Exploring the role of the RNA-binding protein SRSF3 in the developing heart



Irina-Elena Lupu

The Queen's College, University of Oxford

Department of Physiology, Anatomy and Genetics

Supervisor: Dr. Nicola Smart

A thesis presented for the degree of *Doctor of Philosophy*

2019

Abstract

Understanding the molecular processes that govern cardiovascular development has the potential to inform regenerative strategies for disease states. Due to their versatile roles, epicardial cells are an attractive therapeutic target. However, using epicardial cells for therapy is hindered by our limited understanding of epicardial biology.

The embryonic epicardium is one of the main regulators of cardiovascular development, functioning to secrete essential growth factors and produce epicardium-derived cells (EPDCs) that contribute most coronary vascular smooth muscle cells and cardiac fibroblasts. Due to its complex biology, the molecular mechanisms that control epicardial formation and differentiation have not been fully elucidated.

SRSF3 is an RNA-binding protein that has essential roles in RNA processing, and it is highly expressed in the proepicardium and later in the epicardial layer during heart development. Deletion of *Srsf3* from the murine proepicardium using the *Tg(Gata5-Cre)* or embryonic day (E) 8.5 induction of *Wt1*^{CreERT2} led to proliferative arrest and impaired epithelial-to-mesenchymal transition (EMT), which prevented proper formation and function of the epicardial layer. The epicardial requirement for SRSF3 was further assessed in a mouse epicardial cell line using RNA interference, which revealed that SRSF3 is required for production of Cyclin D1 and for EMT in response to TGFβ.

Induction of *Srsf3* deletion with the *Wt1*^{CreERT2} after the proepicardial stage resulted in disrupted sprouting from the sinus venosus and elevated hypoxia at E13.5. Single-cell RNA-sequencing showed SRSF3-depleted epicardial cells were removed by E15.5. The remaining non-targeted cells became hyperproliferative and compensated for the loss, with normal epicardial contribution being detected at E17.5.

Due to the compensation mechanism, the existence of epicardial subpopulations was explored through assessment of published heterogeneous marker genes: *Sema3d, Scx, Tcf21, Tbx18* and *Wt1*, using RNAscope, PrimeFlow and Single-cell RNA-Sequencing, in both wild-type and SRSF3 mutants. Complete overlap of the markers was detected, with no evidence of epicardial subpopulations, raising questions regarding the specificity of previously reported Cre lines.

This research supports a role for SRSF3 as a master regulator of RNA metabolism in epicardial cells, however, further studies are required to dissect the exact molecular mechanisms involved.

Acknowledgments

First, I would like to thank my supervisor, Dr. Nicola Smart, for giving me the opportunity to join this group, and for keeping me motivated and optimistic throughout these past four years.

My DPhil experience would have not been the same without Andia, who taught me so much about research, encouraged me to explore different areas of science, and helped with several aspects of this project. Big thanks to the other members of the Smart, Riley and Mommersteeg groups, especially Will and Helen, for their support and friendship.

I am extremely grateful to my family, especially to my mom, Felicia, for always being there for me, and to my grandma, Florica, who sadly passed away soon after I was accepted onto the DPhil programme, for raising me, and for being one of the strongest women I know.

I couldn't have done it without my friends and fellow DPhil students, Joely and Kathryn. Special thanks to my housemates, Luke and Jack, and to my partner, Matt, for their daily encouragements.

Thanks to everyone who made this research possible: Angela, Richard and all the BMS staff for taking care of the animals, Line and Michal for providing support with the FACS experiments, Neil and Madeleine for helping with the sequencing studies, Prof. David Greaves for all his advice, and the British Heart Foundation for funding this project.

I would also like to acknowledge my mentors before joining Oxford, especially Prof. Bastian Hengerer and my tutors at Manchester Uni, who encouraged me to pursue a career in science.

Finally, I would also like to thank Prof. Shankar Srinivas and Prof. Peter Scambler for taking the time to examine this thesis.

Table of Contents

Chapter I. Introduction 23

1.1 Cardiac development 23

1.1.1 Establishment of cardiogenic progenitors 24

Heart tube formation 24

1.1.2 Chamber formation 26

Heart looping and chamber specification 26

Valve formation and chamber septation 27

Ventricular maturation 28

1.2 Coronary vessel development 30

1.2.1 Developmental sources of coronary endothelial cells 30

The proepicardial organ 30

The sinus venosus and the endocardium 31

1.2.2 Formation of the coronary vasculature 33

Coronary plexus formation 33

Artery specification 33

Mural cell recruitment 34

1.2.3 Robustness and functional heterogeneity 37

1.3 Epicardium function during heart development 38

1.3.1 Formation of the epicardial layer 38

PEO induction 38

Proepicardial cell migration 39

1.3.2 Epicardium-derived cells 40

Epicardial EMT 40

EPDC contribution 42
EPDC differentiation 44
1.3.3 The paracrine function of the epicardial lineage during heart development 44
Compact layer expansion 44
Coronary vessel development 45
Ventricular maturation 45
1.4 The multiple facets of SRSF3 47
1.4.1 The role of SRSF3 in RNA processing 47
1.4.2 SRSF3 as an oncogene 48
1.4.3 SRSF3 in embryonic development 50
1.5 DPhil project 51
1.5.1 Rationale 51
1.5.2 Hypothesis 52
1.5.3 Aims 52
1.5.4 Methodology 52
Chapter II. Materials & Methods 53
2.1 Animal husbandry 53
2.1.1 Mouse lines: 53
2.1.2 Genotyping 54
2.1.3 Tamoxifen induction 54
2.2 Primary cell culture 55
2.2.1 Explant culture 55
PEO explants 55
Epicardial explants 55

2.2.2 Explant treatment 55
4-Hydroxytamoxifen 55
Cell cycle inhibitors 55
2.3 Cell culture 56
2.3.1 RNA interference 56
2.3.2 Induction of EMT & differentiation 56
Epithelial-to-mesenchymal transition 56
Vascular smooth muscle cell differentiation 56
Cardiac fibroblast differentiation 57
Endothelial cell differentiation 57
2.3.3 Inhibition of cell cycle 57
2.4 Molecular Techniques 57
2.4.1 DNA extraction and genotyping 57
Embryo 57
Adult 58
2.4.2 Reverse-transcription quantitative PCR (RT-qPCR) 58
RNA extraction 58
cDNA preparation 58
2.4.3 Western Blot 59
2.5 Imaging 60
2.5.1 Cryosections 60
2.5.2 Immunohistochemistry (IHC) 60
2.5.3 Whole mount antibody staining 60
2.5.4 Immunocytochemistry 61
2.5.5 RNAscope 62
2.5.6 Microscopy 62

2.6 Flow cytometry 63

2.6.1 Tissue dissociation 63

2.6.2 Cell cycle analysis 63

2.6.3 PrimeFlow staining protocol 63

2.6.4 Acquisition 64

2.7 Single-cell RNA-sequencing 64

2.7.1 E 10.5 analysis 64

2.7.2 E 15.5 SMART-Seq2 65

2.7.3 E 13.5 and E 17.5 10X Chromium 66

2.8 Statistical Analysis 66

Chapter III. SRSF3 is required for epicardium formation 67

3.1 Background 67

3.1.1 Proepicardial cell migration 67

3.1.2 The role of proliferation in epicardium formation 68

3.1.3 SRSF3 in heart development 69

3.1.4 Aims 69

3.2 Results 70

3.2.1 Characterisation of SRSF3 expression during development 70

3.2.2 *Tg(Gata5-Cre); Srsf3*$^{fl/fl}$ mutants are embryonic lethal 71

Targeting SRSF3 in the murine PEO 71

Tg (Gata5-Cre); Srsf3$^{fl/fl}$ mutants die mid-gestation 74

Genetic targeting of SRSF3 results in cardiomyocyte defects 75

SRSF3 loss leads to impaired formation of the epicardial layer 77

3.2.3 SRSF3 is required for PEO proliferation 81

3.2.4 SRSF3 is involved in epicardial cell proliferation 83

SRSF3 is required for epicardial explant growth 83
SRSF3 promotes proliferation in an epicardial cell line 86
Determination of cell cycle stage is problematic in the immortalised epicardial cell line 88
3.3 Discussion 91
3.3.1. SRSF3 expression during development 91
3.3.2. *Tg(Gata5-Cre); Srsf3$^{fl/fl}$* mutants are embryonic lethal 91
3.3.3. Fibronectin deposition is decreased in *Tg(Gata5-Cre); Srsf3$^{fl/fl}$* proepicardia 92
3.3.4. SRSF3 is required for PEO proliferation 93
3.3.5. SRSF3 is required for epicardial proliferation *in vitro* 94
3.3.6. Conclusions 95
Chapter IV. SRSF3 is required for epicardial EMT 96
4.1 Background 96
4.1.1 Epicardial EMT regulation 96
4.1.2 Epicardium-derived cell fate specification 97
4.1.3 Epicardial function in coronary vasculature development 98
4.1.4 SRSF3 and mesenchymal state 98
4.1.5 Aims 98
4.2 Results 99
4.2.1 SRSF3 depletion prevents epicardial EMT 99
Wt1^{CreERT2} specifically targets epicardial cells 99
Epicardial SRSF3 deletion leads to heart formation defects 101
SRSF3 is required for epicardial EMT *in vitro* 103
4.2.2 Cell proliferation and EMT 106

Cell cycle inhibition alters EMT response in *vitro* 106

Cell cycle inhibition prevents epicardial explant outgrowth..... 109

4.2.3 Induction of SRSF3 deletion at various developmental stages alters phenotype..... 111

4.2.4 Epicardial cell line differentiation assays 115

SRSF3 knockdown impairs differentiation to vascular smooth muscle *in vitro*..... 116

4.3 Discussion 118

4.3.1 Early induction of SRSF3 deletion leads to failure of EPDC formation 118

4.3.2 Inhibition of CDK4/6 affects epicardial EMT 119

4.3.3 Timing of tamoxifen induction affects phenotype 120

4.3.4 SRSF3 is required for differentiation to vascular smooth muscle *in vitro*..... 121

4.3.5 Conclusions..... 122

Chapter V. Heterogeneity of the epicardial lineage 123

5.1 Background 123

5.1.1 Proepicardial heterogeneity..... 123

5.1.2 Epicardial markers and cell fate choice 124

5.1.3 Aims..... 125

5.1.4 Acknowledgment of contribution..... 125

5.2 Results 126

5.2.1 Overlap of proepicardial markers 126

5.2.2 Expression of epicardial markers throughout development..... 130

E9.5 induction of $Wt1^{CreERT2}$ efficiently labels epicardial cells ... 130

Epicardial markers are downregulated as development progresses 132
Non-specificity of epicardial markers at later stages 133
5.2.3 Heterogeneity of EPDCs and restriction of cell fate 135
EPDCs lose epicardial signature 135
Pseudotime analysis of epicardial markers 139
5.2.4 Epicardial markers are not altered in SRSF3 mutants 141
5.3 Discussion 142
5.3.1 Expression of proepicardial markers in the developing heart 142
PEO 142
Epicardium 143
Non-specific expression 143
5.3.2 Specification of cell fate in epicardium-derived cells 144
5.3.3 Conclusions 144
Chapter VI. Single-cell transcriptomics to explore the molecular mechanisms of SRSF3 function in the epicardium 145
6.1 Background 145
6.1.1 Coronary vessel development 145
6.1.2 Single-cell RNA-sequencing 146
6.1.3 Aims 147
6.2 Results 148
6.2.1 Tamoxifen induction at E9.5/E11.5 results in increased tdTomato+ endothelial cells in *Wt1*^{CreERT2}; *Srsf3*$^{fl/fl}$ hearts 148
6.2.2 Sprouting from the SV and the endocardium is impaired in *Wt1*^{CreERT2}; *Srsf3*$^{fl/fl}$ mutants 151

6.2.3 Unbiased single-cell RNA-sequencing of whole hearts at E13.5 . 153
Identification of cell populations 153
E13.5 *Wt1*^{CreERT2}*; Srsf3*$^{fl/fl}$ mutant hearts are hypoxic 157
6.2.4 Single-cell transcriptomics of the epicardial lineage at E15.5 159
Clustering of cell populations 159
Epicardium-derived population is comprised of cells that escaped recombination 161
6.2.5 Single-cell transcriptomics of whole hearts at E17.5 162
Identification of cell populations 162
Single-cell transcriptomics indicate epicardial contribution to the heart is normal 164
PrimeFlow validates the single-cell RNA-sequencing results 166
Wt1^{CreERT2}*; Srsf3*$^{fl/fl}$ mutants do not show differences compared to littermate controls 168
6.3 Discussion 170
6.3.1 Impaired coronary sprouting in *Wt1*^{CreERT2}*; Srsf3*$^{fl/fl}$ mutants 170
6.3.2 E13.5 whole-heart single-cell transcriptomics indicates *Wt1*^{CreERT2}*; Srsf3*$^{fl/fl}$ hearts are hypoxic 171
Global changes 171
Epicardial lineage defects 172
6.3.3 E15.5 SMART-Seq2 data reveals that the epicardial lineage is hyperproliferative in E15.5 *Wt1*^{CreERT2}*; Srsf3*$^{fl/fl}$ mutants 173
SRSF3 depleted cells are eliminated in mutant hearts 173
EPDC differentiation 174
6.3.4 E17.5 analysis reveals no difference in epicardial contribution at the whole heart level in *Wt1*^{CreERT2}*; Srsf3*$^{fl/fl}$ mutants 174

6.3.5 Conclusions 175

Chapter VII. General discussion 176

7.1 Main findings 176

7.1.1 SRSF3 is required for formation of the epicardial layer 178

7.1.2 SRSF3 is required for EPDC formation 181

7.1.3 Cell-cycle regulators might be involved in epicardial EMT 184

7.1.4 Proepicardial markers significantly overlap during heart development 185

7.1.5 Incomplete SRSF3 targeting results in compensation 187

7.2 General conclusions 189

7.3 Future work 190

7.3.1 Determine the molecular role of SRSF3 in (pro)epicardial proliferation 191

7.3.2 Investigate the molecular mechanism of impaired EPDC formation in *Wt1*^{CreERT2}*; Srsf3*$^{fl/fl}$ mutants 192

7.3.3 Examine the molecular mechanisms of impaired vessel sprouting in *Wt1*^{CreERT2}*; Srsf3*$^{fl/fl}$ mutants 193

7.3.4 Determine how compensation is achieved in *Wt1*^{CreERT2}*; Srsf3*$^{fl/fl}$ mutants 193

7.4 Final remarks 194

Appendix 195

Publications 195

Figures 196

References 207

List of Abbreviations

4-OHT	4-hydroxy-tamoxifen
ANG1	angiopoietin 1
AVC	atrioventricular canal
AVCu	atrioventricular cushion
AVG	atrioventricular groove
BMP	bone morphogenic protein
BRG1	Brahma-related gene 1
BSA	bovine serum albumin
CC3	cleaved caspase 3
CDC42	cell division control protein 42
CDK	cyclin-dependent kinase
CEC	coronary endothelial cell
CF	cardiac fibroblast
CTNT	cardiac muscle troponin T
CTRL	control
CX40	connexin 40
CYR61	cysteine-rich angiogenic inducer 61
DAPI	4′,6-diamidino-2-phenylindole
DHRS3	short-chain dehydrogenase/reductase 3
E	embryonic day
ECM	extracellular matrix
EGM	endothelial growth medium
EMCN	endomucin
EMT	epithelial-to-mesenchymal transition
EndoMT	endothelial-to-mesenchymal transition
EPDC	epicardium-derived cell
ERα	estrogen receptor α
FBS	fetal bovine serum
FGF	fibroblast growth factor
FMO	fluorescence minus one

FN	fibronectin
gMFI	geometric mean fluorescence intensity
HA	hyaluronic acid
HF	heart field
IFNγ	interferon gamma
IGF	insulin growth factor
IGFR	insulin growth factor receptor
IHC	immunohistochemistry
ITS	insulin-transferrin-selenium
IVS	interventricular septum
LATS	large tumour suppressor kinase
MHC	myosin heavy chain
MI	myocardial infarction
NCC	neural crest cell
NEXT	nuclear exosome targeting complex
NF1	neurofibromin 1
NFX1	nuclear transcription factor X
NRG1	neuregulin 1
O/N	overnight
OFT	outflow tract
P/S	penicillin-streptomycin
PBS	phosphate-buffered saline
PCA	principle component analysis
PDCD4	programmed cell death 4
PDGF	platelet derived growth factor
PDGFR	platelet derived growth factor receptor
PEO	proepicardial organ
PFA	paraformaldehyde
PHH3	phospho-histone H3
PIM1	proto-oncogene serine threonine protein kinase 1
PRC2	Polycomb repressive complex 2

RA	retinoic acid
RB	retinoblastoma
RRM	RNA-recognition motif
RT	room temperature
RT-qPCR	reverse-transcription quantitative-polymerase chain reaction
RV	right ventricle
SCX	scleraxis
SEM	standard error of the mean
SEMA	semaphorin
siRNA	small interfering RNA
SMA	smooth muscle actin
SMART	switch mechanism at the 5' end of RNA template
SRSF	serine arginine rich splicing factor
ST	septum transversum
SV	sinus venosus
TBX	T-box transcription factor
TCF21	transcription factor 21
TGF	transforming growth factor
TPM	transcripts per kilobase million
tSNE	t-distributed stochastic neighbour embedding
Tβ4	thymosin β4
UMAP	uniform manifold approximation and projection
UTR	untranslated region
VCAM1	vascular cell adhesion molecule 1
VEGF	vascular endothelium growth factor
VSMC	vascular smooth muscle cell
WT1	Wilms tumour 1
YAP	yes-associated protein

List of Tables

Table 1.1 Endothelial cell lineage tracing in the developing murine heart 32

Table 1.2 Vascular smooth muscle cell lineage tracing in the developing murine heart 35

Table 1.3 Epicardium contributes mural and fibroblast cells before E14.5 42

Table 1.4 The role of SRSF3 in cancer cell lines 49

Table 1.5 Phenotype of cardiac-specific SR protein mutants 50

Table 2.1. Transgenic mouse lines 53

Table 2.2 Primers used for genotyping 54

Table 2.3 PCR programes used for genotyping 54

Table 2.4 Primers used for qPCR 59

Table 2.5 List of antibodies used 61

Table 2.6 RNAscope probes used 62

Table 2.7 PrimeFlow probes used 64

Table 3.1. Survival of *Tg(Gata5-Cre); Srsf3*$^{fl/fl}$ embryos 74

Table 7.1 Summary of *Srsf3* mutant phenotypes 189

Appendix Table 4.1 *Wt1*^{CreERT2}*; Srsf3*^{fl} timed matings produce few embryos 199

List of Figures

Figure 1.1 Specification of cardiac progenitors in the early mouse embryo 24

Figure 1.2 Murine heart formation 25

Figure 1.3 Heart chamber specification 26

Figure 1.4 Chamber septation and valve formation 27

Figure 1.5 Trabecular formation and compaction in the mouse heart 29

Figure 1.6 Embryonic development of the coronary vasculature 36

Figure 1.7 PEO formation 38

Figure 1.8 Molecular mechanisms involved in PEO cell migration 39

Figure 1.9 Model of molecular regulation of epicardial identity 41

Figure 1.10 Epicardium-derived cell formation during murine heart development 43

Figure 1.11 Schematic showing the different roles epicardial cells and EPDCs have during heart development 46

Figure 1.12 The role of SRSF3 in RNA processing 48

Figure 3.1 Schematic of migration strategies used by proepicardial cells 67

Figure 3.2 SRSF3 is expressed in the developing heart 70

Figure 3.3 Breeding strategy used to generate conditional *Srsf3* deletion mice 72

Figure 3.4 *Tg(Gata5-Cre)* lineage tracing with tdTomato 72

Figure 3.5 SRSF3 is downregulated in targeted cells 73

Figure 3.6 Increased cell death and decreased proliferation in *Srsf3* mutants 76

Figure 3.7 Epicardium formation is impaired in *Tg(Gata5-Cre); Srsf3*$^{fl/fl}$ embryos 78

Figure 3.8 Proepicardial cells fail to reach the heart in *Tg(Gata5-Cre); Srsf3*$^{fl/fl}$ mutants 80

Figure 3.9 SRSF3 loss in the PEO leads to defective proliferation 81

Figure 3.10 Decreased proliferation in *Tg(Gata5-Cre); Srsf3*$^{fl/fl}$ proepicardial explants .. 82

Figure 3.11 Strategy used to induce SRSF3 deletion in epicardial explants 83

Figure 3.12 Optimisation of 4-OHT delivery *in vitro* 84

Figure 3.13 *Wt1*^{CreERT2}*; Srsf3*$^{fl/fl}$ explants are less proliferative than controls 85
Figure 3.14 Optimisation of plating densities for the siCtrl 87
Figure 3.15 Cyclin D1 is decreased in siSRSF3 transfected cells 88
Figure 3.16 The cell cycle is perturbed in the immortalised epicardial cell line 90
Figure 4.1 Schematic summarizing the main regulators of epicardial EMT 96
Figure 4.2 Schematic of EPDC differentiation cues 97
Figure 4.3 Breeding strategy used to obtain conditional *Wt1*^{CreERT2}*; Srsf3*$^{fl/fl}$*; Rosa26*^{tdTomato} mice 99
Figure 4.4 Optimisation of tamoxifen delivery *in vivo*. 100
Figure 4.5 *Wt1*^{CreERT2} labels the epicardium before E12.5 101
Figure 4.6 E8.5-induced *Wt1*^{CreERT2}*; Srsf3*$^{fl/fl}$ hearts present failure of EPDC formation, coronary vasculature defects and myocardial non-compaction 102
Figure 4.7 Methodology used to assess EMT in the epicardial cell line 104
Figure 4.8 SRSF3 knockdown inhibits TGFβ1-induced EMT *in vitro* 105
Figure 4.9 Epicardial EMT is altered after cell cycle inhibition *in vitro* 107
Figure 4.10 TGFβ treatment alters cell cycle profile *in vitro* 108
Figure 4.11 FUCCI epicardial explants fail to grow in the presence of cell cycle inhibitors 110
Figure 4.12 Lineage tracing of *Wt1*^{CreERT2} targeted cells in controls and *Srsf3*$^{fl/fl}$ hearts after tamoxifen induction at different timepoints 112
Figure 4.13 Endothelial labelling with different tamoxifen administration regimes 114
Figure 4.14 Differentiation protocols for the mouse epicardial cell line. 116
Figure 4.15 Knockdown of SRSF3 impairs TGFβ1-induced differentiation *in vitro*. 117
Figure 5.1 Epicardial cell fate choice and marker expression 124
Figure 5.2 Proepicardial markers overlap only in the PEO 127
Figure 5.3 Epicardial cells co-express all markers at E10.5 129

Figure 5.4 Wt1^{CreERT2} induction at E9.5 efficiently labels the epicardium 131
Figure 5.5 Epicardial marker expression decreases throughout development 133
Figure 5.6 Expression of epicardial markers throughout development 134
Figure 5.7 EPDCs downregulate expression of epicardial markers. 136
Figure 5.8 E15.5 Single cell RNA-sequencing of the epicardial lineage 138
Figure 5.9 Epicardium-derived cell fate choice and marker expression 140
Figure 5.10 SRSF3 loss does not alter epicardial marker profile 141
Figure 6.1 Comparison between single-cell transcriptomic techniques. 147
Figure 6.2 TdTomato+ cells switch cell identity in *Wt1^{CreERT2}; SRSF3$^{fl/fl}$* mutants 150
Figure 6.3 *Wt1^{CreERT2}* targeted SRSF3 mutants have impaired coronary endothelium formation 152
Figure 6.4 Single-cell RNA-Seq on E13.5 whole-hearts from controls and *Wt1^{CreERT2}; Srsf3$^{fl/fl}$* mutants 155
Figure 6.5 Trabeculae are disorganised in E13.5 *Wt1^{CreERT2}; Srsf3$^{fl/fl}$* mutants 156
Figure 6.6 Iterative clustering of the epicardial lineage reveals increased hypoxia in E13.5 *Wt1^{CreERT2}; Srsf3$^{fl/fl}$* mutant hearts. 158
Figure 6.7 Single-cell transcriptomics of the epicardial lineage from E15.5 controls and *Wt1^{CreERT2}; Srsf3$^{fl/fl}$* mutant hearts 160
Figure 6.8 Tdtomato+ cells are hyperproliferative in *Wt1^{CreERT2}; Srsf3$^{fl/fl}$* mutant hearts 161
Figure 6.9 Single-cell RNA-Seq on E17.5 whole-hearts from controls and *Wt1^{CreERT2}; Srsf3$^{fl/fl}$* mutants 163
Figure 6.10 Sub-clustering of E17.5 tdTomato+ cells 165
Figure 6.11 PrimeFlow shows normal contribution of epicardial cells to various lineages in *Wt1^{CreERT2}; Srsf3$^{fl/fl}$* mutant hearts 167
Figure 6.12 Labelling of coronary endothelium in *Wt1^{CreERT2}; Srsf3$^{fl/fl}$* mutants is not different from controls 169

Figure 7.1 Schematic summarising the phenotype of *Tg(Gata5-Cre); Srsf3*$^{fl/fl}$ embryos179
Figure 7.2 Schematic showing the distinct phenotypes resulting from induction of Wt1-CreERT2 at different developmental stages 183
Figure 7.3 Schematic showing the different treatments used to investigate cell proliferation and EMT in the epicardial cell line. 184
Figure 7.4 Expression of established proepicardial markers throughout development. 187
Figure 7.5 Schematic summarising the early phenotype of *Wt1*^{CreERT2}*; Srsf3*$^{fl/fl}$ embryos tamoxifen induced at E9.5/E11.5 188
Appendix Figure 3.1 SRSF3 expression decreases throughout development..... 196
Appendix Figure 3.2 SRSF3 is not changed in Tβ4 null or WT1 null embryos 196
Appendix Figure 3.3 SRSF3 expression is not affected in heterozygotes 197
Appendix Figure 3.4 Epicardial cells differentiate to smooth muscle cells by 24 h in culture 197
Appendix Figure 3.5 Optimisation of SRSF3 knock down using RNA interference 198
Appendix Figure 3.6 Cell cycle inhibition results in cell death in the mouse epicardial cell lines..... 199
Appendix Figure 4.1 SRSF3 immunostaining in early and late embryonic hearts. 200
Appendix Figure 4.2 Epicardial explants differentiate to vSMC in response to TGFβ and PDGF-DD..... 200
Appendix Figure 5.1 *Wt1* expression is reduced in epicardium-derived cells, whereas *Tcf21* expression is maintained..... 201
Appendix Figure 5.2 Expression of *Sema3d* and *Tbx18* are reduced in epicardium-derived cells..... 202
Appendix Figure 5.3 Non-specificity of epicardial markers at later developmental stages 203
Appendix Figure 5.4 *Scx* and *Tbx18* expression decrease in epicardium-derived cells.204

Appendix Figure 6.1 Tamoxifen is not active four days post administration 204
Appendix Figure 6.2 Smooth muscle coverage is normal in E9.5/11.5 induced *Wt1*^{CreERT2}; *Srsf3*$^{fl/fl}$ hearts 205
Appendix Figure 6.3 Comparison of tSNE and UMAP visualisation of clusters using the E13.5 whole-heart data. 205
Appendix Figure 6.4 No increase in CC3 in E13.5 *Wt1*^{CreERT2}; *Srsf3*$^{fl/fl}$ mutants 206
Appendix Figure 6.5 Comparison of tdTomato labelling at E17.5 after E9.5 and E9.5/E11.5 tamoxifen administration. 206

Chapter I.

Introduction

1.1 Cardiac development

Understanding cardiac morphogenesis is essential for designing better therapies to treat heart disease. In the past decade, efforts have been taken to develop strategies to replace interventional therapies with regenerative treatments, however, they have been largely unsuccessful due to our limited understanding of the regenerative process [1–3]. Lower vertebrate species, which possess cardiac regenerative capacity, have revealed that developmental mechanisms are re-employed during regeneration [4–6], therefore, a better understanding of developmental processes could lead to the design of efficient regenerative therapies.

The outer tissue layer of the heart, the epicardium, is a major player in cardiovascular regeneration [4,5,7–9]. The epicardium was shown to promote cardiomyocyte proliferation and vessel growth in developing embryos and in species that regenerate their hearts, through providing growth factors and perivascular support, [3,5,9–12]. The crucial role of the epicardium during regeneration is highlighted by the formation of a scar after epicardial ablation in the normally regenerative zebrafish [13]. Further understanding of epicardial biology in higher vertebrates could lead to its manipulation for treating conditions such as myocardial infarction and coronary heart disease, which are the leading causes of death worldwide [14].

1.1.1 Establishment of cardiogenic progenitors

Extensive research into early embryo formation showed that the heart is the first organ to form, through specification and migration of progenitors derived from splanchnic mesoderm [15]. Cardiac progenitors are specified by inductive signalling from anterior pharyngeal endoderm, which secretes bone morphogenic protein 2 (BMP2), fibroblast growth factor 8 (FGF8) and Wnt inhibitors that lead to expression of multiple heart identity genes, such as *Nkx2.5* [15–17]. Heart formation is prevented posteriorly through Wnt signalling from the neural tube and BMP inhibitors secreted from the notochord [16,18–20] (Fig 1.1).

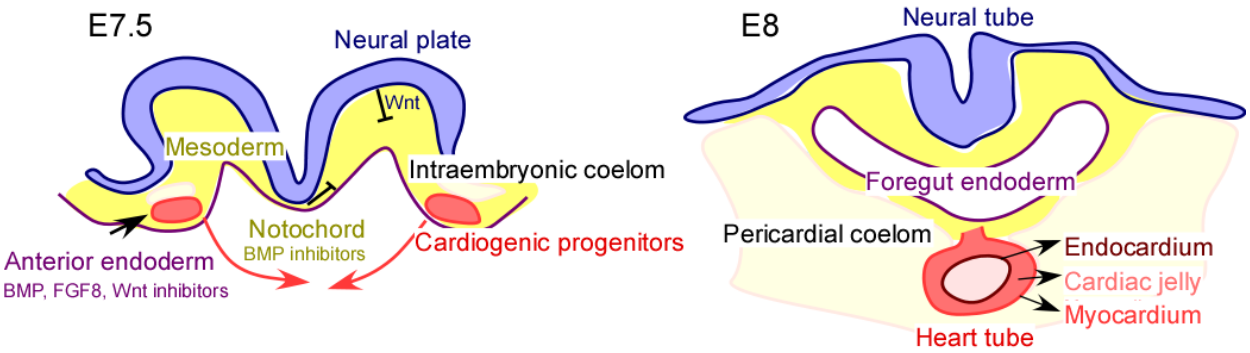


Figure 1.1 Specification of cardiac progenitors in the early mouse embryo

Heart progenitors are specified from splanchnic mesoderm upon inductive signalling from anterior endoderm. Production of Wnt and BMP inhibitors from neural structures prevents ectopic heart formation. Migration of heart progenitors towards the midline is closely associated with formation of the foregut. Figure adapted from Cyganek et al. [21].

Heart tube formation

Cardiac progenitors initially arise on either side of the midline, but eventually fuse around embryonic day (E) 7.75 in mouse and form what is known as the cardiac crescent [18,22,23]. This fusion is intimately connected to the migration of neighbouring foregut endoderm [24]. Endoderm closure defects lead to formation of two separate hearts [25].

During cardiac progenitor migration, the intraembryonic coelom is formed through separation of splanchnic mesoderm from somatic mesoderm [18]. The somatic mesoderm will form the pericardium, whereas the intraembryonic coelom will be separated by the septum

transversum (ST) into the pericardial and pleural cavities. Within the splanchnic mesoderm, two populations segregate: myocardium and endocardium, followed by the organisation of the cardiac crescent into a tube-shaped structure, with an inner endothelial tube separated by extracellular matrix (ECM), known as cardiac jelly, from myocardial cells [26–30].

The cardiogenic regions include two cell populations named the first and second heart field (HF) [23,31]. It is still under debate if these populations are inherently different or if they represent distinct developmental states. The 1st HF has limited proliferative capacity and forms the scaffold of the heart, which will become the left ventricle and most of the atria, whereas the 2nd HF is distinguished by expression of *Islet1* and is maintained in a high proliferative state by its contact with pharyngeal endoderm, which sustains FGF production [31–35]. The 2nd HF contributes cells to the anterior and posterior sides, forming the right ventricle (RV) and outflow tract (OFT) anteriorly, whereas retinoic acid production posteriorly specifies the atria and the sinus venosus (SV) [36] (Fig 1.2).

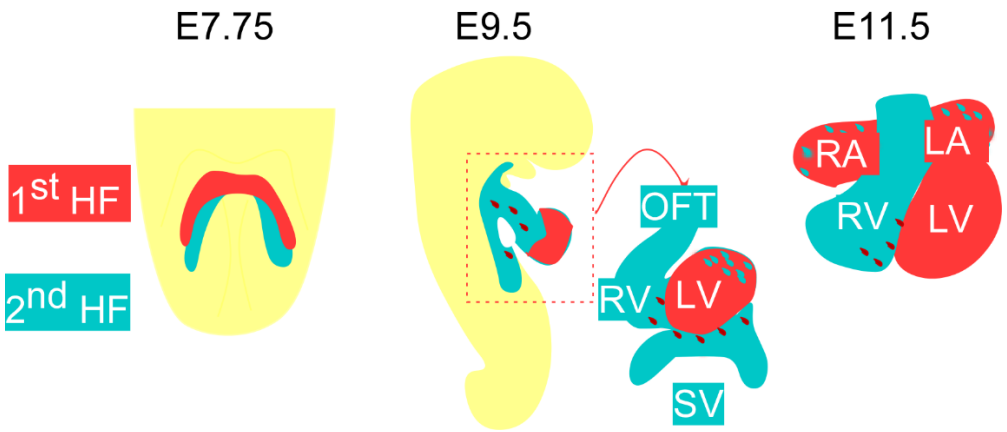


Figure 1.2 Murine heart formation

The cardiac crescent is formed after fusion of cardiogenic progenitors at the midline. The heart tube forms from first heart field progenitors that will mainly contribute to the left ventricle and atria, with second heart field progenitors added to form the right ventricle and outflow tract. HF-heart field, OFT-outflow tract, RV-right ventricle, LV-left ventricle, SV-sinus venosus, RA-right atrium, LA-left atrium. Figure adapted from Laugwitz et al [37].

1.1.2 Chamber formation

Heart looping and chamber specification

The heart tube begins to loop around E8.5, after the initial connection to the mediastinum is partially severed, which allows the tube to bend [38]. The looping process is still not entirely understood, but regionalised tissue growth and mechanical constraints are thought to promote looping to the right [39,40].

As the heart loops, a transcriptional programme that enables more efficient conduction through expression of gap junction proteins, such as connexin 40 (CX40), is initiated in the outer curvature, specifying pre-chamber myocardium [41] (Fig 1.3). Here, sustained expression of the cardiac genes T-box transcription factor (TBX) 5 and TBX20 promote proliferation, leading to ballooning and chamber formation, whereas TBX2 expression in the OFT and atrioventricular canal (AVC) prevents proliferation and chamber specification in these regions [42].

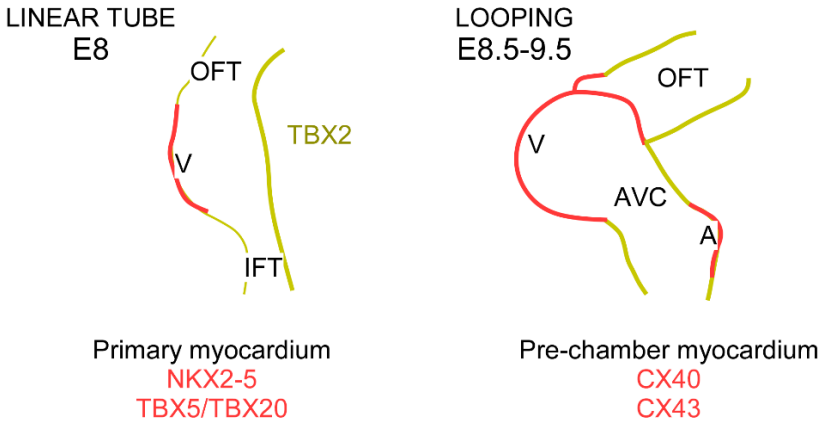


Figure 1.3 Heart chamber specification

TBX5/TBX20 expression in the first heart field, together with expression in the right ventricle, promote cardiomyocyte proliferation and chamber specification. TBX2 expression in the outflow tract and atrioventricular canal prevent chamber formation in these regions. OFT-outflow tract, V-ventricle, IFT-inflow tract, A-atria, , AVC-atrioventricular canal.

Valve formation and chamber septation

Heart valve precursors, known as endocardial cushions, are established during looping through proliferation of endocardial progenitors and addition of cells from the neural crest to the OFT valves and epicardium-derived cells (EPDCs) to the parietal leaflets of the atrioventricular valves [18,43,44].

Endocardial cushion formation is induced by non-chamber myocardium that secretes factors such as BMPs, transforming growth factor β (TGFβ) and vascular endothelial growth factor (VEGF) [45–47]. These factors stimulate cardiac jelly accumulation and endocardial-to-mesenchymal transition (EndoMT). Neural crest cells (NCCs) are also important for proper formation of the OFT cushions through secretion of semaphorin 3C (SEMA3C) [48]. Further maturation of the cushions, together with chamber separation, will give rise to two circulatory systems: pulmonary and systemic, and it will also prevent retrograde flow (Fig 1.4).

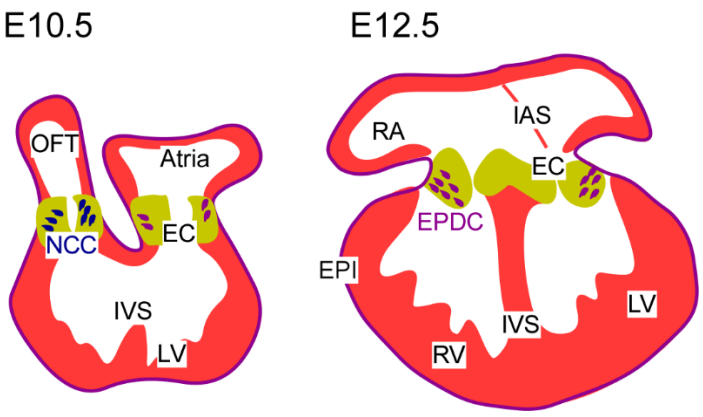


Figure 1.4 Chamber septation and valve formation

Endocardial cushions (yellow) are populated with endocardial cells and neural crest cells (blue) in the outflow tract and epicardium-derived cells (purple) in the atrioventricular canal. During heart looping they start to separate the atria and the outflow tract from the ventricles, eventually forming the valves. The interatrial and interventricular septum also start forming. OFT-outflow tract, NCC-neural crest cell, EC-endocardial cushion, IVS-interventricular septum, LV-left ventricle, RA-right atrium, IAS-interatrial septum, EPDC-epicardium-derived cell, EPI-epicardium, RV-right ventricle.

Ventricular maturation

During looping, at the outer curvature, the myocardium remodels and trabeculation is initiated. Proper formation of the trabeculae is essential for maintaining cardiac output in the embryo and for nutrient exchange before coronary vessels are established [49].

The molecular mechanisms involved in trabeculation are not well-understood, but, in zebrafish, Samsa et al. showed that contraction is required to activate Notch1 signalling in the endocardium, which leads to Neuregulin 1 (NRG1) expression and trabecular formation [50]. Delta-mediated Notch signalling is crucial for trabeculation in both mammals and zebrafish [51–53]. Other signalling pathways, such as BMP10, are also required to maintain proliferation and formation of trabeculae [53]. In mouse, cell proliferation, especially oriented cell division is thought to be required for invasion of myocardial cells into the subendocardial space [54,55], however, in zebrafish, proliferation does not seem to be required for initiation of trabeculation, only needed for subsequent growth [52].

Trabecular myocardium is less proliferative than compact myocardium and expresses genes such as CX40, which facilitate conduction, whereas the compact layer maintains TBX20 expression and proliferation [49]. Signals originating from the endocardium are thought to inhibit proliferation at the apical side of the trabeculae, whereas epicardium-derived signals maintain proliferation in the compact layer [56].

As the myocardium proliferates and expands, diffusion becomes insufficient in supplying the entire muscle wall and coronary vessels form to meet the demand for oxygen and nutrients.

After coronary vessels are formed, trabecular growth ceases. The expression of Manic Fridge, which promotes activation by Delta-like receptors, decreases, allowing Jagged1 ligands from the myocardium to activate endocardial Notch, which promotes trabecular compaction [57].

During compaction, some endocardial cells are trapped in the myocardium, where they differentiate to coronary endothelial cells (CECs) (Fig 1.5). The mechanisms involved in this differentiation remain to be elucidated, but hypoxia and VEGF signalling are thought to play a key role [58].

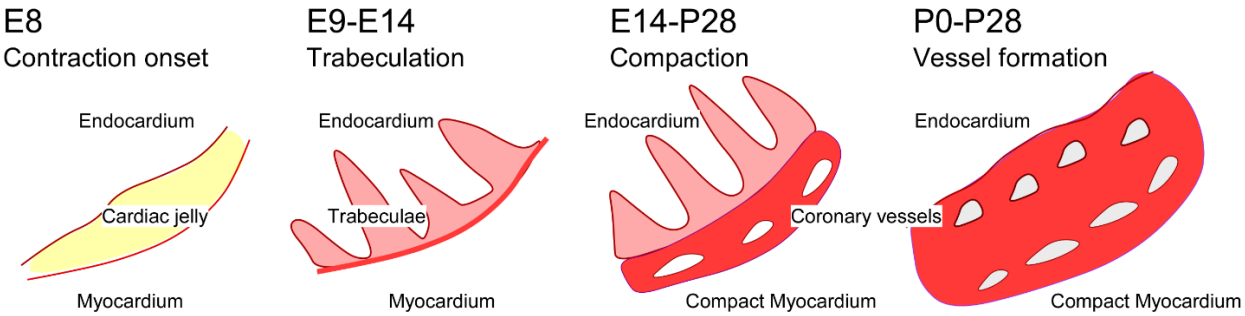


Figure 1.5 Trabecular formation and compaction in the mouse heart

The heart tube contains a smooth endocardial layer that is separated from the myocardial layer by extracellular matrix known as cardiac jelly. Contraction activates Notch signalling in the endocardium, which leads to proliferation and formation of trabeculae. Later in development, endocardial Notch is activated by Jagged1 from the myocardium which results in compaction of the trabeculae. Endocardial cells that are trapped during compaction give rise to blood vessels in the inner heart wall.

1.2 Coronary vessel development

1.2.1 Developmental sources of coronary endothelial cells

The proepicardial organ

Historically it was thought the coronary network was derived from the aorta, however, embryonic studies showed coronary vessels connect to the aorta after they form [59,60].

Retroviral labelling in avian embryos identified the proepicardial organ (PEO) as the main source of coronary endothelium [61,62], which was further supported by quail-chick transplantation experiments [63,64]. However, lineage tracing studies done later in mice using proepicardial Cre lines such as *Wt1*^{CreERT2} [65], *Tcf21*^{MerCreMer} [66] or *Tbx18*^{Cre} [67] found little to no contribution of these precursor cells to coronary endothelium, indicating the origin of CECs might be species-dependent.

In 2012, Katz et al. reported the existence of non-overlapping cell populations within the mouse PEO, roughly defined as either Wilms Tumour 1 (WT1)+/TBX18+ or SEMA3D+/ Scleraxis (SCX)+ [68] . Lineage tracing using *Sema3d*^{Cre} or *Tg(Scx-Cre)* partially labelled the coronary endothelium, suggesting that a PEO subcompartment untraced by previously used Cre lines is responsible for the proepicardial contribution to CECs. Another study supporting the existence of an endothelial progenitor population in the PEO region used the PEO/ST *Tg(G2-Gata4-Cre)* line to trace cells and reported 22.7% of coronary endothelium contribution by PEO/ST [69].

Lineage tracing with the Cre/loxP systems relies on Cre recombinase specificity to the population of cells under investigation [70]. Specificity is achieved by placing the Cre recombinase under the control of a regulatory sequence of a cell-type specific gene, however, in the case of the PEO, none of the genes used to map its lineage are solely

expressed in this region [66,69,71–74]. This non-specificity, together with other technical drawbacks, such as incomplete recombination and tamoxifen toxicity or persistence in the case of inducible Cre lines [65,75,76], makes the Cre/loxP system prone to errors, therefore, caution must be taken in interpreting findings.

Of importance, cells labelled with *Sema3d*^{Cre} also contributed to the SV [68], whereas *Tg(Scx-Cre)* and *Tg(G2-Gata4-Cre)* labelled a subset of ventricular endocardium [69], both known sources of CECs [77]. This might indicate the CEC progenitor population present in the PEO/ST region contributes to coronary endothelium via these vasculogenic sources. Migration of these progenitors to the epicardial layer is unlikely since studies using inducible Cre lines to trace epicardial cells found negligible contribution to coronary endothelium [65,66].

The sinus venosus and the endocardium

Seminal work published in 2010 revealed the main sources of coronary vessels are the SV endothelium and the endocardium [78]. Chen et al. further analysed the percentage contributed by each source and found the SV is the main contributor of CECs in the embryonic mouse heart, populating the dorsal and lateral regions, being complemented by the endocardium in the interventricular septum (IVS) and on the dorsal side [77].

Interestingly, the endocardium becomes the main source of CECs postnatally through trabecular compaction and endothelial differentiation of trapped endocardial cells [58]. These endocardial-derived CECs populate the inner muscle wall, which, together with vessels in the IVS, irrigate 60% of the adult heart, as opposed to the SV-derived vasculature present in the outer muscle wall that irrigates the remaining 40% [58].

A recent avian paper confirmed the SV and the ventricular endocardium are the main sources of the coronary endothelium in chick [79], arguing against species specific origin of the coronary vasculature.

The Cre lines used to investigate the origins of CECs are summarised in Table 1.1.

Table 1.1 Endothelial cell lineage tracing in the developing murine heart

Endothelium

Cre	**Specificity**	**Induction**	**Stage analysed**	**CECs labelled**	**Ref**
Apln^{CreER}	**CECs**	E10.5	P28	OMW	58
		E13.5		IVS	
		P4/6		IMW	
Nfatc1^{CreERT2}	**Endo**		P0	IVS	
		E8.5	P7	IVS, IMW	
Npr3^{CreER}	**Endo**	E8.5	E15.5	IVS	80
Nfatc1^{Cre}	**Endo**	constitutive	E16.5	IVS, lateral	77
Apj^{CreERT2}	**SV**	E10.5	E16.5	OMW dorsal side	
Wt1^{CreERT2}	**Epi**	E10.5	E18.5	rare labelling	65
Tcf21^{MerCreMer}	**Epi** **AVCu**	E10.5	E18.5	none observed	81
Tbx18^{Cre}	**PEO/Epi**	constitutive	adult	none observed	67
Tg(Gata5-Cre)	**PEO/ST/Epi**	constitutive	P3	none observed	82
Sema3d^{Cre}	**PEO/Epi** **AVCu**	constitutive	E16.5	6.9% labelled some SV labelling	68
Tg(Scx-Cre)	**PEO** **AVCu**	constitutive	P4-P7	24.3% labelled some endocardial labelling	
Tg(G2-Gata4-Cre)	**PEO/ST/Epi**	constitutive	E17.5	22.7% labelled some endocardial labelling	69

CEC-coronary endothelial cell, Endo-endocardium, Epi-epicardium, SV-sinus venosus, EPDC-epicardium-derived cell, PEO-proepicardial organ, ST-septum transversum, CM-cardiomyocyte, AVCu-atrioventricular cushion, OMW-outer muscle wall, IVS-interventricular septum, IMW-inner muscle wall.

1.2.2 Formation of the coronary vasculature

Coronary plexus formation

The coronary vasculature initially forms by vasculogenesis as progenitors coalesce to establish the primitive plexus [83,84]. The developmental mechanisms that regulate this vasculogenic process are not entirely understood, but signalling from multiple cell types, such as epicardium and myocardium, have been implicated [85].

Interestingly, the SV and the endocardium appear to respond to different signals to initiate vessel formation. Epicardium-derived signals, such as VEGF-C, are required for the SV to induce sprouting [77,86], whereas, the endocardium is sensitive to hypoxia-related signals such as VEGF-A, originating from myocardium [58,86].

It remains to be determined how the different sourced progenitors come together and connect to form the coronary plexus.

Artery specification

Soon after the primitive coronary plexus is established, the endothelial tubes connect to the aorta, as guided by signalling factors, such as VEGF-C and CXCL12 [87,88]. The established view is that connection to the aorta and onset of blood flow initiates plexus remodelling, where vessels are reorganised, and fates specified.

Novel observations based on single-cell RNA-sequencing data revealed that pre-artery differentiation starts at E12.5 in mouse, prior to aortic connection and onset of blood flow [89]. Surprisingly, the specification of pre-artery fate was linked to lower proliferation rate [89]. Inhibition of cell cycle *in vitro* was sufficient to promote pre-artery fate; however, it remains to be determined how proliferation affects arterial differentiation at the molecular level.

Immunostaining for arterial genes showed that pre-artery cells are initially interspread throughout the coronary plexus, then coalesce and become artery in response to flow [86,90]. These findings indicate that, *in vivo*, arteries do not grow through proliferation, but through recruitment and migration of other arterial cells, which has important implications for regenerative strategies.

Mural cell recruitment

The coronary vessels require perivascular support for proper function, the arteries being surrounded by multiple layers of smooth muscle, whereas the capillaries are in direct contact with pericytes.

The epicardium is the main contributor of mural cells in the mammalian heart. This view is supported by lineage tracing studies using an extensive list of epicardial Cres [65,67,81,91]. Interestingly, the vascular smooth muscle cells (vSMCs) of the postnatal vasculature, derived through compaction-entrapment of the endocardium explained previously, originates from pre-existing mural cells of epicardial origin that expand and invade the inner wall [92].

The neural crest has a minor, but important, contribution to mural cells in the heart, providing vSMCs for the proximal arteries and the septal branches [93]. Another modest, but unexpected, source of mural cells is the endocardium. Chen et al. reported that endocardial-derived cushion mesenchyme can differentiate to mural cells which mainly contribute vSMCs in the IVS [94].

The different Cre lineages used to identity the origins of vSMCs in the heart are shown in Table 1.2. A schematic of coronary vasculature formation in shown in Figure 1.6.

Table 1.2 Vascular smooth muscle cell lineage tracing in the developing murine heart

Vascular smooth muscle cells

Cre	Specificity	Induction	Stage analysed	vSMCs labelled	Ref
Wnt1^{Cre}	**NC**	constitutive	E17.5	proximal arteries	93
Wt1^{CreERT2}	**Epi**	E10.5	8 weeks	>80% labelled	92
Tcf21^{MerCreMer}	**Epi, AVCu**	E10.5	E18.5	substantial labelling	81
Tg(Gata5-Cre)	**PEO/ST/Epi**	constitutive	E18.5 4 months	>80% labelled	91
Tbx18^{Cre}	**PEO/EPI**	constitutive	P14	substantial labelling	67
Tie2^{Cre}	**ECs**	constitutive	E16.5	10.75% labelled	94
Apln^{CreERT2}	**SV-derived CECs**	E10.5	E16.5	none observed	
Nfatc1^{CreERT2}	**Endo**	E8.5	E16.5	some labelled	

NC-neural crest, vSMC-vascular smooth muscle cell, Epi-epicardium, CEC-coronary endothelial cell, CM-cardiomyocytes, AVCu-atrioventricular cushion, CF-cardiac fibroblast, PEO-proepicardial organ, ST-septum transversum, EC-endothelial cell, SV-sinus venosus, Endo-endocardium.

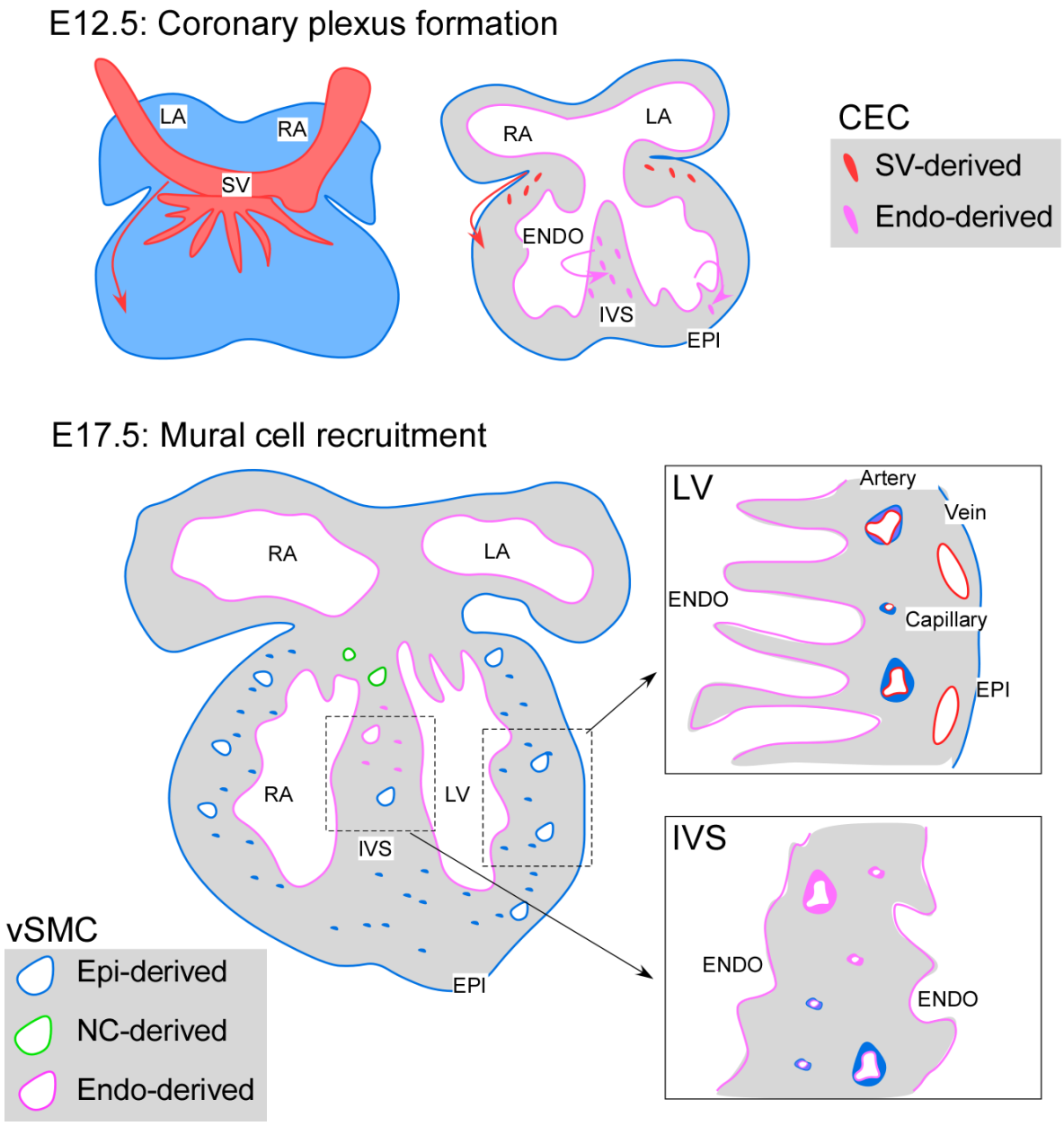


Figure 1.6 Embryonic development of the coronary vasculature

Formation of the coronary plexus is initiated at E11.5, when sinus venosus derived endothelial cells start migrating downwards on the dorsal side of the heart. Endocardial cells start sprouting in the interventricular septum and in the lateral walls towards the apex. Starting from E15.5, pericytes and vascular smooth muscle cells are recruited to the forming vessels. Most mural cells arise from the epicardium, with a small contribution from the neural crest near the base and endocardial-derived mural cells in the interventricular septum. LA-left atrium, RA-right atrium, SV-sinus venosus, ENDO-endocardium, IVS-interventricular septum, EPI-epicardium, NC-neural crest.

1.2.3 Robustness and functional heterogeneity

It is unclear whether the multiple origins of coronary vessels are of functional relevance or if this heterogeneity reflects a rapid response that employs all available cells. Sharma et al. reported that endocardial-derived vessels are morphologically different from SV-derived ones, suggesting the former [86].

Intriguingly, the endocardium is able to compensate for defects in SV-derived vessel formation. This was first reported in vascular cell adhesion molecule 1 (VCAM1) mutants, where subepicardial sprouts failed to form, resulting in an increased number of endocardial-derived blood islands ventrally [95]. The compensation mechanism was better characterised in Elabela mutants, where SV sprouting was impaired, similarly resulting in increased production of endocardium-derived vessels [86]. It remains unexplored if the SV is able to compensate for an endocardial-sprouting defect. This might not be possible, since the endocardium sprouts in response to hypoxia, which is upregulated in the case of SV-sprouting defects, whereas the SV requires non-hypoxic signals to initiate sprouting.

The different sources of vSMCs can also provide compensation for each other. Platelet derived growth factor receptor β (PDGFRβ) loss in the epicardium resulted in absence of epicardium-derived vSMCs and expansion of vSMCs near the aortic root, presumably NCC-derived [96]. Epicardium-specific perturbation of Notch signalling similarly led to failure of the epicardium to provide vSMC and expansion from an untargeted source [91]. Remarkably, later in life, the compensating vSMCs were prone to leakage and susceptible to disease, suggesting the different origins of vSMCs confer functional diversity. In other systems, such as the aorta, the sources of vSMCs determine resistance to atherosclerotic stimuli [97], and it is likely the heterogeneous vSMCs of the coronaries also have different functional characteristics.

1.3 Epicardium function during heart development

1.3.1 Formation of the epicardial layer

PEO induction

The PEO arises from 2nd HF progenitors that downregulate expression of *Nkx2-5* and *Islet 1* (*Isl1)* and gain *Tbx18* expression [98–101]. At the cardiac crescent stage, these progenitors are found in the caudal region of the crescent and, as the heart loops, they relocate to the apical side of the ST [102]. The progenitors still retain the potential to become myocardium and, upon BMP2 signalling, they contribute cardiomyocytes to the inflow tract, whereas at the ventral side of the ST, FGF2 and other signals from the liver bud induce expression of *Wt1 and Transcription factor 21 (Tcf21)*, specifying these cells to become PEO [99,101,103] (Fig 1.7). Overexpression of BMP2 commits all the progenitors to myocardial fate, suppressing PEO formation [101], whereas liver bud implantation induces expression of proepicardial genes ectopically [103].

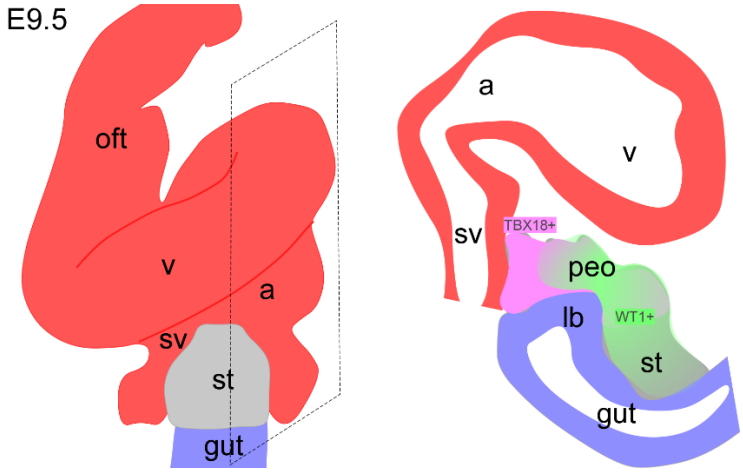


Figure 1.7 PEO formation

The PEO forms in the septum transversum region from TBX18+ second heart field progenitors. Near the inflow tract TBX18+ cells are specified to become myocardium, whereas the liver bud induces proepicardial fate and WT1 expression. WT1 is also expressed in other cells in the septum transversum. v-ventricle, a-atrium , peo-proepicardial organ, lb-liver bud, st-septum transversum, sv-sinus venosus.

Proepicardial cell migration

After proepicardial identity is established, cells of the PEO extrude from the ST and migrate towards the heart surface (Fig 1.8). The apical extrusion of PEO cells is thought to result from regionalised proliferation and polarity cues that lead to accumulation of cells at the midline [104,105]. Migration is induced by BMPs and ECM secreted from the AVC region, such as hyaluronic acid (HA), which act as chemoattractants for PEO cells[106,107].

Proepicardial cells deposit a fibronectin bridge that is used as a substrate during migration [108]. Contraction of the heart is required for transfer of PEO cells onto the heart surface, through mediating release and survival of migrating cells [104,109]. Cell adhesion proteins are also involved in PEO cell attachment, expression of myocardial VCAM1 and proepicardial α4β1 integrin being crucial for epicardium formation [110–112].

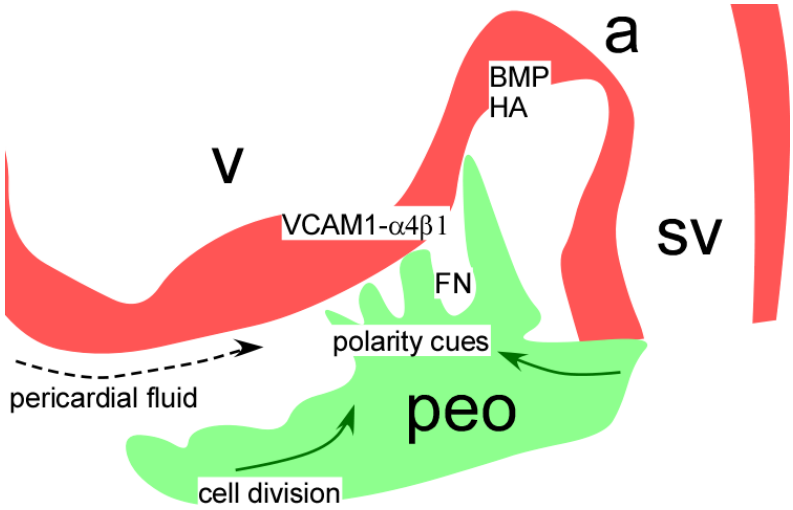


Figure 1.8 Molecular mechanisms involved in PEO cell migration

Higher rates of cell division laterally causes accumulation of PEO cells near the midline, where cell polarity cues lead to apical extrusion. Signals secreted from the atrioventricular groove region such as BMP and hyaluronic acid attract PEO cells. Proepicardial cells express Itga4, that mediates movement onto the fibronectin bridge towards the heart. Myocardial cells express VCAM-1, which promotes adhesion of PEO cells. Heartbeat generates pericardial fluid movement, which enables PEO cell attachment to the myocardium. Peo-proepicardial organ, FN-fibronectin, sv-sinus venosus, a-atrium, v-ventricle, HA-hyaluronic acid.

1.3.2 Epicardium-derived cells

Epicardial EMT

Soon after the epicardial layer is formed, some epicardial cells lose adherence to the epithelium and invade the myocardium in a process known as epithelial-to-mesenchymal transition (EMT). EMT is a fundamental process frequently utilized during development to generate the germ layers and tissues of the embryo, through production of migratory cells as a result of cellular adhesion changes, loss of apico-basal polarity and cytoskeleton reorganisation[113].

The interaction between myocardial VCAM1 and epicardial α4β1 integrin is crucial in limiting epicardial EMT, with loss of either components leading to an increased number of epicardial cells leaving the outer layer [110]. However, what initiates the EMT process is not well defined. Wu et al. reported that oriented cell division is required to promote EMT, with cells dividing perpendicular to the basement membrane entering the myocardium [114]. Junctional adhesion proteins like β-catenin are important for determining the plane of division [114,115]; however, the exact mechanisms that control spindle orientation in the epicardium remain unknown.

The epicardial master transcription factor WT1 is required for β-catenin activity and retinoic acid production, which controls cell proliferation, polarity and EMT [116–119]. Retinoic acid also promotes TCF21 expression, which together with TBX18, prevents premature differentiation of epicardial cells to vSMC fate [120,121].

The Hippo signalling pathway, known to regulate organ size [122], has also been connected to epicardial EMT. Deletion of the transcription factors Yes-associated protein (YAP)/TAZ from the epicardium led to failure of epicardial cells to proliferate and undergo EMT [123], whereas depletion of the large tumor suppressor kinase (LATS) resulted in higher

production of EPDCs that failed to differentiate [124]. YAP/TAZ maintain homeostatic retinoic acid levels through production of Dehydrogenase/Reductase 3 (DHRS3), an enzyme that converts retinaldehyde to retinol [118]. YAP/TAZ also sustain expression of the epicardial master genes *Wt1* and *Tbx18* [123].

Since the Hippo pathway can be triggered by density and substrate changes [122], it is possible that epicardial cell division perpendicular to the heart plane leads to the displacement of one daughter cell from the outer layer, changing parameters that suppress activity of YAP/TAZ, leading to the loss of epicardial identity and onset of differentiation (Fig 1.9).

Another factor required to maintain epicardial identity is Thymosin β4 (Tβ4), a monomeric actin sequestering protein, which promotes expression of epicardial genes through recruitment of the chromatin remodeling complex Brahma-related gene 1 (BRG1) at epicardial gene loci, such as *Wt1, Tbx18* and *Tcf21* [12,125].

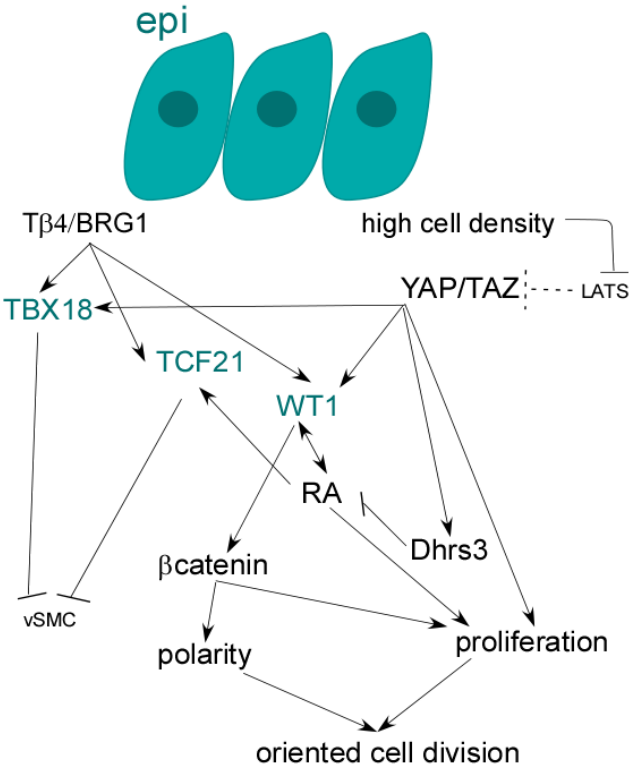


Figure 1.9 Model of molecular regulation of epicardial identity

Epicardial cells express TBX18, TCF21 and WT1, sustained by Thymosin β4 (Tβ4)/BRG1 and Hippo effectors YAP/TAZ. WT1 leads to production of retinoic acid (RA) and β-catenin, both required to promote proliferation and maintain epithelial integrity. YAP/TAZ also mediate expression of Dhrs3, which moderates production of retinoic acid. TCF21 and TBX18 both repress epicardial differentiation to smooth muscle. epi-epicardium, vsmc-vascular smooth muscle cell.

EPDC contribution

Epicardial cells that undergo EMT and invade the heart are known as EPDCs. EPDCs contribute most vSMCs and cardiac fibroblasts (CFs) in the heart [65,67,68,82,91,92].

Tamoxifen dosing at different embryonic stages using the only inducible epicardial Cre lines: *Wt1*^{CreERT2} and *Tcf21*^{MerCreMer}, suggest EPDCs form before E14.5 in mouse. Tamoxifen induction at E10.5 led to more than 80% of the vSMCs being labelled, whereas induction past this stage labelled very few epicardium-derived mural cells and resulted in significant labelling in non-epicardial domains due to *Wt1* expression within CECs and *Tcf21* expression in CFs.

Table 1.3 Epicardium contributes mural and fibroblast cells before E14.5

Epicardium lineage tracing

Cre	Specificity	Induction	Stage analysed	Contribution			Ref
				CF	Mural	CEC	
***Wt1*^{CreERT2}**	Epi	E10.5	E18.5	most	>80%	rare	65,92,126,
	Epi, CEC	E14.5		rare	<5%	most	127
***Tcf21*^{MerCreMer}**	Epi, AVCu	E10.5	E18.5	most	most	none	66,81
	CF	E14.5		most	none	none	

Epi-epicardium, CEC-coronary endothelial cell, AVCu-atrioventricular cushion, CF-cardiac fibroblast, CM-cardiomyocyte

Less convincing evidence has been presented for the contribution of EPDCs to cardiomyocytes and CECs. Most Cre lines used to report cardiomyocyte contribution are also expressed in some myocardial cells [72], making it impossible to distinguish between epicardial contribution and direct labelling.

The constitutive *Wt1*^{Cre} line has been used to show epicardial contribution to coronary endothelium [69], however, expression of *Wt1* in CECs has been documented in several studies [65,128,129] . Restricting activity of the inducible *Wt1*^{CreERT2} by tamoxifen delivery at E10.5, before vessels are formed, led to negligible staining of coronaries, indicating endothelial labelling with *Wt1*^{Cre} was due to its expression in CECs.

In summary, reported findings show epicardial cells contribute more than 80% of vSMCs and CFs in the heart, but they do not contribute significantly to cardiomyocytes or CECs (Fig 1.10).

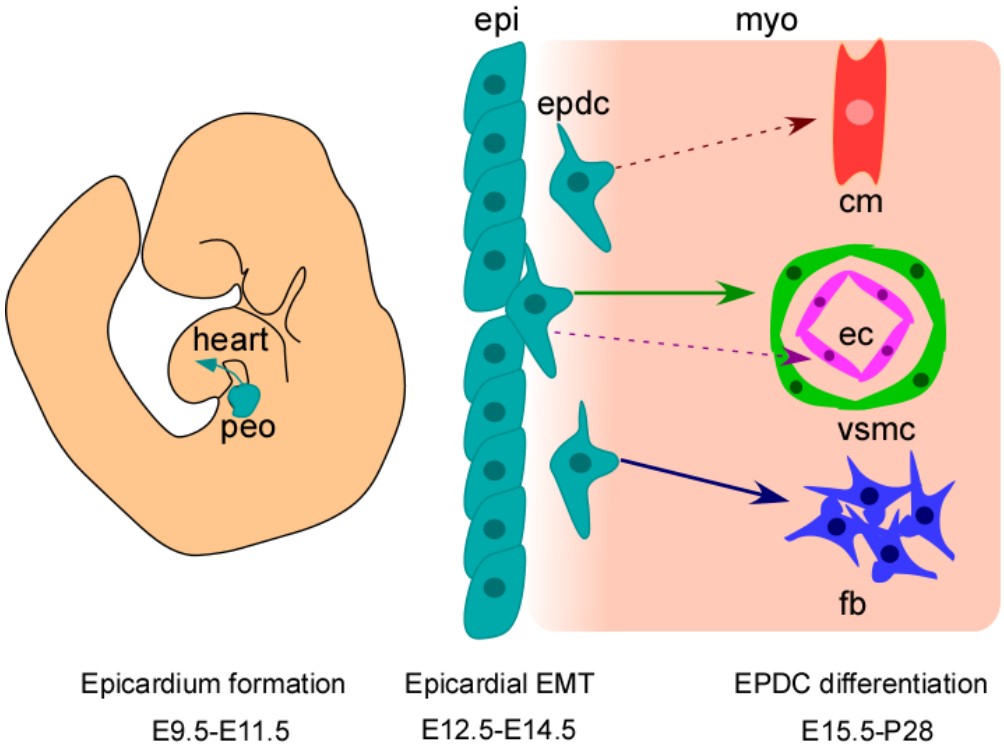


Figure 1.10 Epicardium-derived cell formation during murine heart development

The epicardium forms from the proepicardial organ. After epicardial layer formation is complete, some epicardial cells undergo epithelial-to-mesenchymal transition, producing epicardium-derived cells that later contribute to different cardiovascular lineages. peo-proepicardial organ, epi-epicardium, epdc-epicardium-derived cell, cm-cardiomyocyte, myo-myocardium, vsmc-vascular smooth muscle cell, ec-endothelial cell, fb-fibroblast.

EPDC differentiation

Even though it is accepted that EPDCs contribute CFs and vSMCs, the molecular mechanisms that control EPDC differentiation remain to be determined.

One signalling pathway that has been linked to EPDC cell fate choice is platelet-derived growth factor (PDGF). PDGFRs are co-expressed in the epicardium before E13.5, where they are required for EPDC formation [127]. Surprisingly, deletion of only PDGFRα led to selective loss of CFs [127], which indicated PDGFRα is only required for formation of epicardium-derived CFs. However, it remains unclear if CF progenitors fail to undergo EMT or if their differentiation is compromised in the absence of PDGFRα. Similarly, PDGFRβ loss in the epicardium exclusively prevented mural cell formation [96,127]. In the heart, pericytes act as precursors for vSMCs and PDGFRβ is needed for the transition of EPDCs to pericytes [130]. Further differentiation to vSMCs is triggered by endothelial Notch signalling in response to blood flow [130].

1.3.3 The paracrine function of the epicardial lineage during heart development

Apart from directly contributing to various cardiovascular populations, the epicardial lineage has multiple paracrine functions during heart development.

Compact layer expansion

Early in development, formation of the epicardial layer marks the onset of myocardial patterning and growth. Historical studies have observed that myocardial proliferation rate is highest near the epicardial surface [131]. Mutant embryos that fail to form an epicardium have hypoplastic non-compacted ventricles [82,111] and multiple studies have determined that epicardial cells secrete growth factors, such as FGF9 and insulin growth factor 2 (IGF2), that mediate myocardial proliferation [132–135].

Intriguingly, growth factors, such as FGFs, are also secreted from the endocardium, showing that epicardial growth factor gradient is not sufficient to determine the distinct proliferation rates observed in the myocardial wall. Pennisi et al. showed that distribution of FGF receptors in the myocardium is uneven, with higher expression in the compact layer [135]. Prevention of epicardial formation did not alter the FGF receptor distribution, showing the myocardium is pre-patterned by non-epicardial determinants to undergo regionalised proliferation.

Coronary vessel development

As previously mentioned, factors released from epicardial cells are also needed for coronary vessel growth. Sprouting from the SV is induced by epicardium-derived factors, such as VEGF-C and Elabela [77,86]. Other epicardium-derived factors, such as FGF9, stimulate expression of pro-angiogenic factors in the myocardium, such as VEGF-A and angiopoietin 1 (ANG1), that further support vessel formation [136–138].

Later in development, epicardium-derived CFs release ECM components that promote vessel formation [124], whereas epicardium-derived mural cells are required to physically support the forming vessels [130].

Ventricular maturation

The epicardium has an important paracrine role in early development, whereas as the myocardial wall thickens, diffusion of epicardium-derived factors becomes limited and their function is taken over by cardiac fibroblasts and coronary endothelium [132,139]. Deletion of the IGF receptor (IGFR) from the myocardium showed that epicardium-derived signals are required to promote compact wall proliferation until E14.5 [132]. IGFR mutants had thin walls until this stage, after which proliferation resumed, indicating that epicardial signals are only required in the early stages of development.

Ieda et al. showed that epicardium-derived CFs are important for sustaining cardiomyocyte proliferation at later embryonic stages through secretion of ECM components and growth factors [140]. Moreover, studies in which epicardial function was not altered, but coronary vessel formation was defective, resulted in hearts with ventricular non-compaction [139]. These findings indicate that factors released from CFs and coronary endothelium are important for sustaining myocardial growth maturation at later developmental stages (Fig 1.11).

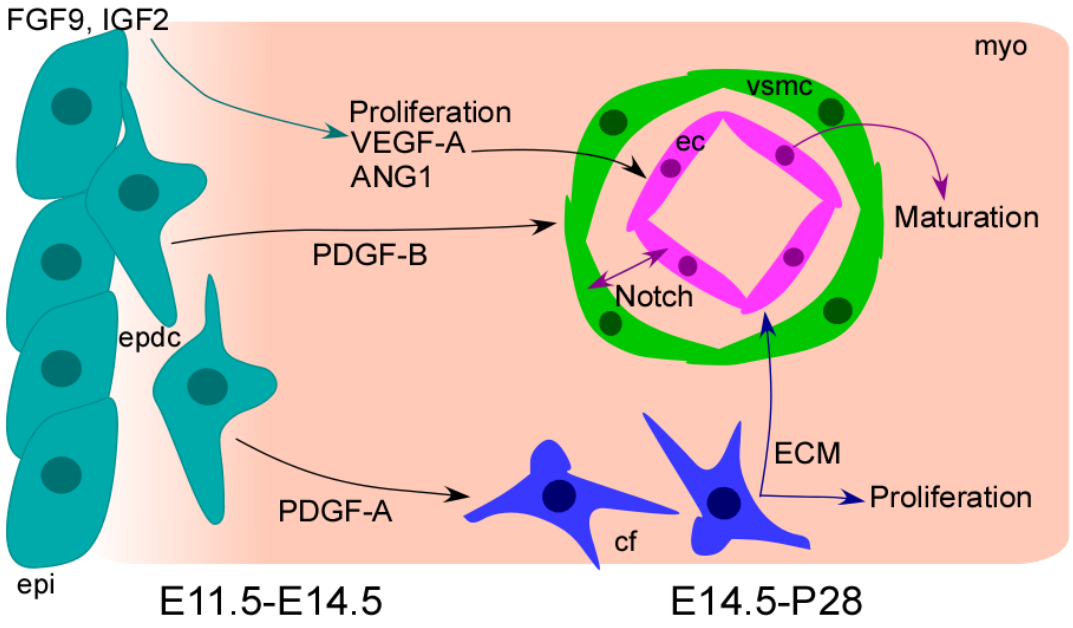


Figure 1.11 Schematic showing the different roles epicardial cells and EPDCs have during heart development

In early development, epicardium secretes mitogenic factors to the myocardium and releases attractants for endothelial cells in the sinus venosus. Later in development, epicardium-derived cells such as cardiac fibroblasts and vascular smooth muscle cells further promote growth of the myocardium and formation of the coronary vessels. epi-epicardium, epdc-epicardium derived cell, vsmc-vascular smooth muscle cell, ec-endothelial cell, cf-cardiac fibroblast. FGF-fibroblast growth factor, IGF2-insulin growth factor, VEGF-vascular endothelial growth factor, PDGF-platelet derived growth factor, ANG-angiopoietin, ECM-extracellular matrix.

1.4 The multiple facets of SRSF3

1.4.1 The role of SRSF3 in RNA processing

Serine/arginine-rich splicing factor 3 (SRSF3) is the smallest member of the serine/arginine rich (SR) family of proteins which have been initially classified as splicing proteins due to their ability to recognise cis-acting elements and promote spliceosome assembly [141–143]. However, further reports that SR proteins also bind intronless mRNA showed they are involved in other aspects of RNA processing unrelated to splicing [144,145].

Even though SR proteins have similar structures, studies that compared their RNA targets found very little overlap, indicating non-redundant roles [144]. Although their targets are largely non-overlapping, SR proteins have low binding specificity and rely on combinatorial control for RNA processing [141,146]. Apart from binding to each other, SR proteins also cross-regulate. For example, SRSF3 modulates expression of itself and of SRSF1 [147,148].

Some SR proteins, including SRSF3, shuttle from the nucleus to the cytoplasm to couple splicing and export [149]. SRSF3 has been implicated in mRNA export through mediating splicing of the exporter protein nuclear RNA export factor 1 (NXF1)/TAP [150] and promoting NXF1 binding to mRNA [144,149]. In agreement with these findings, SRSF3 depletion led to the decreased production of NXF1 and impaired mRNA export.

SRSF3 is also required for expression of chromatin modifiers such as members of the Polycomb repressive complex 2 (PRC2), depletion of SRSF3 being associated with loss of H3K27me3 marks in pluripotent cells and onset of differentiation [150].

Another function of SRSF3 is regulating RNA stability. SRSF3 was shown to promote degradation of intronless genes, such as viral genes, by association with the nuclear exosome targeting complex (NEXT) [151]. SRSF3 can also promote mRNA stability through binding to the 3' untranslated region (3' UTR) of target genes [149,152].

These findings show SRSF3 is a global regulator of RNA processing. Studies that investigated the mechanism through which SRSF3 regulates specific target genes showed SRSF3 uses multiple levels of regulation on the same target [150,153]. (Fig 1.12)

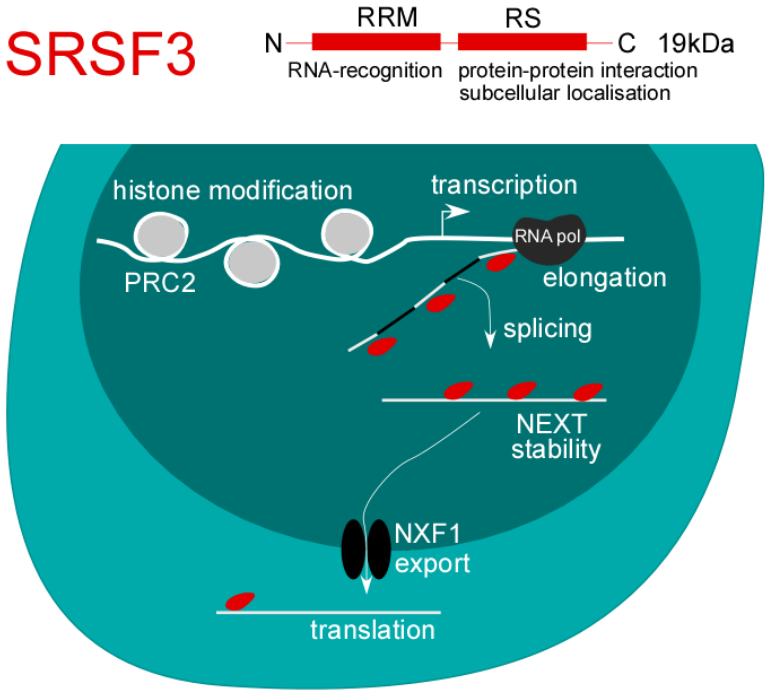


Figure 1.12 The role of SRSF3 in RNA processing

SRSF3 is the smallest member of the SR family of proteins, characterized by the presence of an arginine serine rich domain (RS domain) and an RNA-recognition domain (RRM). SRSF3 mediates production of RNAs through mediating transcription, splicing, export and translation.

1.4.2 SRSF3 as an oncogene

SRSF3 expression is increased in multiple cancers, being involved in proliferation, malignant transformation, survival, genome integrity and metabolism [147,154–160]. The role and targets of SRSF3 in different cancers are summarised in Table 1.4.

Table 1.4 The role of SRSF3 in cancer cell lines

Cancer line	SRSF3 function	SRSF3 targets	Ref
Colorectal cancer HCT116 cells	G1/S progression Survival	*CCND1, CCND3* *E2F1* *HIPK2*	[155]
Ovarian cancer A2780, IGROV1, SKOV3	Cell growth Survival	*INSR* *TAU*	[161]
Osteosarcoma U2OS	Cell growth Cell cytoskeleton	*KIF23, TGFβ2, ANXA1, MAP4, SRSF1 etc.*	[154]
Triple-negative breast cancer MDA-MB231	Cell proliferation Cell polarity	*PAR3, NUMB*	[156]
Cervical cancer, Renal cell carcinoma, Osteosarcoma 33A, HeLa, CaSki, 786-O, U2OS	G2/M progression Survival Malignant transformation	*FOXM1* *CDC25* *PLK1*	[162]
Liver cancer, Cervical cancer, Non-small cell lung cancer PLC/PRF/5, HepG2, HeLa, H35	Genome stability Cell growth	*SRSF3* *CDCA5*	[147]
Breast cancer SKBR3	Malignant transformation	*HER2*	[163]
Oral squamous cell carcinoma FaDu	Malignant transformation	*SNAI2, CHD2*	[157]
Glioblastoma U87	Cell proliferation Malignant transformation	*ETV1, NDE1*	[159]
Colorectal cancer HCT8, Colo205, HCT116	EMT	*MAP4K4*	[160]
Colorectal cancer DLD-1	Metabolic switch Survival	*PKM2*	[164]

1.4.3 SRSF3 in embryonic development

Oocytes that lack SRSF3 have an altered transcriptome that prevents them from entering mitosis [165]. Zygotes that lack SRSF3 die after maternal mRNA is depleted, when they reach morula stage [166]. *In vitro*, SRSF3 is required to maintain induced-pluripotent stemness through mediating Nanog production [150].

Later developmental transitions are also dependent on SRSF3. The pluripotent P19 cell line requires SRSF3 for expression of neural identity genes and differentiation to the neural lineage in response to stimuli [167]. SRSF3 is needed for hepatocyte maturation and liver development *in vivo,* through mediating production of genes involved in metabolism [168]. Interestingly, only 26% of all altered genes in SRSF3-depleted livers were direct targets of SRSF3, further supporting a role for SRSF3 in mediating production of other important regulators of RNA processing.

SRSF3 is also required during heart development. SRSF3 cardiomyocyte-specific knockout embryos have impaired myocardial proliferation, and therefore do not progress through mid-gestation. Induction of SRSF3 deletion in adult cardiomyocytes results in heart failure and death of mice within one week, due to impaired production of sarcomeric proteins as a result of mRNA instability [152]. Other SR proteins are also required for heart development and function, but at later stages, being involved in production of calcium handling proteins (Table 1.5).

Table 1.5 Phenotype of cardiac-specific SR protein mutants

Protein	Viability	Phenotype	Target genes	Ref
SRSF1	6-8 weeks	Hypercontractility	*CamKIIδ*	[169]
SRSF2	viable	Dilated cardiomyopathy	*RyR2*	[170]
SRSF3	E12.5	Impaired proliferation	*mTOR*	[152]
SRSF10	E15.5	Contraction defects	*Triadin*	[171]

1.5 DPhil project

1.5.1 Rationale

As previously mentioned in this introduction, Tβ4 has crucial roles in the epicardium during heart development, being required for activation of epicardial genes through recruitment of the chromatin remodeler BRG1 at epicardial loci such as *Wt1, Tcf21* and *Tbx18* [125]. Loss of Tβ4 from developing hearts resulted in impaired production of EPDCs, defective coronary vessels and myocardial non-compaction [12].

The adult epicardium is quiescent, however, following myocardial infarction (MI) the developmental programme is re-activated [10]. Tβ4 knockout mice failed to re-activate the developmental epicardial programme post-MI, which resulted in a worse outcome [172]. In contrast, delivery of exogenous Tβ4 before MI enhanced reactivation of the epicardium, promoted EPDC production and led to increased neovascularisation and better cardiomyocyte survival [173,174]. Intriguingly, Tβ4 treatment resulted in EPDC differentiation to cardiomyocytes, albeit with very low efficiency [173].

Even though multiple roles have been assigned to Tβ4 [174–177], the mechanism through which Tβ4 modulates EPDC production and cell fate determination remain unknown.

Following a yeast two-hybrid screen, SRSF3 was identified as an interactor of Tβ4, which was further confirmed by co-immunoprecipitation using E11.5 embryonic lysate (unpublished data). SRSF3 has been previously implicated in developmental transitions [166–168], therefore, Tβ4 might regulate certain aspects of epicardial function through SRSF3.

1.5.2 Hypothesis

We hypothesize that changes in RNA processing governed by SRSF3 play a critical role in epicardial activity during development, influencing different aspects of epicardial function, including proliferation, EMT and cell fate decision.

1.5.3 Aims

The following experimental objectives were used to test the hypothesis:

- Characterise SRSF3 expression during heart development
- Investigate if SRSF3 is needed for epicardial layer formation
- Determine if SRSF3 is required for epicardial EMT
- Explore a role of SRSF3 in EPDC cell fate choice

1.5.4 Methodology

The floxed *Srsf3* mouse line[166] was crossed with two epicardial Cre strains; the constitutive *Tg(Gata5-Cre)* [82] to address the proepicardial role of SRSF3 and the inducible *Wt1*^{CreERT2} [65] to investigate epicardial SRSF3 function. These studies were complemented by *in vitro* assays in a mouse epicardial cell line [178]. Single-cell RNA-sequencing was further used to determine molecular mechanisms of SRSF3 function.

Chapter II.

Materials & Methods

2.1 Animal husbandry

2.1.1 Mouse lines

All transgenic mice used in this study were on a C57/BL6 genetic background and are presented in Table 2.1. Conditional targeting of SRSF3 was achieved by crossing epicardial Cre lines with mice that had exons 2 and 3 of *Srsf3* flanked by loxP sites. The targeted lineages were traced with tdTomato. For embryonic studies, 12-20 week old mice were paired overnight (O/N). Females were checked the next morning for the presence of a mating plug. The day the mating plug was observed was designated as E0.5. The animals were housed in the BSB (biomedical services building) and the procedures carried out were approved by the University of Oxford Animal Welfare and Ethical Review Boards in accordance with Animals (Scientific Procedures) Act 1986 (Home Office, United Kingdom) under PPL 30/3450 and 30/3155.

Table 2.1. Transgenic mouse lines

Allele	Integration	Integration site	Reference
Tg(GATA5-cre)^{1Krc}	*Cre*	Random integration	82
Wt1$^{tm2(cre/ERT2)Wtp}$	*CreERT2*	*Wt1* exon1	126
Srsf3^{tm1Pjln}	*loxP*	*Srsf3* exon2/3	166
Gt(ROSA)26Sor$^{tm14(CAG-tdTomato)Hze}$	*tdTomato*	*Rosa26* locus	179
Gt(ROSA)26Sor$^{(Fucci2)Sia}$	*Fucci2*	*Rosa26* locus	180
Tmsb4x^{tm1Prri}	*deletion*	*Tmsb4x* exon2	181

2.1.2 Genotyping

The presence of the modified alleles was detected using the primers described in Tables 2.2 and the PCR programes presented in Table 2.3.

Table 2.2 Primers used for genotyping

Allele	Forward primer (5'->3')	Reverse primer (5'->3')
Wt1$^{tm2(cre/ERT2)}$	AGGAGCGGAGAACCGTC	TCTTGCGAACCTCATCACTC
Tg(Gata5-Cre)	GTGGGCTGGTGACTGGGTG	ACCGGCAAACGGACAGAAG
Srsf3^{tm1}	GCGCAGGTACTTGAGAGA	CCCTTTTATTGGTCAGTGA
tdTomato	CTGTTCCTGTACGGCATGG AAGGGAGCTGCAGTGGAGTA	GGCATTAAAGCAGCGTATCC CCGAAAATCTGTGGGAAGTC
mCherry	GCTTCAAGGTGCACATGGAG	CATGAACTGAGGGGACAGGA
Venus	ATGGTGAGCAAGGGCGAGGAG	CTTGTACAGCTCGTCCATGCCG

Table 2.3 PCR programes used for genotyping

Allele	Initial denaturation	No. of cycles	Cycles			Final extension
			Denaturation	Annealing	Extension	
Wt1$^{tm2(cre/ERT2)}$	94°C 2'	X35	94°C 50''	60°C 50''	72°C 75''	72°C 5'
Tg(Gata5-Cre)	94°C 3'	X30	94°C 30''	60°C 30''	72°C 60''	72°C 1'
Srsf3^{tm1}	94°C 3'	X37	94°C 30''	56°C 45''	72°C 30''	72°C 7'
tdTomato	94°C 5'	X35	94°C 30''	61°C 30''	72°C 30''	72°C 7'
mCherry/Venus	96°C 2'	X35	96°C 30''	65°C 30''	72°C 30''	72°C 5'

2.1.3 Tamoxifen induction

Tamoxifen powder (Sigma #T5648) was prepared in peanut oil (Sigma) with 10% ethanol at a final concentration of 10 mg/ml. Pregnant females were oral gavaged with either 80 mg/kg once or 40mg/kg twice, on two separate days, as described.

2.2 Primary cell culture

2.2.1 Explant culture

PEO explants

Proepicardia were dissected as previously described [111]. The dissections were facilitated by visualisation of proepicardia using tdTomato fluorescence. Proepicardial explants were cultured on 1% w/v gelatine (Sigma #G1393) coated coverslips in DMEM GlutaMax (Gibco #61965059) with 15% fetal bovine serum (FBS) (Gibco #11550356) and 1% penicillin-streptomycin (P/S) (Gibco #15140122) at 37°C for 3 days.

Epicardial explants

Embryonic epicardial explants were obtained as previously described [96]. Briefly, the heart was cut into two pieces, corresponding to each ventricle. The ventricular explants were cultured in DMEM GlutaMax with 15% FBS and 1% P/S for 3 days at 37°C on coverslips coated with 1% w/v gelatine (Sigma #G1393).

2.2.2 Explant treatment

4-Hydroxytamoxifen

Wt1^{CreERT2}*; Rosa26*^{tdTomato} explants were cultured as described above, with the addition of 1 μM 4-hydroxytamoxifen (4-OHT) (ToCris #3412) to the media at the time of plating.

Cell cycle inhibitors

For the cell cycle inhibitor treatment, epicardial explants were cultured as described above, with the addition of 10 μM either PD 0332991 isethionate (Sigma #PZ0199) or 1μg/ml Aphidicolin (Millipore #178273) to the culture media at the time of plating.

2.3 Cell culture

2.3.1 RNA interference

For the small interfering RNA (siRNA) treatment, a mouse epicardial cell line was used. The production and maintenance of this cell line was previously described [178]. Briefly, cell growth was maintained in Immorto medium consisting of DMEM GlutaMax, 10% FBS, 1% P/S, 0.1% interferon gamma (INFγ) (ThermoFischer #PHC4033) and 1X Insulin-Transferrin-Selenium (ITS) (ThermoFischer #41400045) at 33°C. The cells were seeded O/N in Immorto media, then transfected with 40 nM of siRNA for 48h at 33°C using Lipofectamine RNAiMAX Transfection Procedure (Life Technologies #13778-100), according to the manufacturers' instructions. The following siRNAs were used: s73613 and s73615 against SRSF3 (Life Technologies, pre-designed silencers) and silencer siRNA negative control (Life Technologies #4390843).

2.3.2 Induction of EMT & differentiation

Epithelial-to-mesenchymal transition

For EMT induction, cells were plated O/N in 24 well plates, 35 000 cells/well for siControl and 50 000 cells/well for siSRSF3 wells. The cells were transfected as described above, followed by treatment with 10 ng/ml TGFβ1 (Peprotech #100-21C) and 20 ng/ml PDGF-DD (R&D #1159-SB-025) in DMEM Glutamax 10% FBS with 1x ITS for 24h at 37°C.

Vascular smooth muscle cell differentiation

For vSMC differentiation, cells were plated O/N in 24 well plates, 20 000 cells/well for siControl (Ctrl) and 30 000 cells/well for siSRSF3. The cells were transfected as described above, followed by treatment with 10 µg/ml TGFβ1 and 20 ng/ml PDGF-DD in 10% FBS with 1x ITS for 72h at 37°C.

Cardiac fibroblast differentiation

For differentiation to CFs, cells were plated O/N in 24 well plated, 30 000 cells/well, then treated with 50 ng/ml bFGF (Peprotech # 100-18C) and 20 ng/ml PDGF-AA (Peprotech #100-13A) in DMEM Glutamax with 0.5% FBS, 0.1X ITS, 1% P/S for at least 6 days at 37°C.

Endothelial cell differentiation

For endothelial cell differentiation, cells were plated O/N in 24 well plates, 30 000 cells/well, then cultured in endothelial growth medium 2 (EGM-2) (Lonza #CC-4176) with 100 ng/ml VEGF-A (R&D #494-VE-005) for at least 6 days at 37°C.

2.3.3 Inhibition of cell cycle

For cell cycle inhibition, cells were plated O/N 100 000 cells/well in 24 well plates. The cells were treated for 24 h with 2.5 µg/ml Aphidicolin or for 48 h 10 µM PD0332991 isethionate. For EMT induction, 10 ng/ml TGFβ and 20 ng/ml PDGF-DD was added together with Aphidicolin, or after 24h for PD 0332991 isethionate.

2.4 Molecular Techniques

2.4.1 DNA extraction and genotyping

Embryo

The tails were collected from dissected embryos and digested with the REDExtract-N-Amp™ Tissue PCR Kit extract kit (Sigma) as per manufacturers' instructions.

Adult

Ear clips were collected from 2-week-old mice and digested using 5 µl of 10 mg/ml Proteinase K (Sigma #2308) in 100 µl Tail lysis buffer (100mM Tris-HCl pH 8.5, 5mM EDTA, 0.2% SDS, 200mM NaCl) for 2 h at 56°C, followed by 10 min incubation at 95°C. For the PCR reaction, 2 µL of the lysate was added to PCR beads (GD Healthcare), according to manufacturers' instructions, together with 0.5 µM of primer.

2.4.2 Reverse-transcription quantitative PCR (RT-qPCR)

RNA extraction

RNA was extracted using RNeasy Purification Kits, as per manufacturers' instructions, as follows: the RNeasy Micro kit (Qiagen #74034) for the mouse epicardial cell line and the RNeasy Mini kit (Qiagen #74134) for mouse embryonic hearts, which had been frozen in liquid nitrogen.

cDNA preparation

Following extraction, RNA was converted to cDNA using the High-Capacity cDNA Reverse Transcription Kit (ThermoFisher Scientific #4368814). Viia 7 Real-Time PCR System was used to run the PCR reaction which contained 1X Fast SYBR™ Green Master Mix (ThermoFisher Scientific #4385612), 2 ng/µL of cDNA and 0.2 µM primer. All reactions were run in duplicate under the following program: 95°C for 15 minutes, 40 cycles of 95°C for 15 seconds and 60°C for 1 minute. *Hprt, βactin* and *Gapdh* were used as housekeeping genes as determined as most stable after testing a panel of housekeeping genes. The average of the housekeeping CT values was subtracted from the CT value of each gene, followed by subtraction of the normalised CT value of the control sample and conversion to linear scale by 2^-ΔΔCT to obtain relative expression [182]. All the primers used are summarised in table 2.4.

Table 2.4 Primers used for qPCR

Gene	Forward (5' -> 3')	Reverse (5' -> 3')
Srsf3	GCGCAGGTACTTGAGAGA	ATCGGCTACGAGACCTAGAGA
Srsf3 isoform 2	GATGGAAGAACACTGTGTGGCTG	GAGACATGATGGTGACTCTGCG
Snai1	AGCCCAACTATAGCGAGCTG	CCAGGAGAGAGTCCCAGATGA
Acta2	TCCACGAAACCACCTATAACAGC	CGTTCTGGAGGGGCAATGAT
Cnn1	ACATCATTGGACTGCAGATG	CAAAGATCTGCCGCTTGGTG
Hprt	TCAGTCAACGGGGGACATAAA	GGGGCTGTACTGCTTAACCAG
Gapdh	AGGTCGGTGTGAACGGATTTG	TGTAGACCATGTAGTTGAGGTCA
βactin	CTGTCGAGTCGCGTCCACC	GCTTTGCACATGCCGGAGC

2.4.3 Western Blot

Protein was extracted using RIPA buffer (50 mM Tris-HCl pH 7.4, 1% TritonX, 0.1% SDS, 150 mM NaCl, 2 mM EDTA) with Protease Inhibitors (Sigma #P8340) and Phosphatase Inhibitors (Sigma #P5726). Protein concentration was quantified using Pierce BCA Protein Assay kit (ThermoScientific #23227), then 6 µg of protein was loaded on a 4-20% MiniProtean Gel (BioRad #4561096). The samples were transferred using the Trans-Blot Turbo Transfer Pack (BioRad #1704456), blocked in 8% skimmed milk powder/ TBST (20 mM Tris, pH 7.5, 150mM NaCl, 0.1% Tween 20) for 1h, then incubated in 1:1000 SRSF3 (Abcam #ab73891) and 1:5000 GAPDH (Abcam #ab8245) in blocking buffer (5% skimmed milk powder/TBST) O/N at 4°C, followed by 3 washes of 5 min each in TBST and incubation with HRP-conjugated secondary antibodies, diluted 1:2500 in blocking buffer. The blot was rinsed 3 times for 5 min in TBST, then the samples were detected using ECL™ Western Blotting Detection Reagent (Sigma #GERPN2209).

2.5 Imaging

2.5.1 Cryosections

Embryos younger than E11.5 were fixed intact, whereas hearts were dissected from later stages embryos. All samples were fixed for 2h with 4% paraformaldehyde (PFA)/ phosphate-buffered saline (PBS) at room temperature (RT). The tissue was washed with PBS twice, equilibrated O/N at 4°C in 30% sucrose/PBS, then gradually immersed in Tissue-Tek OCT by incubation in 50:50 30% sucrose/PBS:OCT, followed by 100% OCT. Samples were stored at -80°C, then cryosectioned in 8-12 µm thick sections and collected on Super Frost Plus slides (VWR).

2.5.2 Immunohistochemistry (IHC)

Cryosections were rehydrated in PBS, permeabilised with 0.5% Triton X-100 in PBS for 15 mins, then blocked for 1 h at RT using 1% bovine serum albumin (BSA) and 10% donkey serum diluted in 0.1% Triton X-100 in PBS (PBST). Primary antibodies diluted in blocking buffer were added and left O/N at 4°C (Table 2.5). Sections were washed with PBST, then secondary antibody solutions diluted 1:200 in blocking buffer were added and left to incubate for 1 hour, RT, followed by three washes with PBST, 5 min/wash and 5 min incubation with 4',6-diamidino-2-phenylindole (DAPI) nuclear stain. The slides were mounted in Vectashield (Vector Laboratories #H-1000).

2.5.3 Whole mount antibody staining

Embryonic hearts were placed in 4% PFA in 1.5 ml tubes after dissection, then left O/N at 4˚C on a rotator. In between each of the following steps, hearts were washed three times in PBST (0.1% triton), 15 min/wash on the rotator. Hearts were blocked with 5% goat serum in PBST for 1h. An antibody against PECAM-1, 1:500 dilution in PBST with 1%BSA, was added O/N at 4˚C. Hearts were incubated in biotinylated secondary antibody (Goat

Anti-Armenian hamster Biotin #ab5744) 1:250 dilution in PBST for 1h. Avidin-biotin horseradish peroxidase complex (ABC Elite #Vector PK-4000) 1:50 in PBS was added for 30 min. Hearts were placed in DAB substrate (Vector peroxidase substrate kit #SK-4100). When vessels were visible, the reaction was stopped by rinsing the hearts with ddH2O. The hearts were imaged on a stereo microscope.

Table 2.5 List of antibodies used

Antibody	Company	Catalogue No.	Species	Dilution
WT1	Abcam	Ab89901	Rabbit	1:100
SRSF3	Abcam Millipore	Ab73891 MABE116	Rabbit Mouse	1:200 1:100, ICC
αSMA	Sigma	C6198	Mouse	1:200
SM-MHC	Abcam	Ab125884	Rabbit	1:250
Vimentin	Abcam	Ab89901	Rabbit	1:100
PECAM1	Abcam	Ab119341	Ar. Hamster	1:100
Ki67	eBioscience	Ab569882	Rat	1:100
CC3	Cell Signaling	9664	Rabbit	1:100
PHH3	Santa Cruz	Sc-8656	Rabbit	1:100
α-s-actinin	Abcam	Ab9465	Mouse	1:100
Cyclin D1	Abcam	Ab16663	Rabbit	1:100
Endomucin	Santa Cruz	Sc-65495	Rat	1:100
βcatenin	Abcam	Ab32572	Rabbit	1:100
Calponin 1	Abcam	Ab46794	Rabbit	1:200
SOX17	R&D	AF1924	Goat	1:50
GLUT1	Abcam	Ab40084	Rabbit	1:100
NG2	Abcam	Ab129051	Rabbit	1:100
SM22α	Abcam	A14106	Rabbit	1:100
PDCD4	Cell Signalling	9535	Rabbit	1:50

2.5.4 Immunocytochemistry

The coverslips were fixed for 10 minutes with 4% PFA, then permeabilised for 10 min with PBST. The antibody staining was performed as described above for IHC.

2.5.5 RNAscope

RNAscope is an *in-situ* hybridization technique commercially available from Advanced Cell Diagnostics. The RNAscope Multiplex Fluorescent Reagent Kit v2 assay was used according to manufacturers' instructions, except for the target retrieval time which was decreased to 10 min and the Protease Plus digestion which was done at RT. TSA plus fluorophores (PerkinElmer, NEL753001KT, NEL745E001KT) were added at 1:500 dilution for Fluorescein, 1:1000 for Cy3 and 1:1500 for Cy5. The RNAscope probes used are summarised in table 2.6.

Table 2.6 RNAscope probes used

Probe	Catalogue No.
Wt1	432711
Sema3D	488111
Tcf21	508661
Tbx18	515221
Scx	439981
tdTomato	317041
Vegfc	429701
dapB (negative control)	320878

2.5.6 Microscopy

The samples were imaged using a Leica DM6000 fluorescence microscope or Olympus Fluoview-1000 confocal microscope and processed using Fiji. Nuclei were counted using the automated particle analysis in Fiji, whereas other staining was counted manually using the cell counting plug-in.

2.6 Flow cytometry

2.6.1 Tissue dissociation

Embryonic hearts were digested using the Neonatal Heart Dissociation Kit (#130-098-373) and the gentleMACS Octo Dissociator with heaters (#130-096-427) from Milteny Biotec, according to the manufacturers' instructions.

2.6.2 Cell cycle analysis

Cells were fixed in BD CellFix (BD #340181) RT for 20 min, permeabilised in Perm Buffer (eBioscience #00-8333-56), then incubated with primary antibody Ki67-FITC conjugated (eBioscience #11-5698-82) for 0.5 h on ice. The samples were washed with Perm Buffer, resuspended in PBS, then incubated in FxCycle (ThermoFisher #10347) 1:1000 final concentration for 0.5 h on ice in the dark. Cells were stored in IC fixation buffer (ThermoFisher #00-8222-49) until acquisition.

2.6.3 PrimeFlow staining protocol

After dissociation, cells were stained with the Zombie Aqua Fixable Viability Kit (Biolegend #423101) for 0.5 h at RT, 1:1000 dilution, followed by incubation for 5 min on ice with 1:50 TruStain FcX (anti-mouse CD16/32) antibody (Biolegend #101319), then stained with BV421 or BV605 conjugated rat anti-CD31 antibody (Biolegend #102423, #102427) for 0.5 h on ice, 1:50 dilution. Fixation and permeablisation was performed as instructed in the PrimeFlow RNA Assay Kit from ThermoFisher Scientific (#88-18005). Intracellular staining was done using BV421 mouse anti-cardiac troponin T antibody (BD Bioscieces #565618) for 0.5 h on ice, 1:200 dilution. The subsequent hybridisation steps were performed as per manufacturers' instructions. The probes used are summarised in Table 2.7.

Table 2.7 PrimeFlow probes used

PrimeFlow Probe	Catalogue No.
Scx	VB1-3028071-PF
Tbx18	VB4-3113124-PF
Tcf21	VB6-3197774-PF
Sema3d	VB1-3044712-PF
Wt1	VB4-13886-PF
Npr3	VB1-3031000-PF
Dpt	VB1-3034260-PF
Rgs5	VB4-3116783-PF
DapB (negative control)	VF1-11712-PF, VF6-10407-PF VF4-10408-PF
Actb (positive control)	VB6-12823-PF, VB1-10350-PF VB4-10432-PF

2.6.4 Acquisition

All samples were processed on BD LSRFORTESSA X-20 cytometer and analysed using FlowJo software. Geometric mean fluorescence intensity (gMFI) was calculated by extracting fluorescence minus one value (FMO) gMFI from the gMFI of the sample.

2.7 Single-cell RNA-sequencing

2.7.1 E 10.5 analysis

The E10.5 transcriptome data was downloaded from Expression Omnibus (GSM3027035) [183] as TPM (transcript per kilobase million) values. These values were log10 transformed and processed with the Seurat pipeline [184,185] in R (http://www.R-project.org/). Cells were classified into identity clusters using principal component analysis (PCA). The tSNE (t-Distributed Stochastic Neighbor Embedding) method was used to plot the clusters in 2D [186].

2.7.2 E 15.5 SMART-Seq2

Ventricles of E15.5 hearts were dissected below the valves and dissociated as described above. Six *Wt1*^{CreERT2}*; Rosa26*^{tdTomato} hearts were used for the control sample and four *Wt1*^{CreERT2}*; Srsf3*$^{fl/fl}$*; Rosa26*^{tdTomato} hearts for the mutant sample. Cells were sorted for tdTomato fluorescence using BD FACSAria III, then processed according to the SMART-Seq2 (Switching Mechanism At the end of the 5′-end of the RNA Transcript sequencing) protocol [187]. Briefly, tagmentation, library preparation and sequencing were performed using the Nextera XT DNA Library Prep kit and the NextSeq 500/550 High Output Kit v2 (75 cycles) 400 million reads (Illumina, #FC-404-2005) on Illumina NextSeq 500 platform. The bcl files were converted to FastQ with bcl2fastq (Illumina, v.2.19.1.403). Samples that had a lower number of reads than empty wells were eliminated from the analysis. The remaining reads were trimmed and aligned to the mouse genome (GRCm38/Mm10) using STAR (v.2.3.3a) with Gencode (v.M16) annotations. Splice junctions were combined after the first alignment, then junctions that were non-canonical or covered by less than 10 reads were removed before the second alignment.

Seurat 2 [188] was used to process the samples. Genes with less than 200 reads and genes not expressed in at least 3 cells were discarded. Cells were filtered for less than 5% mitochondrial content and less than 10 000 expressed genes to remove doublets. Reads were normalized for depth, then scaled. Cell cycle scores (G2M and S) were calculated using G2/M and S phase genes [189]. The score difference between the G2M and S was removed using the alternative cell cycle regression Seurat vignette. The data was imported from Seurat into Monocle2 for performing semi-supervised pseudotime analysis as described in the Monocle2 pipeline [190].

2.7.3 E 13.5 and E 17.5 10X Chromium

Whole hearts from E 13.5 and E 17.5 embryos were dissociated as described above, then processed using the Chromium Single Cell 3' Reagent Kit (v3 chemistry) (10x Genomics #PN-1000092) as indicated by manufacturers' instructions. The samples were sequenced in three rounds using the NextSeq® 500/550 High Output Kit v2 (150 cycles) 400 million reads (8000 cells) (Illumina #FC-404-200) on the Illumina NextSeq 500 platform. The reads were processed using CellRanger (10x Genomics), then analysed with Loupe (10x Genomics), or analysed in Seurat 3 as described above. Cells with more than 20% mitochondrial reads and more than 7000 genes were removed from the analysis. UMAP (Uniform Manifold Approximation and Projection) was used to visualise samples with large number of clusters [191]. For clusters subsets, tSNE was used instead. For E 13.5 three control hearts and two *Wt1*^{CreERT2}*; Srsf3*$^{fl/fl}$*; Rosa26*^{tdTomato} hearts were used, whereas one control heart and two *Wt1*^{CreERT2}*; Srsf3*$^{fl/fl}$*; Rosa26*^{tdTomato} hearts were used for E17.5.

2.8 Statistical Analysis

The statistical analysis was performed in GraphPad Prism 5 software. An unpaired, two tailed t-test was used for comparing two experimental groups, including Welch's correction if the variances differed significantly. For more than two groups, one-way ANOVA was used with Tukey's multiple comparisons post-hoc test. For comparing cell composition in single-cell RNA-sequencing data, chi-squared test was used. The P value used to determine statistical significance is shown in corresponding figure legend.

Chapter III.

SRSF3 is required for epicardium formation

3.1 Background

3.1.1 Proepicardial cell migration

The epicardial layer originates from the proepicardial organ (PEO), a transient embryonic structure located at the venous pole of the developing heart [192]. The proepicardial cells use multiple strategies to migrate onto the heart. Until recently, the migration strategy was thought to be species-specific, with avian PEO shown to project villi to the heart surface [106,108], whereas mammalian proepicardial cells were reported to form free-floating vesicles that contact the heart and coalesce to form the epicardial layer [105,111]. However, multiple studies have challenged this species-dependent mode of migration and reported that, in addition to vesicle release, mouse proepicardial cells are able to project villi, directly contact the heart and migrate alongside the inflow tract [193,194] (Fig 3.1).

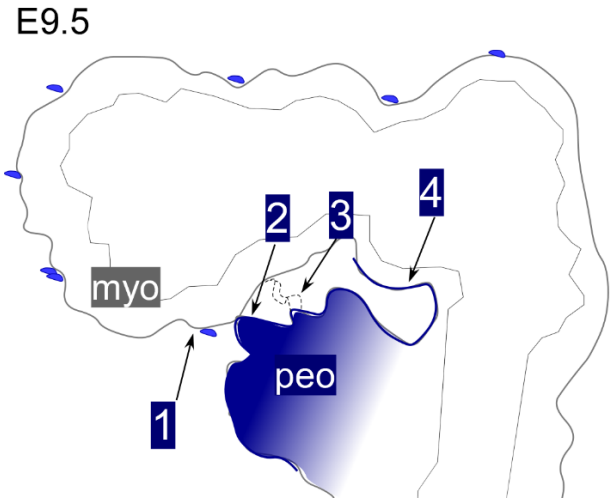


Figure 3.1 Schematic of migration strategies used by proepicardial cells

Proepicardial cells use multiple ways to contact the heart surface: 1-vesicle formation, 2-direct contact, 3-villi formation and extracellular matrix bridge, 4-direct migration on the inflow tract. peo-proepicardial organ, myo-myocardium

Even though these studies showed proepicardial cells use several mechanisms to reach the heart in the same species, the mechanism by which these different modes of migration are deployed remains to be determined. Interestingly, cell division control protein 42 (CDC42) mutants, that have defective PEO villi and vesicle formation, seem to increase the number of proepicardial cells that directly contact the heart [194]. This suggests that different modes of PEO migration are dependent on distinct molecular mechanisms to confer robustness, since proper formation of the epicardium is a crucial process in heart development. Failure of proepicardial cells to reach the heart leads to embryonic lethality by embryonic day (E)15.5 in mouse, due to secondary defects in cardiomyocyte proliferation and coronary vessel formation [116,195,196].

3.1.2 The role of proliferation in epicardium formation

Another important process involved in epicardium formation is cellular proliferation. Collective cell migration and proliferation have been linked in a number of biological systems, from cultured cells [197] to gastrulation [198], where proliferation was shown to be an important factor in controlling tension, velocity and coordination of migration. Recently, it was shown that PEO cluster emergence in zebrafish is also dependent on tension generated through regionalised proliferation of mesodermal progenitors [104].

The importance of cell division in the epicardium has also been highlighted, where orientation of the mitotic spindle was reported to dictate which cells remained on the surface versus which cells invaded the myocardium [114]. The peak of epicardial proliferation was at E11.5 in embryonic mice, where all cells underwent planar division to form the epicardial layer. Later in development, epicardial cells started dividing perpendicular to the heart plane, which promoted myocardial invasion. This showed cell proliferation is not only required for the completion and maintenance of the epicardial layer, but also for epicardial cell invasion into the myocardium.

3.1.3 SRSF3 in heart development

The RNA-binding SRSF3 is the smallest member of the SR family of proteins, labeled as an oncogene due to its role in promoting cellular proliferation and migration in multiple cancers [155,157,158,199–201]. SRSF3 is known to be required for multiple processes associated with progression through the cell cycle, both G1/S [155,201] and G2/M transition [162].

Recently, SRSF3 was shown to be required for cardiomyocyte proliferation during embryonic development, with conditional deletion of SRSF3 in NKX2.5 or myosin heavy chain α (αMHC) expressing cells resulting in embryonic lethality [152]. The role of SRSF3 in the formation of the epicardium has not been previously investigated.

3.1.4 Aims

The aims of this chapter were to study the expression and distribution of SRSF3 during heart development and determine if SRSF3 is implicated in epicardium formation.

3.2 Results

3.2.1 Characterisation of SRSF3 expression during development

First, the expression pattern of SRSF3 during heart development was investigated by IHC on embryonic sections and RT-qPCR (Fig 3.2). SRSF3 was expressed throughout the developing heart in all cell types. The highest levels of SRSF3 were found in the PEO and in the early epicardium (E9.5 - E11.5), after which SRSF3 production started to decrease until postnatal stages, where SRSF3 levels were very low (Appendix Fig 3.1).

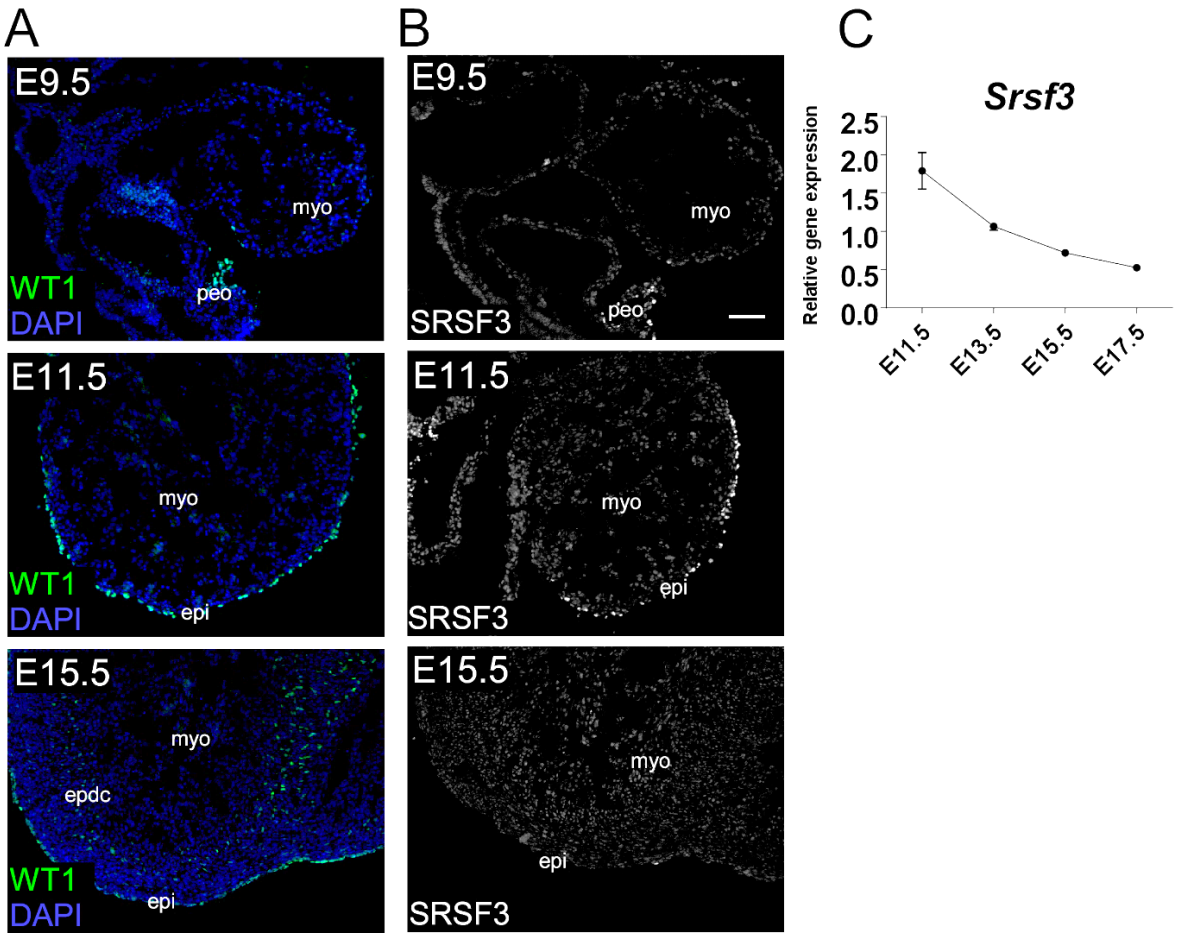


Figure 3.2 SRSF3 is expressed in the developing heart

(A) *Immunostaining for WT1 and* ***(B)*** *SRSF3 on heart cryosections from E9.5, E11.5 and E15.5 mouse embryos (additional stages shown in Appendix Fig 3.1), shows SRSF3 expression is high in PEO and early epicardium. myo-myocardium; peo-proepicardial organ; epi-epicardium; epdc-epicardium-derived cell. n>4. Scale bar: 100 μm.* ***(C)*** *qPCR for Srsf3 on whole heart RNA extracts confirms a decrease in Srsf3 expression between E11.5, E13.5, E15.5 and E17.5 embryos (n=5).*

Since the master regulator of epicardial identity, WT1 [196], was shown to modulate production of SRSF3 [202], expression of SRSF3 was also investigated in WT1 null embryos. SRSF3 levels were also checked in Tβ4 null embryos since previous work in the group showed SRSF3 interacts with Tβ4. No difference was found in SRSF3 levels between control embryos and embryos that lacked either Tβ4 or WT1 (Appendix Fig 3.2).

3.2.2 *Tg(Gata5-Cre); Srsf3$^{fl/fl}$* mutants are embryonic lethal

Targeting SRSF3 in the murine PEO

To investigate what role SRSF3 plays in the PEO, the Gata5-Cre was used to specifically target SRSF3 deletion to the PEO using the Cre/loxP system. Genetic targeting systems such as the Cre/loxP allow conditional deletion of a gene of interest through placing the expression of Cre recombinase under the control of an enhancer or a promoter that is specific to a certain population of cells [203].

The Gata5-Cre uses a chick enhancer of *Gata5* that becomes active at E9.25 in mouse and drives Cre recombinase expression in the PEO [82]. This Cre line was crossed to a modified *Srsf3* line where *Srsf3* had exon 2 and 3 flanked by loxP sites [166]. Upon Cre expression, the loxP sites are recombined, resulting in a mutant *Srsf3* mRNA that contains an in-frame deletion of exon 2 and 3. Exons 2 and 3 encode the RNA-recognition motif (RRM), leading to the production of a non-functional SRSF3 protein. The tdTomato fluorescence was used to identify targeted cells (Fig 3.3). The tdTomato reporter [179] has the tdTomato gene preceded by a STOP cassette flanked by loxP sites, which is removed by the Cre recombinase.

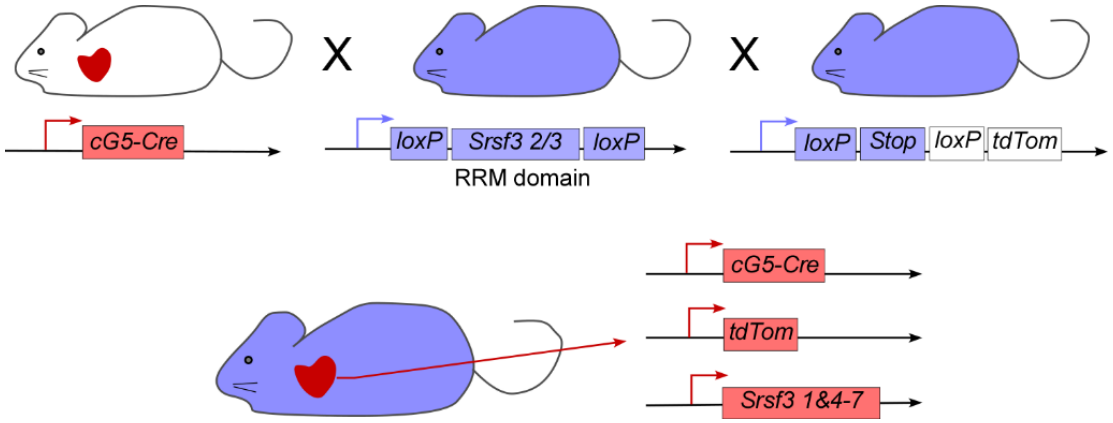


Figure 3.3 Breeding strategy used to generate conditional *Srsf3* deletion mice

Tg(Gata5-Cre) mice were bred with mice that had exons 2 and 3 of the Srsf3 gene flanked by loxP sites and with mice that had the tdTomato gene inserted in the Rosa26 locus, preceded by a STOP codon, flanked by loxP sites. Exons 2 and 3 of the Srsf3 gene constitute the RNA-recognition domain (RRM).

First, the specificity of the Gata5-Cre was investigated with the use of the tdTomato reporter (Fig 3.4). As previously reported, the Cre was active in PEO cells at E9.5, but expression was also found in the pericardium, the septum transversum (ST) and in a subset of cardiomyocytes, showing recombination is not confined to the PEO. At later embryonic stages, tdTomato was found in the epicardium, in some of the right ventricle cardiomyocytes and widespread in the cardiomyocytes of the left ventricle.

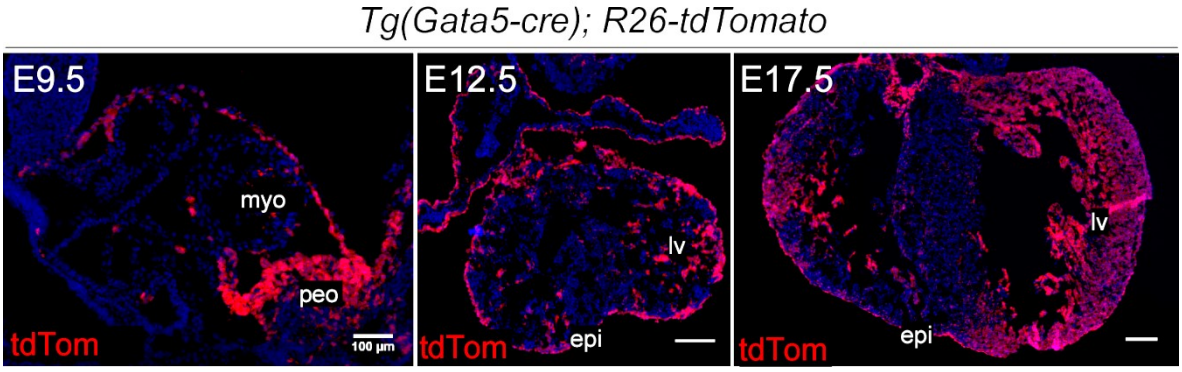


Figure 3.4 *Tg(Gata5-Cre)* lineage tracing with tdTomato

Fluorescence of tdTomato shows Cre activity driven by a chick enhancer of Gata5 and its lineage. The tdTomato is expressed in the PEO, pericardium, epicardium and a subset of cardiomyocytes. myo-myocardium; peo-proepicardial organ; epi-epicardium; lv-left ventricle. Scale bar: 100 µm. Images representative of n>3.

Since floxed alleles are reported to have different recombination efficiencies, either due to the length of the floxed region or due to chromatin complexity, the presence of the tdTomato might not necessarily reflect loss of SRSF3 [204–207] .To determine the efficiency of *Srsf3* targeting, immunocytochemistry was performed on epicardial explants from mutant embryos (Fig 3.5). Even though none of the available SRSF3 antibodies target the RRM domain, which is removed by the Cre recombinase, the removal of the RRM domain reduces the stability of the *Srsf3* mRNA, leading to decreased SRSF3 production by 70% [168], therefore, cells that lost SRSF3 could still be identified through antibody staining in culture.

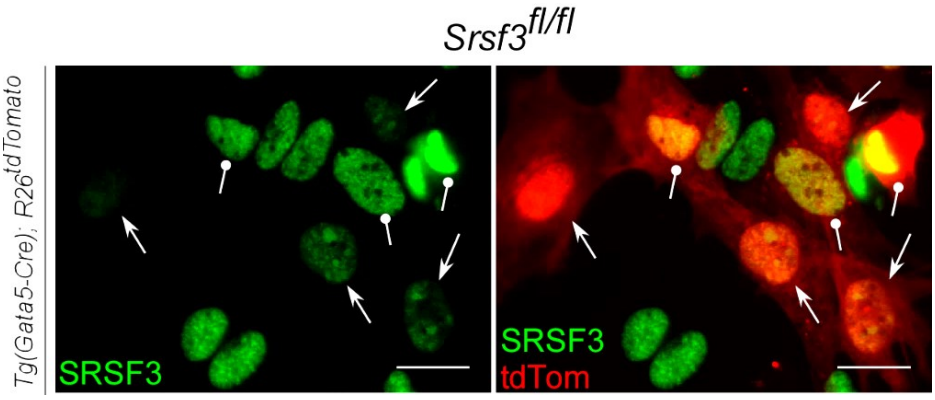


Figure 3.5 SRSF3 is downregulated in targeted cells

Immunocytochemistry for SRSF3 on E11.5 epicardial explants reveals SRSF3 production is reduced in targeted cells (arrows). TdTomato fluorescence does not fully overlap with SRSF3 reduction (dots). n=6. Scale bar: 20 μm. Representative images of N=8.

SRSF3 production was decreased in targeted cells and no longer localized in nuclear speckles, where splicing proteins are normally found [144], instead it was accumulated in structures that resembled nucleoli (Fig 3.5, arrows). However, the expression of tdTomato did not fully overlap with SRSF3 reduction, indicating the recombination of the *Rosa26* locus is more efficient than that of *Srsf3*.

The expression of SRSF3 was also investigated in embryos heterozygous for the floxed *Srsf3* allele. The heterozygous embryos did not show a reduction in *Srsf3* levels, however, the production of an alternative isoform of *Srsf3* that contains exon 4 was decreased (Appendix Fig 3.3). SRSF3 auto-regulates its levels by inclusion of exon 4 [148], which contains a premature STOP codon and it is not present in the predominant isoform of *Srsf3.* The decrease in production of *Srsf3* mRNA inclusive of exon 4 in heterozygotes indicates compensation of SRSF3 levels by auto-regulation.

Tg (Gata5-Cre); Srsf3$^{fl/fl}$ mutants die mid-gestation

No *Tg(Gata5-Cre); Srsf3* homozygous (*Srsf3$^{fl/fl}$*) mutants were born or recovered alive past E12.5 (Table 3.1). Expected Mendelian ratios could not be calculated due to the fact that *Tg(Gata5-Cre)* is a transgene randomly inserted in the genome, however, the number of heterozygotes should be similar to the number of homozygotes from *Srsf3$^{fl/fl}$* x *Srsf3$^{fl/+}$; Tg(Gata5-Cre)* crosses. The number of homozygotes and heterozygotes was similar in litters obtained before E12.5. After this stage, fewer to no homozygous embryos were recovered and none of them was alive at the time of dissection (Table 3.1), indicating mid-gestation lethality.

Table 3.1. Survival of *Tg(Gata5-Cre); Srsf3$^{fl/fl}$* embryos

Stage	Cre negative	Cre positive		Litters
		Het	Hom	
E11.5	28	12	13	9
E12.5	11	5	3+1 dead	2
E13.5	9	11	2 dead	3
Born	10	6	0	4

Het-heterozygote, Hom-homozygote

Genetic targeting of SRSF3 results in cardiomyocyte defects

Tg(Gata5-Cre); Srsf3$^{fl/fl}$ embryos presented gross morphological abnormalities of the heart such as dilated atria and hypoplastic ventricles (Fig 3.6 A). Since the ventricles were smaller, cell death and proliferation were investigated by IHC. There was increased cell death in mutant hearts as indicated by cleaved-caspase 3 (CC3) staining as early as E10.5 in targeted cardiomyocytes, as shown by the presence of tdTomato (Fig 3.6 B). Deceased mutant embryos dissected at E13.5 had widespread presence of CC3 in the left ventricle, where tdTomato is highly expressed (Fig.3.6 C).

Quantification of the number of cells expressing CC3 was done at E12.5, the last stage viable embryos were recovered (Fig 3.6 D, E). Cell proliferation was also quantified based on the presence of phospho-histone H3 (pHH3), a mitotic marker (Fig 3.6 D, E). There was significantly more apoptosis and less proliferation in mutant hearts (Fig 3.6 E). The cells expressing CC3 were positive for sarcomeric-α-actinin (s-α-actinin), indicating that SRSF3 is only required for cardiomyocyte survival (Fig 3.6 D). The tdTomato cells that showed lower levels of pHH3 were a mixture of both cardiomyocytes and epicardial cells, suggesting that SRSF3 is required for the proliferation of both cell types (Fig 3.6 D).

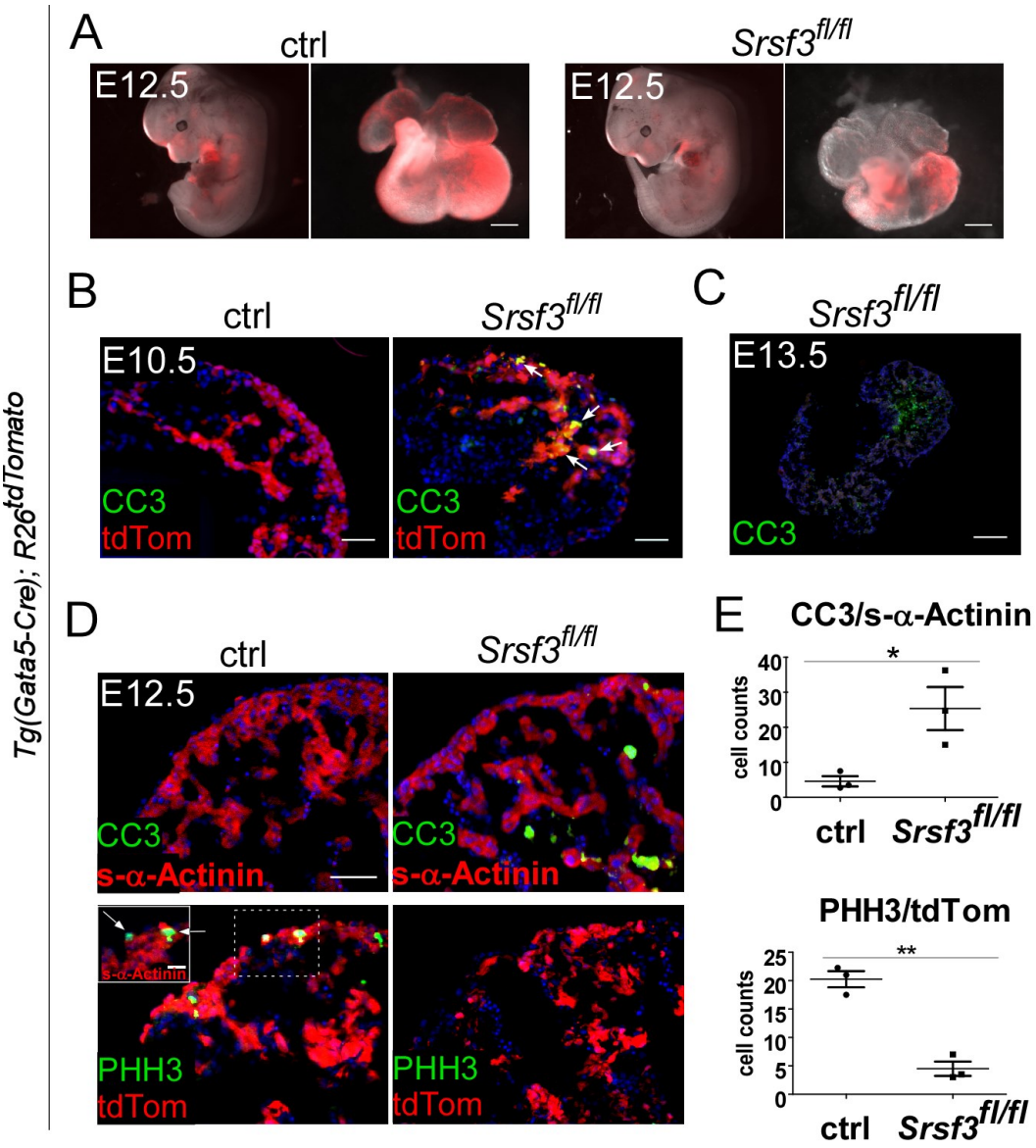


Figure 3.6 Increased cell death and decreased proliferation in *Srsf3* mutants

(A) *Fluorescence stereo microscope images of control and Srsf3 mutant embryos positive for tdTomato and their dissected hearts at E12.5 reveal morphological defects. n=3. Scale bar: 500 µm.* ***(B)*** *Immunohistochemistry for cleaved-caspase 3 (CC3) in Srsf3$^{fl/fl}$ mutants indicates increased apoptosis of tdTomato+ cardiomyocytes starting E10.5. n=1.Scale bar: 50 µm.* ***(C)*** *CC3 staining of E13.5 mutant embryo heart shows widespread apoptosis. n=1. Scale bar: 200 µm* ***(D)*** *Immunostaining for CC3/s-α-actinin and phospho-histone H3 (pHH3) on E12.5 sections shows apoptosis is increased in targeted cardiomyocytes of mutant hearts, whereas proliferation is decreased in both epicardium and cardiomyocytes (arrows, insert, scale bar: 20 µm). Scale bar: 50 µm.* ***(E)*** *Cell counts from stained E12.5 sections of control and mutant hearts for CC3/s-α-actinin and pHH3. Data presented as mean +/- SEM. P<0.01(**), P<0.05(*), student's t-test. n=3, 4 sections per embryo.*

SRSF3 loss leads to impaired formation of the epicardial layer

Because this study was focused on epicardial biology, future steps were aimed at understanding how the epicardium is affected in mutant hearts.

Due to the lower number of proliferating epicardial cells detected in mutants, WT1 immunostaining was used to investigate epicardial formation in both control and *Tg(Gata5-Cre); Srsf3*$^{fl/fl}$ E12.5 hearts (Fig 3.7 A). There were significantly fewer WT1+ cells on the surface of mutant hearts compared to controls (Fig 3.7 B). The proportion of epicardial cells positive for tdTomato was also significantly decreased in mutants: 50.05 % (SEM ± 6.358) vs 88.71 % (SEM ± 0.4276) in controls (Fig 3.7 C), suggesting non-targeted cells are either more proliferative or more likely to reach the heart.

Next, epicardial explants from both control and mutant hearts were cultured to assess growth. The mutant explants were significantly smaller (Fig 3.7 D, E, F, G). Mutant ventricular explants were more affected than atrial explants, however, the proportion of tdTomato+ cells as compared to controls, was significantly lower in both (Fig 3.7 E, G). The percentage of cells positive for tdTomato in controls was 92.17 % (SEM ± 1.349) for ventricular explants and 80.16% (SEM ± 2.451) for atrial explants , whereas mutants had only 25.56 % (SEM ± 4.558) tdTom+ cells in ventricular explants and 17.21 % (SEM ± 3.054) in atrial explants, indicating mutant cells either fail to migrate or expand. The lower tdTomato percentage in control atria, as compared to ventricle, suggests that atrial epicardium is either less likely to be targeted by the Gata5-Cre or atrial explants are contaminated with other cells, such as sinus venosus, that do not express this Cre.

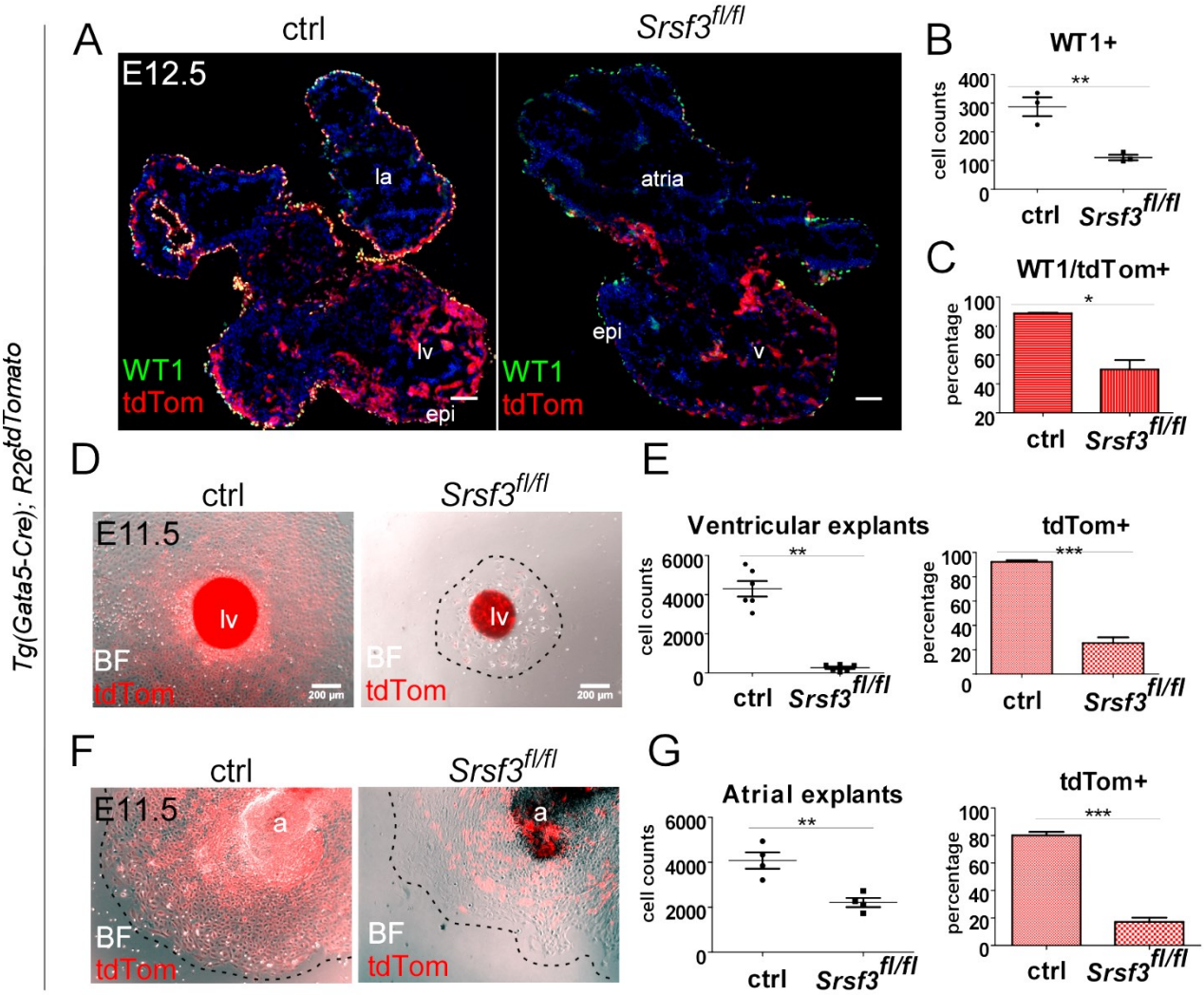


Figure 3.7 Epicardium formation is impaired in *Tg(Gata5-Cre); Srsf3$^{fl/fl}$* embryos

(A) *Immunostaining for WT1 was performed on heart sections from E12.5 mouse embryos from both control and Gata5$^{Tg(Cre)+}$; SRSF3$^{fl/fl}$ mutants. Scale bar: 100 µm.* ***(B)*** *Quantification of WT1+ cells from whole sections. n=3, 4 sections/heart. Data shown as mean +/- SEM, p value < 0.01 (**), student's t-test.* ***(C)*** *The percentage of tdTomato+ cells of total WT1+ cells was quantified. The mutant hearts had a lower percentage of WT1/tdTomato+ cells. Data shown as mean +/- SEM, p value< 0.05 (*), t-test with Welch's correction.* ***(D)*** *Brightfield and red fluorescence images of day 3 ventricular explants. lv-left ventricle, Scale bar: 200 µm.* ***(E)*** *Quantification of total cell number and tdTomato+ percentage in control and mutant E11.5 day 3 ventricular explants shows a significant decrease in the mutants, n=6. Data shown as mean+/- SEM, t-test with Welch's correction. p<0.01 (**), p<0.001 (***).* ***(F)*** *Brightfield and red fluorescence images of day 3 atria explants from control and mutant hearts. a-atria.* ***(G)*** *Quantification of total cell number and tdTomato+ cells in E11.5 day 3 atria. n=4. Data shown as mean+/- SEM, t-test with Welch's correction. p<0.01 (**), p<0.001 (***).*

Since most epicardial cells in mutants were not tdTomato positive, and therefore not targeted by the Cre, an investigation into the migration of PEO cells was performed.

By E10.5, proepicardial migration is almost complete [195], therefore, immunostaining for WT1 at E10.5 was used to assess if PEO cells migrated onto the heart in *Tg(Gata5-Cre); Srsf3$^{fl/fl}$* mutants. Very few WT1+ cells were found on the surface of mutant hearts, whereas control hearts were covered in WT1+ epicardial cells (Fig 3.8 A). Interestingly, in mutant hearts, only the dorsal side was covered by WT1+ cells, with very few WT1+ cells present on the ventral surface (Fig 3.8 A arrow). This indicated PEO cells fail to properly migrate onto the heart in *Tg(Gata5-Cre); Srsf3$^{fl/fl}$* mutants.

The formation of PEO villi and release of PEO vesicles are dependent on extracellular matrix (ECM) components such as fibronectin [105,108,194]. To investigate the cause of failed migration, the mesenchymal marker vimentin and the ECM marker fibronectin were analysed. There was no obvious difference in the expression of vimentin, however, the levels of fibronectin were reduced in mutant proepicardia (Fig 3.8 B). To confirm this result, fibronectin staining was also performed on PEO explants from both control and mutants. The PEO was dissected out, guided by tdTomato fluorescence (Fig 3.8 C dotted box). Mutant explants had fewer cells and deposition of fibronectin filaments was disrupted (Fig 3.8 D). Interestingly, all cells in mutant explants showed decreased fibronectin, even though very few were tdTomato+. This indicated the failure to deposit fibronectin in mutant PEO is not a direct effect of losing SRSF3.

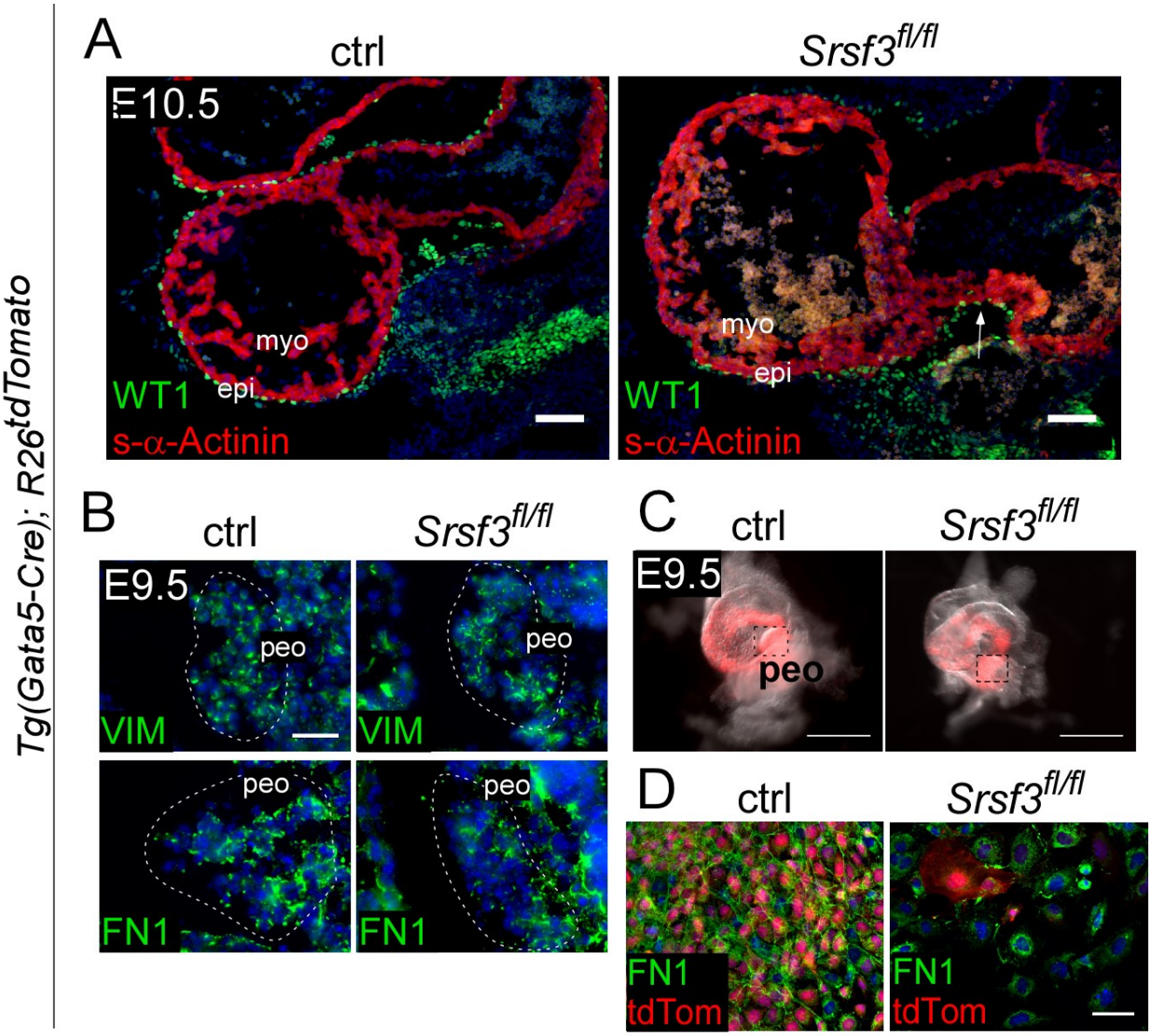


Figure 3.8 Proepicardial cells fail to reach the heart in *Tg(Gata5-Cre); Srsf3$^{fl/fl}$* mutants

(A) *Immunostaining for WT1 and sarcomeric-α-actinin on both control and mutant E10.5 sagittal sections reveal proepicardial cells fail to migrate onto the heart surface in the mutants. epi-epicardium, myo-myocardium. n=2. Scale bar: 100 μm.* ***(B)*** *Immunostaining for vimentin (VIM) and fibronectin (FN1) on E9.5 sagittal sections of control and mutant embryos show no difference in vimentin, but a decrease in fibronectin in the mutant PEO. peo-proepicardial organ. Scale bar: 20 μm. n=3.* ***(C)*** *Fluorescence stereo microscope images of dissected hearts and proepicardia. Dashed box indicates the tissue used for proepicardial explants. Scale bar: 1 mm.* ***(D)*** *PEO explants from both control and mutant hearts immunostained for FN1 reveal reduced deposition of FN1 in the mutant. n=2 control, n=1 mutant. Scale bar: 50 μm*

3.2.3 SRSF3 is required for PEO proliferation

In addition to lack of fibronectin deposition, co-imaging of tdTomato and WT1 revealed that, similar to mutant epicardium, fewer WT1 cells were tdTomato+ in mutant PEO as compared to controls (Fig 3.9 A). This indicated the number of targeted cells is reduced in mutant, therefore, proliferation and apoptosis were assessed by Ki67 and CC3 IHC. Ki67 staining was decreased in the PEO region in mutants, indicating impaired proliferation (Fig 3.9 B). No increase in apoptosis was observed in mutant PEO (Fig 3.9 C).

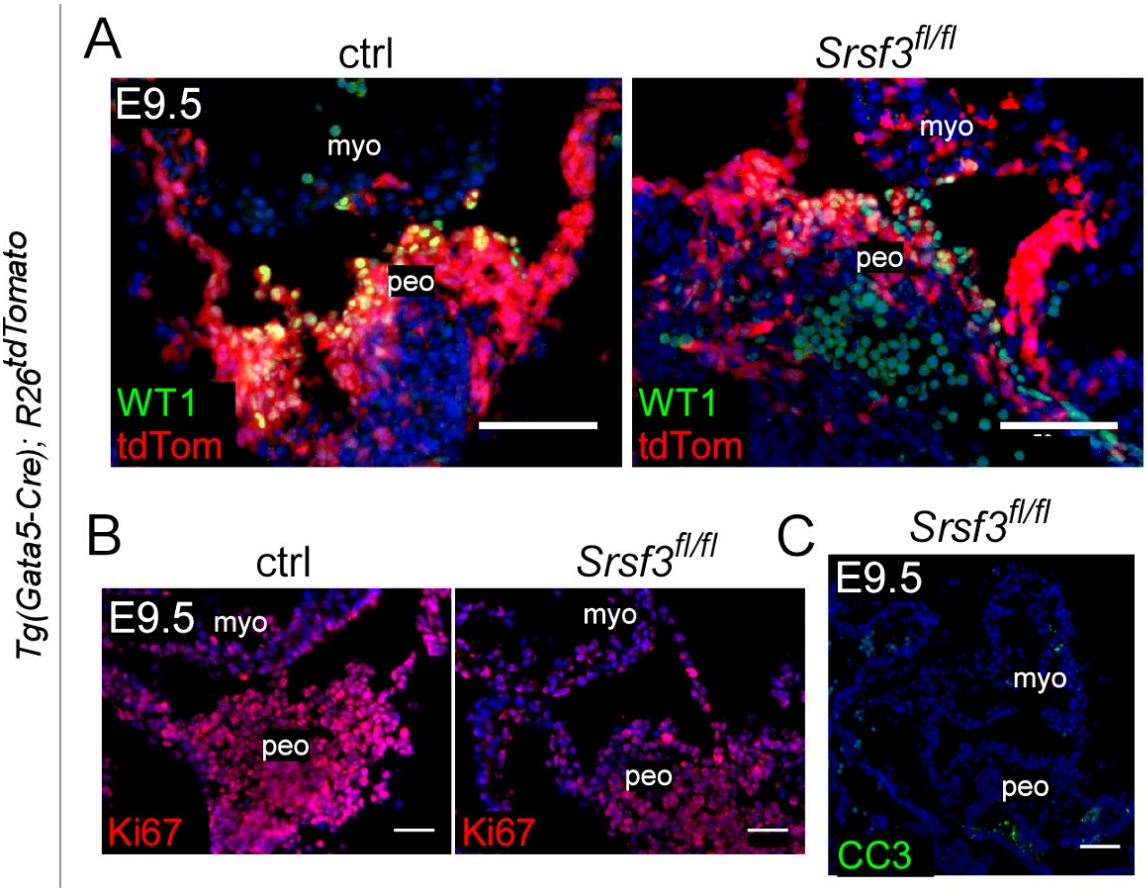


Figure 3.9 SRSF3 loss in the PEO leads to defective proliferation

(A) *Immunofluorescence for WT1 on E9.5 sagittal sections reveals a decrease in the number of proepicardial cells positive for tdTomato in Tg(Gata5-Cre); Srsf3$^{fl/fl}$ mutants. n=3. Scale bar: 50 μm.* ***(B)*** *Staining for Ki67 reveals a decrease in proliferation in the mutants. n=3. Scale bar: 50 μm.* ***(C)*** *No increase in apoptosis is observed in mutant PEO, as shown by immunostaining for CC3. n=2. Scale bar: 100 μm.*

The size of the PEO is difficult to assess in sagittal sections, since the captured area varies in different anatomical regions. To assess if the PEO was smaller in mutants, and to confirm a defect in proliferation, proepicardial explants were assessed. As expected, mutant proepicardial explants were significantly smaller than the controls (Fig 3.10 A, B) and had fewer tdTomato+Ki67+ cells.

Programmed cell death 4 (PDCD4), a protein involved in cellular proliferation, apoptosis and translation, is a known target of SRSF3. [153,208,209]. Co-immunostaining for PDCD4 and SRSF3 on mutant proepicardial explants confirmed this protein is upregulated and translocated to the cytoplasm when SRSF3 is lost (Fig 3.10 C).

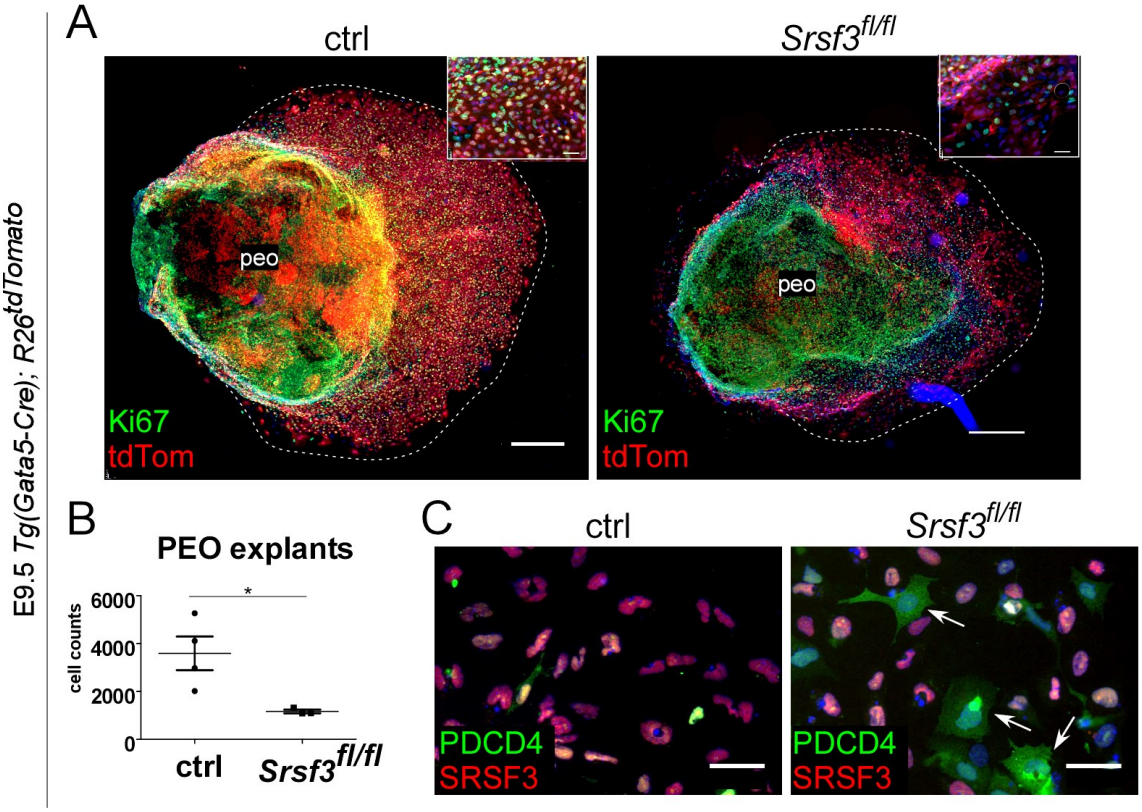


Figure 3.10 Decreased proliferation in *Tg(Gata5-Cre); Srsf3$^{fl/fl}$* proepicardial explants

(A) *Immunostaining for Ki67 and tdTomato reveals less proliferation in E9.5 proepicardial mutant explants. Scale bar: 500 μm. n=2. Close-up scale bar: 50 μm.* ***(B)*** *Quantification of the number of cells present in control and mutant proepicardial explants. n=4 controls, 3 mutants, p<0.05(*), student t-test with Welch's correction.* ***(C)*** *Immunostaining for PDCD4 and SRSF3 reveals cytoplasmic localization of PDCD4 in SRSF3 depleted cells (arrows). n=2. Scale bar: 50 μm.*

3.2.4 SRSF3 is involved in epicardial cell proliferation

SRSF3 is required for epicardial explant growth

Due to defects in PEO proliferation and migration, *Tg(Gata5-Cre); Srsf3*$^{fl/fl}$ mutants did not form an epicardium. The decreased pHH3 staining observed in the few mutant epicardial cells suggested SRSF3 is also needed for epicardial proliferation. Unfortunately, the number of epicardial cells was too small to analyse the proliferation defect in detail and the use of mutant epicardial explants proved unhelpful since most cells were non-targeted.

To enable the recovery of a larger number of SRSF3 depleted epicardial cells, another strategy was pursued. Instead of the constitutive Gata5-Cre, the inducible *Wt1*^{CreERT2} line was used. The Wt1-CreERT2 is not active until tamoxifen is delivered, making it possible to restrict SRSF3 deletion to a specific temporal window (Fig 3.11).

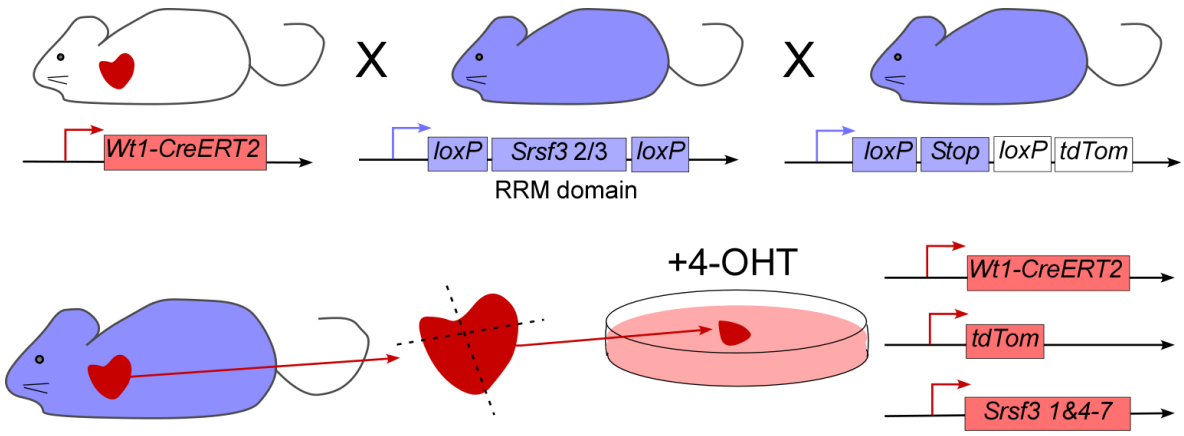


Figure 3.11 Strategy used to induce SRSF3 deletion in epicardial explants

Wt1^{CreERT2} *mice were bred with mice that had Srsf3 exons 2 and 3 flanked by loxP sites and with tdTomato reporter mice. Srsf3 exons 2/3 constitute the RNA-recognition domain (RRM). Embryonic hearts were dissected and cut into four pieces. Ventricular pieces were placed into tissue culture plates that had 4-hydroxytamoxifen (4-OHT) added to the medium. The 4-OHT activated the Cre and induced deletion of regions flanked by the loxP sites.*

To avoid the epicardium formation defects seen *in vivo,* tamoxifen was delivered *in vitro* to epicardial explants from *Wt1*^{CreERT2}*; Srsf3*$^{fl/fl}$ embryos. The rationale was that epicardial explants would be allowed to outgrow, then induced with tamoxifen to assess the consequences of SRSF3 loss. The active form of tamoxifen, 4-OHT, was used to induce recombination *in vitro*. This method of induction has been previously published using the *Wt1*^{CreERT2} allele in spermatogonia explants [210].

First, induction efficiency was optimised using control hearts that had the *Wt1*^{CreERT2} and *Rosa26*^{tdTomato} alleles. The number of cells targeted was highest when 4-OHT was given at the time of plating, whereas delaying addition of 4-OHT until the third day of explant culture decreased the number of cells positive for tdTomato (Fig 3.12). This was due to the spontaneous differentiation of some epicardial cells to smooth muscle cells, as shown by staining for smooth muscle myosin heavy chain (SM-MHC), which no longer express *Wt1*. Surprisingly, differentiation to smooth muscle cells in explants happened as early as 24h post culture (Appendix Fig 3.4), therefore, addition of 4-OHT at the time of plating was required to achieve optimal recombination.

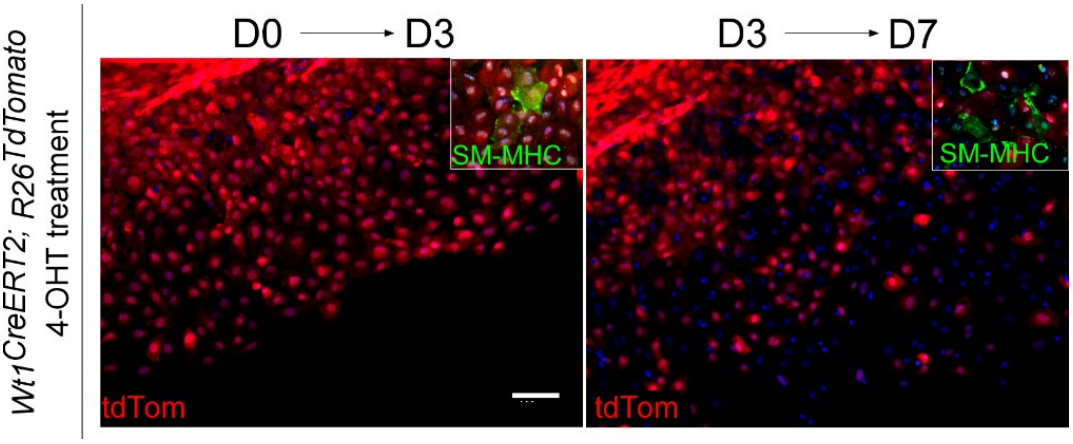


Figure 3.12 Optimisation of 4-OHT delivery *in vitro*

4-OH-Tamoxifen was added either at the time of plating or three days after the explants were put into culture and left for 72h. Recombination efficiency was assessed by the presence of tdTomato. Adding 4-OHT at day 0 (D0) was more efficient than addition at day 3 (D3) due to spontaneous differentiation to smooth muscle cells, as shown by SM-MHC staining. n=2. Scale bar: 100 µm.

4-OHT was added to both control and mutant epicardial explants on the day of culture and explants were left to grow for 72 h. Mutant explants were significantly smaller than controls (Fig 3.13 A, B). Staining for SRSF3 revealed incomplete recombination in mutants and co-staining with Ki67 showed decreased Ki67 staining in recombined cells (Fig 3.13 C), indicating SRSF3 is required for epicardial cell proliferation. Quantification of Ki67+ cells showed that >85% of the proliferating cells still retained had high levels of SRSF3 in *Wt1*^{CreERT2}*; Srsf3*$^{fl/fl}$ explants (Fig 3.13 D).

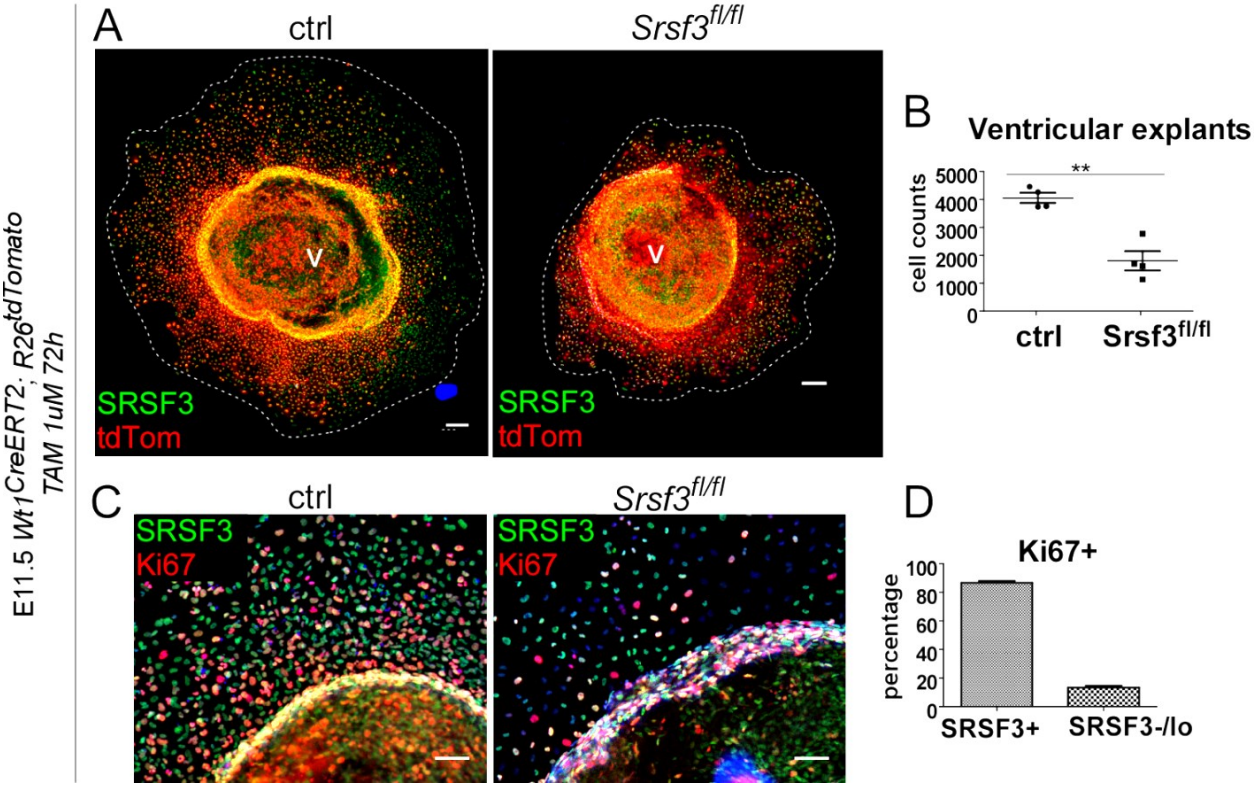


Figure 3.13 *Wt1*^{CreERT2}*; Srsf3*$^{fl/fl}$ explants are less proliferative than controls

(A) *Immunostaining for SRSF3 and tdTomato of both control and Wt1*^{CreERT2}*; Srsf3*$^{fl/fl}$ *explants. Scale bar: 200 µm.* ***(B)*** *Total cell counts of Wt1*^{CreERT2}*; Srsf3*$^{fl/fl}$ *explants are lower than in controls. n=4, student t-test. P<0.01 (**).* ***(C)*** *Immunostaining for SRSF3 and Ki67 reveals decreased levels of Ki67 in the cells that lost SRSF3. Scale bar: 50 µm.* ***(D)*** *The percentage of Ki67 cells that express SRSF3 is higher than those that don't have SRSF3. n=2.*

SRSF3 promotes proliferation in an epicardial cell line

Because the explants obtained from *Wt1*^{CreERT2}*; Srsf3*$^{fl/fl}$ embryos were a mixture of targeted and non-targeted cells, which made analysis of SRSF3-depleted cells difficult, a mouse epicardial cell line was used to test the effects of knocking down SRSF3 using RNA interference. This mouse epicardial line was generated by crossing wild-type mice with Immorto mice that carry an interferon inducible temperature sensitive large T antigen which keeps cells proliferating when cultured at 33°C with IFNγ [211]. Immortalised epicardial cell lines have been extensively used in the field [178,212,213].

Two different siRNAs were used against SRSF3, one siRNA targeted exon 4 and 5 of the predominant isoform of *Srsf3*, whereas the second siRNA targeted exon 2 and therefore, all *Srsf3* isoforms. A siRNA against a non-mouse gene was used as negative siRNA control (siCtrl). Different concentrations and transfection times were tested ranging from 20-80 nM and 24 to 72 h (Appendix Fig 3.5 A, B). Concentrations higher than 40 nM led to very few cells being recovered in the siSRSF3 wells (Appendix Fig 3.5 C), so 40 nM for 48h was chosen as the optimal concentration that resulted in the best knockdown, as shown by RT-qPCR and Western Blot (Appendix Fig 3.5. D, E).

Cells were imaged after 48h of transfection using a brightfield microscope. Fewer cells were recovered in siSRSF3 wells as compared to control wells (Fig 3.14). Because this mouse cell line is sensitive to density fluctuations, with cells becoming more mesenchymal at lower densities (unpublished observation), different concentrations of control cells were compared to match the density of the siSRSF3-treated cells. Starting with ~1/3 fewer cells for control wells led to similar densities at the end of the transfection period (Fig 3.14).

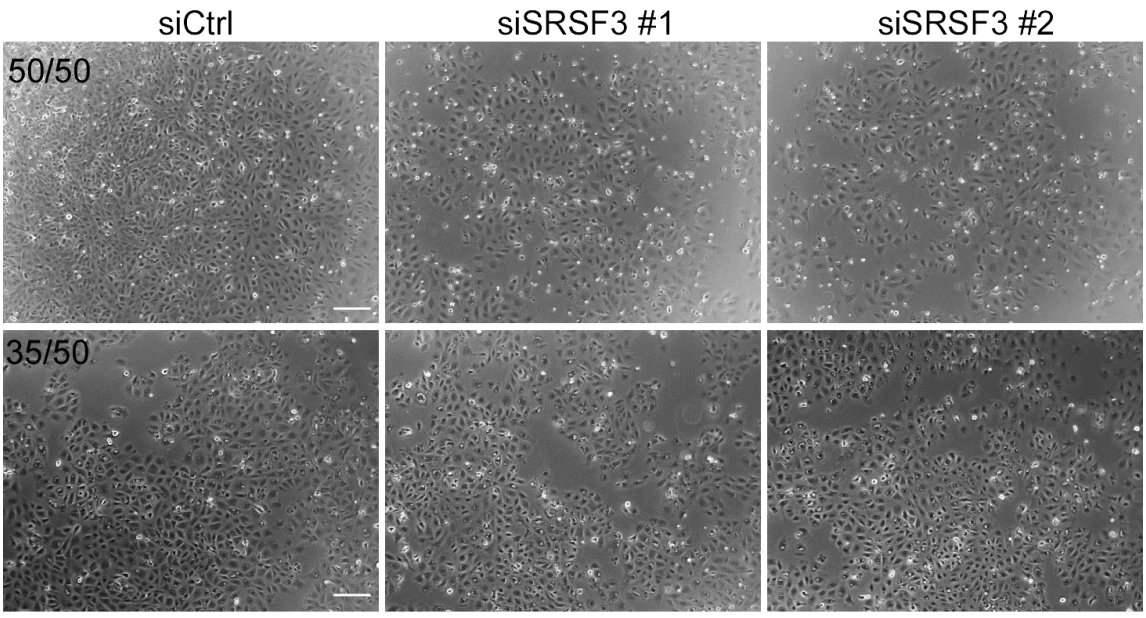


Figure 3.14 Optimisation of plating densities for the siCtrl

A mouse epicardial cell line was transfected with siCtrl and two siRNAs against SRSF3. Starting with the same cell number (50 000 cells/ well in 24 well plate) led to fewer cells being recovered in the siSRSF3 wells, whereas decreasing the starting number of cells in siCtrl wells (35 000/well) led to similar densities being recovered at the end of the 48 h transfection time.

Next, apoptosis and proliferation were tested to explain the lower density of cells in siSRSF3-transfected wells. There was no increase in CC3 (data not shown), however, there were more cells that had detached in siSRSF3 treated wells, which could still reflect increased cell death. Ki67 could not be used to assess proliferation since this immortalised cell line does not undergo quiescence.

Cyclin D1 is a known direct target of SRSF3 [155], therefore, Cyclin D1 levels were tested. There was a severe reduction of Cyclin D1 levels in siSRSF3 transfected wells (Fig 3.15 A, B), suggesting proliferation could be affected and cells might be arrested in G1. Flow cytometry was used to determine cell cycle stage, however, due to the large variation of DAPI content in G1 cells , the G2 stage could not be clearly separated from S (Fig 3.15 C). There was no an increase in the number of cells in G1 in the siSRSF3 cells, raising questions about the involvement of Cyclin D1 in the proliferation of this cell line.

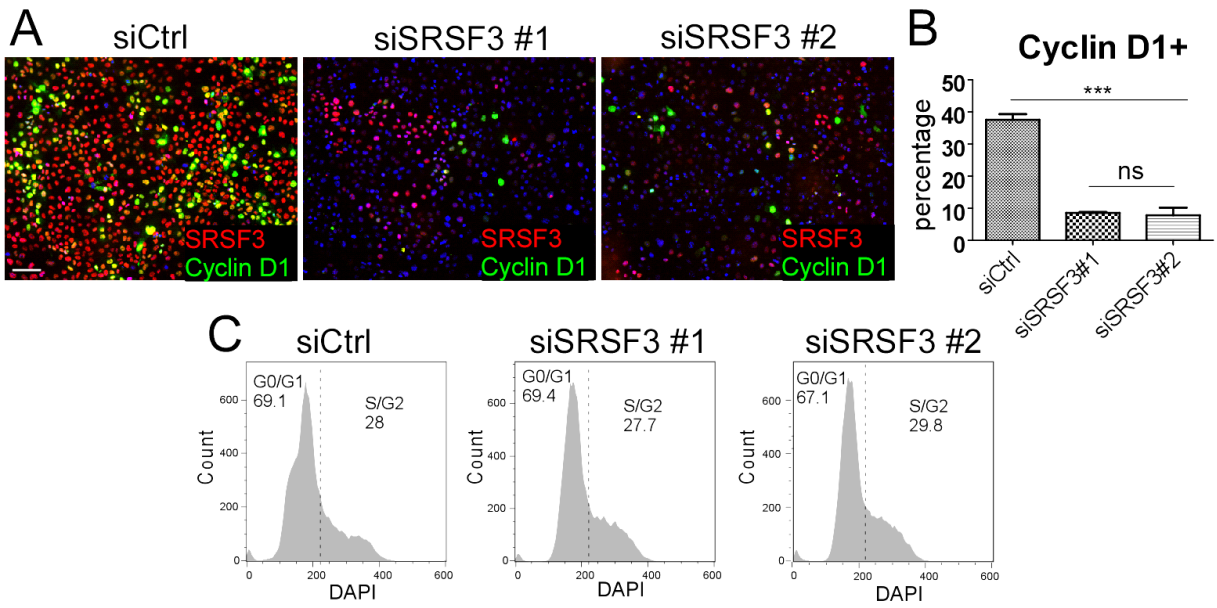


Figure 3.15 Cyclin D1 is decreased in siSRSF3 transfected cells

(A) *Immunostaining for SRSF3 and Cyclin D1 reveals both are decreased in siSRSF3 transfected cells as compared to controls. Scale bar: 100 μm.* ***(B)*** *Quantification of the percentage of cells with high levels of Cyclin D1 in siCtrl and siSRSF3 transfected wells. n=3, 4-5 images/well. Data represented as mean +/- SEM. P<0.0001 (***), one-way Anova with Tukey's post-hoc test.* ***(C)*** *Flow cytometry of siCtrl and siSRSF3 cells stained for DAPI shows the cell nuclei size varies in the G1 phase and that the cells do not have a clear G2 stage n=2.*

Determination of cell cycle stage is problematic in the immortalised epicardial cell line

The large T antigen used to immortalise this epicardial line was reported to complex with Retinoblastoma (RB) to keep cells actively proliferating [214]. Therefore, the Cyclin D1-cyclin-dependent kinases 4/6 (CDK4/6) complex may not be needed for phosphorylation of RB and G1/S progression in these cells, which could explain why there was no increase in the number of cells in G1 in siSRSF3 treated cells even though Cyclin D1 production was reduced. For example, inhibition of CDK4/6 was shown to have no effect on the proliferation of large T antigen immortalised human fibroblasts [215]. However, different studies showed immortalisation happens in a cell-type specific way, with variable dependence on Cyclin D1 [216,217].

To understand more about the cell cycle of this epicardial cell line and determine if the Cyclin D1-CDK4/6 complex is required, well characterized cell cycle inhibitors were used. The activity of CDK4/6 was inhibited with PD0332991 isethionate. A DNA polymerase inhibitor, Aphidicolin, was used to arrest the cells in S phase. The Aphidicolin treatment served as a control for assessing the suitability of the proliferation assays used.

Brightfield images taken after 24 h of cell cycle inhibition revealed reduced cell density in treated wells (Fig 3.16 A). Cells detached *en mass* in treated wells, indicating increased cell death after inhibition with both PD0332991 isethionate or Aphidicolin (Appendix Fig 3.6). Multiple inhibitor concentrations were tested in order to reduce the detachment problem. Decreasing concentration of CDK4/6 inhibitor below 10 μM or Aphidicolin below 2.5 μg/ml was not effective in arresting cell cycle (data not shown), therefore, 10 μM CDK4/6 inhibitor and 2.5 μg/ml Aphidicolin were used in the following assays. The detachment was not observed in vehicle treated controls (water for PD0332991 isethionate and 0.1% DMSO for Aphidicolin).

Flow cytometry was used to determine the cell cycle stage post inhibitor treatment using Ki67 and DAPI (Fig 3.16 B). No cells were found in G0 in either control or treated wells. Nuclear size varied between conditions, likely due to the lower density in treated wells leading to increased cell size. CDK4/6 inhibitor treatment led to no cells undergoing mitosis (M), which was unexpected. As anticipated, Aphidicolin increased the number of cells in S to over 70%. Immunostaining for β-catenin revealed an increase in the number of binucleated cells in wells treated with inhibitors, especially in the case of CDK4/6 inhibition (Fig 3.16 C). Flow cytometry does not distinguish between binucleated cells in G1 and mononucleated cells in G2, adding another drawback to this study.

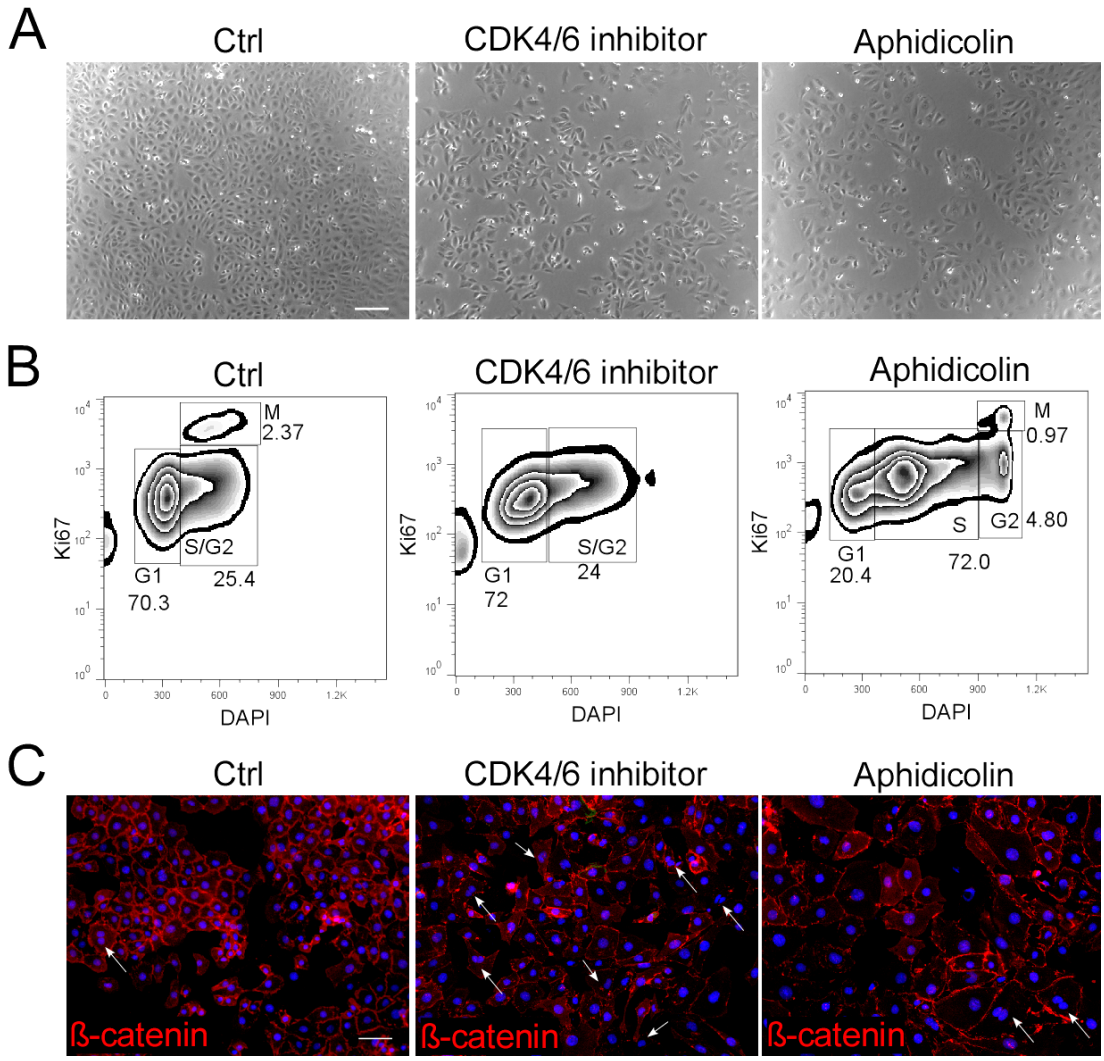


Figure 3.16 The cell cycle is perturbed in the immortalised epicardial cell line

(A) *Brightfield images of control and cell cycle inhibited cells using either CDK4/6 inhibition PD 0332991 isethionate and Aphidicolin shows decreased density and increased cell size in the treatment wells (wells washed pre-imaging to remove dead cells). Scale bar: 100 µm. n=5.* ***(B)*** *Flow cytometry plots of epicardial cells stained for Ki67 and DAPI shows varying cell sizes in treated cells, as compared to controls, no cells in mitosis in the CDK4/6 inhibited cells and an increase in the number of cells in S in the Aphidicolin treated group. n=2.* ***(C)*** *Immunofluorescence of β-catenin on cells treated with cell cycle inhibitors reveals an increase in the number of binucleated cells. n=2. Scale bar: 50 µm.*

These findings indicate that, due to the immortalisation process, the cell cycle is severely perturbed which, together with the varying cell sizes and the presence of binucleation, makes this cell line unsuitable for cell cycle studies.

3.3 Discussion

3.3.1. SRSF3 expression during development

Data presented in this chapter show that SRSF3 expression is widespread in the embryonic heart, with the highest SRSF3 levels detected in the PEO and in the early epicardium (until E12.5). The peak of SRSF3 expression in the epicardium at E11.5 is of significance, because this correlates with published data on epicardial proliferation, where the highest proliferation rate was at E11.5 [114]. SRSF3 levels in the epicardium decrease starting E12.5, correlating with a reduction in epicardial proliferation. SRSF3 expression was also observed in cardiomyocytes. A recent study confirmed SRSF3 is required for the proliferation and survival of both embryonic and adult cardiomyocytes [152] .

3.3.2. *Tg(Gata5-Cre); Srsf3$^{fl/fl}$* mutants are embryonic lethal

To investigate if SRSF3 has a functional role in the embryonic PEO, the Gata5-Cre was used to induce SRSF3 deletion. Unfortunately, expression of the *Tg(Gata5-Cre*) was not restricted to the PEO, as previously reported [82], but was also found in the pericardium and a subset of cardiomyocytes at E9.5. The difference in Cre detection could be due to the higher sensitivity of the tdTomato as compared to the LacZ reporter, which was previously used to characterise Cre expression [82].

Recombination of the *Srsf3* floxed allele was lower than the *Rosa26^{tdTomato}*, however, due to the inability to combine the SRSF3 antibody with other antibodies raised in the same species, tdTomato was often used as a proxy. Moreover, quantification of recombination efficiency could not be calculated since the targeted cells stopped proliferating, whereas the cells that retained SRSF3 continued to expand, especially in the case of explants.

No viable *Tg(Gata5-Cre); Srsf3$^{fl/fl}$* embryos were recovered past E12.5. Mutant embryos had enlarged atria, possibly indicating contractile failure. The ventricles were smaller and widespread apoptosis and reduced proliferation were detected in the cardiomyocytes directly targeted by the Cre. This suggests cell death and loss of proliferation are direct consequences of cardiomyocytes losing SRSF3 and not a downstream effect of misregulated signalling from epicardial cells. This finding confirms other published data, where deletion of SRSF3 using the Nkx2.5-Cre or the αMHC-Cre resulted in embryonic lethality and lack of cardiomyocyte proliferation[152]. Mutant embryos also failed to form an epicardium, however, the early lethality (E12.5) indicates the embryos die due to cardiomyocyte defects. Mutant embryos with defects solely in epicardium formation survive to later stages (~E14.5-16.5), when they usually die due to thinning and non-compaction of the cardiomyocytes and failure of the coronaries to form [116,194].

3.3.3. Fibronectin deposition is decreased in *Tg(Gata5-Cre); Srsf3$^{fl/fl}$* proepicardia

The formation of the epicardium was compromised in *Tg(Gata5-Cre); Srsf3$^{fl/fl}$* mutants. Analysis at E9.5 revealed mutant proepicardia are smaller and fail to deposit fibronectin. The decrease in fibronectin was present in all proepicardial cells, not only in the tdTomato+, indicating it is not a direct consequence of losing SRSF3. Low cell density has been previously associated with decreased fibronectin assembly [218]; thus, the lack of fibronectin deposition could be due to lower cell density in mutant proepicardia.

Fibronectin has been implicated in the proper formation of PEO villi and vesicles[105,108,112], therefore, delamination of cells was expected to be affected in mutants. Analysis of E10.5 *Tg(Gata5-Cre); Srsf3$^{fl/fl}$* mutant hearts revealed few WT1+ cells managed to contact the heart. Of importance, these cells were mainly found on the dorsal side, which remarkably resembled the phenotype of embryos that lack CDC42 [194].

CDC42 mutants fail to form vesicles and villi, but some proepicardial cells migrate through direct contact and along the inflow tract, however, to an insufficient extent, still resulting in epicardium formation defects and embryonic lethality [194]. Proepicardial migration through direct contact and alongside the inflow tract have not been shown to be dependent on fibronectin. Therefore, it can be hypothesized that the proepicardial cells that manage to contact the heart in the *Tg(Gata5-Cre); Srsf3$^{fl/fl}$* transfer via these routes.

3.3.4. SRSF3 is required for PEO proliferation

The *Tg(Gata5-Cre); Srsf3$^{fl/fl}$* mutants had defects in proepicardial cell proliferation both *in vivo* and in explant cultures, which were significantly smaller. Inhibition of proliferation by modulating FGF signalling previously resulted in smaller PEO explants, showing proliferation is an important determinant of explant size [219].

The decrease in proliferation seemed to be confined to tdTomato+ cells, indicating it is a direct consequence of SRSF3 loss. The increased production and cytoplasmic redistribution of the tumour suppressor PDCD4 observed in proepicardial cells that lost SRSF3 might indicate arrest in proliferation due to this protein.

Other studies focused on proteins implicated in PEO proliferation, such as the cell fate determinant MAB21L2, similarly showed the epicardium fails to form when these proteins are depleted [194,220].

Recently it has been shown that proliferation is also required for PEO emergence[104], therefore, SRSF3 deletion might even impact PEO formation if the *Tg(Gata5-Cre)* is expressed in proepicardial progenitors.

3.3.5. SRSF3 is required for epicardial proliferation *in vitro*

To assess the involvement of SRSF3 in epicardial proliferation, *Wt1*^{CreERT2}*;Srsf3*$^{fl/fl}$ explants were used. Due to early spontaneous differentiation to vascular smooth muscle, deletion had to be induced at the same time the explants were cultured. Because of the proliferation defects, this led to few SRSF3 deleted cells being recovered, which impaired further analysis.

A mouse epicardial cell line was used to investigate the effects of SRSF3 loss on proliferation. After siRNA treatment against *Srsf3*, treated wells had fewer cells than controls and the levels of Cyclin D1, a direct target of SRSF3 [155,158], were dramatically reduced. However, flow cytometric analysis did not reveal an increase in the number of cells in G1, which was not entirely surprising, considering large T antigen immortalised cells are not always dependent on Cyclin D1 for G1/S progression [214,215].

The large T antigen was reported to bind only p53 and not RB in MEFs [221]. Therefore, the requirement for Cyclin D1-CDK4/6-mediated G1/S transition was investigated by inhibiting CDK4/6 in the epicardial cell line. Surprisingly, CDK4/6 inhibition had no effect on G1/S progression, but it led to no cells undergoing mitosis. Recently, it was reported that inhibition of CDK4 prevented senescence in fibroblasts, suggesting a role of CDK4 in G2/M transition [215].

Even though this epicardial cell line does not seem to be dependent on Cyclin D1-CDK4/6 for G1/S transition, Cyclin D1 levels also increase in G2, being required for re-entry into G1[222], therefore, Cyclin D1 might still play a role in the proliferation of these cells.

Inhibition of proliferation with either CDK4/6 or Aphidicolin led to a large increase in the number of floating cells. The *en mass* detachment of cells following cell cycle inhibition resembles the “crisis state” cells enter when the large T antigen is inactivated [214]. Immortalised cells seem to undergo apoptosis and not enter cell cycle arrest when proliferation is inhibited.

The cell cycle stage of the epicardial cell line could not be clearly determined due to the variability in cell size and the presence of binucleated cells. This was further complicated by the unexpected way cells responded to CDK4/6 inhibition and the *en mass* detachment following cell cycle inhibition, leading to the conclusion that this cell line is not suitable for cell cycle studies.

3.3.6. Conclusions

This chapter showed SRSF3 is expressed in multiple cell types in the developing heart, such as cardiomyocytes, where it is required for survival and proliferation.

Deletion of SRSF3 using the Gata5-Cre leads to a smaller PEO that fails to deposit fibronectin and migrate onto the heart surface. The defect of proepicardial proliferation and migration leads to the failure of the epicardium to form in *Tg(Gata5-Cre); Srsf3$^{fl/fl}$* mutant hearts. The data presented also support a role for SRSF3 in proliferation of epicardial cells *in vitro*.

Chapter IV.

SRSF3 is required for epicardial EMT

4.1 Background

4.1.1 Epicardial EMT regulation

During embryonic development, a subset of epicardial cells undergo epithelial-to-mesenchymal transition (EMT) and invade the myocardium [81,92,223]. The molecular mechanisms that regulate epicardial EMT are not entirely understood, however, multiple signalling pathways originating from both epicardium and underlying myocardium, including retinoic acid (RA) [82], Hippo[123,124], TGFβ [47,224], PDGF[127] and FGF[225], have been associated with this process (Fig 4.1). Other factors, such as cell polarity and proliferation, are also involved, with the axis of cell division dictating which cells invade the heart [114]. In addition, increasing proliferation rates by Cyclin D1 overexpression[114] or deletion of neurofibromin1 (NF1), a negative regulator of Ras,[226] results in more epicardial cells inside the heart. How these cellular processes are integrated during epicardial EMT remains unknown.

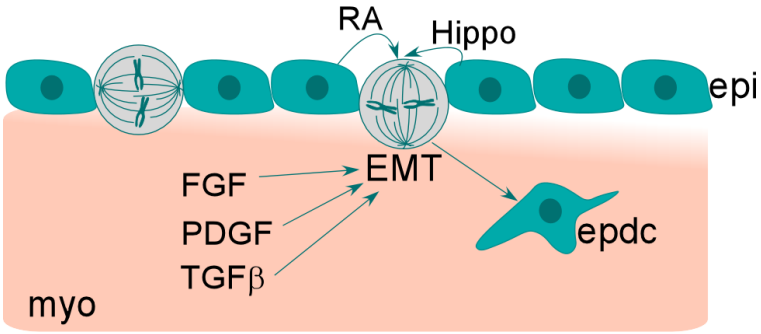


Figure 4.1 Schematic summarizing the main regulators of epicardial EMT

Epicardial epithelial-to-mesenchymal transition (EMT) is induced by multiple signalling pathways from the myocardium and the epicardium and orientation of cell division perpendicular to the basement membrane. epi-epicardium, myo-myocardium, epdc-epicardium-derived cell, TGF-transforming growth factor, PDGF-platelet derived growth factor, FGF-fibroblast growth factor, EMT-epithelial to mesenchymal transition, RA-retinoic acid.

4.1.2 Epicardium-derived cell fate specification

Epicardial cells that invade the myocardium are known as epicardium-derived cells (EPDCs) and directly contribute to multiple cardiovascular lineages, such as cardiac fibroblasts (CFs), mural cells and coronary endothelial cells (CECs). EPDCs primarily differentiate into CFs and mural cells, providing more than 80% of the vascular smooth muscle cells (vSMCs) [91,92] and CFs present in the heart [81]. EPDC contribution to CECs is minor, with the average estimate showing 7% contribution [68,77] .

The factors which regulate EPDC differentiation remain to be determined. Signalling through PDGFRs has been linked to EMT and cell fate choice, with PDGFRα required for CF specification, whereas PDGFRβ was needed for differentiation to vSMC [96,127] (Fig 4.2). Induction of TGFβ signalling in epicardial explants and cell culture has also been reported to promote vSMC fate [178,224]. Differentiation to CECs has only been demonstrated *in vitro*, where VEGF-A was used to specify endothelial fate [68,227].

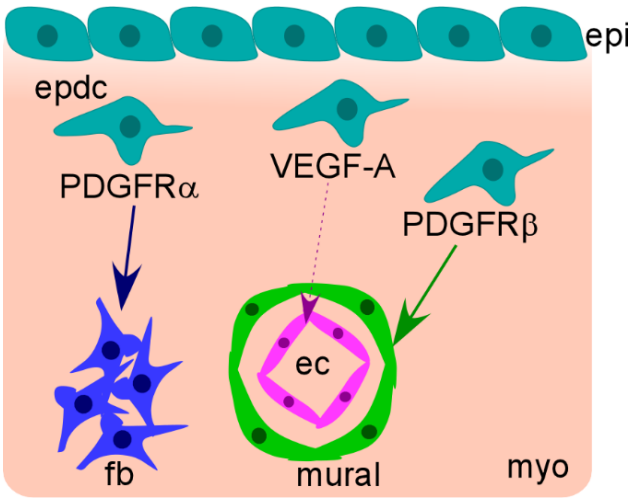


Figure 4.2 Schematic of EPDC differentiation cues

Epicardium-derived cell (EPDC) differentiation to cardiac fibroblast is dependent upon PDGFRα activation, whereas PDGFRβ initiates differentiation to mural fate. VEGF-A induces differentiation of EPDCs to endothelial fate. epdc-epicardium-derived cell, epi-epicardium, myo-myocardium, ec-endothelial cell, fb-fibroblast.

4.1.3 Epicardial function in coronary vasculature development

CECs predominantly originate from the inflow tract of the embryonic heart, the sinus venosus and the inner lining, the endocardium [58,77]. Epicardium-derived signals such as VEGF-C are required for sinus venosus sprouting [77,86], whereas endocardium is sensitive to hypoxia-related signals, such as myocardial VEGF-A [58,228].

All coronary vessels are reliant on EPDCs for maturation, with vSMCs providing physical support and CFs depositing ECM that promote vessel growth [124,226]. Defective epicardial EMT or impaired EPDC differentiation leads to failure of the coronary vasculature to form [124,136,229].

4.1.4 SRSF3 and mesenchymal state

The role of SRSF3 in epicardial EMT has not been investigated. SRSF3 is known to promote mesenchymal transformation in multiple cancers via upregulation of EMT-related genes such as *Snai1* [156,157,160].

SRSF3 has also been implicated in developmental transition and cellular maturation during hepatic [168] and neural [167] development, however, its function in epicardial cell fate determination remains unexplored.

4.1.5 Aims

The aims of this chapter were to investigate the role of SRSF3 in epicardial EMT and epicardium-derived cell fate specification using the inducible *Wt1*^{CreERT2} line.

4.2 Results

4.2.1 SRSF3 depletion prevents epicardial EMT

Wt1^{CreERT2} specifically targets epicardial cells

To determine the role of SRSF3 in epicardium, the inducible *Wt1*^{CreERT2} line [126] was used to delete the RNA-binding domain encoded by exon 2 and 3 of SRSF3 [166]. This targeting method leads to the decreased production of a non-functional SRSF3 mutant protein.

Lineage tracing of targeted cells was achieved with the tdTomato reporter [179] (Fig 4.3). The Cre enzyme leads to irreversible transcription of *tdTomato* which marks the Cre-expressing cell and all its progeny [179,230]. In this way, cell lineages can be followed throughout the course of development.

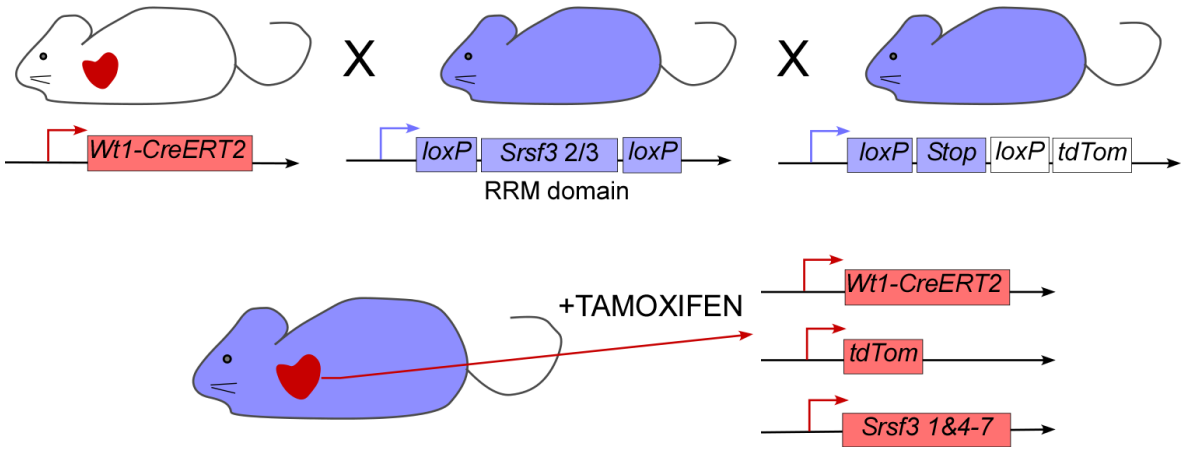


Figure 4.3 Breeding strategy used to obtain conditional *Wt1*^{CreERT2}; *Srsf3*$^{fl/fl}$; *Rosa26*^{tdTomato} mice

Wt1^{CreERT2} *mice were bred with mice that had exons 2 and 3 of the Srsf3 gene flanked by loxP sites and with tdTomato reporter mice. Exons 2 and 3 of the Srsf3 gene constitute the RNA-recognition domain (RRM). Tamoxifen is required to translocate the Cre-ER (estrogen receptor) complex to the nucleus and initiate recombination of regions flanked by loxP sites.*

Inducible Cre lines, such as *Wt1*^{CreERT2}, have the Cre recombinase fused to estrogen receptor α (ERα) and require tamoxifen administration to translocate the Cre-ERα to the nucleus, where recombination takes place [70]. This way, Cre activity is restricted to a defined temporal window, allowing for more specific labelling.

Due to their restricted activity, inducible Cre are not as efficient as constitutive ones; hence, tamoxifen administration was optimised to ensure efficiency. Optimal Cre activation was achieved after two doses of 40 mg/kg delivered via oral gavage, which was superior to intraperitoneal injection (Fig 4.4). Oral administration had lower toxicity and more reproducible activation compared to the intraperitoneal route; where embryos showed different degrees of toxicity and varying recombination rates, confirming other reports [65,231]. Similar to other studies, no difference in recombination efficiency was found between tamoxifen and the active form of tamoxifen, 4-hydroxytamoxifen (data not shown) [232], so tamoxifen oral administration was used in all subsequent experiments.

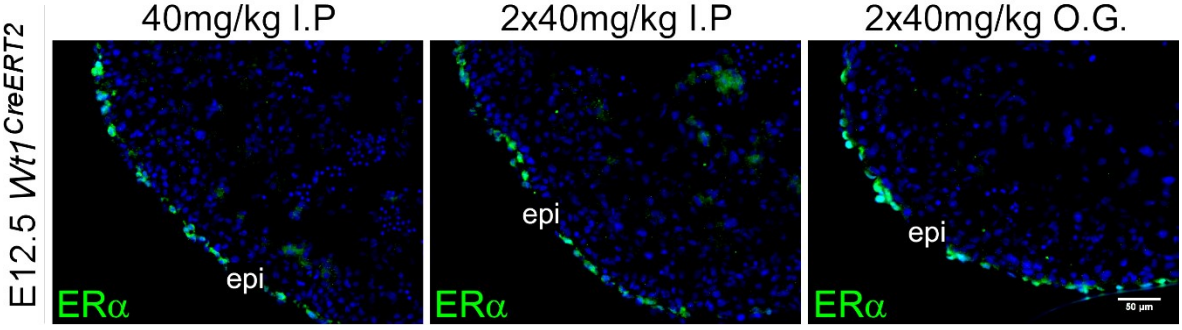


Figure 4.4 Optimisation of tamoxifen delivery *in vivo*.

Intraperitoneal (I.P.) tamoxifen administration with one dose of 40 mg/kg was not very efficient in activating the Cre, as shown by the cytoplasmic localization of the estrogen receptor α (ERα), which is tagged to the Cre. Two doses of 40 mg/kg were more efficient in translocating the Cre to the nucleus, with oral gavage (O.G.) administration superior to I.P. n=2. Scale bar: 50 µm.

WT1 expression was found in endothelial cells at later stages of development [65,76], therefore, the specificity of the *Wt1*^{CreERT2} in early development was assessed using the tdTomato reporter (Fig 4.5). Cre activation with tamoxifen before embryonic stage 12.5 (E12.5) resulted in efficient epicardial targeting, with few endothelial cells labelled.

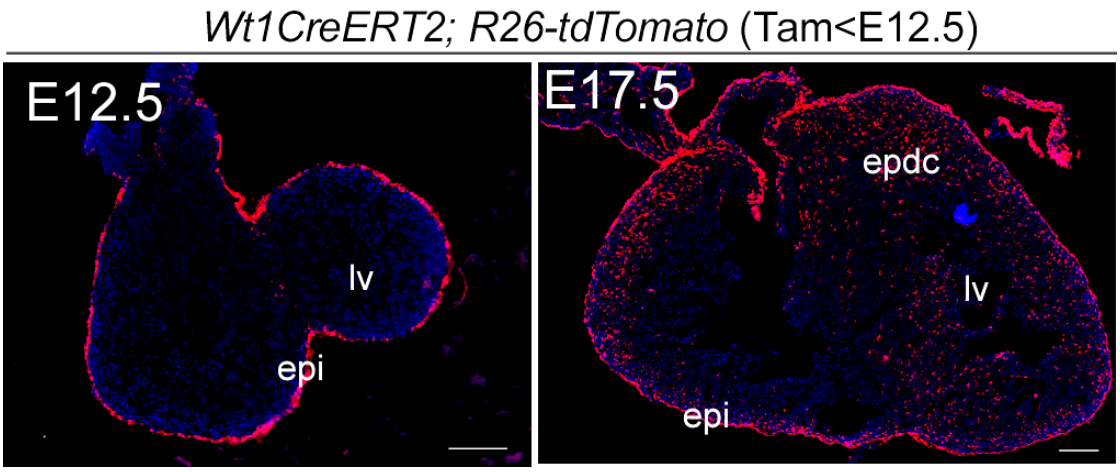


Figure 4.5 *Wt1*^{CreERT2} labels the epicardium before E12.5

Tamoxifen delivery at E9.5/E11.5 leads to restricted activity of the WT1^{CreERT2} *to the epicardium at E12.5. Analysis of the induced hearts at E17.5 shows tdTomato expression in epicardium and traced epicardium-derived cells. epi-epicardium, lv-left ventricle, epdc-epicardium-derived cell. n>5. Scale bar: 200 µm.*

Epicardial SRSF3 deletion leads to heart formation defects

To confirm the role of SRSF3 in epicardium formation presented in Chapter III, tamoxifen was delivered at E8.5 in a double dose of 80 mg/kg. This strategy has been previously used to activate WT1-CreERT2 in the PEO[194], however, there was no detectable tdTomato expression in E9.5 embryos after E8.5 tamoxifen administration (data not shown). This is consistent with previous findings showing highest reporter expression at 48 h post tamoxifen induction, in spite of maximum Cre translocation taking place at 24 h [233], therefore, it is likely tdTomato reporter expression, and possibly SRSF3 depletion, peaked 48h post tamoxifen administration, at E10.5, after proepicardial cells migrated onto the heart.

Analysis of E8.5-induced hearts at E16.5 revealed failed EPDC formation in *Wt1*^{CreERT2}*; Srsf3*$^{fl/fl}$ mutant hearts, as indicated by the absence of tdTomato+ cells inside the myocardium (Fig 4.6 A). Immunostaining for the endothelial marker PECAM1 showed a significant decrease in PECAM1+ cells in mutant hearts, suggesting impaired coronary vasculature formation (Fig 4.6 B). Instead, superficial PECAM1+ structures were found underneath the epicardium (Fig 4.6 B arrows). Mutants also presented myocardial non-compaction, as revealed by the presence of endomucin (EMCN), which marks endocardial cells [234], very close to the epicardial surface (Fig 4.6 C). Impaired coronary vasculature formation, appearance of ectopic subepicardial vessels and myocardial non-compaction are defects frequently reported in mutants with faulty EPDC formation [95,177,235].

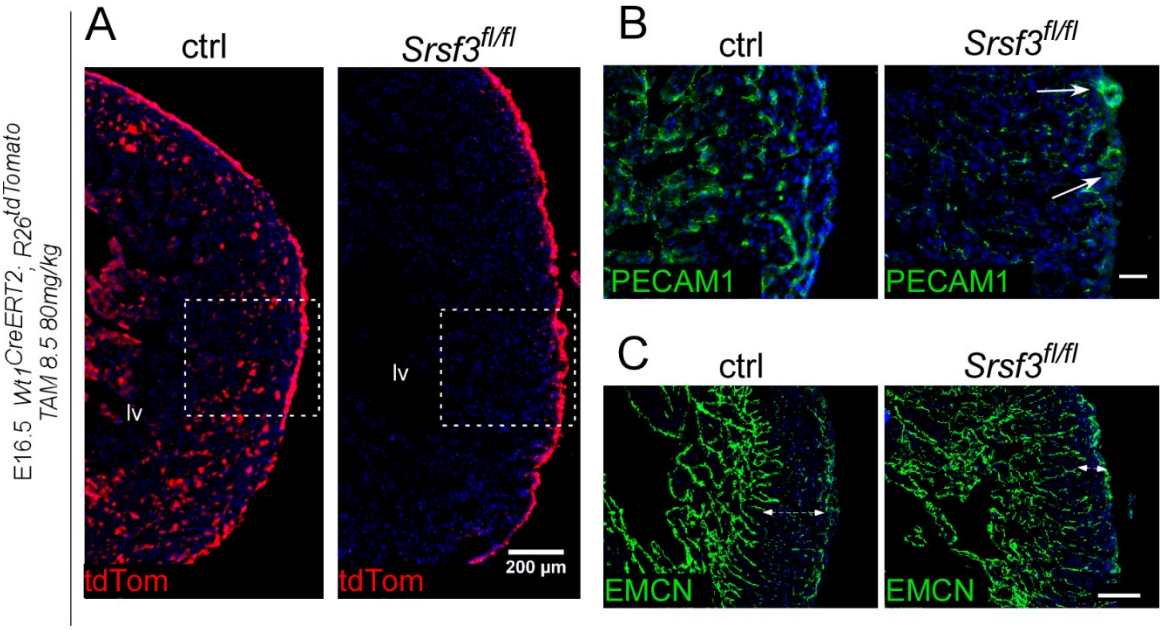


Figure 4.6 E8.5-induced *Wt1*^{CreERT2}*; Srsf3*$^{fl/fl}$ hearts present failure of EPDC formation, coronary vasculature defects and myocardial non-compaction

(A) *TdTomato fluorescence in E16.5 control and Wt1*^{CreERT2}*; Srsf3*$^{fl/fl}$ *hearts tamoxifen induced at E8.5. n=2. Scale bar: 200 µm. lv-left ventricle* ***(B)*** *Immunofluorescence for PECAM1 and tdTomato reveals fewer PECAM1 and tdTomato cells and presence of superficial vessels near the surface (arrows). Scale bar: 50 µm.* ***(C)*** *Endomucin (EMCN) immunostaining indicates non-compaction defects in the mutant heart. Compact layer delimitated by arrows. Scale bar: 200 µm.*

SRSF3 is required for epicardial EMT *in vitro*

The lack of EPDCs in E8.5 tamoxifen-induced *Wt1*^{CreERT2}*; Srsf3*$^{fl/fl}$ mutant hearts suggested SRSF3 depletion in epicardial cells leads to either inability to undergo EMT or failure to migrate. To discriminate between these two possibilities, an immortalised mouse epicardial cell line was used. This epicardial cell line has been shown to undergo EMT and differentiation to vSMC in response to treatment with TGFβ [178].

In order to assess EMT, a cocktail of TGFβ1 (frequently used to induce EMT *in vitro* [178]) and PDGF-DD was used to induce EMT after siSRSF3 treatment. Since this epicardial cell line contains an INFγ-inducible temperature-sensitive large T antigen that keeps cells immortalised, treatment was performed at 37°C, in the absence of INFγ, to inactivate the large T antigen and allow differentiation [178]. Multiple concentrations of TGFβ1 were tested, ranging from 1 ng/ml to 10 ng/ml. The optimal EMT response, as assessed by induction of EMT-related genes, was triggered by treatment with 10 ng/ml of TGFβ1 (data not shown). PDGF-DD was used for PDGFRβ activation , which was reported to trigger epicardial EMT and differentiation to vSMC [96,127]. Since epicardial cells express both PDGFRα and PDGFRβ, 20 ng/ml of PDGF-DD was added to selectively activate PDGFRβ [96] and enhance the EMT response. This concentration has been previously used to efficiently activate PDGFRβ [96].

As presented in Chapter III, siSRSF3 treatment led to reduced proliferation rates and lower cell density in treated wells, as compared to controls. This cell line becomes more mesenchymal at lower densities (observation); therefore, more cells were seeded in treated wells to correct for enhanced mesenchymal response due to reduced density. Methodology summarised in Figure 4.7.

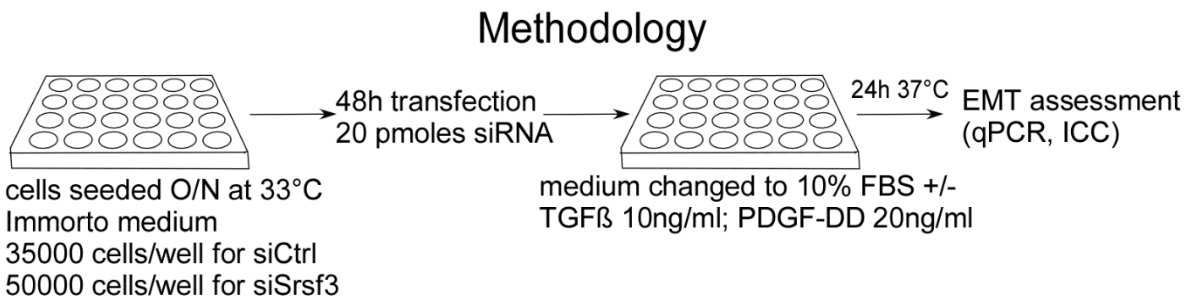


Figure 4.7 Methodology used to assess EMT in the epicardial cell line

Cells were seeded overnight (O/N) at 33°C in 24-well plates at various densities: 35 000 cells/well for siCtrl and 50 000 cells/well for siSRSF3 treatment. Cells were treated with 40 nM siRNA for 48 h, followed by TGFβ1/PDGF-DD treatment for 24 h at 37°C. Epithelial-to-mesenchymal transition (EMT) was assessed by quantitative PCR (qPCR) and immunocytochemistry (ICC).

SRSF3 immunostaining confirmed reduced expression in cells transfected with 40 nM siSRSF3 for 48h (Fig 4.8 A). Post-transfection, cells were moved to 37°C and either treated with TGFβ/PDGF-DD or control medium for 24 h. Immunostaining for the cell-cell adhesion marker β-catenin[116] and the mesenchymal marker α-smooth muscle actin (α-SMA) [236] was used to assess epithelial vs mesenchymal state. Untreated cells had high levels of β-catenin present at adherens junctions, indicative of epithelial morphology (Fig 4.8 B). Control cells that underwent TGFβ1/PDGF-DD treatment had high levels of αSMA, showing mesenchymal transition, whereas cells that had been transfected with siSRSF3 had lower levels of αSMA and preserved cell-cell contacts, as shown by β-catenin staining (Fig 4.8 B).

RT-qPCR was used to quantify expression of EMT-induced genes such as *Snai1* [237] and *Acta2* (α-SMA) post 24 h of TGFβ1/PDGF-DD treatment. RNA interference is reversible [238], therefore, *Srsf3* levels were also measured to assess recovery. Cells that had been treated with siSRSF3 still had lower *Srsf3* expression 24 h after the siRNA was removed and failed to trigger EMT to the same extent as siCtrl cells (Fig 4.8 C). These data indicate that SRSF3 is required for epicardial EMT induction in response to TGFβ1/PDGF-DD .

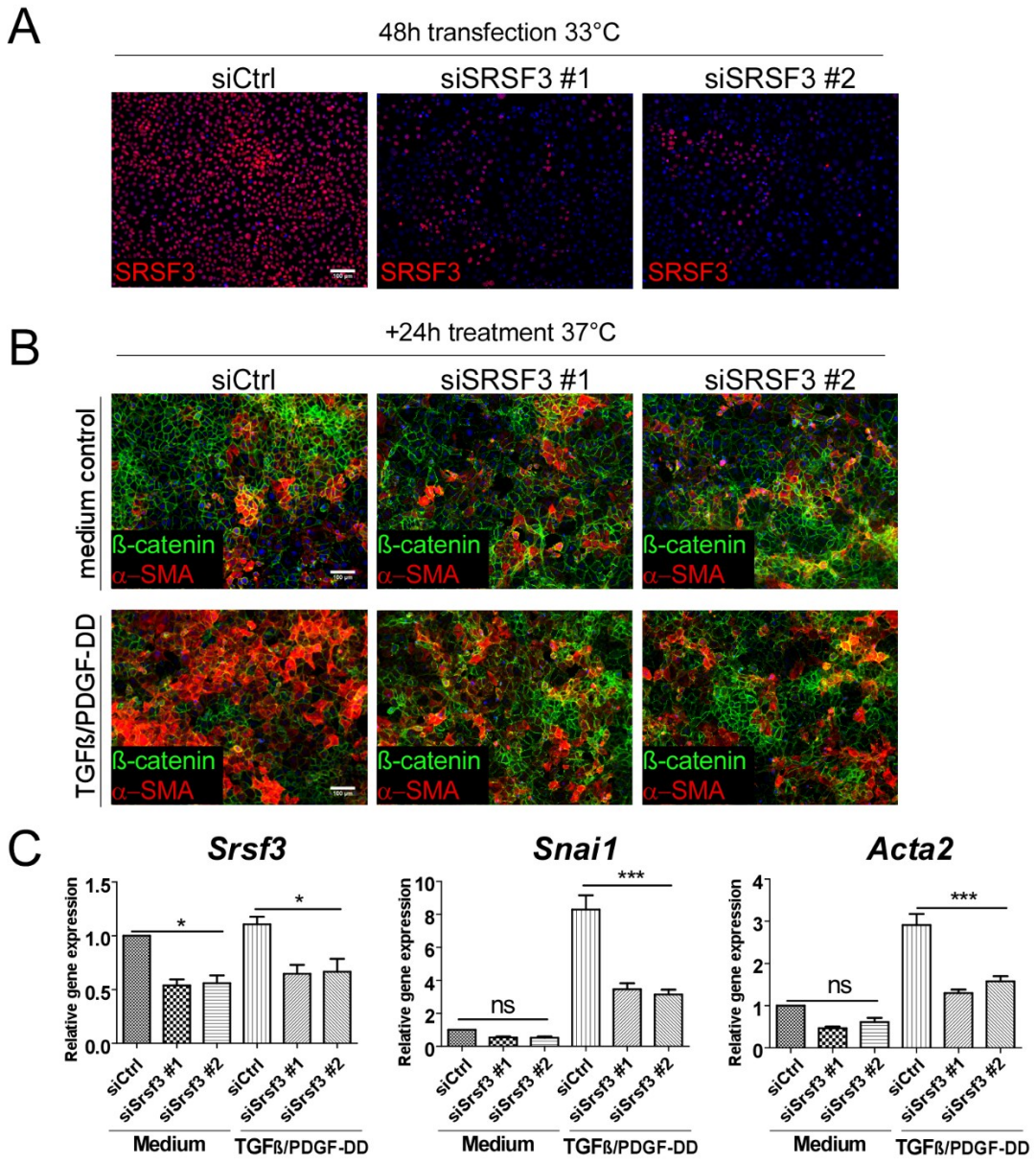


Figure 4.8 SRSF3 knockdown inhibits TGFβ1-induced EMT *in vitro*

(A) *Immunostaining for SRSF3 was performed on cells that had been transfected for 48h with either control siRNA or siSRSF3, showing decreased SRSF3 levels after siSRSF3 treatment. Scale bar: 100 µm.* ***(B)*** *Immunostaining for αSMA and β-catenin was performed on cells that had been transfected for 48h, followed by treatment with TGFβ1/PDGF-DD for 24h. siControl cells lose β-catenin expression and increase αSMA levels after treatment, whereas siSRSF3 transfected cells fail to respond to the same extent. n=3. Scale bar: 100 µm.* ***(C)*** *RT-qPCR for Srsf3, Snai1, Acta2 after 24h treatment with TGFβ1/PDGF-DD post-transfection confirms a decrease in Srsf3 expression and EMT markers in the siSRSF3 transfected cells. Expression relative to untreated control, data shown as mean +/- SEM. One-way Anova with Tukey's post-hoc test. P<0.05 (*), p<0.001(**), ns-not significant. n=3 independent experiments.*

4.2.2 Cell proliferation and EMT

Cell cycle inhibition alters EMT response in *vitro*

SiSRSF3 treatment in the mouse epicardial cell line led to decreased proliferation and failure to undergo EMT in response to TGFβ1/PDGF-DD stimulation. Proliferation was reported to be required for EPDC formation in *vivo,* where cell cycle inhibition with the DNA polymerase inhibitor Aphidicolin led to no cells invading the myocardium, whereas promoting cell division by Cyclin D1 overexpression increased EPDC number [114].

To investigate a link between cell proliferation and EMT, cells were treated with either Aphidicolin (S block) or the CDK4/6 inhibitor PD0332991 isethionate (G1 block) and EMT was induced with TGFβ1/PDGF-DD. For CDK4/6 inhibition, the cells were treated at 33°C for 24 h, followed by addition of TGFβ1/PDGF-DD for another 24 h at 37°C. No cells survived after 48 h Aphidicolin treatment, therefore, Aphidicolin had to be delivered at the same time as TGFβ/PDGF-DD to allow survival of cells. As expected, wells treated with cell cycle inhibitors had far fewer cells than controls. As a result, cells were seeded at a lower concentration in control wells to mitigate differences due to density. The methodology used is summarised in Figure 4.9 A.

Even in the absence of TGFβ1/PDGF-DD, cells treated with Aphidicolin at 37°C were more elongated compared to controls, suggestive of mesenchymal morphology (Fig 4.9 B). Such changes were absent with CDK4/6 inhibition (Fig 4.9 B). RT-qPCR against the EMT markers, *Snai1* and *Acta2* and vSMC marker, Calponin1 (*Cnn1*) [239] revealed cells treated with CDK4/6 inhibitor fail to induce EMT in response to TGFβ1/PDGF-DD, whereas Aphidicolin treated cells upregulate not only EMT-related genes, but also vSMC genes, even in the absence of treatment (Fig 4.9 C).

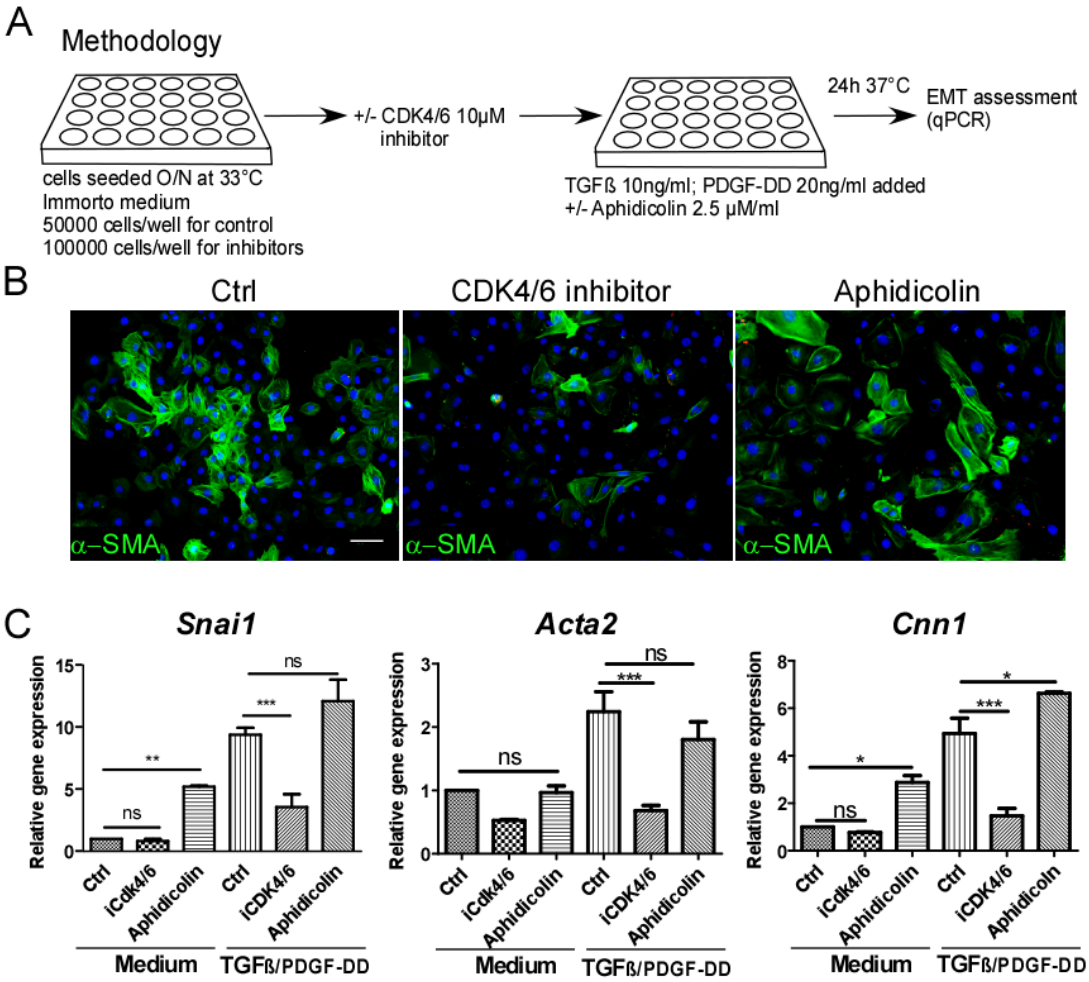


Figure 4.9 Epicardial EMT is altered after cell cycle inhibition *in vitro*

(A) *Methodology used to assess EMT in response to cell cycle inhibitors in a mouse epicardial cell line.* ***(B)*** *Immunostaining for α-smooth muscle actin (αSMA) on cells cultured at 37°C in the presence of cell cycle inhibitors shows elongated cell morphology in Aphidicolin treated cells. Ctrl-control. n=2. Scale bar: 50 µm.* ***(C)*** *RT-qPCR for Snai1, Acta2 and Cnn1 was performed on cells treated with proliferation inhibitors and cultured at 37°C in the presence of TGFβ/PDGF-DD or media control. Data shown as mean +/- SEM. One-way Anova with Tukey's post-hoc test. n=3. Relative gene expression to untreated control. p<0.05 (*), p<0.01 (**), p<0.001 (***), ns-not significant.*

These results indicated that epicardial cells *in vitro* can still undergo EMT when treated with Aphidicolin, therefore, the failure to initiate EMT after CDK4/6 inhibition could not be explained by proliferation arrest, unless only certain stages of the cell cycle, such as S phase, are permissive of EMT.

As shown in Chapter III, this epicardial cell line does not undergo G1 arrest when treated with CDK4/6 inhibitor due to the immortalisation process bypassing the need for retinoblastoma (RB) phosphorylation by CDK4/6 [215]. Instead, CDK4/6 inhibition made cells larger and prevented them from entering mitosis. However, the production of large T antigen should be arrested at 37°C and the normal cell cycle should be resumed [178]. To investigate the cell cycle after CDK4/6 inhibition at 37°C, flow cytometry was performed on control and inhibited cells at 33°C and compared to cells at 37°C treated with TGFβ1/PDGF-DD. Control cells were still proliferating in the non-permissive temperature, although fewer cells were found in S/G2/M, suggesting a longer G1 phase (Fig 4.10 A). Surprisingly, cells under CDK4/6 inhibition at 37°C had more cells in G2, as suggested by DAPI content and by the appearance of a separate G2 population in the flow cytometry plot (Fig 4.10 B), however, most cells were still found in G1. Since control cells were also mostly found in G1, the failure to undergo EMT could not be linked to arrest in a specific cell cycle stage.

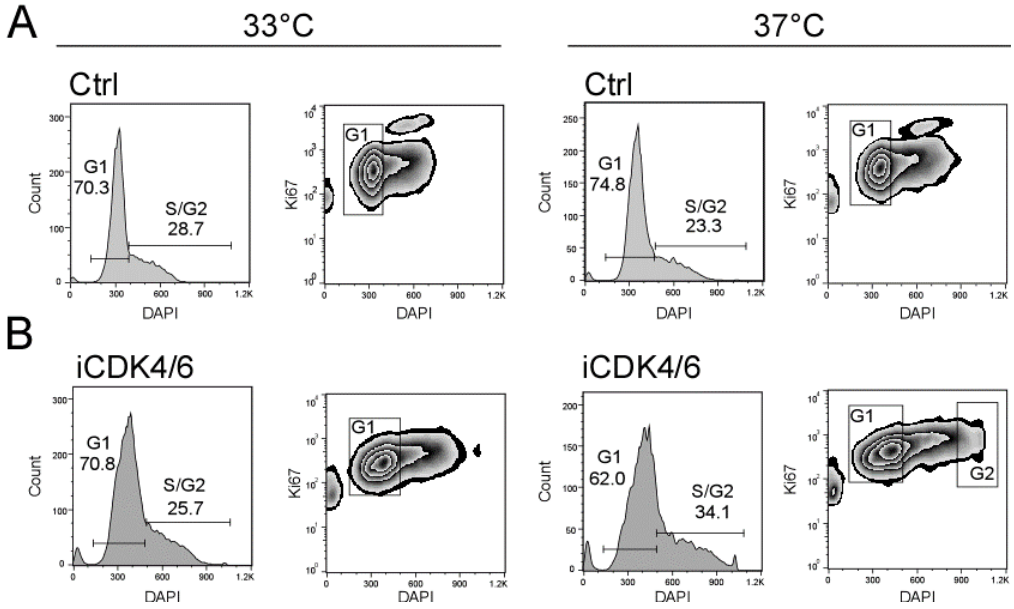


Figure 4.10 TGFβ treatment alters cell cycle profile *in vitro*

(A) *Flow cytometry plots of cells stained for DAPI (histogram) and Ki67 at 33°C versus cells treated with TGFβ at 37°C shows fewer cells in S/G2/M with treatment. n=2.* ***(B)*** *Flow cytometry plots of CDK4/6 inhibited cells stained for DAPI (histogram) and Ki67 at 33°C versus cells treated with TGFβ at 37°C shows more cells in G2 at 37°C. n=1.*

Cell cycle inhibition prevents epicardial explant outgrowth

The cell cycle inhibitor studies showed that epicardial cells *in vitro* can still respond to EMT cues in S phase. Interestingly, inhibition of CDK4/6 prevented EMT response in the mouse epicardial cell line, however, due to the altered cell cycle profile of these cells, it could not be concluded that failure to undergo EMT is cell cycle related.

To further investigate the link between cell cycle inhibition and EMT in a more physiologically relevant assay, primary FUCCI epicardial explants were used. FUCCI is a system that allows visualization of cell cycle stage by fluorescence, with cells in G1 expressing red fluorescence protein (mCherry), which is tagged to the ubiquitylation domain of the chromatin licensing and DNA replication factor 1 (CDT1), whereas cells in S/G2/M express green fluorescence protein (Venus) tagged to the ubiquitylation domain of the DNA replication inhibitor Geminin [180] (Fig 4.11 A). Cells that are not proliferative (G0) do not fluoresce.

E11.5 FUCCI ventricular explants were grown in the presence of cell cycle inhibitors. Explants were derived at E11.5 because epicardial cells are most proliferative at this stage [114]. Inhibition of cell proliferation prevented explant growth in both CDK4/6 inhibitor and Aphidicolin treatment, indicating outgrowth is dependent on cell division (Fig 4.11 B, C). In spite of impaired outgrowth, SM-MHC+ cells were still present in Aphidicolin treated explants, suggesting epicardial cells in S phase are able to spontaneously undergo EMT and differentiate to smooth muscle (Fig 4.11 B, C). No SM-MHC+ were found in CDK4/6 inhibitor treated explants, however, very few cells were recovered and not all of them were arrested in G1, as shown by GFP fluorescence (Fig 4.11 B).

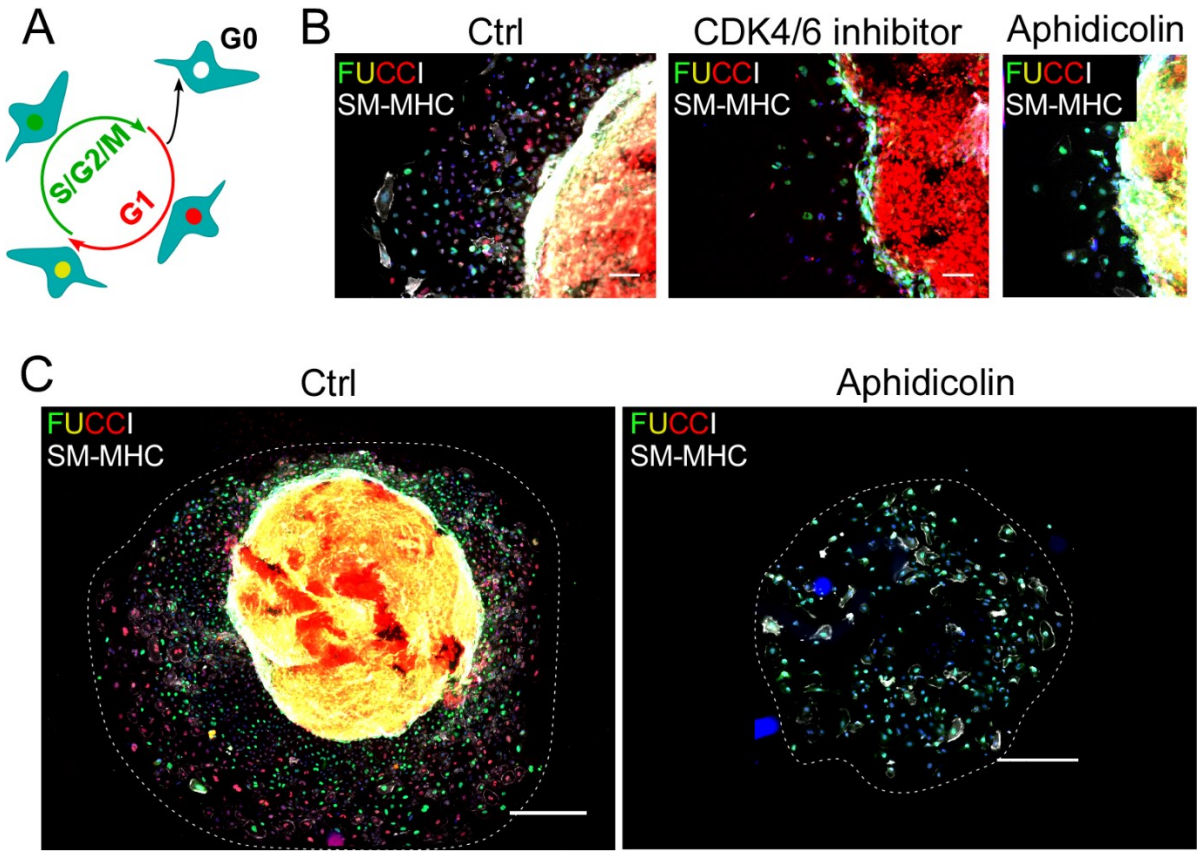


Figure 4.11 FUCCI epicardial explants fail to grow in the presence of cell cycle inhibitors

(A) *Diagram summarizing the fluorescence of FUCCI cells in different stages of cell cycle.* ***(B)*** *E11.5 FUCCI epicardial explants treated with 10 μM PD0332991 isethionate or 1 μg/ml Aphidicolin fail to outgrow. Immunostaining for smooth muscle myosin heavy chain (SM-MHC) shows SM-MHC+ cells present in control and Aphidicolin treated cells, but not with CDK4/6 inhibition. Scale bar: 100 μm.* ***(C)*** *Low magnification view of right ventricle control explant and Aphidicolin treated explant (ventricle piece detached) stained for SM-MHC. n=2. Scale bar: 500 μm.*

Because proliferation is required for epicardial explant outgrowth, no meaningful analysis or further cell cycle inhibition studies were possible using epicardial explants.

4.2.3 Induction of SRSF3 deletion at various developmental stages alters phenotype

To examine the role of SRSF3 after epicardium formation, tamoxifen was administered past E8.5. Multiple dosage regimes were tested: a single high dose of 80 mg/kg at E9.5 to target the early epicardium, a single high dose at E11.5 to target the epicardium during EMT and two smaller doses of 40 mg/kg at both E9.5 and E11.5 to attempt to maximise targeting efficiency in the epicardium through sustained recombination. Since tamoxifen is highly effective up to 48 h post-delivery [233], induction after E11.5 was not possible due to WT1 expression in endothelial cells at later stages [65].

The *Wt1*^{CreERT2};*Srsf3*^{fl}; *Rosa26*^{tdTomato} crosses were very inefficient at producing embryos, with half of the plugged females either not pregnant or having resorptions (Appendix Table 4.1). The average number of embryos per litter was ~3.5, for both heterozygous Srsf3$^{fl/+}$/Srsf3$^{fl/+}$ crosses and homozygous Srsf3$^{fl/fl}$/Srsf3$^{fl/fl}$ crosses. Cre- females were better at producing embryos than Cre+ females, possibly due to SRSF3 being required in WT1+ cells in adults. Due to the low embryo number in both heterozygote and homozygote crosses, tdTomato+ control embryos had to be obtained from different litters.

First, control embryos were investigated to determine targeting efficiency and specificity with different tamoxifen induction regimes. (Fig 4.12 A). Surprisingly, tamoxifen induction with one high dose at E9.5 seemed slightly more effective than two lower doses at E9.5 and E11.5, by assessing the number of tdTomato+ cells. One high dose at E11.5 was less effective and missed the first wave of epicardial EMT that contributes to the AV valves [44,240], as shown by lack of tdTomato+ cells in the valve region, whereas more tdTomato+ cells were present throughout the IVS. EPDCs are usually confined to the apical portion of the IVS [44], therefore this result suggested labelling of endothelial cells in the IVS.

Srsf3$^{fl/fl}$ mutant hearts had distinct patterns of tdTomato expression depending on the timing of tamoxifen induction (Fig 4.12 B). Embryos which received a high dose of tamoxifen at E9.5 had fewer tdTomato cells inside the heart as compared to controls, especially in the AV valve and apex region. Embryos treated with two lower doses of tamoxifen at E9.5 and E11.5 appeared normal, however, tdTomato+ cells were closer to the surface. Embryos induced with one high dose at E11.5 also had fewer tdTomato+ cells near the apex and in the IVS as compared to tamoxifen-matched controls and presented abnormally large vessels (Fig 4.12 B arrow).

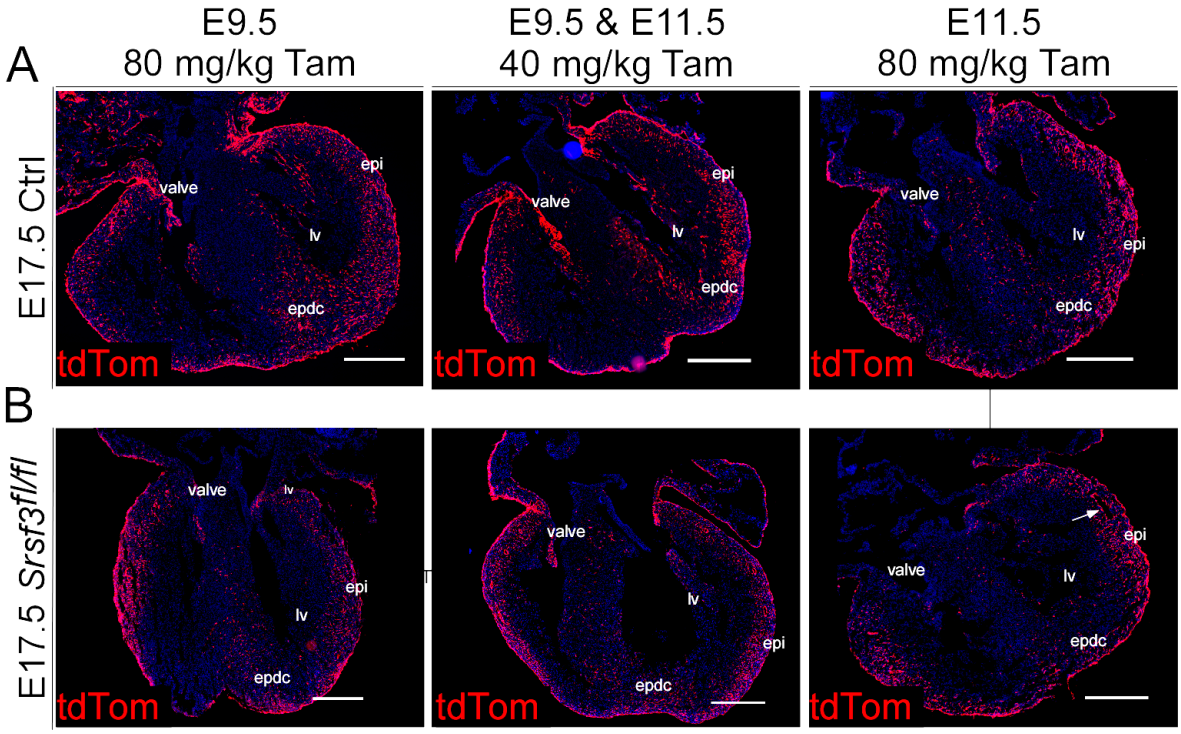


Figure 4.12 Lineage tracing of *Wt1*^{CreERT2} targeted cells in controls and *Srsf3*$^{fl/fl}$ hearts after tamoxifen induction at different timepoints

(A) *Control hearts induced with tamoxifen at different stages of development show distinct patterns of labelling. n=2 E9.5, E11.5 tamoxifen, n=4 E9.5/11.5. Scale bar: 500 μm.* ***(B)*** *Srsf3*$^{f/fl}$ *embryos present different phenotypes depending on the timing of tamoxifen-induced Srsf3 deletion. Enlarged vessel indicated by arrow. n=2 E9.5, E11.5 tamoxifen, n=4 E9.5/11. Scale bar: 500 μm. lv-left ventricle, epi-epicardium, epdc-epicardium derived cell.*

The presence of a significant number of tdTomato+ cells inside the heart in these mutants was difficult to reconcile with the phenotype produced by induction of SRSF3 deletion at E8.5, where no EPDC formed. One possibility is that later tamoxifen induction is less effective due to a larger number of epicardial cells requiring targeting as development progresses, therefore, SRSF3 depleted cells still fail to enter the myocardium, but more epicardial cells escape recombination and produce EPDCs. Another possibility is that later tamoxifen induction triggers SRSF3 loss in EPDCs after they have entered the myocardium.

Unfortunately, it could not be determined by IHC if SRSF3 was lost in EPDCs in mutant hearts. Early in development, when SRSF3 levels are high (E13.5), IHC can be used to distinguish between cells that had undergone recombination and have low levels of SRSF3, however, IHC cannot be used later in development to indicate recombination because SRSF3 levels are already low (Appendix Fig 4.1). In addition, tdTomato fluorescence could not be used as a proxy for SRSF3 loss since the recombination efficiency of floxed *tdTomato* construct was superior to that of floxed *Srsf3* (discussed in previous chapter).

Since the E8.5-tamoxifen induced mutants presented coronary vasculature defects, the pan-endothelial marker PECAM1 was used to assess vessel growth in the mutants induced at the later stages. Control hearts had normal coronaries independent of tamoxifen induction stage, however, labelling of CECs was higher with later stage induction, probably due to persistence of Cre activity when WT1 starts to be expressed in endothelium (Fig 4.13 A). CEC labelling was low with both E9.5 and E9.5/11.5 induction, consistent with reports showing that EPDCs do not significantly contribute to coronary vessels [65,81,91]. In contrast, the higher dose at E11.5 led to substantial labelling of endothelial cells (Fig 4.13 A, arrows).

Surprisingly, the expected number of vessels were also present in mutant hearts. More tdTomato+ CECs were found in *Srsf3*$^{fl/fl}$ mutants induced either at E9.5 or E9.5/E11.5 compared to tamoxifen-matched controls (Fig 4.13 B). This phenotype was most pronounced with E9.5/E11.5 tamoxifen administration. Mutants induced at E11.5 did not show an increase in the number of tdTomato+PECAM1+ cells compared to controls, however, some vessels were enlarged, possibly due to mis-targeting of SRSF3 deletion to endothelial cells. (Fig 4.13 B, boxed region).

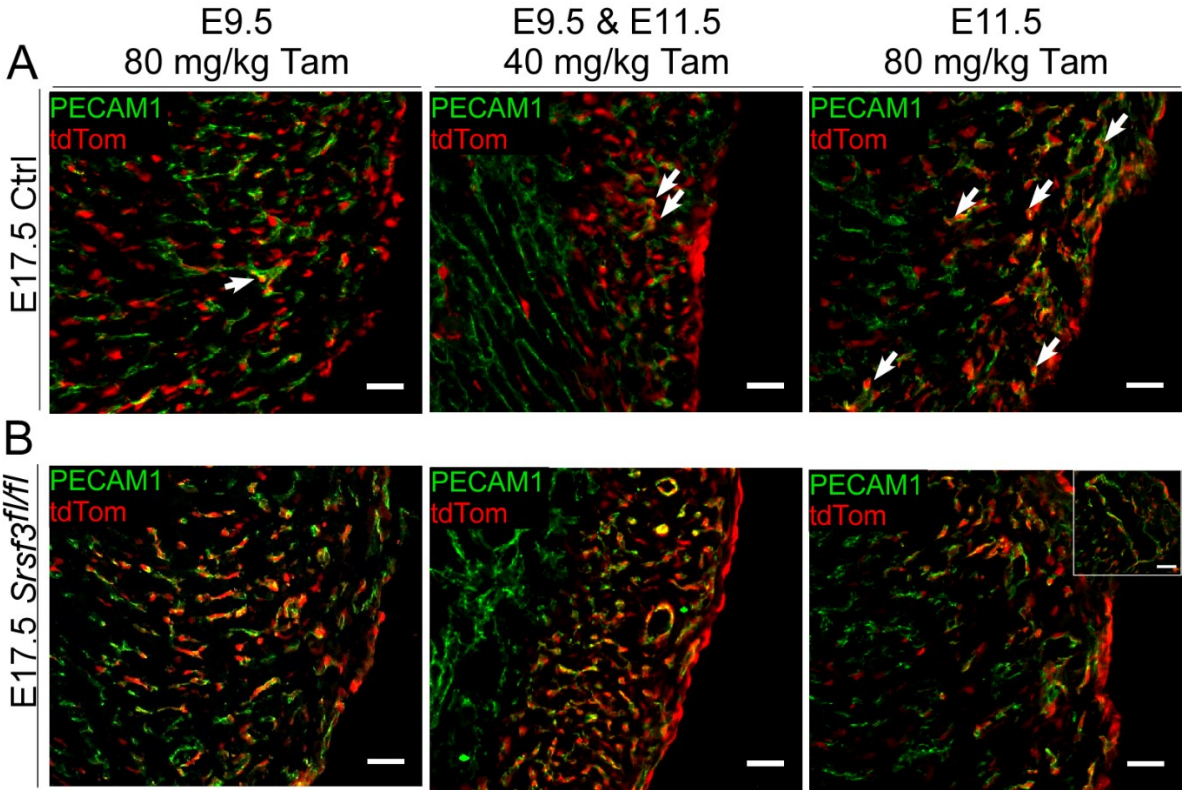


Figure 4.13 Endothelial labelling with different tamoxifen administration regimes

(A) *Immunofluorescence for PECAM1 and tdTomato on E17.5 Wt1*^{CreERT2} *control hearts shows negligible contribution of epicardium-derived cells, shown by tdTomato, to coronary endothelium, after E9.5 and E9.5/11.5 tamoxifen. A high dose of tamoxifen administration at E11.5 led to increased labelling of endothelial cells. Arrows point to tdTomato+ endothelial cells.* ***(B)*** *E17.5 Srsf3*$^{fl/fl}$ *mutant hearts have an increased number tdTomato+PECAM1/+ cells with early tamoxifen induction and enlarged vessels with later induction (boxed region). Scale bar: 50 μm. n=2 E9.5, E11.5 tamoxifen, n=4 E9.5/11.5.*

The increase in tdTomato+ PECAM1+ cells could indicate a compensation mechanism through which EPDCs differentiate to CECs if SRSF3 depleted epicardial cells fail to secrete the required factors to initiate coronary formation from the conventional sources: SV and endocardium. This would also explain why inducing deletion after sprouting is initiated (E11.5) does not result in more tdTomato+ CECs. Another possibility is that SRSF3 loss in EPDCs directly promotes differentiation to CECs.

4.2.4 Epicardial cell line differentiation assays

To determine if SRSF3 loss impacts EPDC cell fate choice by making differentiation to endothelium more likely, multiple differentiation assays were optimised in the mouse epicardial cell line. Using different growth factor cocktails, epicardial cells were pushed towards vSMC, CF or CEC fate (Figure 4.14). Upon consulting the literature; PDGF-AA in combination with bFGF was used to activate PDGFRα and induce CF fate [127,225,241], whereas TGFβ1/PDGF-DD was used to initiate PDGFRβ signalling and promote vSMC fate [96,178,241]. There are no studies that achieved differentiation of murine EPDCs to CECs *in vitro*, however, a recent study on human iPS-derived epicardial cells used EGM-2 media and VEGF-A to promote endothelial fate [227].

The epicardial cell line preferentially differentiated to vSMC fate, upregulating vSMC markers such as Calponin1 within 72h of exposure to TGFβ1/PDGF-DD. Primary epicardial explants treated with the same growth factors dramatically increased the number of SM-MHC+ cells, indicating this vSMC differentiation protocol is also relevant in primary cultures (Appendix Figure 4.2). Differentiation to CF took longer, possibly due to increased cell proliferation rates in response to FGF treatment, however, after a week the cells upregulated fibroblast markers such as vimentin.

Endothelial cell differentiation was the least successful, cells were cultured in EGM-2 media with high concentrations of VEGF-A for at least a week to obtain very few endothelial cells. Unfortunately, since SRSF3 levels fully recover within a few days after siRNA transfection, assessment of differentiation to CF and CEC was not possible due to the extended timeframe required.

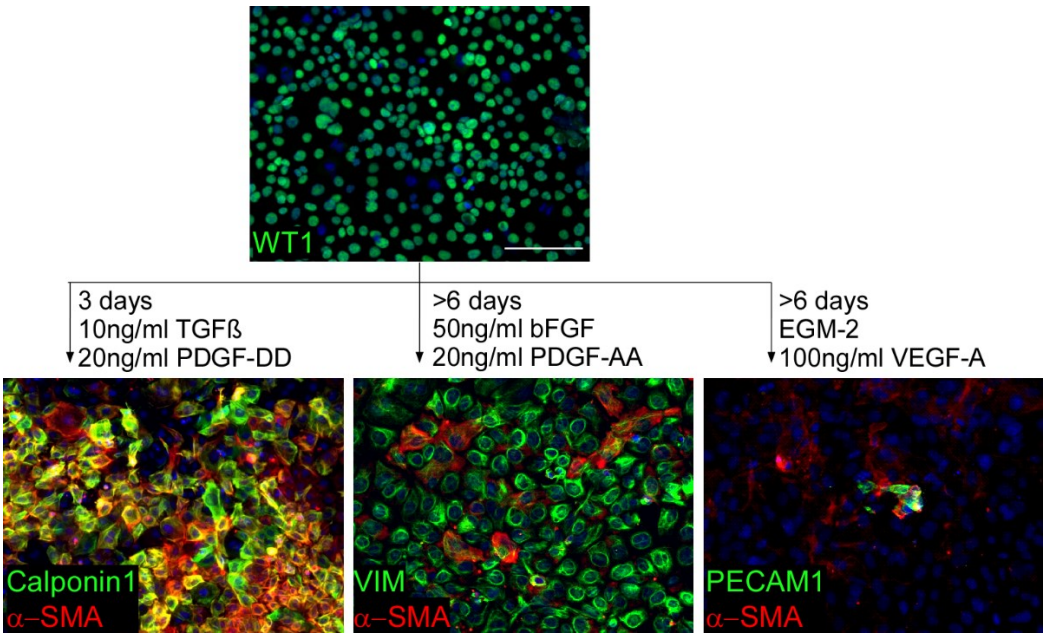


Figure 4.14 Differentiation protocols for the mouse epicardial cell line.

The mouse epicardial cell line was treated with different growth factors to induce differentiation to multiple cardiovascular fates. Immunostaining for α-smooth muscle actin (α-SMA) was used to check mesenchymal state, whereas Calponin1 was used as an indicator of vascular smooth muscle fate, vimentin as fibroblast marker and PECAM1 for identification of endothelial cells. n=>1. Scale bar: 50 µm. TGF-transforming growth factor, PDGF-platelet-derived growth factor, VEGF-vascular endothelium growth factor, EGM-endothelium growth medium.

SRSF3 knockdown impairs differentiation to vascular smooth muscle *in vitro*

Differentiation to vSMC post siSRSF3 transfection was assessed using TGFβ1 and PDGF-DD treatment (Fig 4.15 A). Immunostaining showed that control cells upregulated smooth muscle markers, such as Calponin1 in response to treatment, whereas their expression was reduced in siSRSF3 treated wells (Fig 4.15 B). Quantification using RT-qPCR showed *Srsf3* levels start to recover 72 h post-transfection (Fig 4.15 C).

The expression of *Acta2* was decreased in siSRSF3 cells, but not to a significant extent, indicating cells are starting to respond to TGFβ1 as SRSF3 starts being re-expressed, whereas expression of the smooth muscle marker *Cnn1* was still significantly decreased. These findings suggest SRSF3 is required for EPDC differentiation to vSMC.

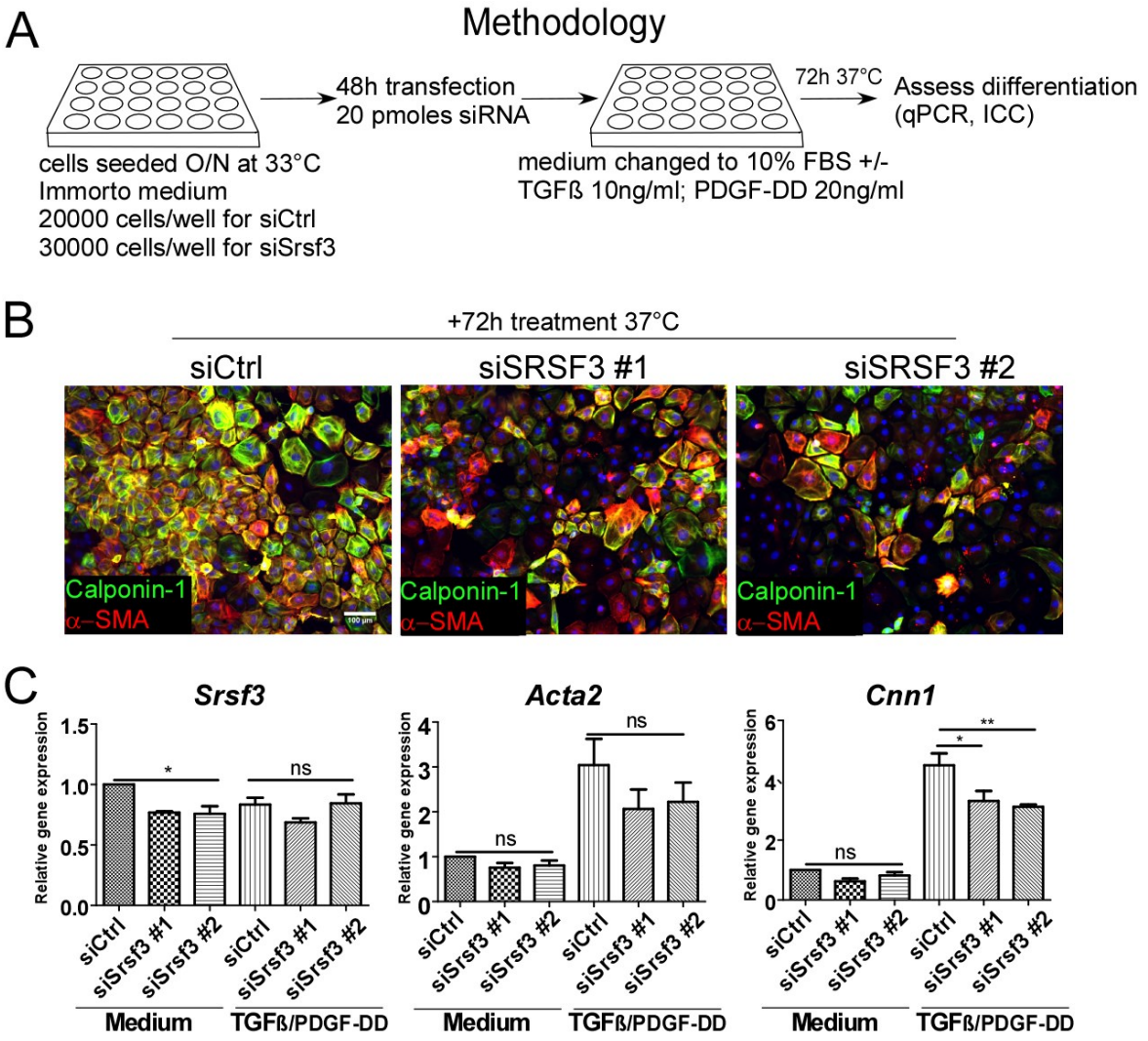


Figure 4.15 Knockdown of SRSF3 impairs TGFβ1-induced differentiation *in vitro*.

(A) *Methodology used to assess smooth muscle differentiation after TGFβ/PDGF-DD treatment.* ***(B)*** *Immunostaining for αSMA and Calponin1 was performed on cells that had been transfected for 48h, followed by treatment with TGFβ1/ PDGF-DD for 72 h. siSRSF3 treated cells have decreased levels of smooth muscle markers. n=3. Scale bar: 100 μm.* ***(C)*** *RT-qPCR for Srsf3, Acta2 and Cnn1 after 72h treatment with TGFβ1/PDGF-DD post-transfection shows decreased levels of Cnn1 in the siSRSF3 transfected cells. n=3. Data shown as mean +/- SEM. Relative expression to untreated control. One-way Anova with Tukey's post-hoc test. P<0.05 (*), p<0.01(**), ns-not significant.*

4.3 Discussion

4.3.1 Early induction of SRSF3 deletion leads to failure of EPDC formation

E8.5 tamoxifen induction of *WT1*^{CreERT2} has been previously used to induce recombination in the PEO [194], however, no tdTomato expression was detected at E9.5 after E8.5 tamoxifen treatment in SRSF3 mutants, suggesting SRSF3 depletion was achieved after the proepicardial cells reached the heart. Nonetheless, immunostaining for SRSF3 at E9.5 and E10.5 will be required to determine the timing of deletion since tdTomato fluorescence may not be strong enough to be detected soon after recombination, thus tdTomato accumulation might happen later than SRSF3 deletion.

E8.5 induced mutants formed an epicardium as shown by the presence of tdTomato on the heart surface, however, no tdTomato+ cells were found inside the heart, indicating impaired EPDC formation. This coincided with myocardial non-compaction and defective coronary vessel formation. Similar phenotypes have been previously described in other mutants that have epicardial EMT defects such as Fog-2 [242], β-catenin [114,229], Tβ4 [12], PDGFR [127] , Yap/Taz [123], FGFR2 [225] epicardial-knockout embryos.

The requirement for SRSF3 in epicardial EMT was investigated *in vitro*, using a mouse epicardial cell line that undergoes EMT in response to TGFβ [178]. Cells failed to upregulate EMT-response genes after SRSF3 knockdown, confirming that SRSF3 is required for TGFβ1-induced epicardial EMT.

However, TGFβ1 is not the main driver of epicardial EMT in vivo, being exclusively expressed in endocardial cells [56] . Other TGFβ ligands are only expressed in small regions of the myocardium near the atrioventricular canal and outflow tract [243,244] therefore, more studies are required to understand the role of SRSF3 in modulating EMT *in vivo*.

4.3.2 Inhibition of CDK4/6 affects epicardial EMT

Epicardial proliferation is known to be one of the factors that facilitates EMT *in vivo*, with increased rates of cell division leading to higher EPDC production [114,226]. Due to SRSF3 being involved in proliferation [152–155,158], a link between proliferation and EMT was explored using the mouse epicardial cell line. Cells were treated with cell cycle inhibitors and then exposed to TGFβ1 and PDGF-DD, two factors that drive EMT [127,178].

Interestingly, cell cycle inhibition with the S block Aphidicolin, which has been previously shown to decrease EPDC production *in vivo* [114], did not prevent EMT *in vitro*. Aphidicolin treatment even enhanced expression of mesenchymal genes in the absence of TGFβ1, but this could be due to lower density in treated wells.

Epicardial explants from FUCCI mice were used to further explore the role of Aphidicolin. SM-MHC+ cells were still found in Aphidicolin treated explants, indicating cells spontaneously underwent EMT and differentiated to vSMC when arrested in S phase. The difference between Aphidicolin treated hearts *in vivo* and treated cells *in vitro* could be due to cell division being required to physically push epicardial cells inside the heart and initiate migration, but not needed for EMT *per se*. The requirement for cell division to displace and rearrange cells has been described in other developmental processes such as gastrulation [198]. Future studies are required to determine the molecular mechanism of impaired EPDC formation after cell cycle arrest *in vivo*.

Of significance, treatment with CDK/6 inhibitor prevented upregulation of EMT-related genes in TGFβ1/PDGF-DD treated cell line. CDK4/6 inhibition did not lead to G1 arrest in the immortalised mouse epicardial cell line; instead it prevented cells from entering mitosis. Since Aphidicolin treated cells still respond to TGFβ, it is unlikely that CDK4/6 prevents EMT through proliferation arrest. CDK4/6 has been shown to influence gene

expression by preventing SMAD signalling through phosphorylation of Smad2/3 in their linker region [245]. Even though TGFβ induction of epicardial EMT is not dependent on Smad2/3, but on non-canonical RhoA/ROCK [213,224], the phosphorylation activity of CDK4/6 could result in inhibition of other proteins required for EMT.

These findings indicate that cell cycle arrest does not affect EMT *in vitro*, suggesting SRSF3 loss may inhibit the TGFβ response through another pathway that does not involve proliferation. However, the role of SRSF3 in epicardial proliferation might still be of importance *in vivo* where cell division is required to facilitate EPDC invasion.

4.3.3 Timing of tamoxifen induction affects phenotype

Multiple phenotypes emerged from analysis of *Wt1*^{CreERT2}*; Srsf3*$^{fl/fl}$ mutants. Complete lack of EPDC formation was observed after E8.5 induction, whereas delivery of tamoxifen at later stages did not prevent EPDC formation. Since SRSF3 is required for EPDC formation, the presence of EPDCs suggests either incomplete recombination or targeting of EPDCs after EMT. Due to the inability to detect SRSF3 depletion by immunostaining at later developmental stages, it remained unclear if SRSF3 was still present in mutant EPDCs.

Delivery of a high dose of tamoxifen at E11.5 resulted in ectopic labelling of coronary endothelium in both controls and mutants. This was unexpected, since most studies that investigate epicardial function used E11.5 induction of Wt1-CreERT2. Mutants presented enlarged vessels, possibly due to targeting of CECs themselves. SRSF3 is expressed in endothelial cells (unpublished observation), therefore, a phenotype could be expected if SRSF3 is lost in CECs.

Interestingly, with both E9.5 and E9.5/11.5 gavage, there was an increase in the number of tdTomato+PECAM1+ cells in mutant hearts. There was no increase in the number of tdTomato+PECAM1+ cells in E11.5 induced mutants compared to tamoxifen-matched controls, suggesting the increase in tdTomato+PECAM1+ cells with earlier induction timepoints is not due to direct labelling of endothelial cells.

The lack of increase in tdTomato+PECAM1+ cells after E11.5 induction also argues against EPDC cell fate switch due to loss of SRSF3. If loss of SRSF3 should result in EPDC fate switch to CEC, E11.5-targeted EPDCs would also be expected to show increased differentiation to CECs. However, if differentiation is due to compensation, which is not required in the case of E11.5 induction, since sprouting is initiated before targeting takes place, then no increase would be expected, as is the case.

4.3.4 SRSF3 is required for differentiation to vascular smooth muscle *in vitro*

Differentiation assays were optimised in the mouse epicardial cell line to further address the role of SRSF3 in cell fate choice. Only assessment of vascular smooth muscle cell differentiation was possible, due to the extended timeframe required for fibroblast and endothelial differentiation being incompatible with the reversible nature of siRNA treatment.

Moreover, differentiation to endothelial fate was very inefficient, with only a few PECAM1+ cells present after a week of treatment. This process could probably be improved by the use of Matrigel instead of gelatin-coating [246], however, it is unlikely such optimisation would shorten the timeframe required for differentiation. A slower cell cycle has been associated with increased cell differentiation in a number of systems from neural development to muscle growth [247]. Both FGF [225,248] and VEGF/EGM-2 [249,250] , the growth factors used to drive differentiation to CFs and CECs in these assays, are pro-mitotic agents,

which prolong time to differentiation, whereas TGFβ slows down proliferation [56,251], making differentiation to vSMCs more likely.

Cells treated with siSRSF3 expressed lower levels of vSMC markers in response to TGFβ1/PDGF-DD. Since SRSF3 is required for TGFβ1-induced EMT, the inability to differentiate to vSMC is most likely a consequence of impaired EMT.

However, it is unclear if the same EMT process precedes all epicardial differentiation processes or if cell fate choice is coupled with EMT, as has been suggested in the case of CFs [81], where loss of TCF21 impaired EMT and differentiation to CFs, but left vSMC fate unaffected. The implications of lineage-specific EMT would mean SRSF3 might not be required for other epicardial cell fates, however, if the same EMT process precedes all cell fate specification, then SRSF3 is required for EPDC differentiation independent of lineage.

4.3.5 Conclusions

This chapter showed that epicardial SRSF3 is required for EPDC formation in developing murine hearts.

Deletion of epicardial SRSF3 early in development resulted in myocardial non-compaction and coronary vasculature defects due to impaired EPDC production, whereas SRSF3 targeting at later stages led to an increased presence of tdTomato+ CECs, possibly as a result of EPDC differentiation to coronary endothelium.

In vitro data support a role for SRSF3 in TGFβ-induced EMT and vascular smooth muscle specification, however, the role of SRSF3 in CF or CEC differentiation remains unclear.

Chapter V.

Heterogeneity of the epicardial lineage

5.1 Background

5.1.1 Proepicardial heterogeneity

The epicardial layer originates from a transient embryonic structure known as the proepicardial organ (PEO), which arises in the septum transversum (ST) area from posterior second heart field progenitors [99,252] .

The cellular composition of the PEO was concluded to be heterogenous on the basis of Cre-dependent fate mapping [4,68,109,253]. For example, PEO cells expressing *Sema3d* or *Scx* were reported to make a significant contribution to coronary endothelium [68], whereas *Wt1*, *Tbx18* or *Tcf21* expressing cells did not contribute endothelium, but instead differentiated to vascular smooth muscle cells (vSMCs) and cardiac fibroblasts (CFs) [65,72,81].

Intriguingly, several studies reported ubiquitous expression of *Wt1, Tcf21* and *Tbx18* in the early epicardium [81,91], indicating that these non-overlapping PEO subpopulations may not translate to the epicardium.

Fate-mapping with Cre/loxP relies heavily on the specificity of Cre expression in the cells of interest. Since Cre recombinase leads to permanent transcription of a reporter gene in Cre-expressing cells and all their descendants, any ectopic recombination can have significant impact. This is especially concerning in the case of constitutive Cre lines, where Cre activity is not temporally restricted, increasing the chances of non-specific labelling.

Such problems have been highlighted in the case of constitutive *Tbx18*^{Cre} [72] and *Wt1*^{Cre} [65], where Cre expression was detected in cardiomyocytes and endothelial cells respectively, at certain developmental stages, raising questions about reported proepicardial cell contribution to these lineages. Moreover, expression of *Tbx18, Tcf21* and *Wt1* was also found in the extended ST [69,72,254–256], which further complicates delimitation of PEO versus ST contribution based on lineage tracing. In addition, *Sema3d*^{Cre} and *Tg(Scx-Cre)* traced cells in the sinus venosus and the endocardium [68], indicating that these proepicardial cells might contribute endothelium via a non-epicardial route.

5.1.2 Epicardial markers and cell fate choice

Most proepicardial genes are also expressed in the epicardium and have been connected to epicardium-derived cell (EPDC) fate choice. TCF21 is thought to be a pre-determinant of CF fate and expressed in epicardial cells that are destined to become CFs [81,120], whereas TBX18 activation was shown to promote vSMC fate [67,121] (Fig 5.1). However, the widespread expression of these genes suggests they are not sufficient to restrict fate, therefore, it remains unclear if EPDCs are multipotent or if their fates are pre-determined at the proepicardial level.

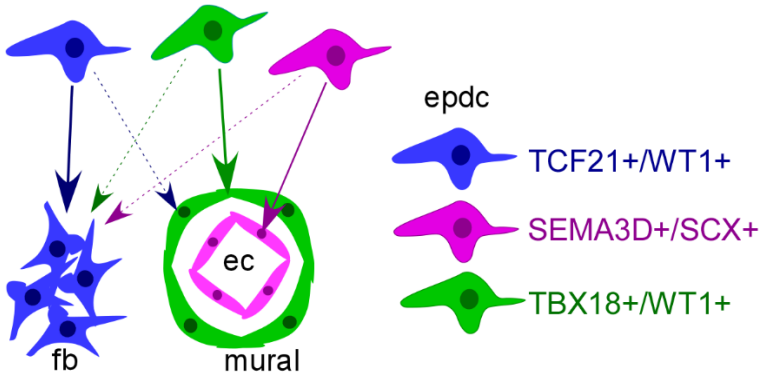


Figure 5.1 Model of epicardial cell fate choice and marker expression

Epicardium-derived cell (EPDC) differentiation is reported to be dependent on marker expression with TCF21 promoting fibroblast fate, TBX18 mural fate, whilst Sema3d and Scx expressing cells differentiate to endothelial fate. fb-fibroblast, ec-endothelial cell, epdc-epicardium-derived cell.

5.1.3 Aims

Data presented in the previous chapters showed that Gata5-Cre mediated removal of *Srsf3* led to impaired epicardium formation; suggesting Gata5-Cre targets all epicardial subpopulations, whereas *Srsf3* deletion driven by the WT1-CreERT2 resulted in decreased EPDC production and increased differentiation to CEC, indicating a switch in EPDC fate.

The aims of this chapter were to examine the expression of known proepicardial markers throughout heart development and determine if marker expression correlates with epicardium-derived cell fate choice, in order to examine the effect of SRSF3 loss on epicardial cell fate and identity, and also verify the targeting domain of the Cre lines used.

5.1.4 Acknowledgment of contribution

The flow cytometry and single-cell RNA-sequencing experiments presented in this chapter were conducted together with Dr. Andia Redpath.

5.2 Results

5.2.1 Overlap of proepicardial markers

RNAscope was used to detect expression of PEO markers in wild-type E9.5 sagittal mouse embryonic sections. RNAscope is an *in-situ* hybridisation technique that detects mRNA with single molecule resolution. The following canonical PEO markers: *Sema3d, Scx, Wt1, Tcf21 and Tbx18* were chosen because their regulatory sequences have been used to generate proepicardial Cre lines and determine contribution to the developing heart [65,67,68,120].

RNAscope allows for simultaneous detection of up to three genes, therefore, three probes were multiplexed onto the same section to assess marker co-expression.

Surprisingly, complete overlap of the chosen markers was observed in the PEO (Fig 5.2 A) and in cells translocating onto the heart (Fig 5.2 A, boxed region). The marker genes displayed different domains of expression below proepicardial protrusions, in the extended ST region (Fig 5.2 B). The PEO has been morphologically defined as protrusions that form on top of the ST [257,258]. Therefore, these findings suggest the *bona fide* PEO co-expresses all marker genes.

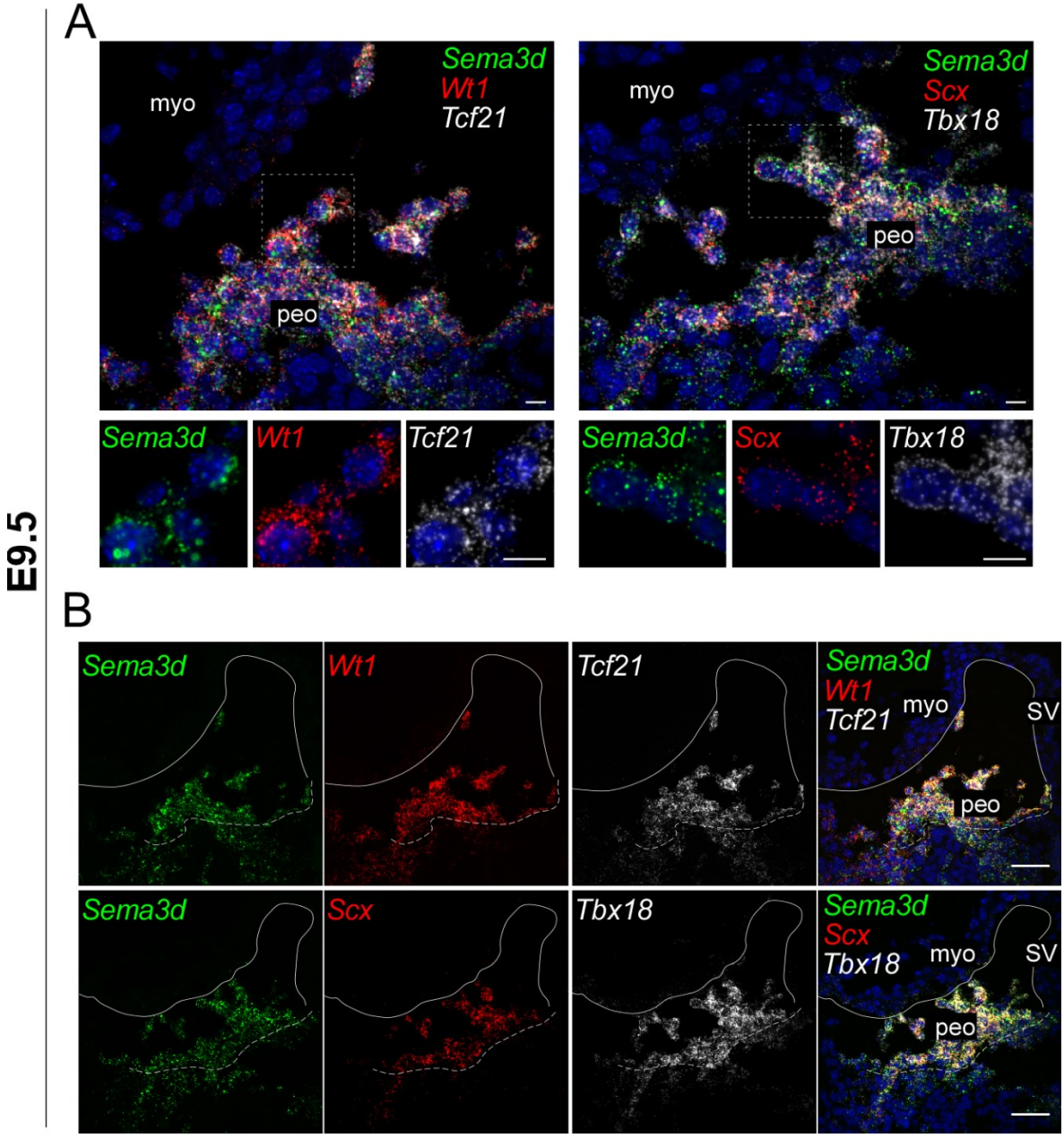


Figure 5.2 Proepicardial markers overlap only in the PEO

(A) *RNA ISH staining of E9.5 embryo cryosections shows overlapping expression of Sema3d, Wt1, Tcf21, Scx, and Tbx18 mRNA in proepicardial cells (dashed line magnified in inset) (n=5 embryos). Scale bar: 10 μm.* ***(B)*** *Proepicardial markers only overlap in the PEO (dashed line), the underlying septum transversum mesenchyme showing non-overlapping expression. Scale bar: 50 μm. peo-proepicardial organ, myo-myocardium, SV-sinus venosus.*

To confirm that proepicardial cells which form the epicardium co-express all selected markers, RNAscope was used on E10.5 sagittal sections (Fig 5.3 A). Markers completely overlapped in the forming epicardium. *Scx* expression was significantly lower than in PEO cells (Fig 5.3 B), confirming published data on non-detectable *Scx* expression in the epicardium from E11.5 [68].

To further validate the RNAscope data, published E10.5 heart single-cell RNA-sequencing data [183] were re-analysed. Using principal component analysis (PCA), cells were divided into three separate clusters. The identity of the clusters was determined using the top 10 expressed genes (Fig 5.3 C). The cardiomyocyte (CM) cluster showed high expression of *Titin (Ttn)* and other myosin-related genes, the epicardium (Epi) expressed mesothelial genes such as *Uroplakin 3b* (*Upk3b)*, whereas the endocardium/atrioventricular cushion (Endo/AVCu) highly expressed *Periostin (Postn)*. T-distributed Stochastic Neighbor Embedding (t-SNE) was used to visualise the clusters in 2D (Fig 5.3 D).

The percentage of cells in the epicardial clusters expressing *Wt1, Sema3d, Tcf21, Tbx18 and Scx* was calculated (Fig 5.3 E). *Wt1, Sema3d, Tcf21* and *Tbx18* expression was found in 97-100% of cells with epicardial identity, like other epicardial genes such as *Upk3b*, *Upk1b and Podoplanin (Pdpn). Scx* expression was only found in 26% of the epicardial cluster, however, this could reflect low expression, since STRT-Seq only captures highly expressed genes.

These results show proepicardial founder cells that give rise to the epicardium co-express all marker genes.

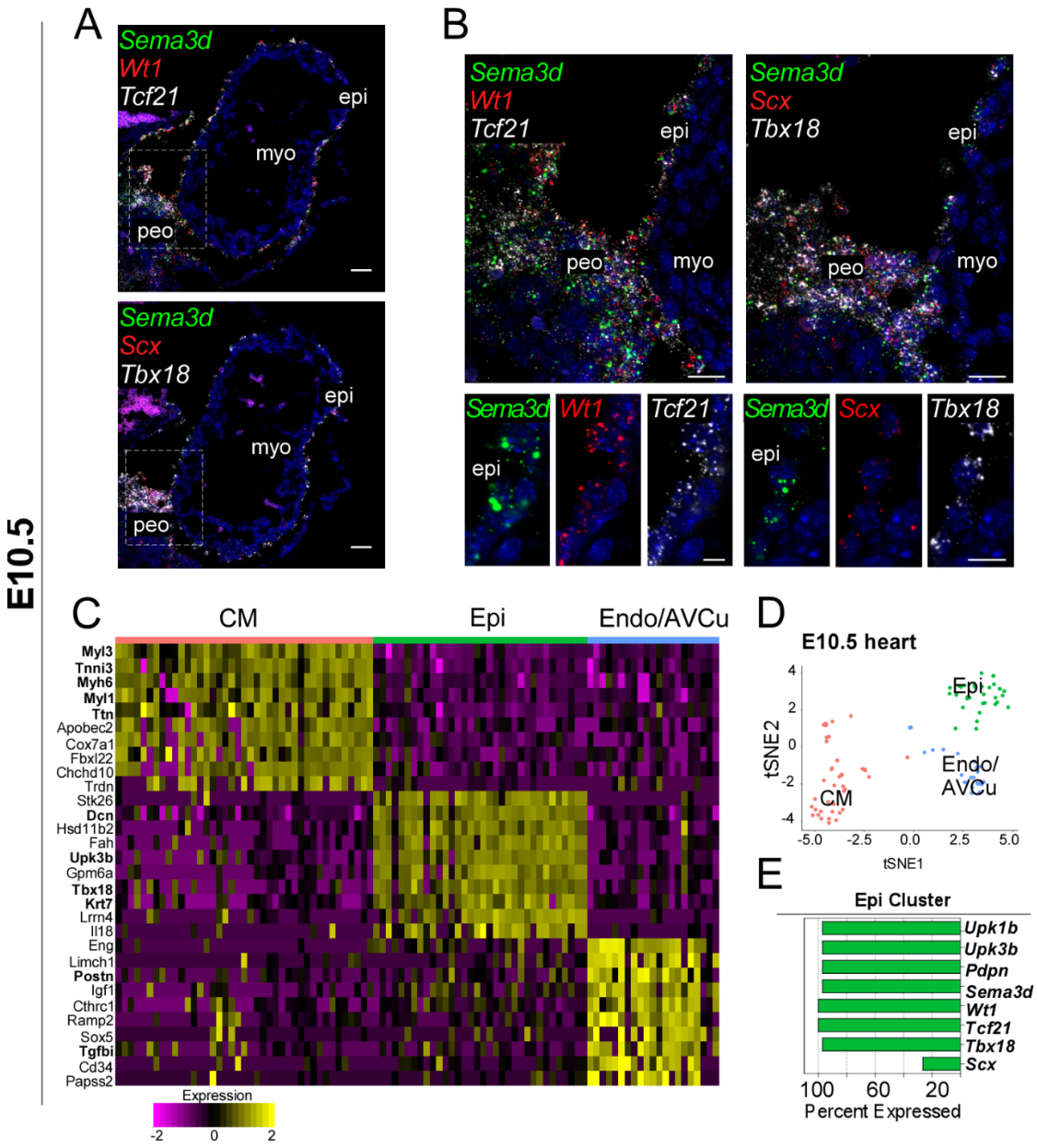


Figure 5.3 Epicardial cells co-express all markers at E10.5

(A) *RNA ISH staining of E10.5 embryo cryosections. Dashed box indicates magnified PEO. Scale bars: 50 μm.* ***(B)*** *High power images of E10.5 stained cryosections demonstrate co-expression of Sema3d, Wt1, Tcf21, Scx and Tbx18 mRNA in migrating proepicardial cells and forming epicardial cells (n=2 embryos). Scale bars: 50 μm (upper panel), 10 μm (lower panel).* ***(C)*** *Heatmap of top 10 differentially expressed genes for each cluster in E10.5 scRNA-Seq.* ***(D)*** *tSNE plot showing clustering of cardiomyocytes (CM), endocardium/atrioventricular cushion (Endo/AVCu), and epicardial cells (epi) from scRNA sequenced E10.5 hearts (total 96 cells; n=2 hearts).* ***(E)*** *Percentage of cells within the epicardial cluster (Epi) expressing selected epicardial genes. epi-epicardium; peo-proepicardial organ, myo-myocardium.*

5.2.2 Expression of epicardial markers throughout development

E9.5 induction of Wt1^{CreERT2} efficiently labels epicardial cells

To evaluate marker expression in epicardial cells and EPDCs at later embryonic stages, cells were labelled with the tdTomato reporter [179], driven by Wt1-CreERT2 [126]. Tamoxifen was administered at E9.5 to initiate tdTomato expression in the early epicardium (E10.5-E11.5), since recombination efficiency is highest 24 to 48 h after induction [233], and to avoid non-specific labelling at later embryonic stages, when *Wt1* becomes expressed in the coronary endothelium [65].

To determine the tdTomato labelling efficiency, RNAscope probes against the selected markers and tdTomato were multiplexed (Fig. 5.4 A). TdTomato expression was found throughout the epicardial layer, and inspection of high-power images revealed overlap between the markers and tdTomato (Fig. 5.4 A insets). Consistent with the earliest epicardial EMT taking place near the atrioventricular groove (AVG) [243], there was a tdTomato+ population of cells in the AVG that retained *Tcf21* expression and downregulated *Wt1, Tbx18, Sema3d* and *Scx.* Expression of some markers was also detected in non-epicardial cells: *Tbx18* was detected in cardiomyocytes, *Scx* and *Tcf21* in AVCu, confirming other reports [72,120,259].

To quantitatively assess marker expression in the entire epicardial layer, PrimeFlow was used on dissociated E11.5 hearts. PrimeFlow is a commercially available flow cytometry-based RNA *in-situ* hybridisation technique [260]. Co-expression of *Wt1, Tcf21, Sema3d* and *Tbx18* was found in >95% of tdTomato+ cells, whereas *Scx* expression was low and only detected in 88.7% (Fig 5.4 B). Out of the *Wt1*+ cells, 90.6±0.2% were tdTomato positive, indicating Wt1-CreERT2 efficiently labels the epicardium and its derivatives (Fig 5.4 C).

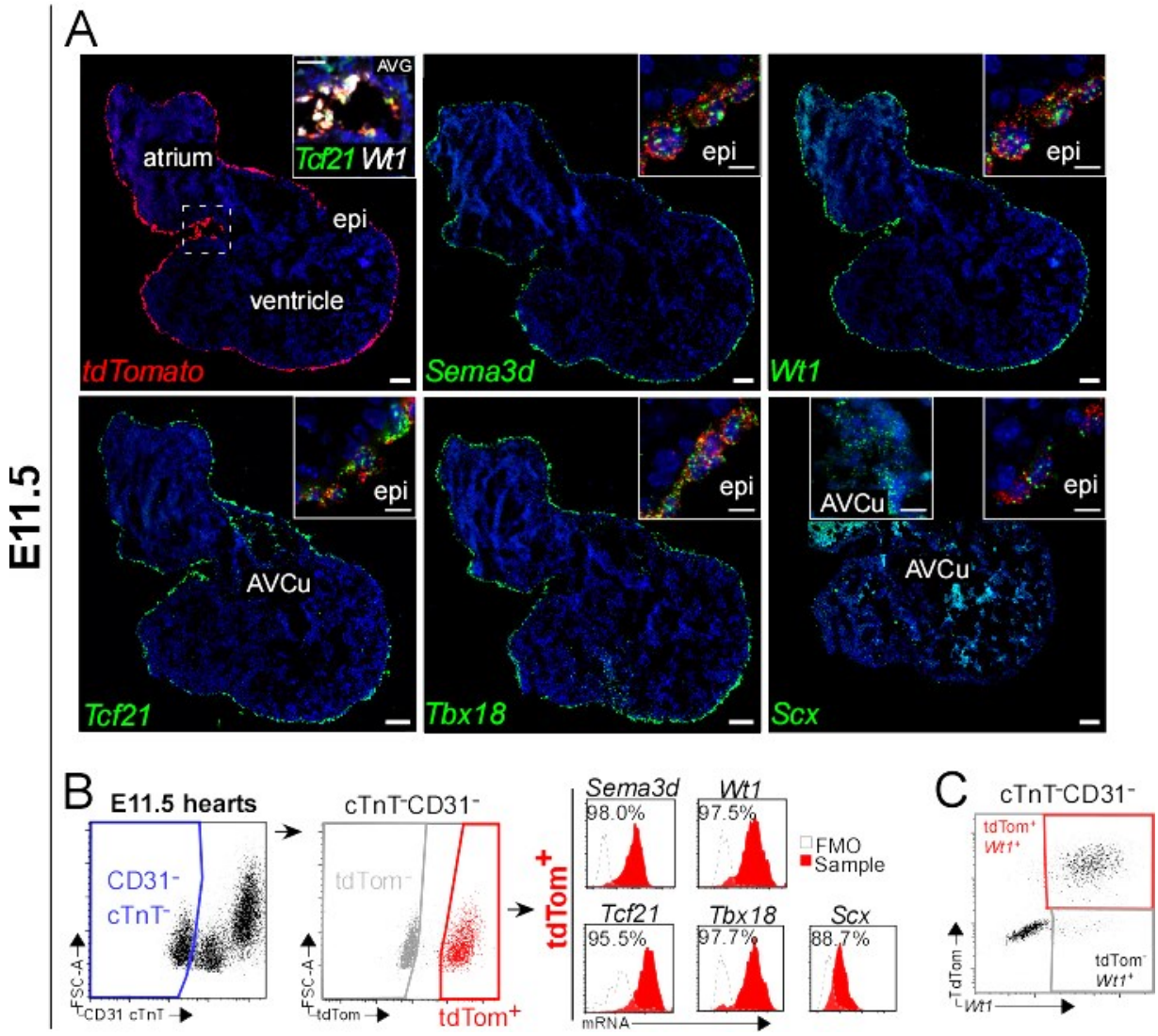


Figure 5.4 Wt1^{CreERT2} induction at E9.5 efficiently labels the epicardium

(A) *RNA ISH staining of E11.5 heart cryosections shows tdTomato labelling of the epicardium in E9.5 tamoxifen induced Wt1^{CreERT2};Rosa26^{tdTomato}embryos and reveals co-expression of Sema3d, Wt1, Tcf21, Tbx18 and Scx in tdTomato-labelled epicardium (n=3 hearts). Inset shows cells in the atrioventricular groove (AVG) co-expressing Tcf21 and tdTomato.* ***(B)*** *Flow cytometry plots of dissociated E11.5 hearts. Epicardial cells, selected by gating CD31$^-$cTnT$^-$tdTomato$^+$, show co-expression of Sema3d, Wt1, Tcf21, Tbx18, and Scx (n=31 hearts, three independent experiments). Fluorescence minus one (FMO) control and percent positive shown.* ***(C)*** *Labelling efficiency of tdTomato. epi, epicardium; AVG-atrioventricular groove, AVCu-atrioventricular cushion, epi-epicardium. Scale bars: 100 µm, 10 µm in insets.*

Epicardial markers are downregulated as development progresses

RNAscope and PrimeFlow were used to assess expression of selected markers in the epicardial layer throughout development.

Four key developmental stages were chosen for analysis: E11.5, when epicardium formation is complete; E13.5, when EPDCs start forming; E15.5, when epicardial EMT stops and E17.5, when EPDCs have differentiated.

Expression of *Sema3d, Wt1, Tcf21* and *Tbx18* peaked within the epicardium at E11.5 (Fig 5.5), then continuously decreased. Expression of epicardial *Scx* was very low throughout development. *Tcf21* and *Tbx18* were significantly reduced beyond E13.5 in the epicardium, being almost undetectable in some of the cells, coinciding with the cessation of epicardial EMT by E15.5 [92,120], whereas *Wt1* and *Sema3d* remained co-expressed in epicardial cells at later stages, but at lower levels (Appendix Fig 5.1, 5.2). There was minimal variation in the level of marker expression between cells at the same stage, as reflected by the SEM in the gMFI plots (Fig 5.5 B).

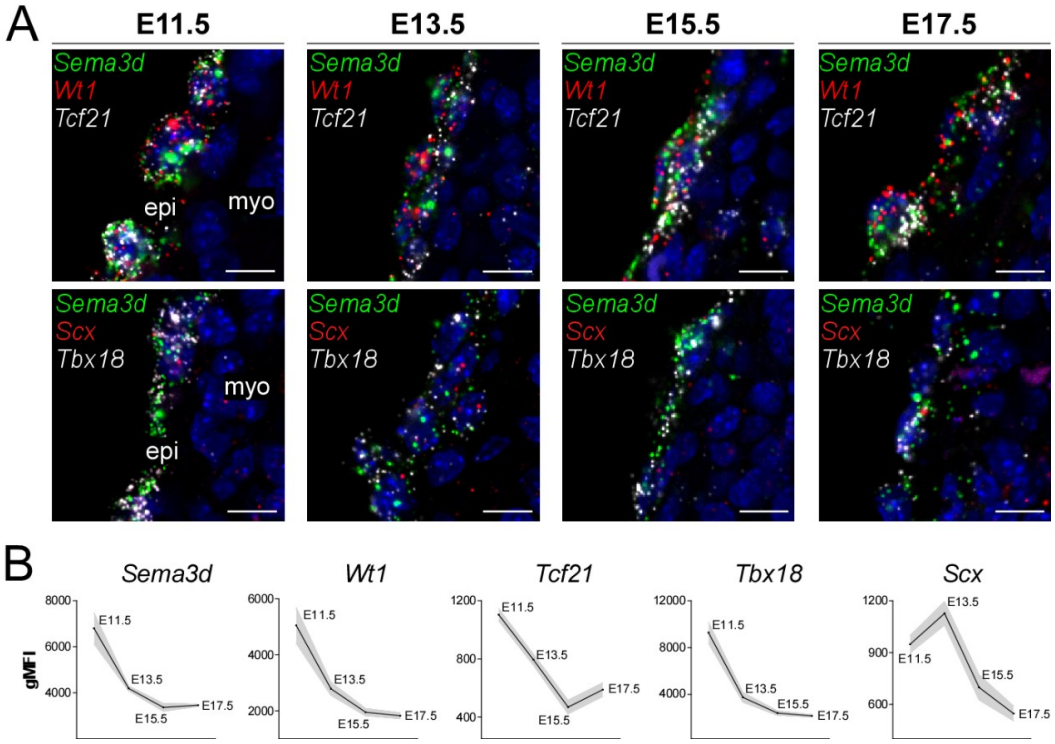


Figure 5.5 Epicardial marker expression decreases throughout development

(A) *RNA ISH staining of E11.5, E13.5, E15.5 and E17.5 heart cryosections shows expression of Sema3d, Wt1, Tcf21, Tbx18*, and *Scx in the epicardium. Scale bar: 10 μm.* ***(B)*** *Flow cytometric analysis of Sema3d, Wt1, Tcf21, Tbx18, and Scx in the epicardial population reveals a rapid decrease in expression at later developmental stages. (data shown as mean gMFI ± SEM of n=4 independent experiments with exception of Tbx18, n=2). gMFI-geometric Mean Fluorescence Intensity.*

Non-specificity of epicardial markers at later stages

The specificity of selected markers to the epicardial lineage, labelled with tdTomato, was assessed at the four developmental stages (Fig 5.6 A-E). The markers were widely expressed at later developmental stages in non-epicardial domains. *Tbx18* was expressed in vSMCs, both of non-epicardial (aorta) and epicardial origin (coronary vessels), as well as in the cardiomyocytes of the left ventricle and IVS (Appendix Fig 5.3 A). *Wt1* expression was found in the endothelium, starting at E13.5 (Appendix Fig 5.3 B). *Sema3d* and *Scx* were expressed in the AVCu and *Tcf21* was found in AVG and interstitial cells (Appendix Fig 5.3 C). Due to the widespread expression of the markers at later stages, subsequent analysis was focused on the epicardial lineage, represented by tdTomato+ cells.

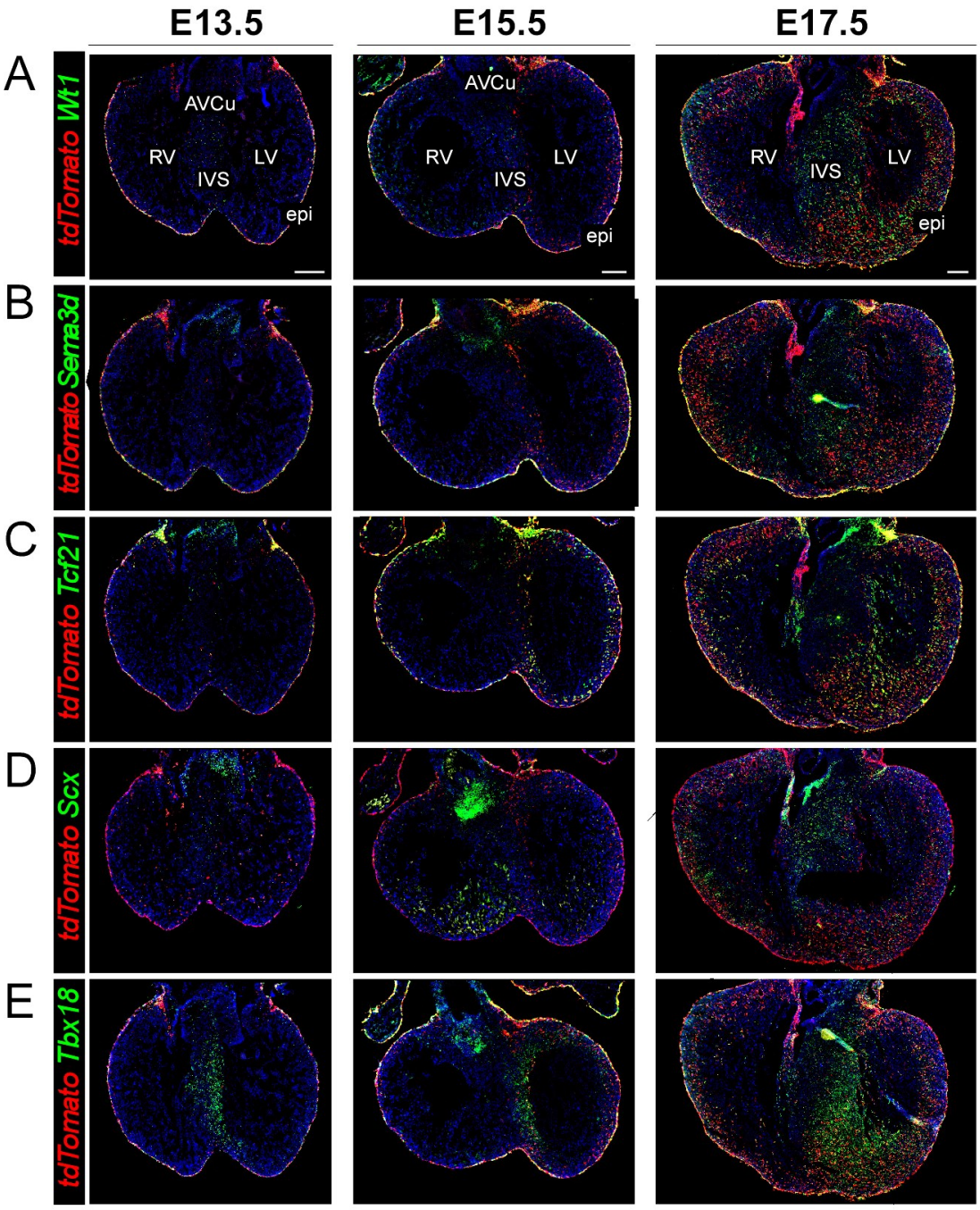


Figure 5.6 Expression of epicardial markers throughout development

(A-E) *RNA ISH co-staining of tdTomato and the epicardial markers Wt1, Sema3d, Tcf21, Scx, Tbx18 at E13.5, E15.5, E17.5. n=>3.* ***(A)*** *Wt1 is expressed in coronary endothelial cells starting E13.5.* ***(B)*** *Sema3d is expressed in the atrioventricular cushion (AVCu).* ***(C)*** *Tcf21 is expressed in EPDCs, AVCu and in interstitial fibroblasts.* ***(D)*** *Scx is highly expressed in the AVCu.* ***(E)*** *Tbx18 is also expressed in cardiomyocytes in the IVS and left ventricle and in vascular smooth muscle cells in the aorta. AVCu-atrioventricular cushion, RV-right ventricle; IVS-interventricular septum, LV-left ventricle, epi-epicardium. Scale bars: 200 μm.*

5.2.3 Heterogeneity of EPDCs and restriction of cell fate

EPDCs lose epicardial signature

Expression of certain epicardial markers, such as *Tcf21*, has been linked to cell fate restriction in EPDCs [81]. To determine the marker expression profile of EPDCs, PrimeFlow was performed on tdTomato+ hearts (Fig 5.7 A). Two probe combinations were used: *Sema3d/Wt1/Tcf21* and *Sema3d/Scx/Tbx18*. Cells were positively selected for tdTomato expression and the expression of each marker was quantified at each of the four embryonic stages.

At E11.5, the tdTomato+ fraction represented the epicardium (>95%) and was positive for all marker genes (Fig 5.7 B, Appendix Fig 5.4). From E13.5, an EPDC population started to emerge, as indicated by tdTomato staining inside the heart and by the appearance of a population of cells in the FACS plots that downregulated *Wt1, Sema3d, Tbx18* and *Scx*, but retained *Tcf21*. All EPDCs expressed *Tcf21* at E13.5, however, from E15.5, *Tcf21* was lost in a small fraction of EPDCs, coinciding with the formation of epicardium-derived mural cells [130]. Quantification of the number of cells found in each fraction revealed the EPDC population increased throughout development, exceeding the number of epicardial cells from E15.5 onwards (Fig 5.7 C).

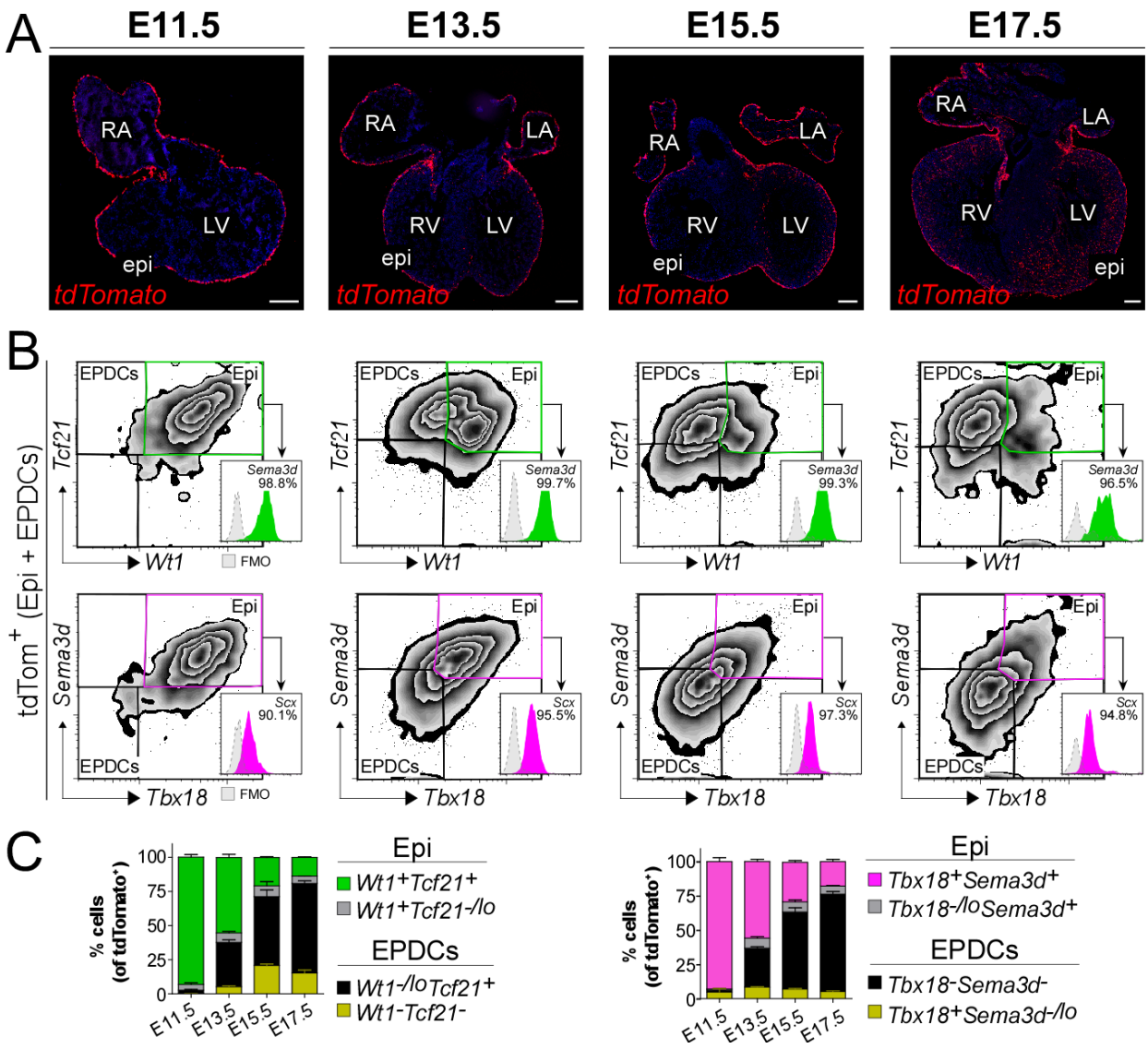


Figure 5.7 EPDCs downregulate expression of epicardial markers.

*(**A**) RNA ISH staining of E11.5, E13.5, E15.5 and E17.5 heart sections reveal tdTomato labelling of the epicardium and lineage-traced EPDCs (n=>3). (**B**) Flow cytometric analysis of dissociated E11.5 (n=31 hearts, three experiments), E13.5 (n=25 hearts, three experiments, E15.5 (n=10 hearts, two experiments) and E17.5 hearts (n=2 hearts, two experiments).TdTomato+ cells, representing the epicardial lineage, selected by gating CD31$^-$cTnT$^-$tdTomato$^+$, show overall loss of Sema3d, Wt1, Tbx18, and Scx as EPDC production increases. Cells co-expressing Sema3d, Wt1, Tcf21, Tbx18, and Scx (green and purple) represent the epicardium. (**C**) Populations expressing Sema3d, Wt1, Tcf21, Tbx18, and Scx, calculated as a proportion of tdTomato$^+$ cells, demonstrate gradual expansion of the EPDC fraction as development progresses. (n= as B; data shown as mean ± SEM of at least two experiments).*

To further assess marker expression during EPDC differentiation, and to investigate a link between certain markers and cell fate choice, single-cell RNA-sequencing was performed on tdTomato+ FACS sorted cells from E15.5 hearts using the SMART-Seq2 protocol [187]. E15.5 is the embryonic stage when epicardial EMT ceases and EPDCs start differentiating [92,130].

Cells were divided into five identity clusters using differentially expressed genes as revealed by PCA in Seurat [184,185] (Fig 5.8 A). A cell cycle regression workflow was run in Seurat to separate the cells found in S/G2/M from cells in G1 to mitigate the effects of cell cycle stage on heterogeneity, but preserve the information about proliferation state [261]. This resulted in the presence of a proliferative cluster, marked by the expression of S/G2/M genes such as *Top2a.* The epicardial cluster (Epi) was identified based on the presence of mesothelial genes such as *Upk3b* [124,262]. Two EPDC clusters were present, one expressing genes found in the subepicardial mesenchyme, such as *Dhrs3* [124], whereas the second (EPDCs2) expressed more mature mesenchymal genes, such as *Postn* [124] . A mural cluster was identified based on expression of pericyte and vSMC genes, such as *Cspg4* (NG2) [263] and *Rgs5* [264].

A dot plot was used to show expression of selected markers in the different clusters (Fig 5.8 B). The percentage of cells positive for each marker was calculated for the Epi cluster (Fig 5.8 C). *Sema3d* and *Wt1* were expressed in 100% of epicardial cells; similar to mesothelial genes (*Upk3b, Upk1b*), however, their expression decreased in the EPDC clusters (Fig 5.8 D). *Tcf21* was low in the epicardium, whereas expression increased in the EPDC clusters. *Tbx18* was mainly found in the epicardium and in the mural clusters. *Scx* was restricted to the Epi cluster, but its expression was very low. These findings confirmed the results obtained with PrimeFlow and RNAscope (Fig 5.8 E).

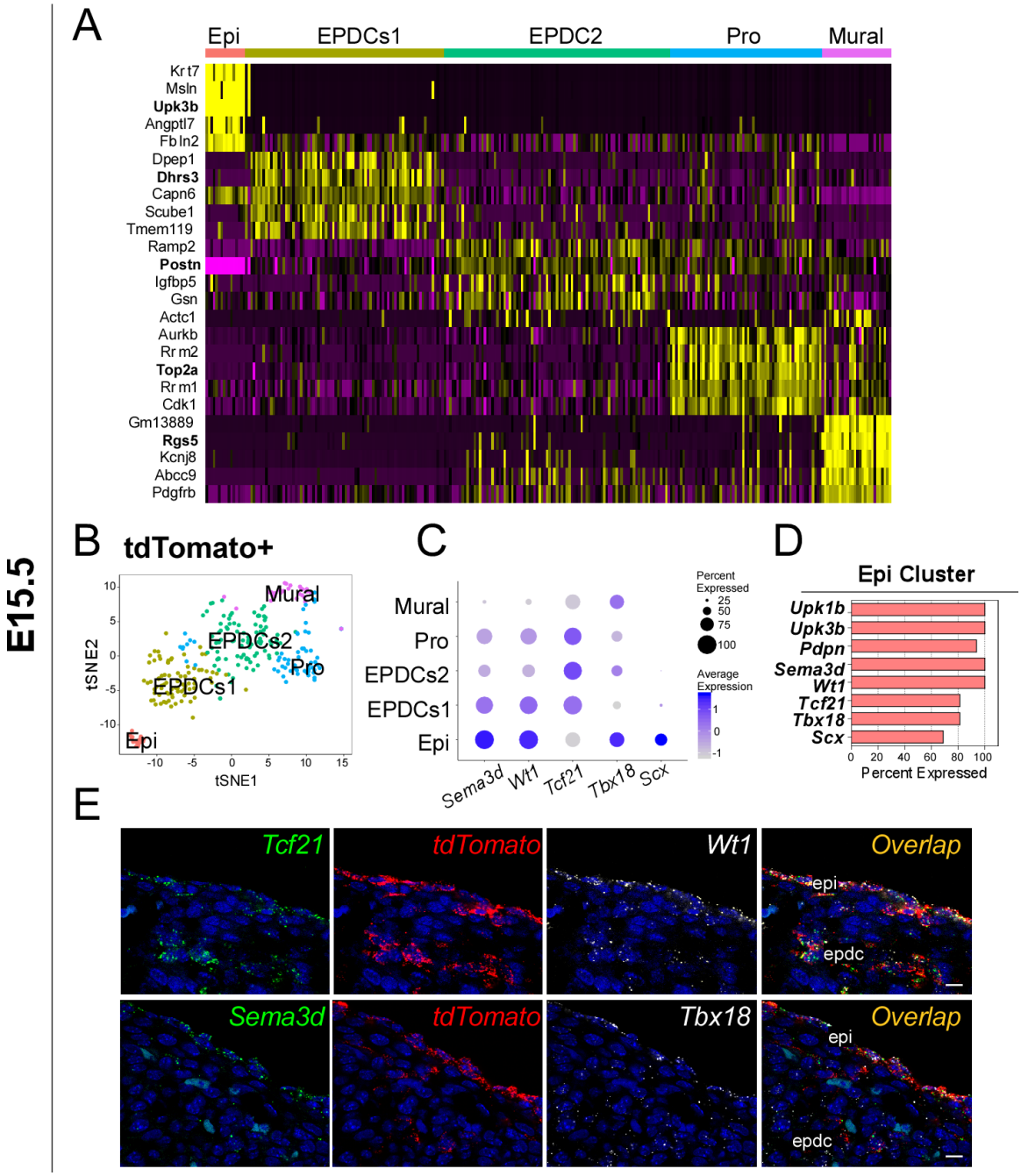


Figure 5.8 E15.5 Single cell RNA-sequencing of the epicardial lineage

(A) *Heatmap of top 5 differentially expressed genes per cluster in the E15.5 single-cell RNA sequenced tdTomato⁺ FACS sorted cells at E15.5 (total 265 cells; n=6 hearts). High expression is indicated in yellow* ***(B)*** *tSNE plot showing clustering of epicardial (Epi), epicardium-derived cells (EPDCs1 and EPDCs2), mural and proliferating (Pro) cells.* ***(C)*** *Dot plot showing proportion of cells in each cluster expressing epicardial markers.* ***(D)*** *Percentage of cells within the epicardial cluster (Epi) expressing selected epicardial genes.* ***(E)*** *RNA ISH shows expression of Tcf21, Wt1, Sema3d and Tbx18 in the epicardium and EPDCs, labelled with tdTomato. Scale bar: 10 μm.*

Pseudotime analysis of epicardial markers

Monocle2 [190] was used to reconstruct the differentiation trajectory of epicardial cells in pseudotime. The trajectory consisted of two branches, one enriched for mural cluster cells (branch A), whereas the other was associated with EPDC cluster 2 (branch B) (Fig 5.9 A). Branch A was associated with mural cell fate, expressing genes such as *Pdgfrβ* and *Rgs5* [81,264], whereas branch B contained cells expressing fibroblast-like genes such as *Pdgfrα* and *Dermatopontin* (*Dpt)* (Fig 5.9 B) [265].

The expression of the selected markers *Sema3d, Wt1, Tcf21, Tbx18 and Scx* was visualised across pseudotime. None of the markers exhibited branch-specific expression, indicating marker expression is not sufficient to restrict cell fate choice (Fig 5.9 C). In addition, the branch point was present after the emergence of EPDCs, suggesting cell fate choice takes place after EMT.

Very few *Pecam*1+ cells were detected in the single-cell RNA-Seq data, therefore, flow cytometry was used to determine the contribution of the epicardial lineage to the coronary endothelium at E17.5 (Fig 5.9 D). Natriuretic peptide receptor 3 (*Npr3)*, a gene expressed only in the endocardium [80], was used to exclude endocardial cells from the analysis. Only 3.39% (+/-0.28% SEM, n=6) of the PECAM1+*Npr3*- cells were positive for tdTomato, indicating that contribution of the epicardium to the coronary endothelium is negligible.

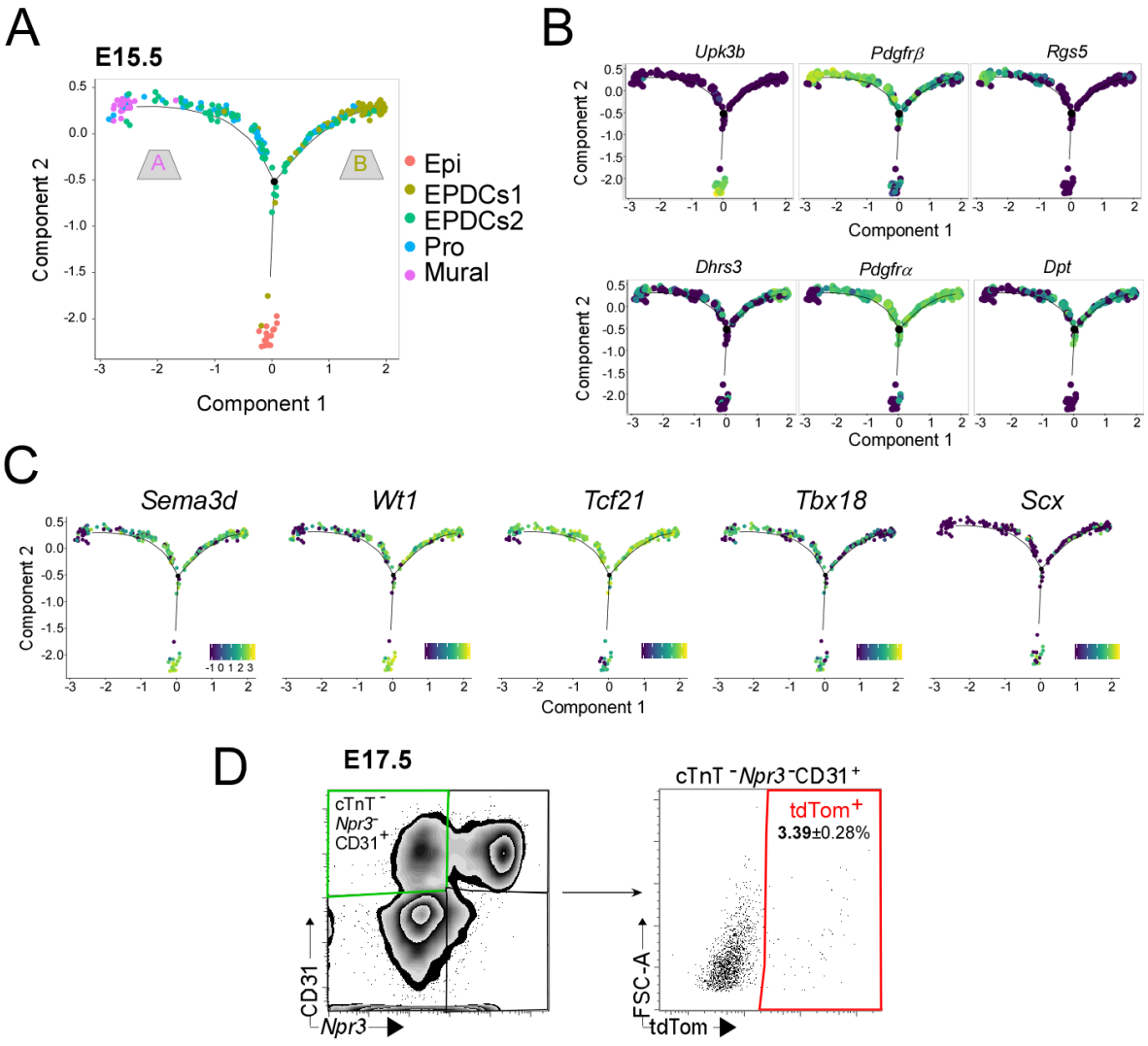


Figure 5.9 Epicardium-derived cell fate choice and marker expression

(A) *Pseudotime trajectory of tdTomato⁺ cells at E15.5, showing two fates, branch A (mural) or branch B (EPDCs1).* ***(B)*** *Visualisation of selected genes in pseudotime reveals one epicardial origin (Upk3b+) and two potential cell fates, one associated with mural genes (Pdgfrβ and Rgs5) and one associated with mesenchymal/fibroblast fate (Pdgfrα and Dpt).* ***(C)*** *Pseudotime trajectory coloured by expression level of epicardial marker genes.* ***(D)*** *Flow cytometric analysis of dissociated E17.5 Wt1^{CreERT2}; Rosa^{26tdTomat} hearts. Endothelial cells were selected by gating cTnT^{-}Npr3^{-}CD31^{+}. Gating for tdTomato^{+} was used to determine epicardial contribution. Percentage expressed as mean ± SEM (n=6 hearts). EPDCs-epicardium-derived cells; Epi-epicardium; Pro-proliferative.*

5.2.4 Epicardial markers are not altered in SRSF3 mutants

To determine if SRSF3 depletion alters the expression of epicardial markers, RNAscope was performed on E9.5 *Tg(Gata5-Cre); Srsf3*$^{fl/fl}$ mutants (Fig 5.10 A) and E12.5 *Wt1*^{CreERT2}*; Srsf3*$^{fl/fl}$ mutants (Fig 5.10 B). No change was detected in the expression level of *Sema3d, Tcf21, Scx or Wt1* in mutant cells, indicating SRSF3 loss does not alter epicardial identity.

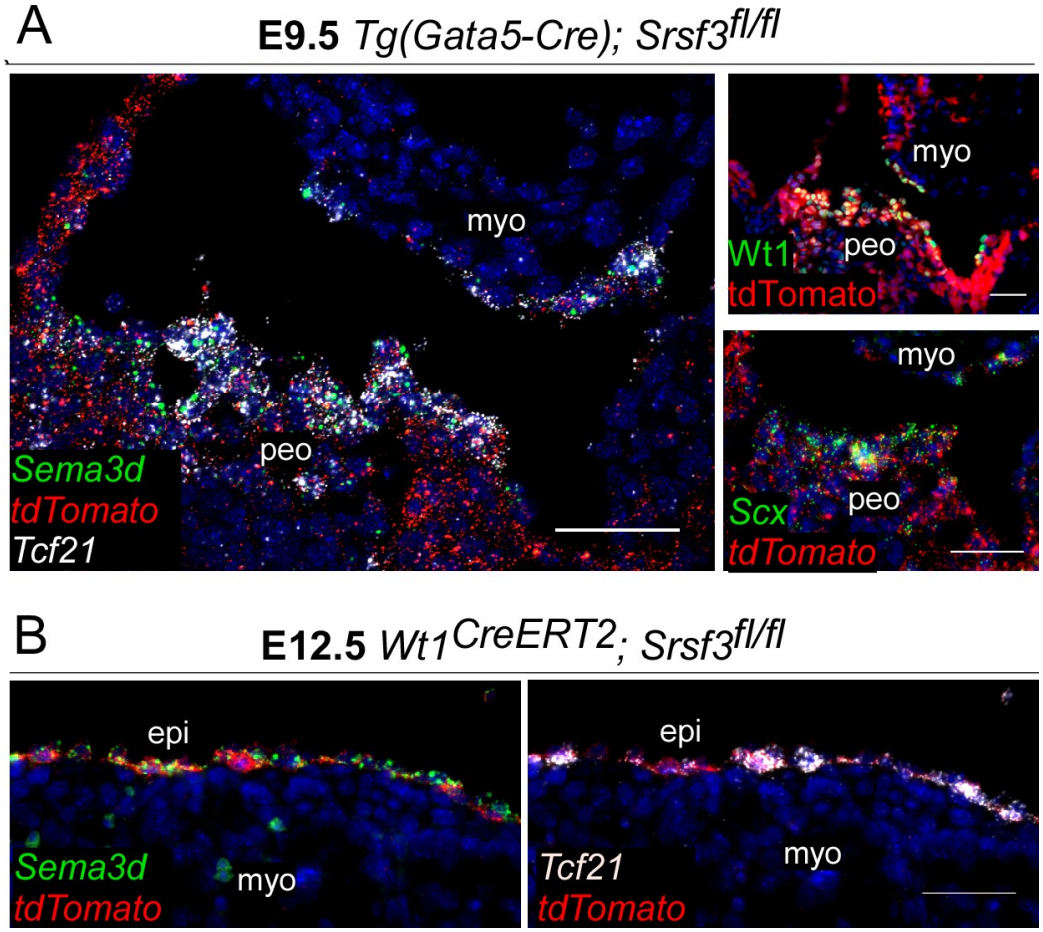


Figure 5.10 SRSF3 loss does not alter epicardial marker profile

(A) *Immunostaining and RNA ISH reveals Tg(Gata5-Cre); Srsf3*$^{fl/fl}$ *E9.5 mutant proepicardial cells express all tested proepicardial markers (Sema3d, Tcf21, WT1, Scx). N=2.* ***(B)*** *RNA ISH shows E12.5 Wt1*^{CreERT2}*; Srsf3*$^{fl/fl}$ *mutant epicardial cells express Sema3d and Tcf21. peo-proepicardial organ, myo-myocardium, epi-epicardium. n=2. Scale bar: 50 μm.*

5.3 Discussion

5.3.1 Expression of proepicardial markers in the developing heart

PEO

The data presented shows the proepicardial markers *Wt1, Tcf21, Tbx18, Sema3d* and *Scx* are co-expressed on the apical side of the ST, where the PEO is specified. Moreover, all cells that transfer onto the heart to give rise to the epicardial layer express all selected markers, as indicated by RNAscope *in situ* hybridization and single-cell RNA-sequencing.

These results challenge other studies that reported non-overlapping PEO expression of the markers [68]. The contrasting findings could reflect a failure to distinguish the PEO from the rest of the ST mesenchyme. Unfortunately, there are no anatomical or molecular boundaries that define the PEO [69] and frequently used markers, such as WT1 or TBX18, are also expressed in other progenitor populations found in the ST, such as hepatic primordia[256] and cardiomyocyte precursors [72].

In addition, previously reported non-overlapping patterns are largely based on immunostaining, which relies on the efficiency and specificity of antibodies and on the presence of the protein [68,120]. However, Cre lines only use the regulatory sequences of marker genes, therefore, the Cre recombinase does not undergo the same post-translational regulation as the endogenous protein, making mRNA expression a more accurate representation of Cre activity.

The controversy surrounding proepicardial contribution to the coronary endothelium, ranging from 0% with *Tbx18*^{Cre} or *Tcf21*^{Cre} to over 20% with *ScxCre* and 7% with *Sema3d*^{Cre} is possibly due to endothelial precursors existing in the ST that do not contribute to the heart via the epicardium. All proepicardial lines used to report endothelial contribution also trace cells in the sinus venosus/endocardium, indicating precursors might contribute directly to these vasculogenic sources [68,69]. This hypothesis also explains why PEO/ST explants can differentiate to endothelial cells, whereas no endothelial cells were ever found in epicardial explants [78,266,267].

Epicardium

Analysis of selected markers throughout development using RNAscope and PrimeFlow revealed overlapping expression of *Wt1, Tcf21, Sema3d, Tbx18* and *Scx* in the early epicardium. *Scx* was the first downregulated marker, its expression being dramatically reduced in the epicardium from E10.5, confirming published data [68]. *Tcf21* was the next marker to be downregulated starting at E13.5 and almost completely lost in some cells by E15.5, coinciding with the arrest of epicardial EMT [92]. The other markers were also downregulated throughout development, but at the same rate in all epicardial cells. No sub-populations were found in the epicardium at any of the stages analysed.

Non-specific expression

Assessment of marker expression throughout the heart revealed widespread presence in non-epicardial domains. *Tbx18* was found in a subset of cardiomyocytes and vSMCs, both in coronary vessels and aorta (epicardium-derived and non-epicardium derived cells) indicating *de novo* expression in this cell type. *Tcf21* was found in interstitial cells and epicardium-derived mesenchyme, whereas *Scx* and *Sema3d* were detected in the AVCu. *Wt1* started to be expressed in coronary endothelium from E13.5.

These results highlight the concern with using constitutive Cre lines to track epicardial lineages based on the regulatory sequences of these genes. None of the selected markers are specifically expressed in the epicardium, therefore, temporal control of Cre activity is crucial to limit non-specific labelling.

5.3.2 Specification of cell fate in epicardium-derived cells

The pseudotime analysis indicated EPDCs downregulate *Wt1, Sema3d, Tbx18* and increase *Tcf21*, whilst maintaining mesenchymal state until differentiation to mural or fibroblast fate.

TCF21 did not seem to specify fibroblast fate since all EPDCs expressed *Tcf21* and downregulation only took place post-differentiation to mural fate. This is in contradiction with a previous report, where TCF21 null mice had PDGFRβ+ cells present in the heart, whereas PDGFRα+ cells were missing, leading to the conclusion that TCF21 is only active in fibroblast progenitors [81]. However, another study reported TCF21 null mice do not form an epicardium, preventing EMT altogether [254]. The recent finding that endocardial cells can contribute mural cells to the heart [94] could indicate that PDGFRβ+ cells found in TCF21 nulls were derived from this compartment and not from TCF21-ve epicardial cells. Future studies using Wt1-CreERT2 to conditionally delete *Tcf21* and trace epicardial cells should solve this controversy.

5.3.3 Conclusions

In conclusion, these data suggest that epicardial cells are not heterogenous based on the expression of selected ‘canonical’ markers, and EPDC fate choice is not pre-determined before EMT. Loss of SRSF3 in epicardial cells does not alter epicardial identity and does not lead to differences in marker expression.

Chapter VI.

Single-cell transcriptomics to explore the molecular mechanisms of SRSF3 function in the epicardium

6.1 Background

6.1.1 Coronary vessel development

Extensive research has been dedicated to understanding how the coronary vasculature forms. Recent discoveries based on genetic lineage tracing irrevocably showed the sinus venosus (SV) and the endocardium are the main contributors of coronary endothelium in the heart, disputing the conventional view the proepicardium is the main source of coronary endothelial cells (CECs) [58,77,78,80,95]. These studies also revealed the coronary vasculature is remarkably compartmentalised, with SV-derived vessels irrigating the outer muscle wall, whereas coronaries originating from the endocardium populate the interventricular septum (IVS) and the inner muscle wall [58,77].

In spite of the origins of coronary endothelium being uncovered, the molecular mechanisms that drive coronary vessel formation are still not entirely understood. Multiple reports have indicated epicardium-derived signals are required to activate sprouting from the SV [77,86] , with other factors, such as myocardial compaction and ECM secretion from epicardium-derived mesenchyme, guiding vessel growth [124,139]. Nonetheless, further investigation is required to understand how all these signals are integrated to achieve successful coronary vasculature formation.

In contrast to the SV, the endocardium relies on hypoxia and VEGF-A signalling to deploy several mechanisms to transition to CECs: sprouting [86,228], budding/blood island formation[78] and compaction/entrapment [58]. These different mechanisms seem to be dependent on spatiotemporal cues, with sprouting being used during embryonic development to contribute vessels to the outer wall, whereas compaction is activated postnatally. How these distinct modes of vessel growth are initiated remains unknown.

The epicardial contribution to coronary endothelium is still under debate. *In vivo* studies have shown epicardial contribution to endothelium is negligible [65,67,81,91], yet, cultured epicardial cells have the potential to become endothelial cells [227]. What prevents this differentiation *in vivo* is unclear, however, data presented in chapter IV indicated that epicardium-derived cells (EPDCs) can differentiate to CECs in the presence of genetic changes.

6.1.2 Single-cell RNA-sequencing

The development of single-cell RNA-sequencing technologies in recent years has provided an unprecedented ability to understand behavior of individual cells, which is essential for deciphering complex biological systems. SMART-Seq2 [187] and 10x Chromium [268] sequencing are the most established single-cell transcriptomics techniques, each with its own advantages and limitations (Fig 6.1).

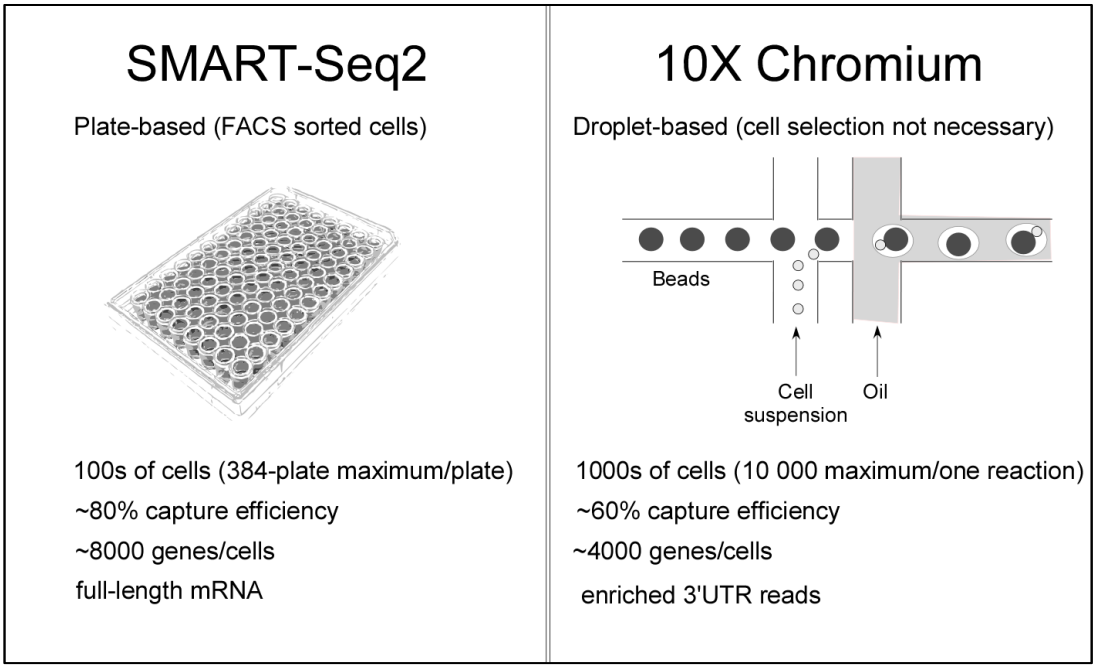


Figure 6.1 Comparison between single-cell transcriptomic techniques.

SMART-Seq2 allows sequencing of hundreds of cells, having a better capture rate and returning superior quality data with more genes/cell and full-length transcripts than 10x Chromium. However, 10x Chromium allows sequencing of thousands of cells, being less labour intensive due to bulk processing of samples.

6.1.3 Aims

The aim of this chapter was to investigate the molecular mechanisms involved in epicardium-derived cell differentiation in E9.5/E11.5 tamoxifen-induced *Wt1*^{CreERT2}*; Srsf3*$^{fl/}$ mutants using single-cell RNA-sequencing.

6.2 Results

6.2.1 Tamoxifen induction at E9.5/E11.5 results in increased tdTomato+ endothelial cells in *Wt1*^{CreERT2}; *Srsf3*$^{fl/fl}$ hearts

Induction of SRSF3 deletion at different developmental timepoints in *Wt1*^{CreERT2};*Srsf3*$^{fl/fl}$ embryos led to a range of phenotypes dependent on the timing of tamoxifen administration, as presented in Chapter IV.

The most intriguing phenotype emerged after tamoxifen was administered at E9.5 and E11.5, which resulted in tdTomato+ CECs throughout the entire compact layer by E17.5, suggesting EPDCs differentiated to endothelium (Figure 6.2 A). CECs in mutant hearts were rounded (Fig 6.2 B), which suggests the cells were less mature and not yet subjected to shear stress, which is known to promote elongated morphology [269]. CECs in the IVS were negative for tdTomato, indicating they did not originate from the epicardium. The IVS vessels are endocardial-derived, whereas vessels in the outer myocardial wall mainly originate from the SV [58,77]. The SV is dependent on epicardium-derived signals to initiate sprouting [77,86], therefore, it is likely SRSF3 loss in the epicardium affects sinus venosus sprouting.

Another possibility for the appearance of tdTomato+ endothelium is ectopic labelling of CECs with tamoxifen dosing at E9.5/E11.5. Staining for estrogen receptor α (ERα) was used to determine the period of tamoxifen activity. ERα tags the Cre and has a cytoplasmic localization when it is not active [70]. Upon tamoxifen induction, the ERα-Cre complex translocates to the nucleus and mediates recombination. The first stage tdTomato+ CECs were detected in mutant hearts was E15.5 (Appendix Fig 6.1 A). The ERα was cytoplasmic at this stage (Appendix Fig 6.1 B), indicating the Cre is not active when tdTomato+ CECs appear.

Since EPDCs normally contribute to mural cells and fibroblasts [65,81], IHC and RNAscope, a commercially available *in situ* hybridisation technique, were used to examine EPDCs differentiation to these fates in mutant hearts.

Multiple pericyte and vSMC markers were tested to assess mural cell contribution. EPDCs are known to first differentiate to pericytes that later become vSMCs [130]. The pericyte marker NG2 was found around vessels in both controls and mutants, however, NG2 was also found in cardiomyocytes [263] , which was problematic when distinguishing pericytes from surrounding cells (Fig 6.2 C). SM-MHC was used to check presence of vSMCs and no difference was found between control and mutant hearts (Appendix Fig 6.2). However, SM-MHC only stains mature arteries [270], therefore, SM22α was used to investigate the smooth muscle coverage of smaller vessels [178]. SM22α was present around vessel-like structures in mutants, however, there were fewer SM22α+tdTom+ cells in the rest of the heart (Fig 6.2 C).

Differentiation to cardiac fibroblasts was assessed using an RNAscope *in situ* probe against *Tcf21*. TCF21 is a known marker of CFs [81,120]. TCF21 is also present in epicardial cells and mesenchymal cells and it is upregulated in CFs. There were fewer tdTomato+ cells that had high levels of *Tcf21* in mutant hearts (Fig 6.2 D), indicating failure of EPDCs to differentiate to CFs. *Tcf21*+ cells that were negative for tdTomato were still present in mutants near the endocardium. Recently, the endocardium has been shown to contribute 20% of CFs [271,272], therefore, CFs in mutant hearts could still originate from here. These results indicated that EPDCs differentiate to CECs instead of CFs and potentially vSMCs.

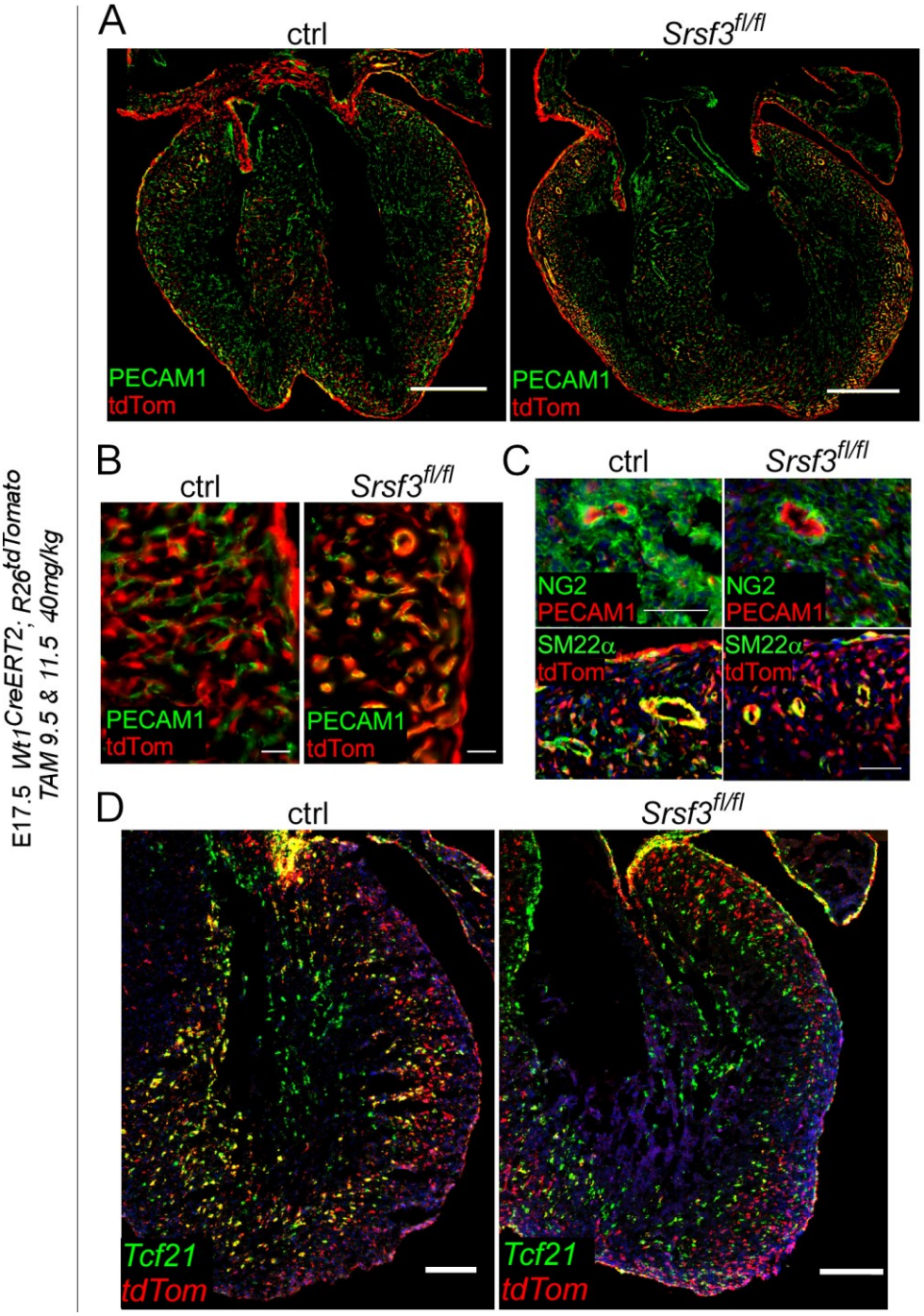


Figure 6.2 TdTomato+ cells switch cell identity in *Wt1^{CreERT2}; SRSF3$^{fl/fl}$* mutants

(A) *Immunostaining for PECAM1 was performed on control and mutant sections from E17.5 embryos. In mutant sections, more PECAM1+ cells were tdTomato+. Scale bar: 500 µm.* ***(B)*** *Higher magnification of PECAM1 staining. Scale bar: 50 µm.* ***(C)*** *Immunostaining for NG2 shows expression in pericytes and cardiomyocytes. SM22α is present around vessels. Scale bar: 100 µm.* ***(D)*** *RNAscope for Tcf21 was performed on E17.5 heart sections. In mutant sections, the tdTomato cells did not overlap with the cardiac fibroblast marker Tcf21. Scale bar: 500 µm.* ***(A-D)*** *n=4.*

6.2.2 Sprouting from the SV and the endocardium is impaired in *Wt1*^{CreERT2}; *Srsf3*$^{fl/fl}$ mutants

Analysis of E17.5 SRSF3 mutant hearts tamoxifen induced at E9.5/11.5 indicated a large percentage of CECs were epicardium-derived. However, the main sources of CECs in embryonic hearts are the sinus venosus and the endocardium [58,77].

To determine the endothelial contribution from conventional sources in mutant hearts, whole-mount PECAM1 staining was performed at E13.5 (Fig 6.3 A). This type of analysis has been extensively used to assess sinus venosus sprouting [77,86,273]. Mutant hearts had significantly reduced vessel coverage at E13.5 compared to littermate controls (Fig 6.3 B), indicating sprouting defects from the sinus venosus.

The failure to sprout is likely due to SRSF3 depleted epicardial cells not producing factors required to promote vessel growth. One such factor is VEGF-C, which has been reported to be secreted by the epicardium to initiate sinus venosus sprouting [77]. However, RNAscope against *Vegfc* showed no decrease in *Vegfc* expression in mutants and revealed VEGF-C is produced not only in the epicardium, but also in myocardial cells (Fig 6.3 C).

There are no sprouting assays available for endocardial cells, however, it was recently reported that endocardial cells destined to sprout into the compact layer express SOX17 [86]. IHC for SOX17 and the endocardial marker Endomucin [234] (EMCN) revealed significantly fewer SOX17+EMCN+ cells in E13.5 mutant hearts (Fig 6.3 D, E), suggesting that endocardial contribution to CECs to the outer wall in mutants may also be reduced.

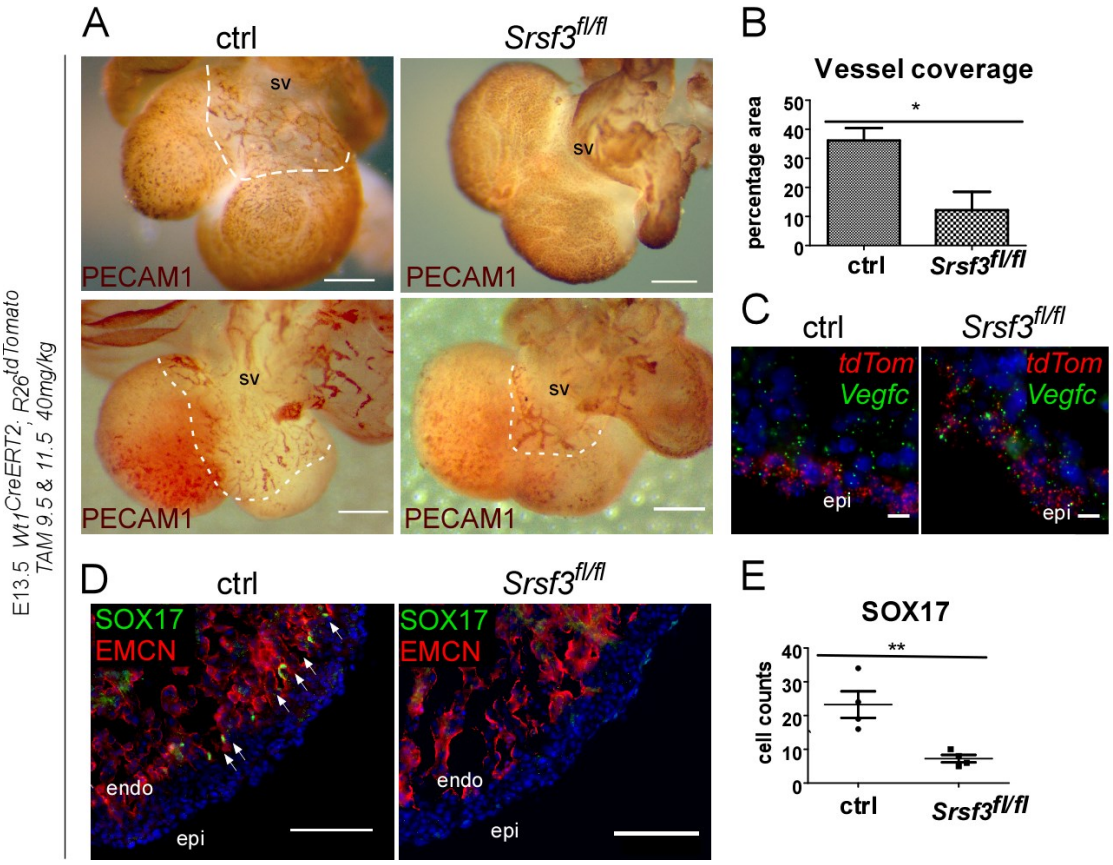


Figure 6.3 *Wt1*^{CreERT2} targeted SRSF3 mutants have impaired coronary endothelium formation

(A) *PECAM1 whole-mount staining was performed on E13.5 hearts from controls and Wt1*^{CreERT2} *E9.5/11.5 targeted SRSF3 mutants. The mutants had fewer surface vessels. Scale bar: 500 µm.* ***(B)*** *Quantification of area covered by vessels as a percentage of total surface area. n=3. Student's t test. P<0.05 (*).* ***(C)*** *RNAscope against Vegfc and tdTomato shows no difference in Vegfc production in mutant hearts. n=2. Scale bar: 10 µm.* ***(D)*** *Immunostaining for SOX17 and Endomucin (EMCN) was performed on E13.5 controls and Wt1*^{CreERT2} *targeted SRSF3 mutants. The SRSF3 mutants have fewer SOX17+ endocardial cells. Arrows point to SOX17+ EMCN+ cells. Scale bar: 50 µm.* ***(E)*** *Quantification of the number of SOX17+ endocardial cells in controls vs mutants. n=4, whole heart frontal sections. Student's t-test. P<0.01(**). sv-sinus venosus, epi-epicardium, endo-endocardium.*

6.2.3 Unbiased single-cell RNA-sequencing of whole hearts at E13.5

Identification of cell populations

Whole hearts were sequenced at E13.5 using Chromium 10X technology to investigate the consequences of SRSF3 loss in epicardial cells and gain insight into the global changes present in mutant cardiac tissue since coronary sprouting defects were detected at this stage. Unfortunately, due to a technical error, fewer mutant cells (4606) were captured compared to control (8212). Because of the lower number of cells captured, the mutant sample was sequenced at higher depth, leading to an average of 3970 genes/cell for mutant cells as compared to 3151 genes/cell for control (Fig 6.4 A).

Principal component analysis (PCA) using cell cycle-associated genes revealed that cells clustered dependent on their cell cycle stage. To avoid heterogeneity due to cell cycle stage, a workflow that regresses differences in expression between cells in S and G2/M was used [261]. This way, differences in cell cycle stage were removed, yet proliferating cells (S/G2/M) were kept separate from non-actively proliferating ones (G1/G0) to preserve information about progenitor states (Fig 6.4 B).

After cell cycle regression, clustering based on the significant principal components was used to separate cells into similar identities. The cells were divided into 23 clusters, falling under eight major classifications (Fig 6.4 C). Most cells were cardiomyocytes (CM) expressing myosin-related genes such as *Myl1* [274]. Sub-clusters included atrial cardiomyocytes expressing *Sln* [275], *Tbx5* [276], trabecular cardiomyocyte expressing *Irx3* [277], *Nppa* [49], *Gja5* [139], ventricular compact cardiomyocytes expressing *Myl3* [278], *Mycn* [139] and atrioventricular canal (AVC) cardiomyocytes expressing *Rspo3* [279] and *Bmp2* [46]. The next most abundant classification was endocardium (Endo), identified by the presence of *Emcn* and *Npr3* [80], with endocardial-to-mesenchymal transition (EndoMT) subclusters expressing *Prox1* [124] and *Klf2* [280].

Most of the remaining cells were mesenchymal, with valve/cushion mesenchyme expressing *Postn* [281], *Sox9* [282], *Twist1* [45], whereas epicardium-derived cell mesenchyme (EPDC) had *Dcn* [283], *Ptn* [124] and other ECM-related genes. Other clusters included epicardium (Epi) identified based on mesothelial markers such as *Upk3b* [262], endothelium (ECs) expressing *Cdh5*, *Fabp4* [284], macrophages (MΦ) expressing *Mrc1* [124] and *Alcam* [285], white blood cells (WBCs) expressing complement genes, red blood cells (RBCs) expressing haemoglobins and platelets (Plt) expressing platelet factor 4 (*Pf4*).

Multiple methods were tested to visualise the clusters in two dimensions. UMAP (Uniform Manifold Approximation and Projection for Dimension Reduction) performed best when processing such complex data (Fig 6.4 D), being superior to tSNE (T-distributed Stochastic Neighbour Embedding) clustering that only preserved distances locally but failed to represent differences globally (Appendix Figure 6.3).

The number of cells assigned to each identity in mutants was compared to controls (Fig 6.4 E). Fewer EPDCs and valve mesenchyme cells were recovered in the mutant dataset, however, the number of proliferating EPDC and valve cells was similar, indicating decreased EPDC formation and contribution to the valves at this early stage. The mutant dataset also contained fewer macrophages and more circulating cells, which could indicate residual blood inside the heart, despite red blood cell lysis being performed prior to sequencing.

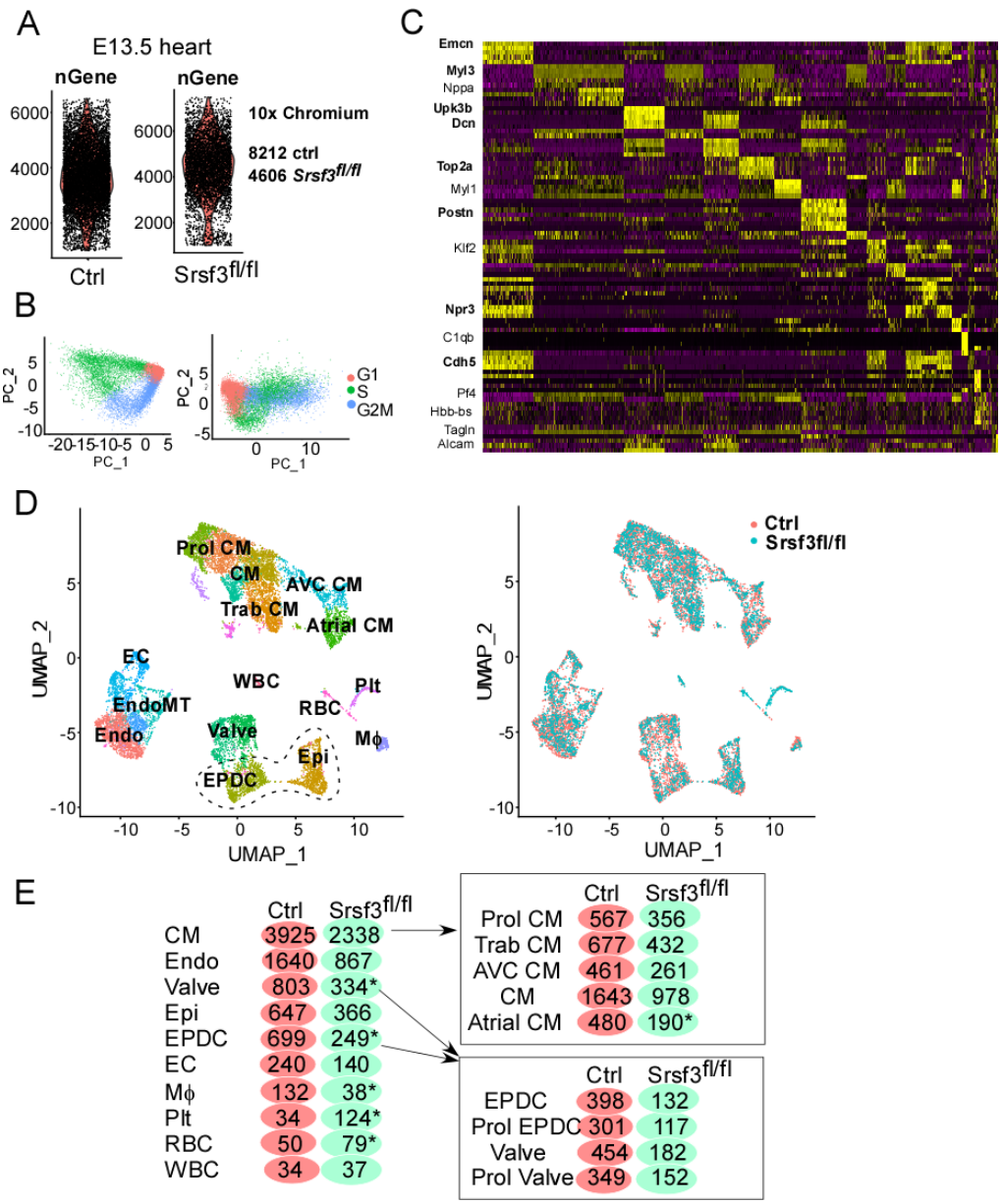


Figure 6.4 Single-cell RNA-Seq on E13.5 whole-hearts from controls and *Wt1*^{CreERT2}; *Srsf3*$^{fl/fl}$ mutants

(A) *Violin plot showing the number of genes per cell from 10x Chromium data performed on whole-hearts from controls (n=3) and mutant (n=2) hearts.* ***(B)*** *Principal component plots indicating clustering on the cells based on cell cycle genes before cell cycle regression and after.* ***(C)*** *Heatmap showing selected differentially expressed genes in the 23 identified clusters.* ***(D)*** *UMAP plot showing the different major clusters in 2D.* ***(E)*** *The number of control and mutant cells per identity. Chi-squared test, p<0.0001(*). MΦ-macrophages; ECs-endothelial cells; Endo-endocardial cells; EndoMT-endocardial-to-mesenchymal transition; Epi-epicardium; CM-cardiomyocytes; Prol CM-proliferative CM; Trab CM- trabecular CM; AVC CM-atrioventricular canal CM; EPDC-epicardium-derived cell; WBC-white blood cell; RBC-red blood cell; Plt-platelet.*

In order to confirm the differences in cellular composition identified by the single-cell RNA-Sequencing, IHC was used. The number of EPDCs inside E13.5 mutant hearts was decreased both apically and in the atrioventricular groove region, as revealed by tdTomato IHC (Fig 6.5 A, B). The mitotic marker pHH3 showed lower proliferation in ventricular walls in mutants (Fig 6.5 A), however, further studies are required to confirm the presence of pHH3 in cardiomyocytes and allow quantification. Assessment of mitotic cells in other populations such as EPDCs was not possible in section, due to the small number of cells actively undergoing mitosis in controls. More blood cells were noticed inside the lumen in mutant sections, confirming the single-cell RNA-Seq data; the trabeculae were disorganised and the compact layer reduced, as shown by EMCN staining (Fig 6.5 B). Aberrant trabecular formation can lead to contraction problems [49] , which could explain the presence of trapped blood inside the heart.

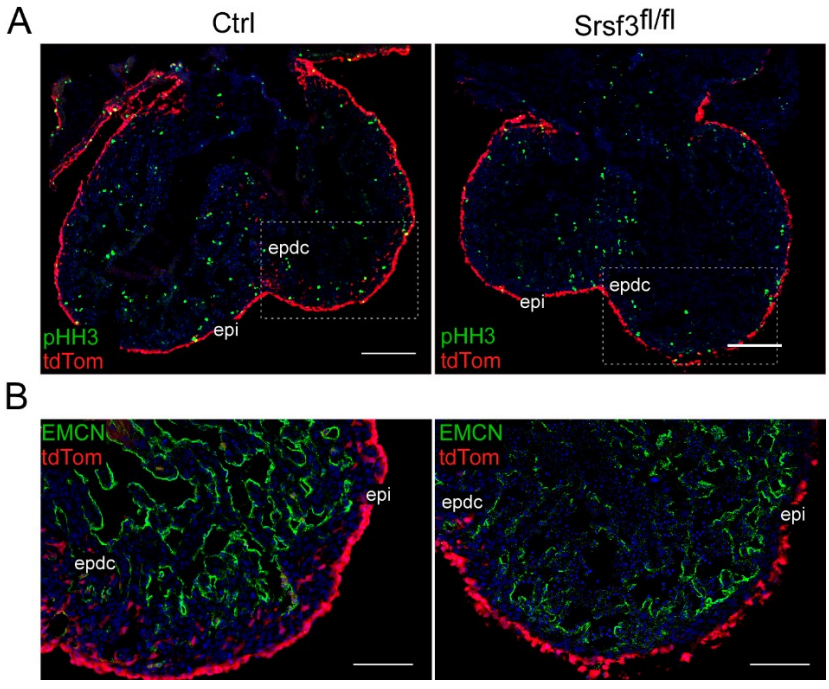


Figure 6.5 Trabeculae are disorganised in E13.5 *Wt1*^{CreERT2}*; Srsf3*$^{fl/fl}$ mutants

(A) *Immunostaining for pHH3 and tdTomato reveals less pHH3+ cells in mutants. n=2. Scale bar: 100 µm.* ***(B)*** *Immunostaining for Endomucin (EMCN) and tdTomato shows disorganised endocardium and fewer tdTomato+ cells inside mutant hearts. n=4. Scale bar: 50 µm. epdc-epicardium-derived cell, epi-epicardium.*

E13.5 *Wt1*^{CreERT2}*; Srsf3*$^{fl/fl}$ mutant hearts are hypoxic

To understand how the epicardial lineage is directly affected by the loss of SRSF3, the epicardial and EPDC clusters subset was analysed separately for control and mutant. The clusters divided into proliferative and non-proliferative sub-clusters. An extra epicardial cluster (Epi2) was detected in mutants (Fig 6.6 A). Differential gene expression indicated Epi2 expresses multiple genes associated with hypoxia such as *Slc2a1* (GLUT1), *Vegfa* and hypoxia-induced cell death genes like *Fam162a* (Fig 6.6 B). IHC for the apoptotic marker cleaved-caspase 3 (CC3) showed no increase in mutants, revealing Epi2 does not undergo caspase-dependent apoptosis (Appendix Fig 6.4).

Apart from hypoxia-related genes, this cluster also had significantly higher expression of tdTomato, suggesting these cells were probably first to recombine and most likely to have lost SRSF3 (Fig 6.6 C). Unfortunately, *Srsf3* reads could not be used to confirm this finding, because the *Srsf3* mutation is an in-frame deletion of exon2 and 3 and Chromium 10x technology does not return the whole length of the mRNA transcript, most reads being assigned to the 3'UTR [286] . To confirm SRSF3 depleted cells were present at this stage, epicardial explants were used. IHC for SRSF3 detected decreased expression in several cells in mutant explants (Fig 6.6 D). The E13.5 mutant explants were smaller than controls, consistent with the role of SRSF3 in epicardial proliferation discussed in Chapter III (Fig 6.6 E).

Of importance, expression of *Slc2a1* was also increased in the other mutant clusters as compared to control (Fig 6.6 F). GLUT1 IHC was used to confirm this result (Fig 6.6 G). In controls, GLUT1 was found mainly in the IVS and in the atrioventricular cushion, confirming other reports about hypoxic regions in E13.5 hearts [287]. In mutants, GLUT1 was widespread in the myocardium, indicating mutant hearts are more hypoxic overall.

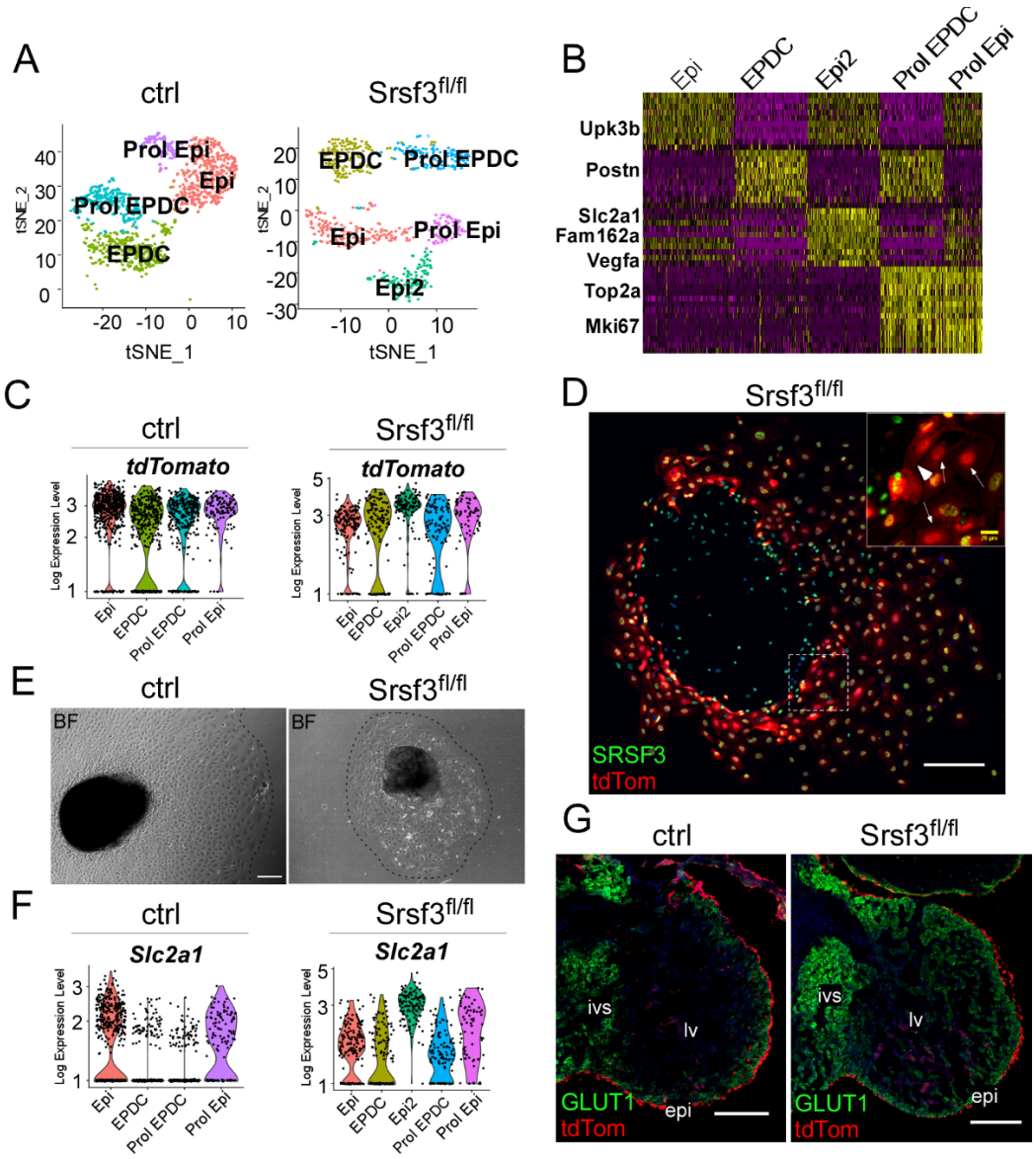


Figure 6.6 Iterative clustering of the epicardial lineage reveals increased hypoxia in E13.5 *Wt1*^{CreERT2}*; Srsf3*$^{fl/fl}$ mutant hearts.

(A) *tSNE plots of the epicardial and EPDCs clusters subset re-analysed separately for control and mutants. The mutants present an extra epicardial cluster associated with hypoxia-related genes.* ***(B)*** *Heatmap of top differentially expressed genes in the mutant subset.* ***(C)*** *Violin plots for tdTomato shows Epi2 has the highest tdTomato expression.* ***(D)*** *Immunostaining of tdTomato and SRSF3 on E13.5 mutant explants reveal loss of SRSF3 in some cells (boxed region arrows, scale bar: 20 µm). Scale bar: 200 µm. n=2.* ***(E)*** *Brightfield images indicate mutant explants are smaller than control explants. (N=2).* ***(F)*** *Violin plots for Slc2a1 shows the Epi2 cluster has the highest hypoxia signature.* ***(G)*** *Immunostaining for GLUT1 performed on E13.5 control and mutant hearts (n=3) indicates mutants have increased hypoxia. EPDCs-epicardium-derived cells; Epi-epicardium; Prol-proliferative.*

6.2.4 Single-cell transcriptomics of the epicardial lineage at E15.5

Clustering of cell populations

The E13.5 analysis revealed mutant hearts have impaired EPDC formation and are more hypoxic. SRSF3 depleted epicardial cells seemed to be most affected by the increased hypoxia, possibly undergoing cell death. This finding suggests mutant cells may be lost at early stages and EPDC differentiation to coronary endothelium might be a compensation mechanism from cells that retained SRSF3.

To investigate EPDC differentiation in mutant hearts, SMART-Seq2 was used to sequence the epicardial lineage; as marked with tdTomato, from control and *Wt1*^{CreERT2}*; Srsf3*$^{fl/fl}$ E15.5 embryos, the stage when the first epicardium-derived endothelial cells were observed (Fig 6.7 A). After quality checks, 265 tdTomato+ control cells and 254 tdTomato+ mutant cells were recovered, averaging 7500 genes/cell (Fig 6.7 B).

Six identity clusters were identified by principal component analysis and tSNE was used for visualisation (Fig 6.7 C). Differential expression revealed transcriptional signatures associated with each cluster (Fig 6.7 D). The epicardial (Epi) cluster was identified based on expression of mesothelial genes like *Upk3b* [124,262], the mural cluster expressed *Cspg4* and *Kcnj8* [264], the proliferative (Prol) cluster had cyclins such as *Ccnb1*, the endothelial (CEC) cluster expressed *Fabp4* [284,288] and two EPDC clusters were identified based on the presence of mesenchymal genes such as *Mfap4* [289]*.* The two EPDC clusters had distinct transcriptional profiles, with EPDC1 cluster expressing genes associated with subepicardial mesenchyme such as *Dhrs3* [124] (Fig 6.7 E). The number of cells associated with each cluster was similar in control vs mutant at this stage. More endothelial cells were found in the mutant dataset; however, the cell numbers were too small to make the comparison meaningful.

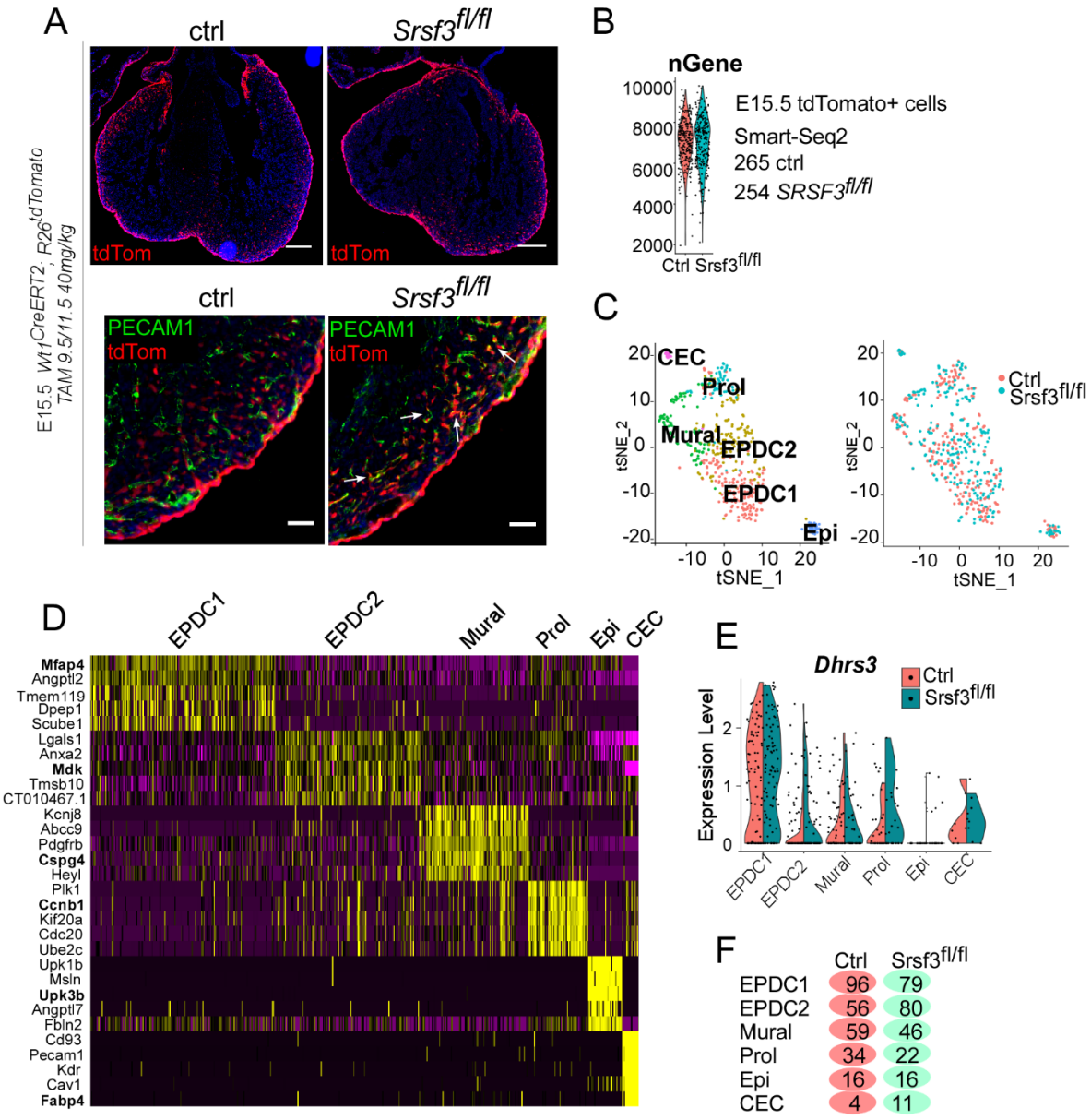


Figure 6.7 Single-cell transcriptomics of the epicardial lineage from E15.5 controls and *Wt1*^{CreERT2}*; Srsf3*$^{fl/fl}$ mutant hearts

(A) *Immunostaining for tdTomato and PECAM1 was performed at E15.5. Arrows indicate tdTom+PECAM1+ cells. Scale bar: 250 µm (top panel), 50 µm (lower panel).* ***(B)*** *Violin plots indicating the number of genes per cell from SMART-Seq2 RNA-Seq performed on FACS sorted tdTom+ cells from both control (n=6) and mutants (n=4 hearts).* ***(C)*** *TSNE plot showing the cell identity clusters.* ***(D)*** *Heatmap showing the top 5 differentially expressed genes in each identity cluster, Yellow indicates high expression.* ***(E)*** *Violin plot indicating the levels of Dhrs3 per cluster.* ***(F)*** *The number of cells from controls and mutants present in each cluster. EPDC-epicardium-derived cells; Epi-epicardium; Prol-proliferative; CEC-coronary endothelial cells.*

Epicardium-derived population is comprised of cells that escaped recombination

Differential gene expression between control and mutant cells revealed proliferation-related genes such as *Srsf3* and the c-MYC co-factor *Pim1* [290] to be significantly increased in mutants (Fig 6.8 A). Since SMART-Seq2 allows recovery of full-length mRNA [187], SRSF3 depleted cells could be identified, however, no cells lacking *Srsf3* exons 2/3 were found in mutants, suggesting that the SRSF3 mutant cells had been cleared by E15.5, the stage at which this analysis was performed. This was consistent with the compensation scenario proposed, where the cells that escape recombination are the ones able to undergo EMT and invade the heart. To confirm epicardial cells in mutant hearts are hyperproliferative, epicardial explants were used. E15.5 explants are normally slow to grow [291], as was seen in control, however, the mutant explants expanded a lot faster, suggesting the cells had higher division rates (Fig 6.8 C). However, n numbers need to be increased to validate this finding. SRSF3 IHC confirmed the presence of SRSF3 in all cells (Fig 6.8 C, boxed region).

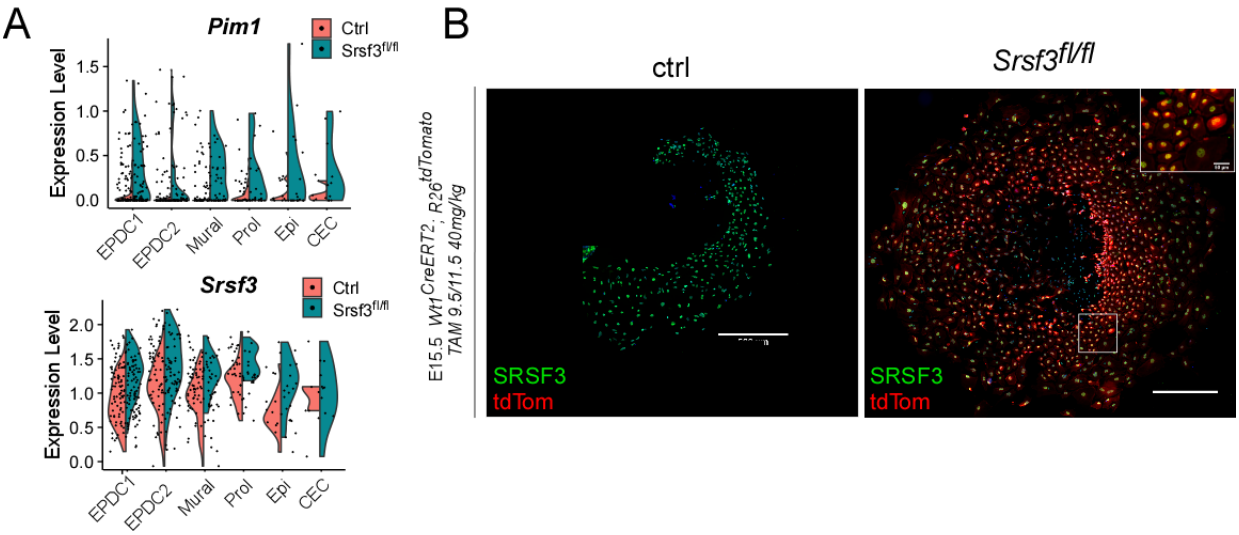


Figure 6.8 Tdtomato+ cells are hyperproliferative in *Wt1*^{CreERT2}*; Srsf3*$^{fl/fl}$ mutant hearts

(A) *Violin plot for Pim1 and Srsf3 reveals increased expression of these markers in mutant cells.* ***(B)*** *Immunostaining for SRSF3 and tdTomato in E15.5 epicardial explants show increased explant size in mutant explants and presence of SRSF3 in all cells. (boxed region, scale bar: 50 μm). n=1 Cre negative littermate control, n=2 mutant. Scale bar: 500 μm. EPDC-epicardium-derived cell; Epi-epicardium; Prol-proliferative; CEC-coronary endothelial cell.*

6.2.5 Single-cell transcriptomics of whole hearts at E17.5

Identification of cell populations

Imaging of E17.5 heart sections showed more tdTomato+Pecam1+ cells in mutants, suggesting increased endothelial cell contribution from EPDCs. To profile the cellular composition of mutant hearts at E17.5, Chromium 10x sequencing was used.

Cell cycle regression and principal component analysis were used as previously described. A similar number of cells were recovered post quality checks from control (6149 cells) and mutant (6145), with control cells averaging 3984 genes/cell, whereas mutant coverage was slightly lower with 3586 genes/cell. Differential gene expression enabled identification of cellular populations based on expression of marker genes (Fig 6.9 A). The clusters identified at E13.5 were also detected in this dataset, plus the emergence of others such as lymphatic endothelial cells (LECs), identified based on expression of *Lyve1* and *Prox1* [292], pericytes and vSMCs expressing *Rgs5* [264], respectively *Eln* [293], which were not present at the E13.5 timepoint. The cellular composition of E17.5 hearts was changed from the E13.5 timepoint, with the percentage of cardiomyocytes increasing from 48% to 61%, and the endocardial fraction decreased from 20% to 9% (Fig 6.9 B).

The E17.5 mutant and control cells were divided into 28 identity clusters, color coded in the UMAP graph (Fig 6.9 C). A similar number of control and mutant cells were assigned to each major classification of clusters, with the exception of mesenchymal and vSMC numbers, that were higher in mutants and cardiomyocytes, which number was increased in controls (Fig 6.9 D).

Due to the complexity of the data, the subsequent analysis focused on the epicardial lineage.

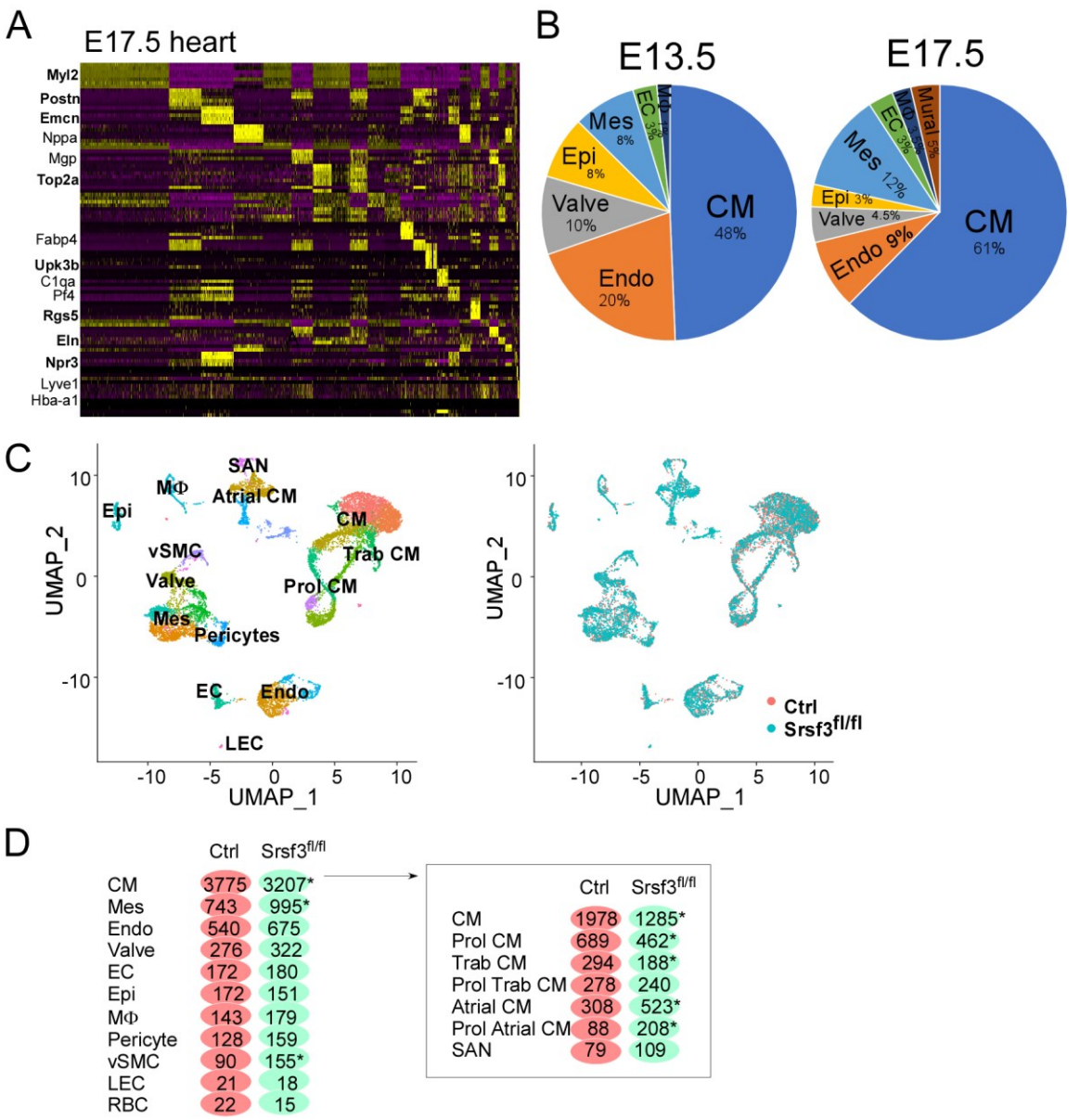


Figure 6.9 Single-cell RNA-Seq on E17.5 whole-hearts from controls and *Wt1*^{CreERT2}; *Srsf3*$^{fl/fl}$ mutants

(A) *Heatmap showing selected differentially expressed genes in the 28 identified clusters from 10x Chromium data performed on whole-hearts from controls (n=1) and mutant (n=2) hearts.* ***(B)*** *Heart composition of E13.5 and E17.5 control hearts from 10x Chromium data reveals increased cardiomyocyte percentage at E17.5 and decreased endocardial proportion.* ***(C)*** *UMAP plot showing the different cell clusters.* ***(D)*** *The number of control and mutant cells per cell identity. Chi-squared test, p<0.0001(*). MΦ-macrophages; ECs-endothelial cells; Endo-endocardial cells; LECs-lymphatic endothelial cells; Mes-mesenchyme, vSMCs-vascular smooth muscle cells; Epi-epicardium; SAN-sinoatrial node; CM-cardiomyocyte; Prol CM- proliferative cardiomyocyte; Trab CM-trabecular cardiomyocyte; Prol Trab CM-proliferative trabecular cardiomyocyte.*

Single-cell transcriptomics indicate epicardial contribution to the heart is normal

Iterative clustering was used to analyse the epicardial lineage, identified by the expression of the reporter gene *tdTomato*. The threshold used for the tdTomato subset was chosen based on the expression level of the epicardial cluster, which was expected to contain mostly tdTomato+ cells (Fig 6.10 A dotted line). The expression level was calculated using the SCtransform command in R [188], which normalises gene expression individually rather than in bulk, being more robust than previous methods of normalising expression by sequencing depth. More *tdTomato*+ cells were found in the mutant dataset (793) compared to control (561), however, this difference could be due to higher detection of *tdTomato* in mutants since the *tdTomato* gene is in homozygosity, whereas controls are heterozygous for this gene.

PCA of tdTomato+ cells revealed 11 identity clusters, visualised using tSNE (Fig 6.10 B). The clusters were assigned identities based on expression of marker genes (Fig 6.10 C). Two epicardial clusters were identified, having similar transcriptional signatures, with variation in expression level of certain genes, possibly indicating onset of quiescence. Three EPDC clusters were identified based on expression of mesenchymal genes. Mural cells were present, most of them were pericytes, further divided into proliferating and non-proliferating. Few cells were identified as valve fibroblasts and CECs.

Surprisingly, apart from the epicardial cluster, no differences were found in the number of mutant cells per cluster compared to control, indicating epicardial contribution is normal in mutant hearts, which was unexpected as it did not support the IHC findings (Fig 6.10 D). Markers for epicardium-derived cells were identified, *Rgs5* being specific to mural cells and *Dpt* expressed in mesenchyme Fig 6.10 E).

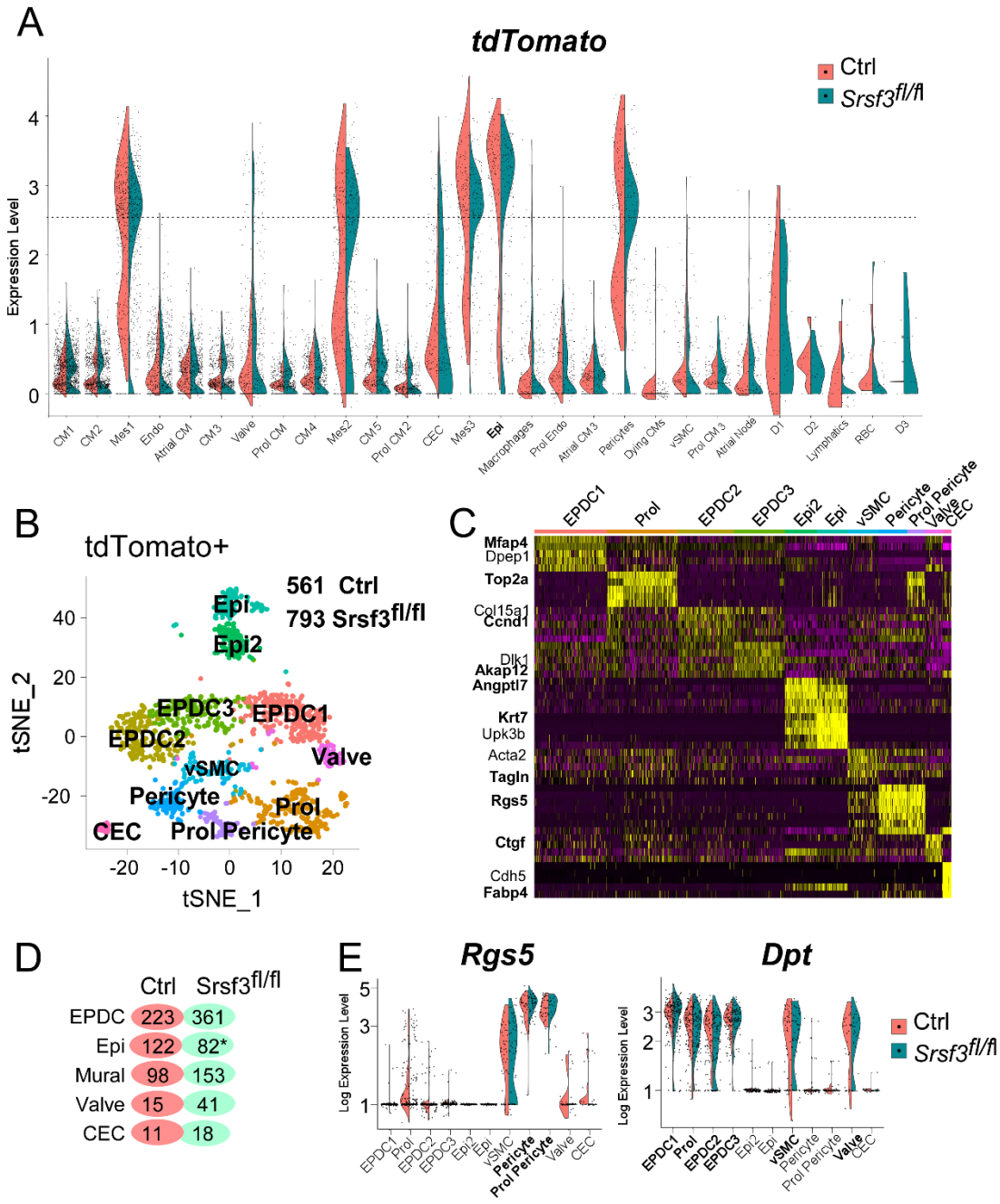


Figure 6.10 Sub-clustering of E17.5 tdTomato+ cells

(A) *Violin plot for tdTomato on E17.5 whole heart data shows the cut-off point for positive expression is 2.5, as indicated by the epicardial cluster.* ***(B)*** *tSNE plots of the tdTomato+ subset re-analysed.* ***(C)*** *Heatmap of top differentially expressed genes in the tdTomato subset.* ***(D)*** *Number of control and mutant cells per tdTomato+ clusters. Chi-squared test, p<0.0001 (*)* ***(E)*** *Violin plots for Rgs5 and Dpt show they are marker genes for mural cells, respectively mesenchyme/fibroblasts. EPDC-epicardium-derived cell; Epi-epicardium; Prol-proliferative; vSMC-vascular smooth muscle cell; CEC-coronary endothelial cells.*

PrimeFlow validates the single-cell RNA-sequencing results

The single-cell transcriptomic data did not show an increased number of epicardium-derived endothelial cells in mutants. To validate this finding, and to enable quantification at the whole heart level, flow cytometry was used. First, the percentage of tdTomato was analysed to check if there were differences in the number of tdTomato+ cells in mutants. Since cardiomyocytes are sensitive to the digestion process, the tdTomato percentage was calculated from the cardiac troponin T (cTNT) negative fraction to exclude differences due to the number of cardiomyocytes recovered (Fig 6.11 A). No increase was detected in tdTomato+ cells from controls (38.65 ± 2.442 SEM, N=6) to mutants (38.73 ± 1.424 SEM, N=6) (Fig 6.11 B). The tdTomato percentage was also not different from embryos that only had tamoxifen induction at E9.5 (Appendix Fig 6.5).

Due to the lack of antibodies available; PrimeFlow probes were used to distinguish the mural and mesenchymal populations based on markers detected in the single-cell RNA-seq. The percentages of *Rgs*+ and *Dpt*+, representing mural cells and mesenchymal fraction, respectively, were calculated from the tdTomato+ population (Fig 6.11 C). No difference was detected in the percentage of *Rgs*+ control cells (19.36 ± 1.165 N=2) compared to mutants (16.54 ± 0.6173, N=5) or *Dpt*+ control cells (68.99 ± 2.781, N=2) compared to mutant (64.93 ± 1.060, N=5) (Fig 6.11 D).

Endothelial cells were selected based on expression of CD31 and exclusion of *Npr3*, an endocardial marker [80] (Fig 6.11 E). E17.5 control hearts tamoxifen induced at E9.5/E11.5 had a similar percentage of tdTomato+ endothelial cells (10.65 ± 2.006, N=2), compared to mutants (7.759 ± 0.7150, N=5) (Fig 6.11 F). However, the percentage of tdTomato+ endothelial cells after tamoxifen administration at E9.5/E11.5 was much higher than E9.5 only induction (3.39 ± 0.250. N=6), indicating ectopic endothelial labelling with later induction.

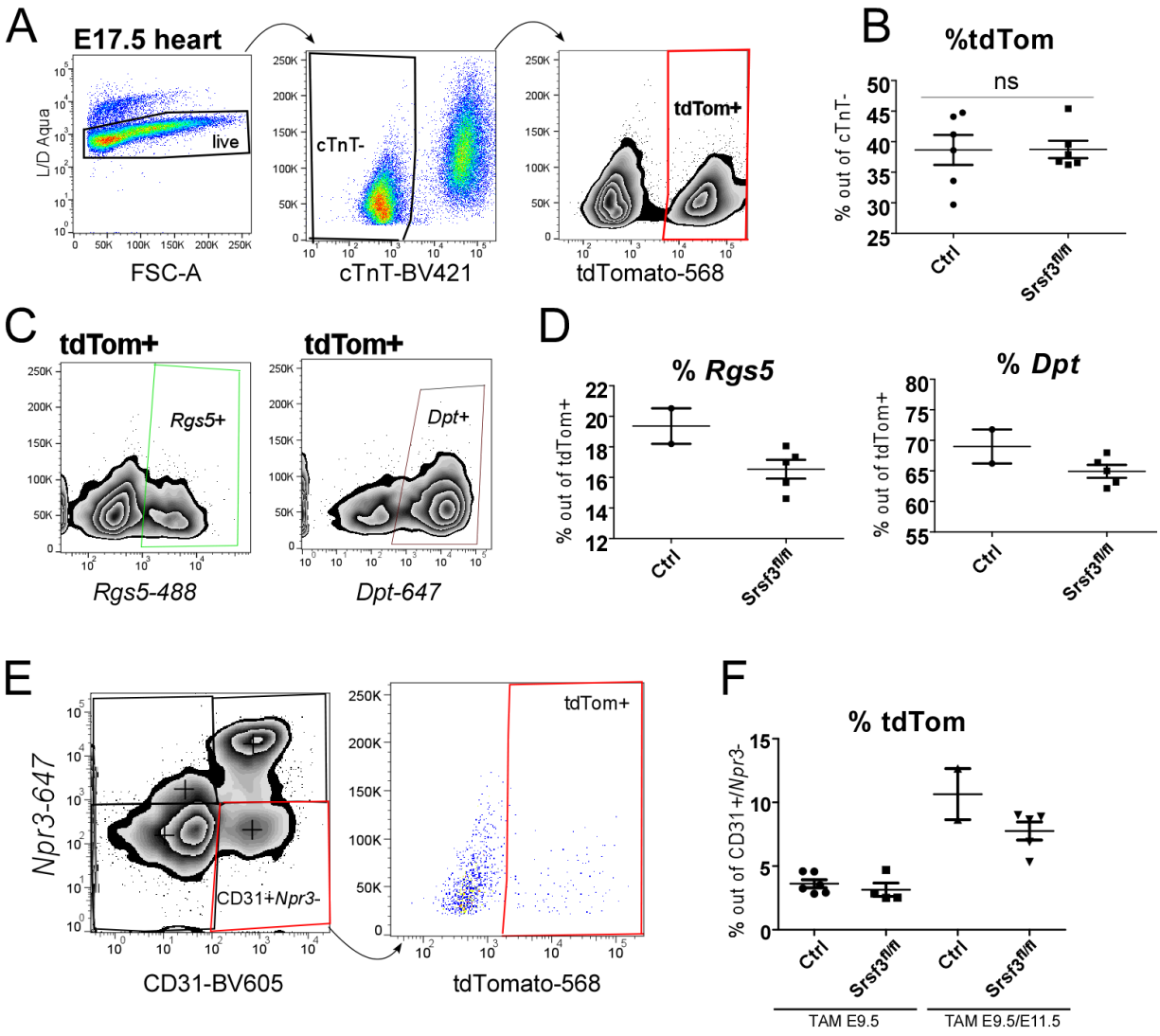


Figure 6.11 PrimeFlow shows normal contribution of epicardial cells to various lineages in *Wt1*^{CreERT2}; *Srsf3*$^{fl/fl}$ mutant hearts

(A) *Flow cytometric analysis of dissociated E17.5 (n=6 hearts, 2 experiments) representing the gating strategy used to select the epicardial lineage.* ***(B)*** *The percentage of tdTomato+ cells out of cTNT-ve cells is not changed in E9.5/E11.5 tamoxifen induced E17.5 mutant hearts. Data shown as mean +/- SEM, ns-not significant, student's t-test.* ***(C)*** *Flow cytometry plots showing tdTomato+ cell populations expressing the mural marker Rgs5 and the mesenchymal marker Dpt.* ***(D)*** *The percentages of Rgs5 and Dpt expressing cells of all tdTomato+ cells was similar in in E9.5/E11.5 tamoxifen induced mutant hearts compared to controls (n=2 controls, n=5 mutants).* ***(E)*** *Flow cytometry plots indicating the gating strategy used to calculate the number of tdTomato+ endothelial cells.* ***(F)*** *The percentage of tdTomato+ cells out of Npr3-CD31+ cells increased after E9.5/E11.5 tamoxifen compared to E9.5. n=6, 1 litter, E9.5 control, n=4, 2 litters, E9.5 mutant, n=2, 1 litter, E9.5/E11.5 control, n=5, 2 litters, E9.5/E11.5 mutant, all samples run together during the same experiment.*

Wt1^{CreERT2}*; Srsf3*$^{fl/fl}$ mutants do not show differences compared to littermate controls

The single-cell RNA-sequencing results were confirmed by flow cytometry studies, which also failed to detect differences between epicardial contribution to various lineages in E17.5 *Wt1*^{CreERT2}*; Srsf3*$^{fl/fl}$ mutants tamoxifen induced at E9.5/E11.5 compared to controls. The reasons for this discrepancy could be either technical or biological.

Since control and mutant hearts were not littermates due to the very small number of embryos recovered from mutant crosses, slight differences in the timing of tamoxifen administration could have led to more endothelial cells being labelled in the hearts used for cryosections due to variable *Wt1* expression in endothelial cells. Another possibility is there are anatomical differences in tdTomato+ CECs distribution, therefore, there is no increase in total number, however, the regions where these cells are found differ in mutants.

To investigate differences due to tamoxifen induction, littermate controls were obtained. Sections were immunostained for PECAM1 (Fig 6.12 A) and no difference was found in the number of tdTomato+ endothelial cells in littermate controls and *Wt1*^{CreERT2}*; Srsf3*$^{fl/fl}$ mutants (Fig 6.12 B), indicating the differences observed in previous sections were due to the coincidental increase of endothelial cell labelling in mutants due to timing of tamoxifen administration, reflecting variable timing of conception between litters.

Wt1 expression was detected in endothelial cells at E13.5 in the single-cell transcriptomic data and ERα was still nuclear at this stage (Fig 6.12 C) indicating that the Cre remains active when *Wt1* start to be expressed in endothelial cells.

Together, these results indicate that *Wt1*^{CreERT2}*; Srsf3*$^{fl/fl}$ mutant hearts fully compensate by E17.5 stage and any differences observed using tdTomato are confounded by the labelling of endothelial cells with E11.5 tamoxifen induction.

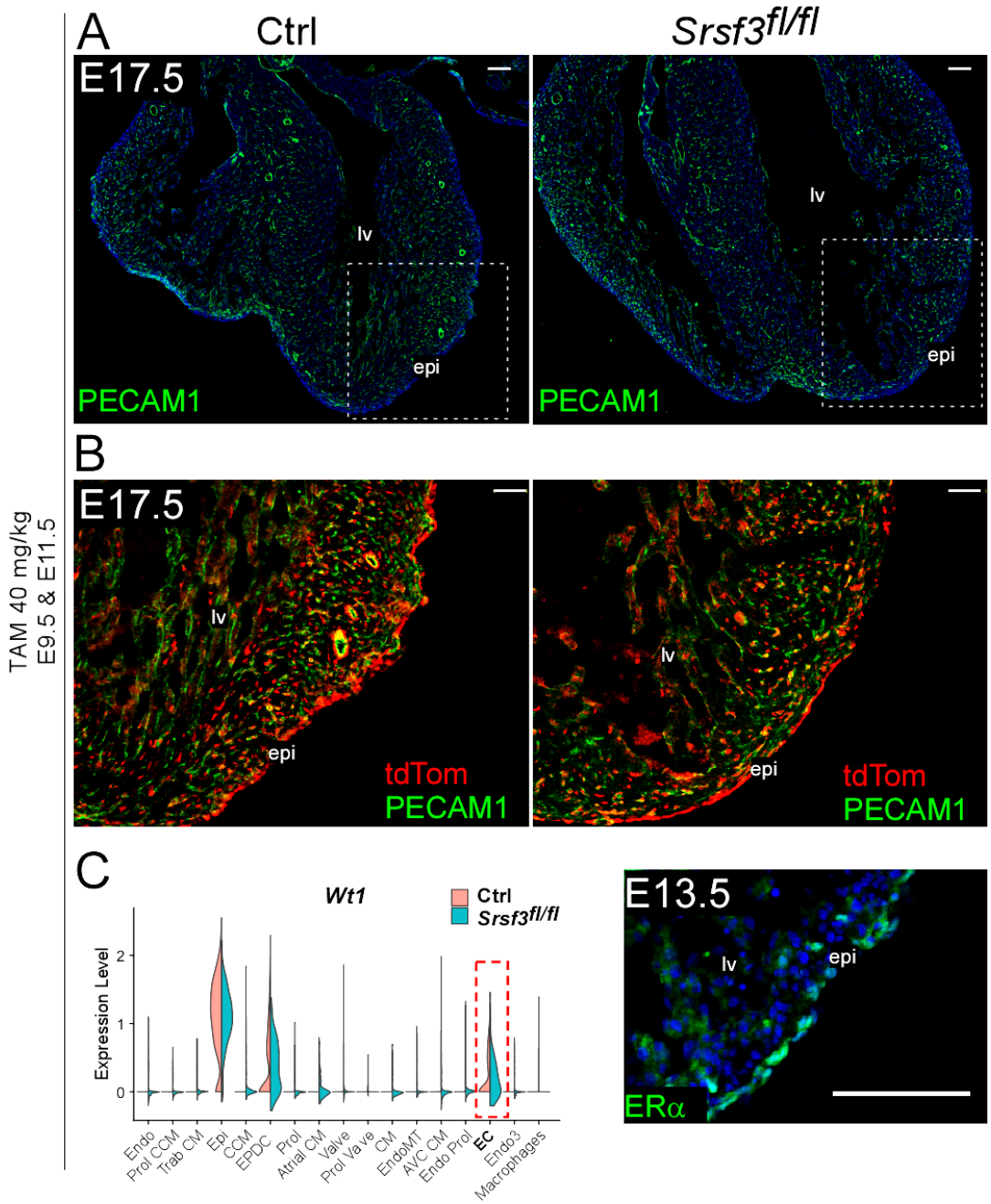


Figure 6.12 Labelling of coronary endothelium in *Wt1^{CreERT2}; Srsf3$^{fl/fl}$* mutants is not different from controls

(A) *Immunostaining for PECAM1 shows normal vessel formation in E17.5 mutants. Scale bar: 100 µm. n=1.* ***(B)*** *Higher magnification (boxed region)) of immunostaining for PECAM1 and tdTomato reveals no increase in the number of tdTom+PECAM1+ cells in mutants. Scale bar: 60 µm.* ***(C)*** *Wt1 is expressed in endothelial cells at E13.5 as revealed by single-cell RNA-sequencing (dotted box). Immunostaining for estrogen receptor α (ERα) shows Wt1Cre is still active at E13.5 after E11.5 administration. Scale bar: 100 µm. n=1.*

6.3 Discussion

6.3.1 Impaired coronary sprouting in *Wt1^{CreERT2}; Srsf3$^{fl/fl}$* mutants

E17.5 *Wt1^{CreERT2}; Srsf3$^{fl/fl}$* mutants that had been gavaged at E9.5/E11.5 presented increased tdTomato+PECAM1+ cells and decreased TdTomato+*Tcf21*+ cells in immunostained cryosections, suggesting that the mutant epicardial lineage contributes more endothelium at the expense of mesenchymal cells.

Since CECs do not normally originate from the epicardium, sprouting from the conventional sources (SV and endocardium) was investigated. Whole-mount PECAM1 staining revealed impaired SV sprouting in E13.5 mutants. Since VEGF-C has been reported to be exclusively secreted from the epicardium to initiate sprouting [77], *Vegfc* production was evaluated. Surprisingly, *Vegfc* expression was widespread in the heart and no decrease was detected in mutants, indicating VEGF-C is not sufficient to promote sprouting from the SV.

No sprouting assays are available for endocardial cells, however, SOX17 has been implicated in endocardial to endothelial transition [86]. In controls, SOX17 was expressed in a subset of endocardial cells near the apex, where the endocardium is thought to contribute vessels to the ventricular walls [77]. SOX17 was largely absent in mutants, indicating endocardial sprouting is affected in the outer ventricular wall, however, the endocardium was still able to contribute vessels in the IVS. It is likely IVS vessel production is not dependent on SOX17 since no SOX17+ endocardial cells were detected near the IVS in controls or mutants.

6.3.2 E13.5 whole-heart single-cell transcriptomics indicates *Wt1*^{CreERT2}*; Srsf3*$^{fl/fl}$ hearts are hypoxic

Global changes

Unbiased single-cell transcriptomics of E13.5 cardiac tissue revealed increased levels of hypoxia-related genes in *Wt1*^{CreERT2}*; Srsf3*^{fl} mutants. IHC for the hypoxia-upregulated gene GLUT1 [294] indicated certain regions of the heart are hypoxic at baseline, such as the IVS and the endocardial cushions, confirming previous reports [287,295]. GLUT1 was more widespread in mutant hearts, however, GLUT1 also has other roles independent of hypoxia [296], therefore, further experiments are needed to assess hypoxic regions with the use of more direct readouts such as Hypoxyprobe [297].

A previous report indicated that endocardial cells upregulate SOX17 in response to hypoxia [86], thus, a curious aspect is the lack of SOX17 expression in the endocardium of mutant hearts. Interestingly, in the previous study, epicardial function was not compromised, which indicates hypoxia is not sufficient to trigger vessel formation from the endocardium and correct epicardial function is also required. However, it is unlikely the epicardium directly signals to the endocardium since they are not in close proximity. *Wt1*^{CreERT2}*; Srsf3*$^{fl/fl}$ hearts also presented reduced myocardial compaction and disorganised trabeculae, probably as a consequence of decreased myocardial proliferation in response to impaired epicardial function [82], consequently, the impaired endocardial response may be due to reduced myocardial compaction.

Epicardial lineage defects

Of importance, the highest expression of hypoxia-related genes was found in a sub-cluster of epicardial cells These genes included *Fam162a* and *Bnip3*, which are associated with hypoxia-induced cell death [298]. No increase in CC3 was detected in these hearts, indicating cell death happens independently of caspase cleavage, which has previously been reported after *Bnip3* induction in response to hypoxic stimuli in cardiomyocytes [299]. Further experiments such as propidium iodide staining or TUNEL assay are required to examine the extent of cell death in mutant hearts.

The presence of hypoxia-induced cell death genes in a sub-cluster of epicardial cells indicated not all epicardial cells are sensitive to elevated hypoxia in mutants. Since these hypoxic cells were associated with increased tdTomato expression, it is likely this cluster represented the SRSF3 depleted cells. SRSF3 has been shown to protect against hypoxia [300,301], therefore, it is possible that loss of SRSF3 leads to more severe defects in elevated hypoxia.

Mutant hearts also presented a decreased number of EPDCs, as revealed by the single-cell RNA-Sequencing data and tdTomato IHC. No decrease in EPDC proliferation was detected, indicating the reduced number is due to impaired EPDC formation from the epicardium. Mutant epicardial explants were smaller, supporting a role of SRSF3 in epicardial proliferation and EPDC formation, as discussed in Chapter IV.

6.3.3 E15.5 SMART-Seq2 data reveals that the epicardial lineage is hyperproliferative in E15.5 *Wt1^{CreERT2}; Srsf3$^{fl/fl}$* mutants

SRSF3 depleted cells are eliminated in mutant hearts

To investigate in greater detail the EPDC differentiation process in *Wt1^{CreERT2}; Srsf3$^{fl/fl}$* hearts, single-cell RNA-Sequencing was performed on control and mutant tdTomato+ cells, representing the epicardial lineage on E15.5 hearts, the first stage tdTomato+PECAM1+ cells were detected.

Surprisingly, no SRSF3 depleted cells were recovered in the mutant dataset at this embryonic stage, indicating cells that lost SRSF3 were no longer present; possibly due to hypoxia-induced cell death or exclusion of these cells at earlier stages.

Differential gene expression revealed proliferation markers were increased in non-recombined cells. Of importance, *Pim1* was significantly upregulated in the epicardial lineage in mutants. Proto-Oncogene Serine/Threonine-Protein Kinase (PIM1) is a known co-factor of c-MYC [290], which has been previously implicated in cell competition in the epicardium [302]. Cell competition is a well-studied conserved developmental process, where "fitter"; usually more proliferative cells, eliminate their less fit neighbours [303]. Data presented in Chapter III showed SRSF3 is required for epicardial proliferation, therefore, it is likely cells that escape recombination outcompete the non-proliferative SRSF3 depleted cells, leading to their exclusion, and become hyperproliferative to compensate for the loss.

A pilot validation experiment showed E15.5 epicardial explants were larger and grew faster than littermate controls, supporting the hyperproliferative behavior of these cells. Moreover, all cells in mutant explants expressed normal levels of SRSF3, validating the disappearance of SRSF3 depleted cells by this stage.

EPDC differentiation

Unlike the E13.5 timepoint, the number of EPDCs was similar in the E15.5 mutant dataset compared to control, showing the hyperproliferative behavior compensated for the reduced EPDC formation observed at earlier stages. All EPDCs in the mutant dataset expressed SRSF3, indicating only epicardial cells that escape recombination are able to produce EPDCs.

6.3.4 E17.5 analysis reveals no difference in epicardial contribution at the whole heart level in *Wt1^{CreERT2}; Srsf3$^{fl/fl}$* mutants

Surprisingly, the E17.5 single-cell RNA-sequencing data failed to support the earlier IHC results. No increase in tdTomato+ endothelial cells or decrease in epicardium-derived fibroblasts was detected in the mutant dataset. This finding was further supported by flow cytometry quantification of epicardial contribution which confirmed no significant difference in epicardial contribution to various cardiovascular lineages in mutants.

The reason for the different results appeared to be due to the lack of littermate controls and possible differences in the time of plugging and tamoxifen delivery; which was confirmed by eventually obtaining littermate controls that failed to show a different phenotype compared to mutants. Moreover, comparison of the number of endothelial cells that were tdTomato+ between controls induced at E9.5 with controls induced E9.5/E11.5 indicates more endothelium is labelled with later tamoxifen administration, due to the persistence of tamoxifen activity when *Wt1* expression is initiated in endothelial cells. Previous reports showed induction of *Wt1^{CreERT2}* at E14.5 leads to all coronary endothelial cells being labelled [65,76], therefore delayed tamoxifen induction can result in increased endothelial labelling, making littermate controls crucial to assess ectopic labelling.

These data highlight the problem of using tamoxifen to activate Wt1-CreERT2 past E10.5. The detection of tdTomato-endothelial cells in the heart from E15.5 led to the assumption that they had evaded targeting by tamoxifen since the ERα was cytoplasmic at this stage, however, the analysis did not assess the coronary endothelium that had started to express *Wt1* by E13.5, as revealed by the single-cell transcriptomic data, a stage when the Cre recombinase was still active.

No difference was detected in the total number of endothelial cells in controls compared to $Wt1^{CreERT2;}$ $Srsf3^{fl/fl}$ mutants at E17.5, indicating the sprouting defects seen at E13.5 are not permanent and vessel growth is delayed, not completely impaired.

6.3.5 Conclusions

The findings presented in this chapter show depletion of SRSR3 by tamoxifen induction at E9.5/E11.5 in epicardial cells results in decreased EPDC production and failure of the SV and the endocardium to produce coronary endothelium at E13.5.

SRSF3 depleted cells are eliminated from mutant hearts at later stages, being outcompeted by epicardial cells that escaped recombination; which become hyperproliferative, compensating for the loss of mutant cells. Coronary sprouting is also resumed, with no differences being detected by E17.5

Chapter VII.

General discussion

7.1 Main findings

Epicardial cells have essential roles during heart development, secreting growth factors that promote cardiomyocyte proliferation and coronary vessel formation and producing epicardium-derived cells (EPDCs) that further differentiate to mural cells and cardiac fibroblasts, which support the growing coronary vasculature [77,123,124,134,229,255,304,305]. However, key aspects of epicardial function remain unknown, such as regulation of epicardial epithelial-to-mesenchymal transition (EMT) and EPDC fate determination.

The main aim of this thesis was to determine the role of the RNA-binding protein SRSF3 in the epicardium during heart development.

This chapter highlights the main findings of this thesis, with reference to the initial aims listed in Chapter I, whilst also discussing the limitations of these findings and their wider implication in the field .

The key questions addressed in this thesis were:

- Is SRSF3 involved in the formation of the epicardial layer?
- Is SRSF3 required for epicardial EMT?
- Is EPDC fate pre-determined?
- Is SRSF3 involved in EPDC fate choice?

The main findings of this thesis are:

- SRSF3 is required for epicardial layer formation through promoting proliferation of proepicardial progenitors
- SRSF3 is required for EPDC formation *in vivo* and TGFβ-induced EMT *in vitro*
- Cell proliferation is not required for epicardial EMT *in vitro,* but cell-cycle regulators might be
- EPDC fate is not pre-specified and inconsistencies within the literature about epicardial contribution to various cardiovascular lineages are due to non-specific Cre activity
- Incomplete targeting of SRSF3 results in hyperproliferation of untargeted cells, which leads to compensation

Limitations of this study:

- Tg(Gata5-Cre) was not specific to the PEO, as previously reported
- TdTomato expression did not reflect loss of SRSF3, due to different recombination efficiencies
- Targeting of *Srsf3* led to production of a non-functional protein that was still detected by antibodies
- Wt1-CreERT2 induction past E10.5 led to labelling of coronary endothelium which became progressively worse with later tamoxifen administration
- Immortalised epicardial cell line had an altered cell cycle which made it sub-optimal for proliferation studies
- Due to its essential role in cellular propagation, depletion was not the optimal way to study SRSF3 function in proliferative systems

7.1.1 SRSF3 is required for formation of the epicardial layer

Data presented in Chapter III shows SRSF3 is widespread in embryonic hearts, being highly expressed in proepicardial cells and in the epicardial layer until E15.5. Of importance, the highest expression was detected at E11.5 in the epicardium, which coincided with the peak of proliferative activity [114].

To determine a functional requirement for SRSF3 in the epicardium, transgenic lines were used to target *Srsf3* deletion to epicardial cells. Embryos that had SRSF3 depletion induced by the Tg(Gata5-Cre)[82] did not survive past E12.5 and presented gross morphological heart abnormalities such as dilated atria and hypoplastic ventricles. Further analysis revealed the epicardial layer failed to form. Investigation of proepicardial progenitors showed the PEO was smaller and less proliferative in these mutants, indicating epicardium formation is compromised due to impaired PEO function (Fig 7.1).

Surprisingly, the Tg(Gata5-Cre) was not confined to the PEO, as previously reported [82], but was also expressed in a subset of cardiomyocytes. The non-specific Cre expression has important implications for other studies that have used this Cre to recombine or lineage trace proepicardial cells and did not address the consequences of protein loss in other targeted cells [82,91,127,229,306–308]. This is specifically problematic in the case of widely expressed proteins, such as SRSF3, that have essential roles in most cell types [166]. The widespread expression of the Tg(Gata5-Cre) contributed to the severity of the phenotype, since other mutants that have impaired epicardial formation die at later stages compared to the SRSF3 mutants [116,194]. The Cre-expressing cardiomyocytes underwent apoptosis after SRSF3 was depleted, likely contributing to the early lethality and confirming a role for SRSF3 in survival and proliferation of cardiomyocytes [152].

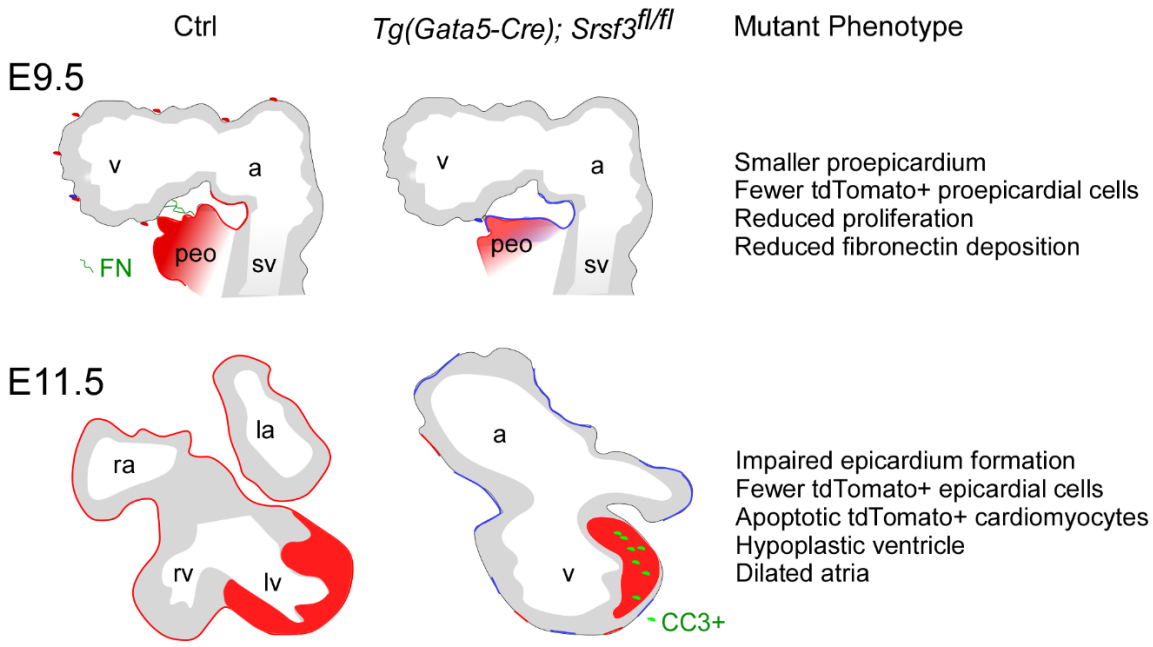


Figure 7.1 Schematic summarising the phenotype of *Tg(Gata5-Cre); Srsf3$^{fl/fl}$* embryos

Mutant embryos have smaller proepicardia that do not produce fibronectin (FN) with fewer tdTomato+ cells present. Most cells that migrate onto the heart in mutants are tdTomato-ve. Mutants do not form a complete epicardium and myocardial cells that express the Cre undergo apoptosis. a-atrium, v-ventricle, peo-proepicardial organ, sv-sinus venosus, ra-right atrium, la-left atrium, lv-left ventricle, rv-right ventricle, epi-epicardium, epdc-epicardium-derived cel, CC3-cleaved caspase 3l.

The SRSF3 requirement for proepicardial proliferation is also translated to epicardial cells, as shown by the failure of both proepicardial and epicardial explant cultures to expand in the absence of SRSF3. This is consistent with the main role of SRSF3 described in the literature being proliferation [154,155,158,162,167,200,309]. SRSF3 is an oncogene, its expression being altered in a wide range of cancers [155,157,160,199,201].

Due to its essential role in cellular propagation, explant cultures from SRSF3 mutants were small and mainly comprised of cells that escaped recombination and continued expanding, as shown by the high percentage of tdTomato negative cells present in these cultures.

A major issue highlighted by this study was the importance of proliferation in explant growth, which was also confirmed by failure to expand of cultures treated with cell cycle inhibitors. This showed growth in explant cultures is mainly due to proliferation and not due to migration. Explant size has been used in a number of studies as a proxy for migration potential [121,306,310], without assessing cellular proliferation.

Since most cells in mutant explants were non-targeted, this complicated the study of SRSF3 depleted cells by means other than immunostaining. Staining for the known SRSF3 target, PDCD4 [153,208] , revealed that SRSF3-depleted proepicardial cells increased PDCD4 production, which is known to lead to cell cycle arrest [311,312]. Ki67 immunostaining showed that epicardial cells that lost SRSF3 stop production of Ki67, suggesting these cells undergo senescence or quiescence [313]. However, it was recently reported that Ki67 levels also drop in G1, therefore, cell cycle arrest of targeted cells in G1 cannot be excluded [314].

To allow recovery of more SRSF3 mutant cells, a mouse epicardial cell line was used. Knockdown of SRSF3 resulted decreased cell density, supporting a role for SRSF3 in epicardial proliferation. The SRSF3 target, CyclinD1 [155,158] was dramatically reduced in the epicardial cell line.

These findings indicate SRSF3 influences (pro)epicardial cell proliferation through multiple pathways, such as repression of PDCD4 and induction of Cyclin D1. Further studies are required to determine the exact molecular mechanism by which SRSF3 influences epicardial cell proliferation.

7.1.2 SRSF3 is required for EPDC formation

Interestingly, induction of SRSF3 deletion using the *Wt1*^{CreERT2} at E8.5 did not result in failure of the epicardium to form, unlike targeting with the Tg(Gata5-Cre). This could be due to a number of factors, such as better efficiency of constitutive Cre as compared to inducible ones, and Cre activation at the onset of proepicardial formation with Tg(Gata5-Cre), as opposed to the lag between tamoxifen delivery and recombination in the case of *Wt1*^{CreERT2} [233]. Although the epicardial layer was established in these mutants, EPDCs failed to form, as shown by the absence of tdTomato+ cells inside the heart at E16.5. This resulted in myocardial non-compaction and impaired coronary vessel formation, being consistent with other studies where EPDC formation was defective [95,116,177,235,237] (Fig 7.2).

In contrast, induction of SRSF3 depletion at E9.5 or E9.5/ E11.5 resulted in normal heart morphology at E17.5 and a similar number of tdTomato+ cells inside the myocardium (Fig 7.2). Single-cell RNA-sequencing revealed tdTomato+ cells that invaded the heart in these mutants retained SRSF3, indicating more cells escape recombination with later tamoxifen induction. These contrasting phenotypes suggest compensation from non-targeted cells requires a certain threshold of targeting inefficiency which is not achieved with E8.5 tamoxifen induction, but present with E9.5 or E9.5/E11.5 administration. The compensation mechanism is probably facilitated by the non-proliferative phenotype of mutant cells and by cell competition mechanisms that are active in the epicardium, as previously demonstrated with overexpression of c-MYC, where the overexpressing cells become hyperproliferative and replaced wild-type cells in epicardial explants [302].

The extent of *Srsf3* recombination in *Wt1*^{CreERT2}*; Srsf3*$^{fl/fl}$ tamoxifen-induced mutants could not be assessed by IHC at later stages because the mutant *Srsf3* allele led to the production of a non-functional protein, still detectable by antibodies. TdTomato could not be used a proxy since this allele recombined more efficiently than *Srsf3*, however, the non-overlapping targeting was likely exacerbated by the difference in proliferation rates of tdTomato+SRSF3+ cells, compared to tdTomato+SRSF3- cells.

Wt1-CreERT2 induction at E11.5 led to CECs being targeted due to *Wt1* expression being initiated in endothelium [128]. Deletion of SRSF3 from E11.5 resulted in enlarged labelled vessels, indicating SRSF3 is required for normal endothelial function. Induction of the Wt1-CreERT2 at E11.5 is a common strategy that has been used in multiple epicardial studies without addressing endothelial labelling [123,124]. This is especially problematic in studies where endothelial defects have been reported as a consequence of impaired epicardial function and the effects of direct endothelial targeting have not been addressed [124]. The overlooking of *Wt1* expression in endothelial cells is a major problem in the epicardial field and has led to false reports about epicardial contribution to coronary endothelium [69].

In this thesis, expression of *Wt1* in endothelial cells at early embryonic stages was not initially observed due to the methods used. Evaluation of WT1 expression was done by IHC, however, very few endothelial cells are present in the heart at E12.5/E13.5. However, the E13.5 single-cell RNA-sequencing showed *Wt1* is expressed in endothelial cells, possibly within the sinus venosus, before they reach the heart. The 3.39% endothelial contribution after E9.5 tamoxifen induction could be due to *Wt1* expression within endothelial cells and not due to epicardial contribution. WT1 has been found in endothelial cells in the PEO [315], therefore, further studies are required to determine the onset of *Wt1* expression within endothelial compartments in the heart.

This study highlights the importance of characterising Cre specificity, restricting Cre activity to a defined temporal window and assessing depletion efficiency through other means rather than relying on reporter expression.

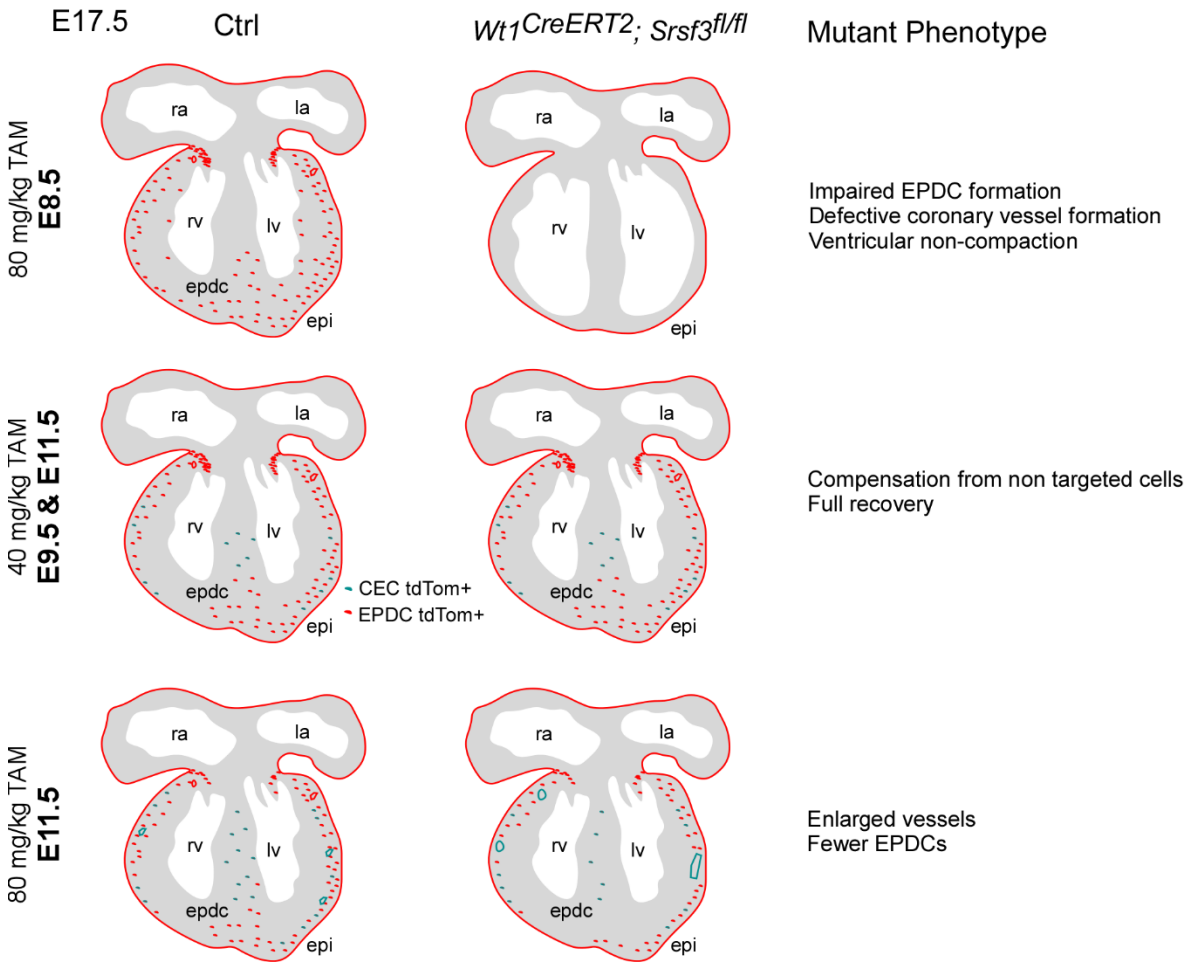


Figure 7.2 Schematic showing the distinct phenotypes resulting from induction of Wt1-CreERT2 at different developmental stages

Depletion of SRSF3 with tamoxifen induction at E8.5 results in lack of EPDC formation and ventricular non-compaction, whereas induction with two lower doses at E9.5/E11.5 leads to full compensation by non-targeted cells. Induction with a high dose of tamoxifen at E11.5 results in targeting coronary endothelial cells, which leads to enlarged vessels. ra-right atrium, la-left atrium, lv-left ventricle, rv-right ventricle, epi-epicardium, epdc-epicardium-derived cell.

7.1.3 Cell-cycle regulators might be involved in epicardial EMT

Cell division has been demonstrated to promote EPDC formation *in vivo* [114,226]. Due to the role of SRSF3 in epicardial proliferation and EPDC formation, a link between cellular proliferation and epicardial EMT was explored. This study was performed using an epicardial cell line, since cell division is more readily manipulated *in vitro* using pharmacological inhibition.

Unfortunately, due to the immortalisation process, the cell line was not suitable for this type of study since inhibition of proliferation led to very high rates of cell death. However, the limited studies conducted indicated that epicardial cells *in vitro* can undergo EMT when cell cycle arrested, which is in contrast with impaired EPDC formation seen *in vivo*. No link was detected between cell cycle stage and ability to undergo EMT (Fig 7.3).

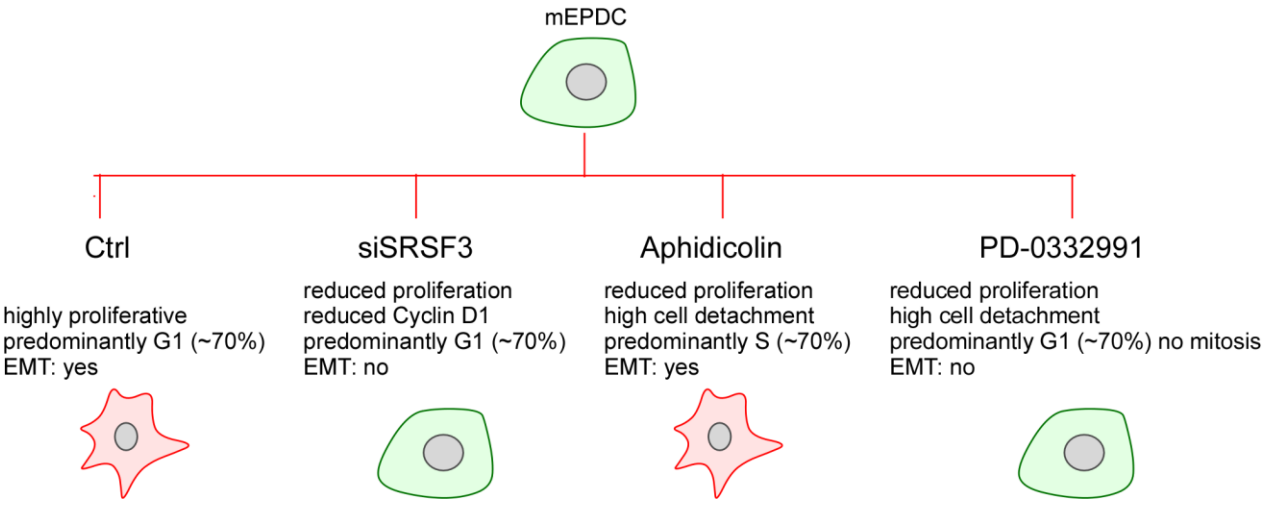


Figure 7.3 Schematic showing the different treatments used to investigate cell proliferation and EMT in the epicardial cell line.

The mouse epicardial cell line (mEPDC) and the effects of siRNA treatment against SRSF3 and cell cycle inhibitors on viability and epithelial-to-mesenchymal transition (EMT).

These findings could indicate that epicardial cells can still undergo EMT when cell cycle arrested, but cell proliferation may be required to relocate cells from the outer layer and expose them to EMT-inducing factors in the sub-epicardium *in vivo* or they could show that this *in vitro* system is not physiologically relevant. Further investigation is needed to determine the mechanism of impaired EPDC production after cell cycle inhibition *in vivo*.

Interestingly, treatment with CDK4/6 inhibitor prevented cells from responding to TGFβ, similarly to siSRSF3 treatment, but did not arrest cells in G1, indicating the reduced EMT response is not necessarily connected to proliferation. CDK4/6 and the SRSF3 target, CyclinD1, have had non-cell cycle related roles described in recent years [245], therefore, CDK4/6 might be required for phosphorylation of proteins needed for EMT, whereas Cyclin D1 might mediate transcription of genes involved in EMT [316]. Furthermore, the high concentration of CDK4/6 inhibitor used may have led to off-target effects. Future studies are required to determine a role for these proteins in EMT. For example, depletion of Cyclin D1 could be used to check if epicardial cells respond to TGFβ in its absence.

7.1.4 Proepicardial markers significantly overlap during heart development

To understand more about the role of SRSF3 in the epicardium, a study into epicardial identity was conducted. SRSF3 depletion did not alter the expression level of the (pro)epicardial markers: *Wt1, Sema3d ,Scx*, *Tcf21,* indicating SRSF3 is not required to maintain epicardial identity. Similarly, depletion of the master epicardial regulator WT1 [196] did not alter expression of SRSF3, further demonstrating SRSF3 is not associated with epicardial identity.

However, this study revealed that proepicardial cells which give rise to the epicardium co-express the previously reported non-overlapping markers *Wt1, Sema3d*, *Tbx18, Scx and Tcf21* [68]. The contrasting results reflect the difficulty of defining the PEO

based on molecular markers, since the domains of expression of proepicardial genes extend into the septum transversum, where expression domains do not fully coincide [69]. In this study, proepicardial cells were defined as the ones translocating to the heart surface to give rise to the epicardium.

The idea that (pro)epicardial cells are heterogenous and pre-specified to contribute to different cardiovascular lineages stems from the use of Cre lines [67,68,81], with each reported Cre line tracing a different number of endothelial, mural or fibroblast cells. The findings presented in Chapter V show that none of the previously used (pro)epicardial markers are specific to this lineage throughout development, therefore, caution must be taken in interpreting cell fate mapping with the Cre-LoxP system, especially in the case of constitutive Cres. For example, *Tbx18* expression is found in vSMCs of both epicardial origin, such as in coronary vessels, and non-epicardial origin, such as aortic vSMCs. The use of the constitutive $Tbx18^{Cre}$ has already led to exaggeration of epicardial contribution to cardiomyocytes [72] and the same may be true for vSMCs. Similarly, *Wt1* is expressed in endothelial cells [69], *Tcf21* in interstitial cells [81] and *Sema3d* in lymphatics (data not shown, E17.5 single-cell RNA-sequencing).

Single-cell RNA-sequencing analysis supports the idea that epicardial cells are not pre-specified to contribute to different lineage and no link was found between marker expression and cell fate specification. The findings presented also suggest that epicardial cells do not contribute to coronary endothelium. The expression of these five markers in the epicardial lineage throughout development is summarised in Fig 7.4.

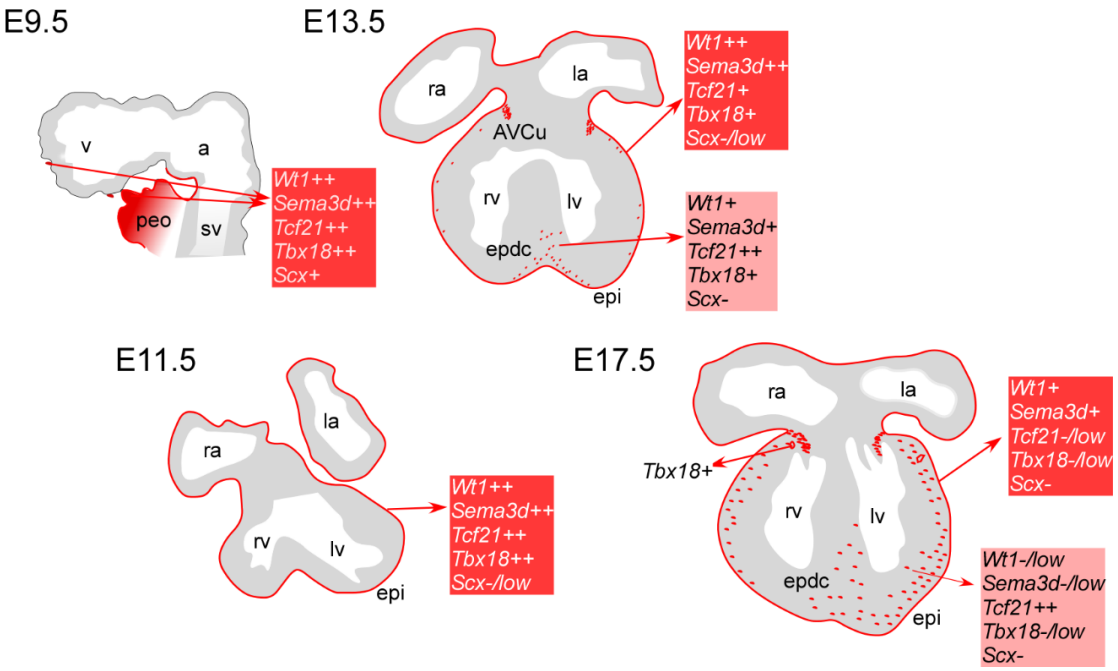


Figure 7.4 Expression of established proepicardial markers throughout development

Expression of proepicardial markers Wt1, Sema3d, Tcf21, Tbx18, Scx was assessed throughout the course of heart development. peo-proepicardial organ, sv-sinus venosus, a-atria, v-ventricle, ra-right atrium, la-left atrium, lv-left ventricle, rv-right ventricle, epi-epicardium, epdc-epicardium-derived cell.

7.1.5 Incomplete SRSF3 targeting results in compensation

The results presented in Chapter VI show that E17.5 *Wt1*^{CreERT2}*; Srsf3*$^{fl/}$ mutants that had tamoxifen administered at E9.5/E11.5 did not have any detectable differences in epicardial contribution to the expected cardiovascular lineages or other changes in cellular composition. This, together with the presence of SRSF3 in all EPDCs, indicates that non-targeted cells compensated in these mutants.

Analysis at E13.5 showed mutant hearts were initially defective, having impaired coronary vessel formation, thinner compact walls, disorganised trabeculae and fewer EPDCs (Fig 7.5). Single-cell RNA-sequencing revealed some epicardial cells that had high tdTomato levels, expressed hypoxia-induced cell death genes. However, no increase in caspase-dependent apoptosis was detected, indicating cell death might occur through other mechanisms in SRSF3 depleted cells.

The E15.5 data showed proliferative markers such as *Pim1* were increased in the non-recombined epicardial cells. PIM1 is a co-factor of c-MYC[290] which has been associated with cell competition in the epicardium [302]. These results show SRSF3 depleted epicardial cells are excluded from the heart, but it remains unclear if this is a result of hypoxia-induced cell death or cell competition due to the non-proliferative phenotype of SRSF-depleted cells.

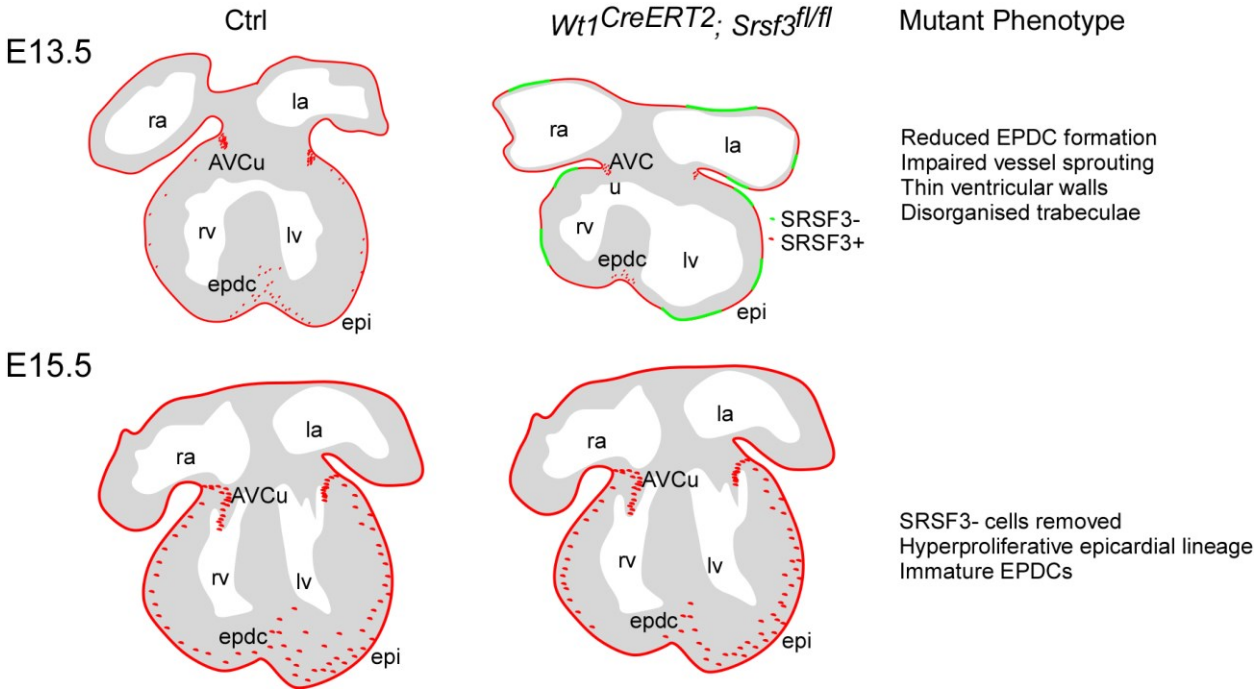


Figure 7.5 Schematic summarising the early phenotype of *Wt1*^{CreERT2}*; Srsf3*$^{fl/fl}$ embryos tamoxifen induced at E9.5/E11.5

Mutant hearts have a thin compact layer, fewer vessels and EPDCs. By E15.5, SRSF3 depleted cells are removed from the heart and cells that escaped recombination become hyperproliferative. EPDC number is recovered. ra-right atrium, la-left atrium, AVCu-atrioventricular cushion, rv- right ventricle, lv-left ventricle, epi-epicardium, epdc-epicardium-derived cell.

Since compensation did not take place after the E8.5 tamoxifen dosage, these findings highlight the importance of achieving and confirming a high level of gene targeting after tamoxifen induction rather than using reporter expression as a proxy.

7.2 General conclusions

The data presented in this thesis revealed an essential role for the RNA-binding protein SRSF3 in proliferation of (pro)epicardial cells and formation of EPDCs. Genetic manipulation of SRSF3 led to a wide range of phenotypes dependent on the efficiency and the specificity of the Cre driver used (Table 7.1).

This thesis also presented data that support a homogeneous composition of the epicardial layer and argues against pre-specification of epicardium-derived cell fate.

Table 7.1 Summary of *Srsf3* mutant phenotypes

Cre		***Tg(Gata5-Cre)***	***Wt1*^{CreERT2}**		
Induction		Constitutive	E8.5	E9.5/E11.5	E11.5
Specificity		PEO, Epi, LV CMs	PEO, Epi	Epi, EPDCs 10% endothelial	Epi, EPDCs, endothelial
Phenotype	**Epi-lineage**	Failed Epi formation	Epi formed No EPDCs	Compensation	Fewer EPDCs
	Non-Epi	Death mid-gestation Targeted CMs apoptotic	No coronary vessels No ventricular compaction		Enlarged vessels

PEO-proepicardial organ, Epi-epicardium, LV-left ventricle, CM-cardiomyocyte, EPDC-epicardium-derived cell

7.3 Future work

The results presented in this thesis have highlighted possible mechanisms of SRSF3 function in the epicardial lineage during heart development. It was argued in this thesis that SRSF3 is required for proliferation of proepicardial progenitors, and later on, for epicardial cell expansion and EPDC formation. The role of SRSF3 in maintaining epicardial identity was also investigated. It was concluded that SRSF3 is not required for expression of epicardial markers or vice versa.

These findings provided multiple leads for further investigations focused on dissecting the molecular mechanisms involved in proliferation, EPDC production and coronary vessel formation. The limitations and challenges of studying SRSF3 have also been highlighted in this thesis. This will inform future studies and help improve experimental design.

The main questions that remain to be addressed are:

- What is the molecular mechanism through which SRSF3 impacts proliferation in proepicardial and epicardial cells?
- How does SRSF3 depletion prevent EPDC formation *in vivo*?
- What are the molecular mechanisms which prevent vessel growth from the sinus venosus and the endocardium in *Wt1*^{CreERT2}*; Srsf3*$^{fl/fl}$ mutants?
- How is compensation triggered in *Wt1*^{CreERT2}*; Srsf3*$^{fl/fl}$ mutants?

7.3.1 Determine the molecular role of SRSF3 in (pro)epicardial proliferation

The results presented in Chapter III showed SRSF3 is required for proliferation of proepicardial and epicardial cells. However, quantification of this phenotype was not possible *in vivo* using proliferation antibodies, such as Ki67 and pHH3. Ki67 staining was widespread in the embryo, making it difficult to separate (pro)epicardial cells from surrounding tissue. Moreover, Ki67 would not reflect cell cycle arrest since it is expressed during all stages of the cell cycle. In the case of pHH3, which only marks mitotic cells, very few cells were positive in the control, making it difficult to assess a difference in mutants. Better proliferation assays, such as EdU incorporation, are required to confirm the non-proliferative phenotype of SRSF3 depleted cells *in vivo*.

Since SRSF3 downregulation has also been shown to trigger cellular senescence [199], a senescence assay could be used to assess if SRSF3 depleted cells are senescent. The lack of Ki67 staining in SRSF3 depleted cells may reflect senescence, but this requires further confirmation.

Furthermore, both Cyclin D1 and PDCD4 were altered in SRSF3 depleted cells. In order to confirm these targets are valid *in vivo*, an RNA-immunoprecipitation assay such as RIP-Seq or iCLIP, could be used to investigate if SRSF3 directly binds to these targets in sorted epicardial cells.

Further studies could also be done *in vitro*, where EdU staining can be to used separate S from G2 phase and determine the cell cycle profile after SRSF3 depletion.

7.3.2 Investigate the molecular mechanism of impaired EPDC formation in *Wt1*^{CreERT2}*; Srsf3*$^{fl/fl}$ mutants

Wt1^{CreERT2}*; Srsf3*$^{fl/fl}$ mutants had reduced EPDC formation early in development, with tamoxifen-induced mutants at E8.5 failing to produce EPDCs throughout the course of development, whereas E9.5 and E9.5/E11.5-induced mutants compensated by non-targeted cells that produced EPDCs, indicating E8.5 administration is more effective in targeting SRSF3.

Basescope, which is a novel RNA *in situ* hybridisation technique that allows labelling of short segments of mRNA and discrimination of different isoforms [317], could be used to determine the extent of *Srsf3* recombination after different tamoxifen regimes and confirm all EPDCs that formed in these mutants had indeed retained SRSF3.

Since signals from other sources, such as myocardium, have been involved in epicardial EMT [305], further analysis of the E13.5 transcriptomics data should reveal if there are any differential expressed genes in other cellular compartments that could explain the failure of EPDC formation.

Further studies could also be performed *in vitro*, where SRSF3 knockdown prevented epicardial cells from undergoing TGFβ-induced EMT. RNA-sequencing could be performed on these cells to determine which genes fail to be upregulated in response to TGFβ, compared to control.

7.3.3 Examine the molecular mechanisms of impaired vessel sprouting in *Wt1*^{CreERT2}; *Srsf3*$^{fl/fl}$ mutants

E13.5 *Wt1*^{CreERT2}; *Srsf3*$^{fl/fl}$ mutants presented impaired sprouting from both the sinus venosus and the endocardium. The defects in sprouting could be a direct result of loss of epicardium-derived signals in SRSF3 depleted cells, or it could be a secondary defect of myocardial non-compaction, which has been shown to be required for vessel formation previously [139]. Further analysis of the E13.5 single-cell transcriptomics data may reveal differentially expressed genes in these vasculogenic compartments. Preliminary data showed that *Cyr6*1 is increased in SV cells in mutants (data not shown). Cysteine-rich angiogenic inducer 61 (CYR61) is a proliferation-inducing ECM-associated gene that can be upregulated by hypoxia [318]. It is possible that increased hypoxia in mutant hearts leads to hyperproliferative behaviour of endothelial cells, which has been shown to negatively affect sprouting [319]. Further studies are needed to assess endothelial cell proliferation in *Srsf3* mutants.

7.3.4 Determine how compensation is achieved in *Wt1*^{CreERT2}; *Srsf3*$^{fl/fl}$ mutants

Wt1^{CreERT2}; *Srsf3*$^{fl/fl}$ mutants, tamoxifen-induced at E9.5/E11.5, present defects at E13.5, but they fully recover by E17.5. E15.5 analysis revealed SRSF3 depleted cells are lost in these hearts, however, it remains to be determined how these cells are eliminated.

E13.5 single-cell RNA-sequencing data revealed that hypoxia-induced cell death genes are upregulated in a subset of epicardial cells, but no increase in cleaved-caspase 3 (CC3) was detected in these hearts, therefore, other apoptotic assays such as TUNEL can be used to determine if, and when, SRSF3 depleted cells undergo cell death. Basescope can be used to simultaneously detect hypoxia-induced cell death genes and the mutant *Srsf3* mRNA, to confirm that only SRSF3 depleted cells undergo hypoxia-induced cell death.

Another factor that might contribute to the elimination of these cells could be cell competition. *Pim1*, a co-factor of c-MYC [290], was upregulated in cells that escaped recombination in E15.5 mutants. Epicardial co-cultures from E15.5 *Wt1*$^{CreERT2;}$ *Srsf3*$^{fl/fl}$ mutants and controls could be used to assess if 'mutant' epicardial cells are hyperproliferative and outcompete control cells. This type of co-culture has been previously used for c-MYC overexpression explants to study cell competition in the epicardium [302]. The c-MYC overexpressing epicardial cells proliferated faster and covered neighbouring epicardial explants, replacing wild-type epicardial cells.

7.4 Final remarks

The data obtained in this thesis demonstrated that SRSF3 is required for proper epicardial function during heart development. The involvement of SRSF3 in several aspects of epicardial function, such as proliferation and EMT, suggests that SRSF3 is a master regulator of RNA metabolism in the epicardium . Further investigation into the molecular mechanisms regulated by SRSF3 could expand our understanding of epicardial biology and contribute towards the design of better regenerative therapies.

Appendix

Publications

Currently in revision at *Stem Cell Reports* (Chapter V results):

Spatiotemporal analysis reveals significant overlap of key proepicardial markers in the developing murine heart
Irina-Elena Lupu*, Andia N. Redpath*, Nicola Smart
bioRxiv 666610; doi: https://doi.org/10.1101/666610

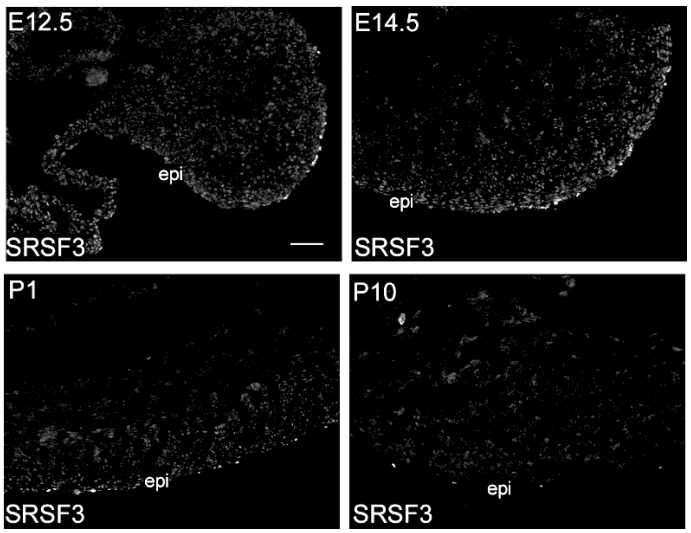
Review in preparation:

Coronary vessel formation in the ischaemic heart: mechanisms and insight towards therapy. Invited review for *Nature Reviews Cardiology.*
Irina-Elena Lupu, Sarah De Val, Nicola Smart

Manuscript in preparation:

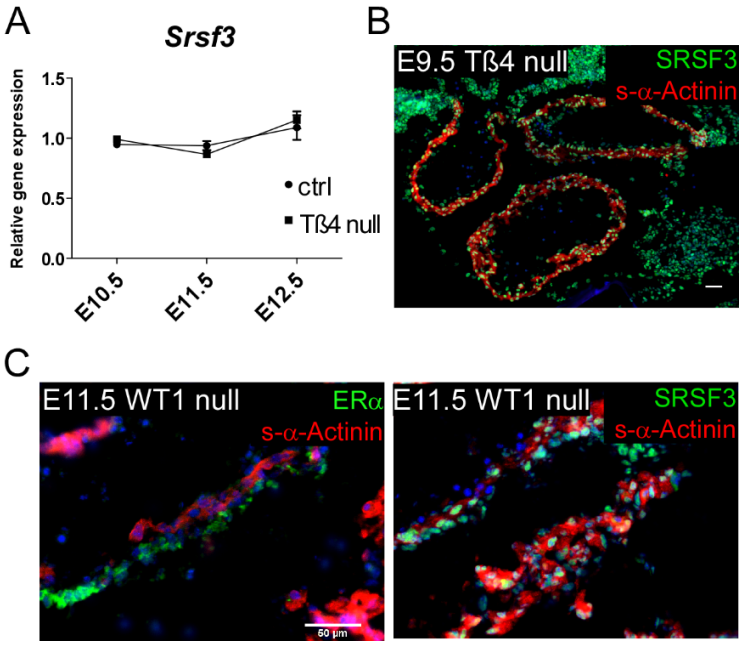
SRSF3 is required for epicardium formation and EMT during heart development.
Irina-Elena Lupu, Andia Redpath, Nicola Smart

Figures



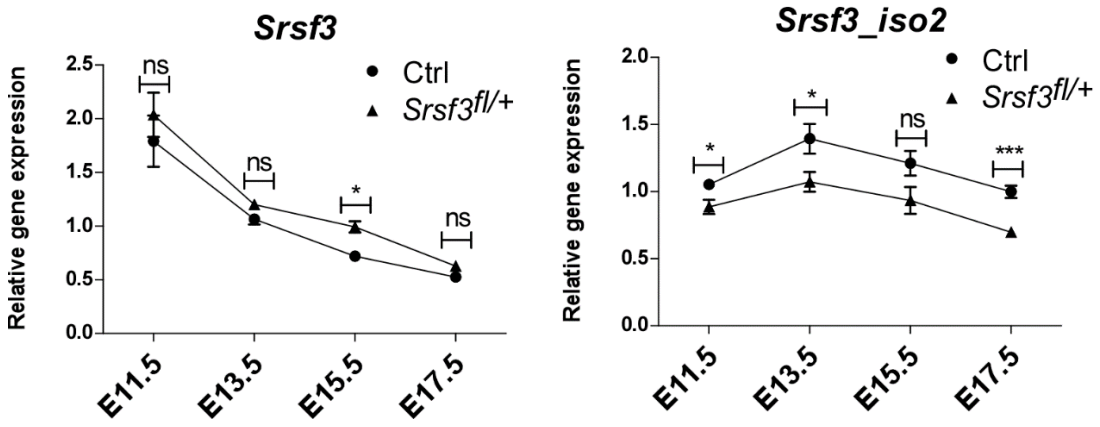
Appendix Figure 3.1 SRSF3 expression decreases throughout development

Immunostaining for SRSF3 was performed on E12.5, E14.5, postnatal day 1 (P1), P10. These stages complete the time course shown in Figure 3.2. The expression of SRSF3 in the heart decreased as development progressed. epi-epicardium. Scale bar: 100 μm.



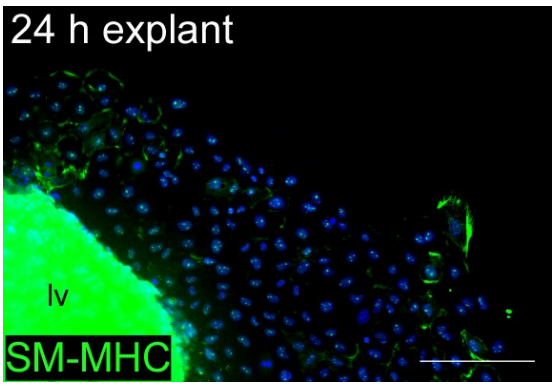
Appendix Figure 3.2 SRSF3 is not changed in Tβ4 null or WT1 null embryos

***(A)** RT-qPCR for Srsf3 on E 10.5, E11.5, E12.5 embryonic hearts shows no difference between Srsf3 expression in control and Tβ4 nulls. n=2 hearts/stage. **(B)** IHC for SRSF3 on E 9.5 sagittal sections from Tβ4 null embryos shows SRSF3 expression. Scale bar: 50 μm. **(C)** IHC for estrogen receptor α (ERα) shows epicardial cells still express SRSF3 in WT1 null hearts. Scale bar: 50 μm.*



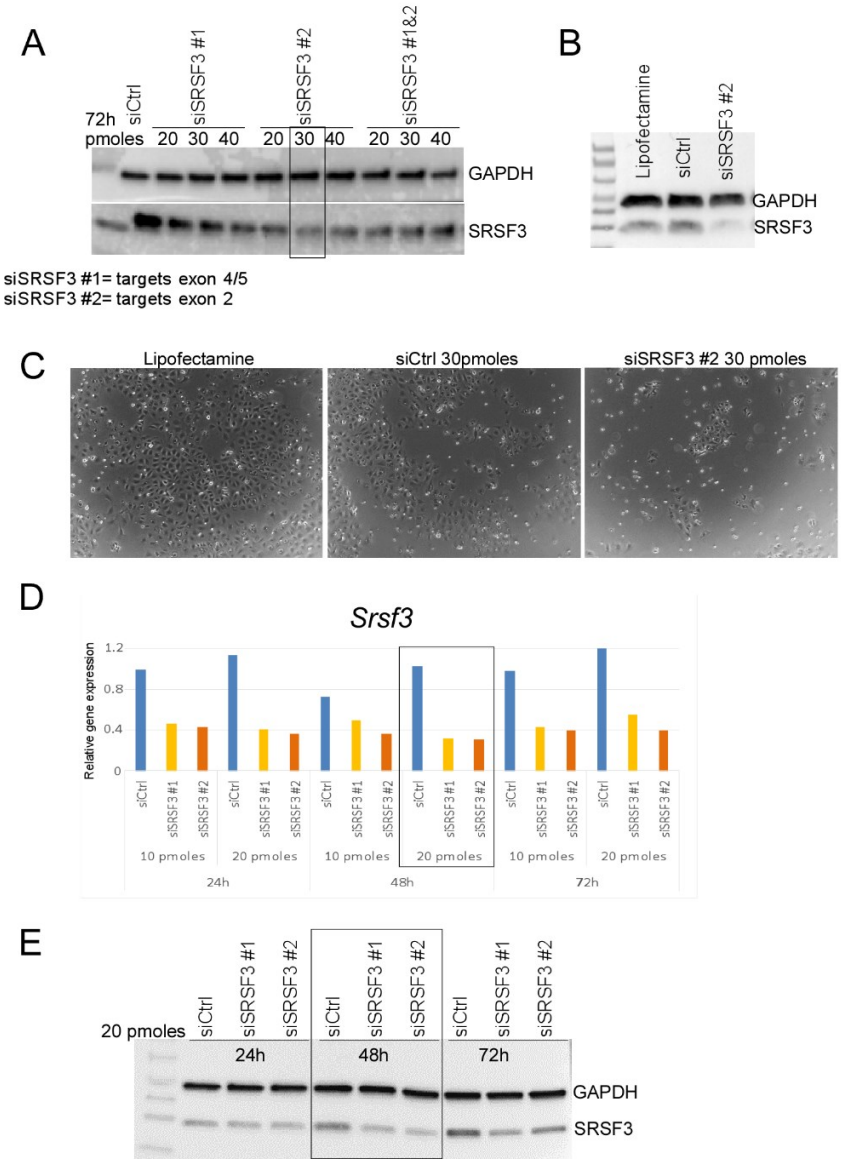
Appendix Figure 3.3 SRSF3 expression is not affected in heterozygotes

RT-qPCR data shows no difference in the expression of the functional isoform of Srsf3 in heterozygote hearts throughout development, whereas the non-functional isoform of Srsf3 is decreased in the heterozygote. Student's t-test, p<0.0.5(*), p<0.001 (***). ns-not-significant. n=5 hearts/stage.



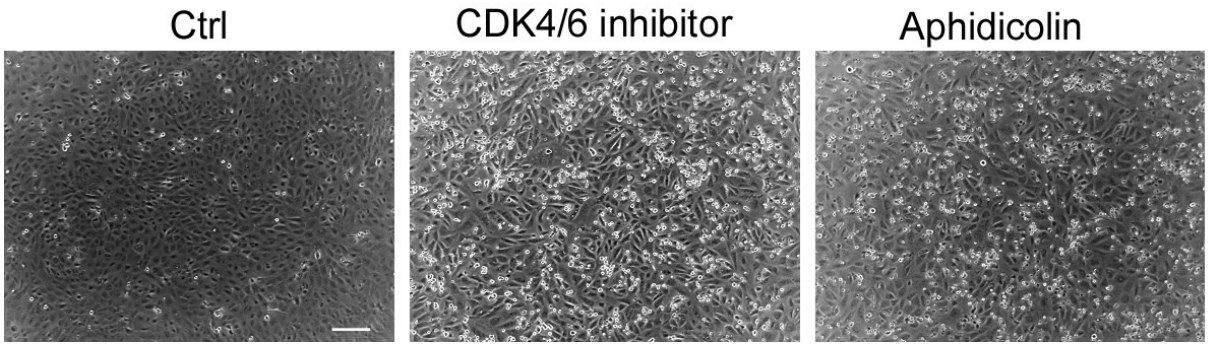
Appendix Figure 3.4 Epicardial cells differentiate to smooth muscle cells by 24 h in culture

Immunostaining for SM-MHC on a left ventricle explant culture for 24 h shows epicardial cells differentiated to vascular smooth muscle. lv-left ventricle. Scale bar: 200 µm.



Appendix Figure 3.5 Optimisation of SRSF3 knock down using RNA interference

(A) Western blot performed on protein extracts from 72 h transfected cells with 20, 30 or 40 pmoles of siControl (siCtrl) or two different siRNAs targeting SRSF3. SiSRSF3 #2 was the most efficient at 60 nM concentration (boxed region). GAPDH was used as loading control (B) Repeat of the transfection with siSRSF3 #2 comparing lipofectamine control and siCtrl. (C) Brightfield images of cells transfected with either just lipofectamine, siCtrl or siSRSF3 #2 for 72 h reveals toxicity of the siSRSF3 #2 at 60nM. (D) RT-qPCR data from epicardial cell line transfected for either 24 h, 48 h or 72 h with 10 pmoles or 20 pmoles of siCtrl, siSRSF3 #1 and siSRSF3 #2. Boxed region shows the highest decrease in Srsf3. (E) Western Blot of protein extract from cells transfected for either 24, 48 or 72 h with 20 pmoles of siCtrl, siSRSF3 #1 and siSRSF3. Boxed region shows the most efficient condition. GAPDH used as loading control.

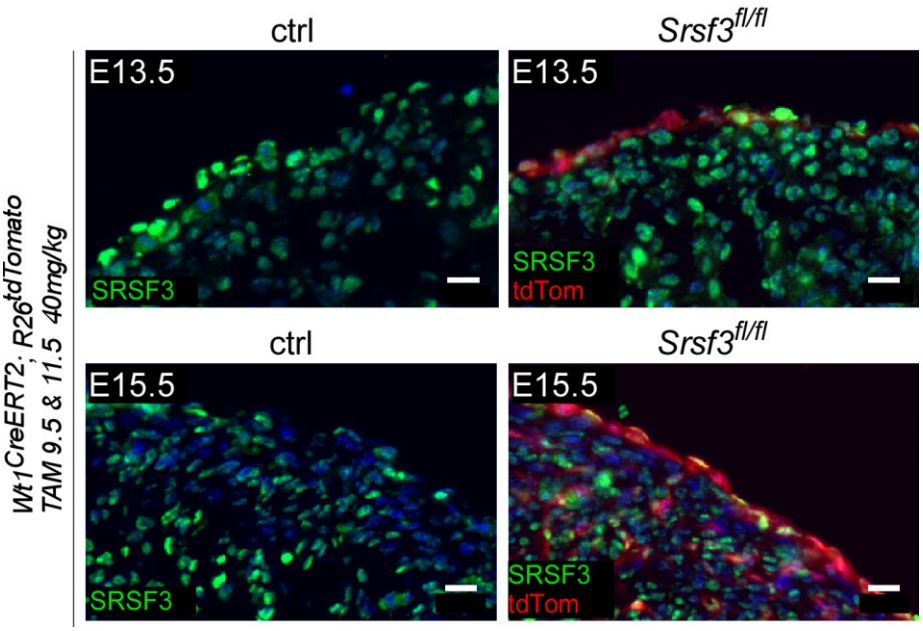


Appendix Figure 3.6 Cell cycle inhibition results in cell death in the mouse epicardial cell lines

Brightfield images of the mouse epicardial cell line treated with cell cycle inhibitors, CDK4/6 inhibitor PD 0332991 isethionate or Aphidicolin. N>5. Scale bar: 100 µm.

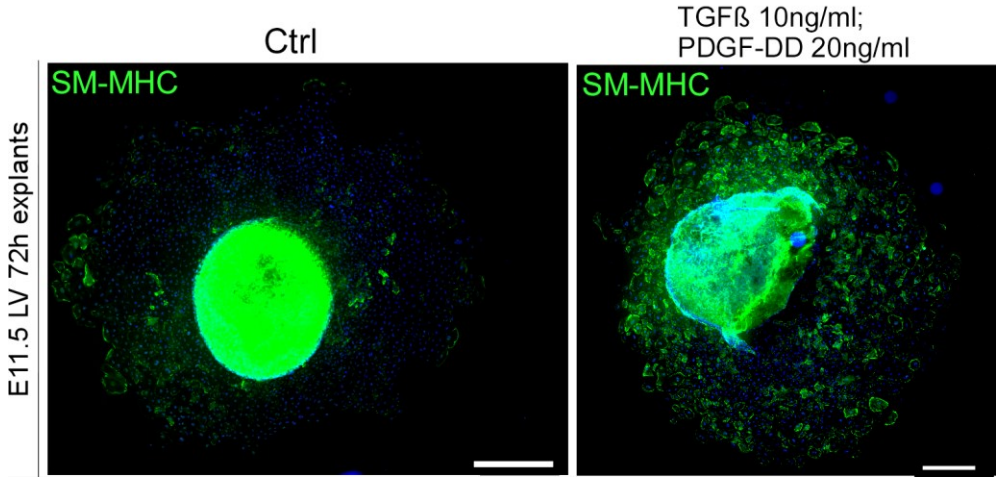
Appendix Table 4.1 *Wt1*^{CreERT2}*; Srsf3*^{fl} timed matings produce few embryos

Mother			Embryos	
Genotype	Plugged	Pregnant	Cre+	Cre-
Cre+	16	7	2	10
Cre-	47	26	50	51



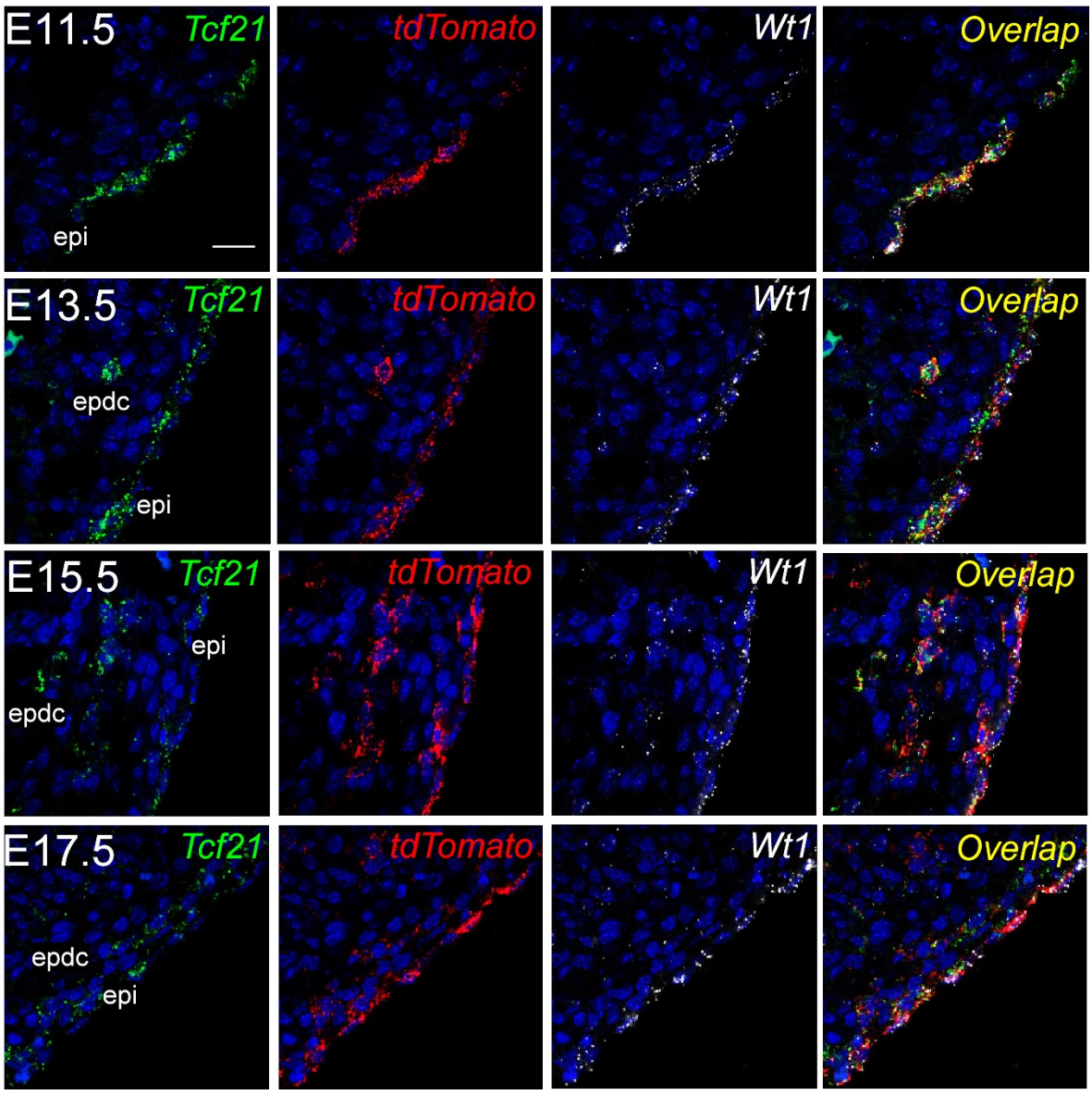
Appendix Figure 4.1 SRSF3 immunostaining in early and late embryonic hearts.

Immunostaining for SRSF3 was performed on E13.5 and E 15.5 control and mutant hearts that received tamoxifen at E9.5/E11.5. SRSF3 levels are high in the epicardium at E13.5 and decreased in mutant hearts. At E15.5, SRSF3 production is decreased in the heart in both control and mutants. N=3. Scale bar: 20 µm.



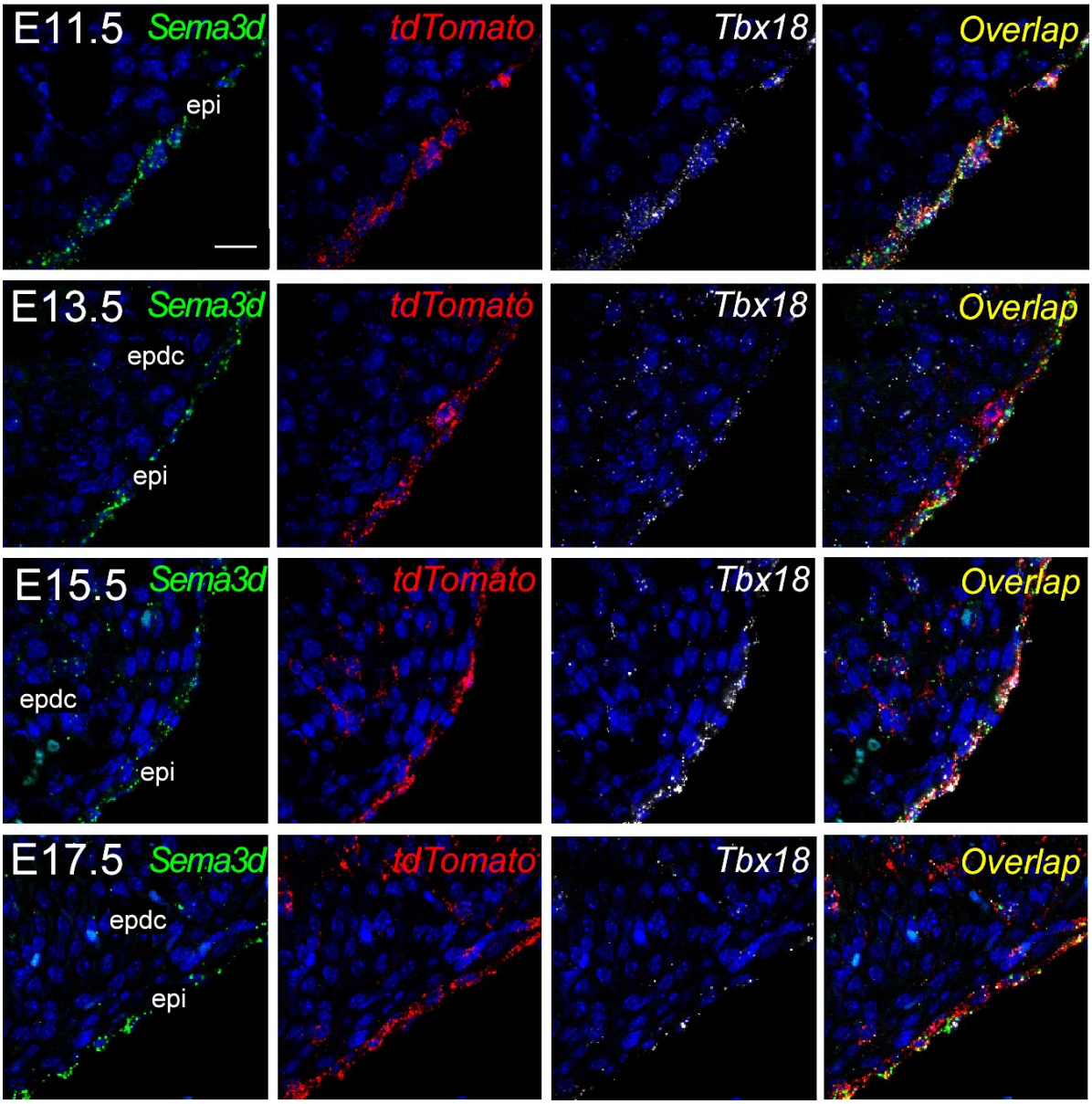
Appendix Figure 4.2 Epicardial explants differentiate to vSMC in response to TGFβ and PDGF-DD

Immunostaining for smooth muscle myosin heavy chain (SM-MHC) was performed on E11.5 ventricular explants grown either in medium or in the presence of TGFβ/PDGF-DD for 72h shows increased differentiation to vascular smooth muscle (vSMC) with treatment, Scale bar: 500 µm.



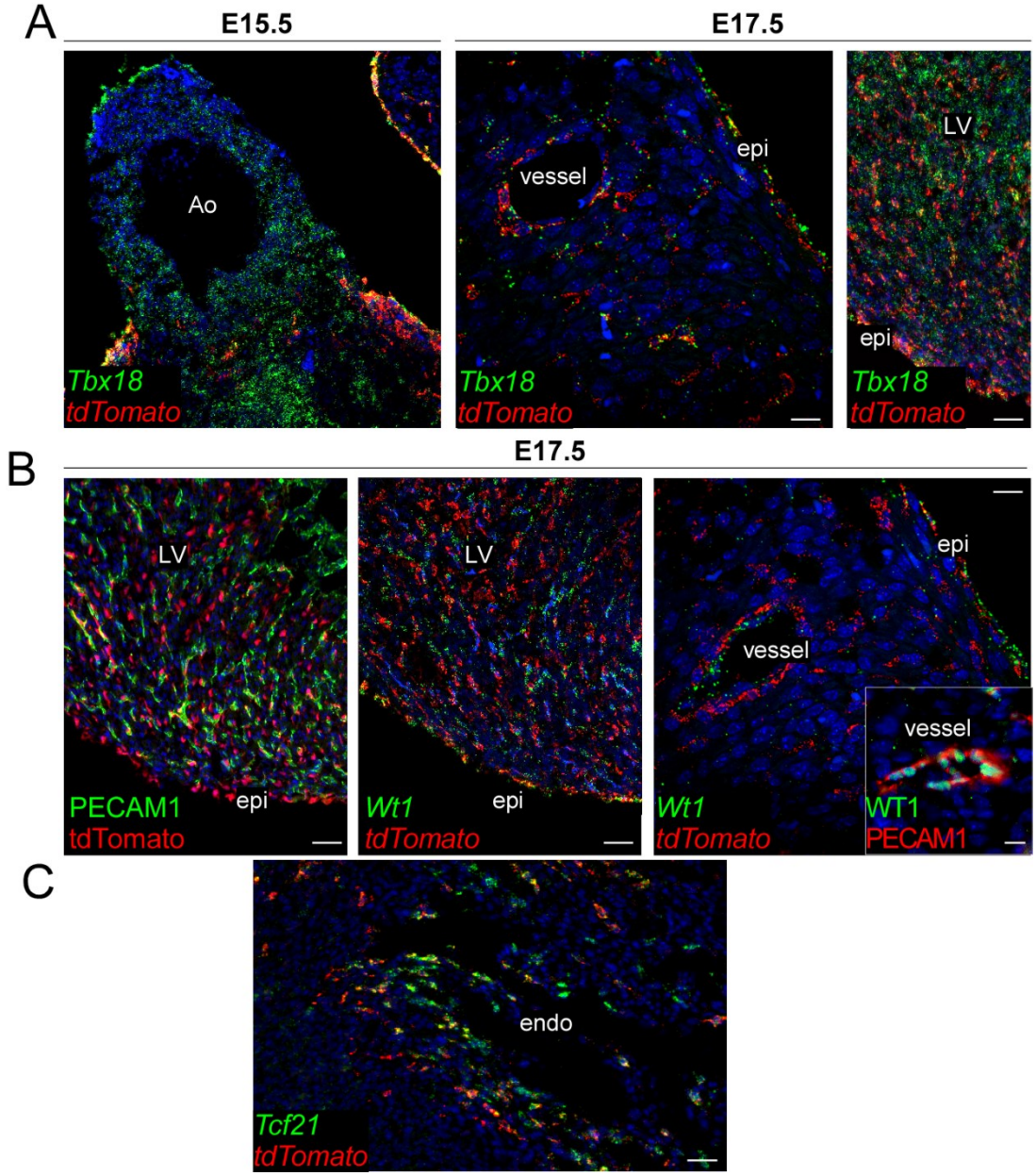
Appendix Figure 5.1 *Wt1* expression is reduced in epicardium-derived cells, whereas *Tcf21* expression is maintained

RNA ISH co-staining of tdTomato and the epicardial markers Tcf21 and Wt1 at E13.5, E15.5, E17.5 shows overlap in the epicardium at E11.5. Tcf21 expression in the epicardium decreases at later stages, whereas expression is maintained in epicardium-derived cells. Wt1 is continuously expressed in the epicardium, decreased in epicardium-derived cells. Epi-epicardium, epdc-epicardium-derived cells. n=3. Scale bar: 20 μm.



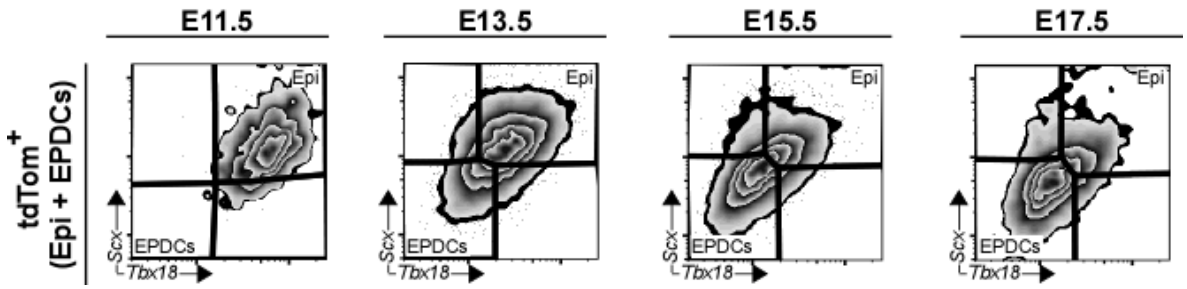
Appendix Figure 5.2 Expression of *Sema3d* and *Tbx18* are reduced in epicardium-derived cells

RNA ISH co-staining of tdTomato and the epicardial markers Sema3d and Tbx18 at E13.5, E15.5, E17.5 shows overlap in the epicardium and decreased expression in epicardium-derived cells. Epi-epicardium, epdc-epicardium-derived cells. n=3. Scale bar: 20 μm.



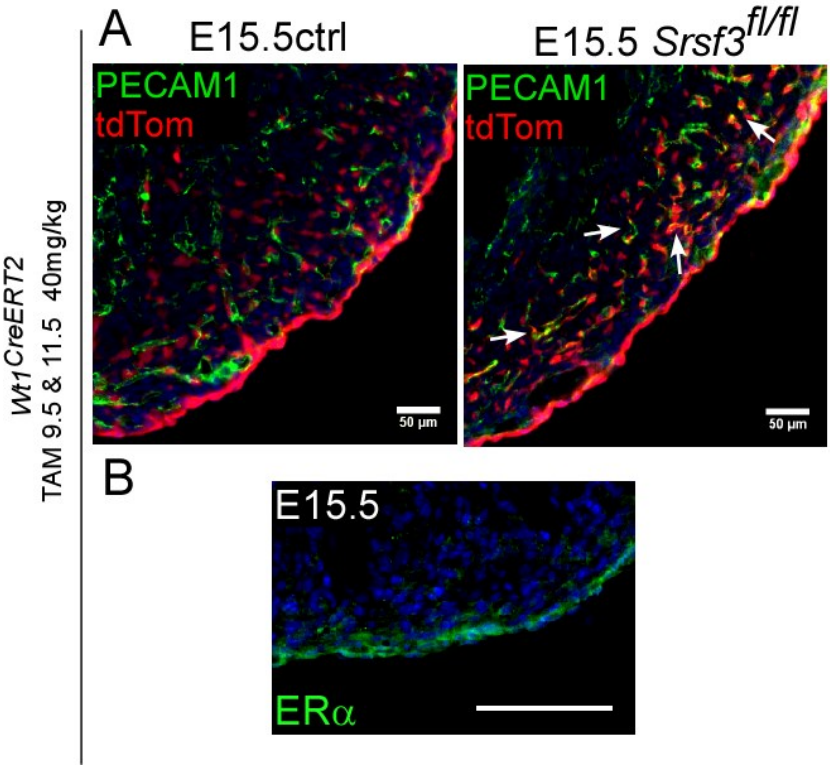
Appendix Figure 5.3 Non-specificity of epicardial markers at later developmental stages

*(**A**) RNA ISH co-staining of Tbx18 and tdTomato reveals Tbx18 expression in vascular smooth muscle cells derived from both non-epicardial (aorta) and epicardial sources (coronary). Tbx18 is expressed in cardiomyocytes. (**B**) Co-immunostaining of PECAM1 and tdTomato shows no contribution of the epicardial lineage to coronary endothelium. Immunohistochemistry co-staining of WT1 and PECAM1 reveals Wt1 expression in coronary endothelium cells. (**C**) Tcf21 is expressed in all cardiac fibroblasts, independent of origin. epi-epicardium; EPDCs-epicardium-derived cells; Ao-aorta; LV- left ventricle. Scale bars: 50μm; 10μm in inset B.*



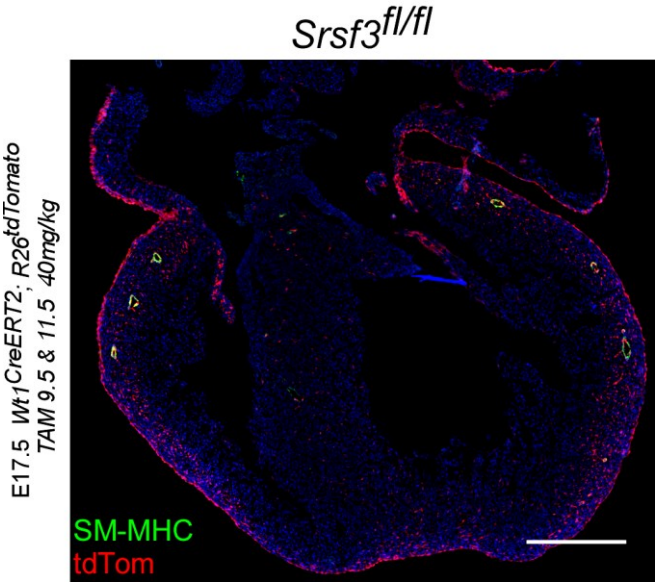
Appendix Figure 5.4 *Scx* and *Tbx18* expression decrease in epicardium-derived cells.

Flow cytometric analysis of dissociated E11.5 (n=31 hearts), E13.5 (n=25 hearts, three experiments, E15.5 (n=10 hearts) and E17.5 hearts (n=2 hearts, two experiments).TdTomato+ cells, representing the epicardial lineage, selected by gating CD31-cTnT-tdTomato+, show overall loss of Tbx18 and Scx as development progresses.



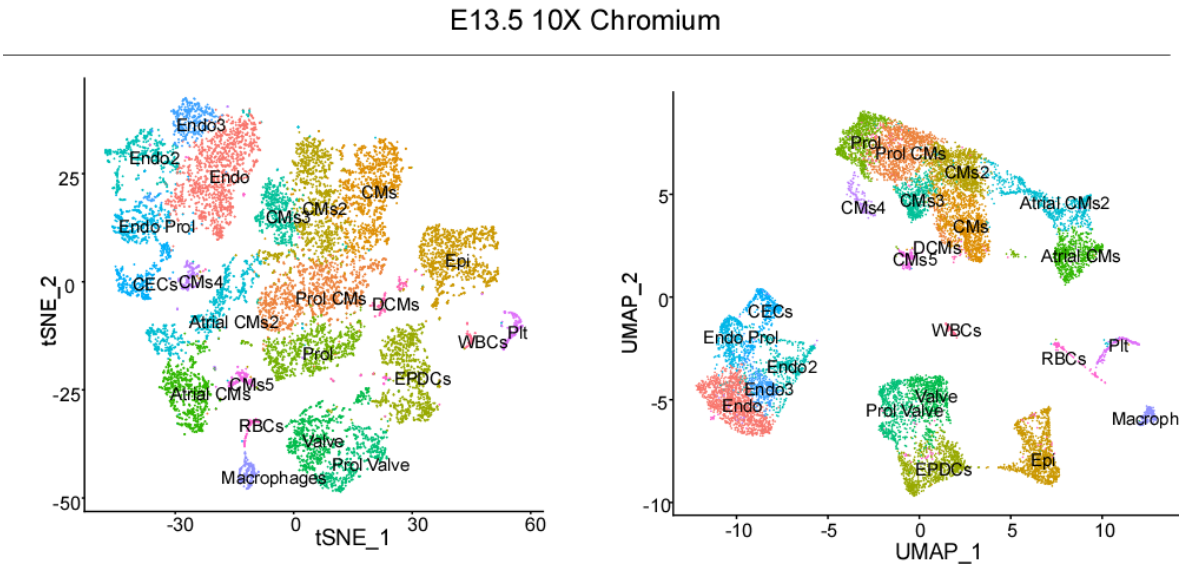
Appendix Figure 6.1 Tamoxifen is not active four days post administration

(A) *Immunofluorescence for tdTomato and PECAM1 shows differentiation to endothelial cells at E15.5 in mutant hearts. n=3. Scale bar: 50 µm.* ***(B)*** *Immunostaining for estrogen receptor α (ERα) was used to assess the effects of tamoxifen administration. Four days after delivery (E15.5), ERα was cytoplasmic, showing the tamoxifen is no longer active. n=2. Scale bar: 100 µm.*



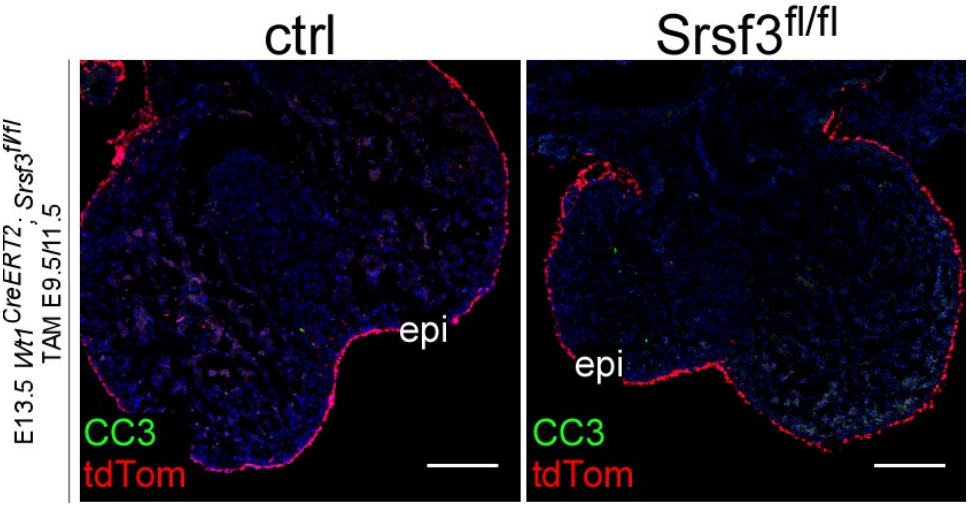
Appendix Figure 6.2 Smooth muscle coverage is normal in E9.5/11.5 induced *Wt1^{CreERT2}; Srsf3$^{fl/fl}$* hearts

Immunostaining for smooth muscle myosin heavy chain (SM-MHC) shows staining around large arteries in E17.5 mutant hearts tamoxifen induced at E9.5/11.5 n=4, Scale bar: 500 μm.



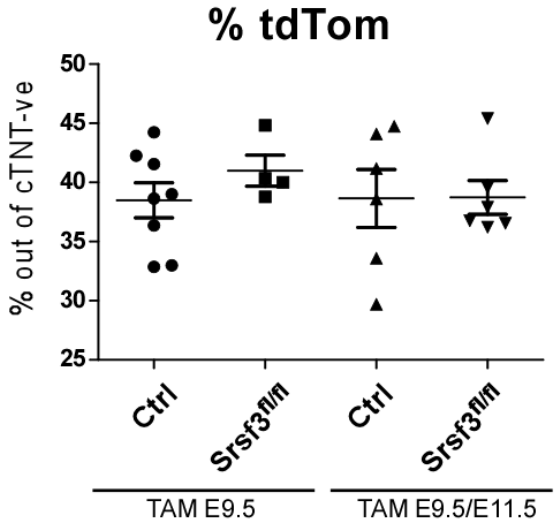
Appendix Figure 6.3 Comparison of tSNE and UMAP visualisation of clusters using the E13.5 whole-heart data.

Visualisation of clusters with UMAP (Uniform Manifold Approximation and Projection for Dimension Reduction) is superior to tSNE (t-distributed stochastic neighbor embedding), due to better preservation of global distances in high-dimensional data. ECs-endothelial cells; Endo-endocardial cells; Epi-epicardium; CMs-cardiomyocytes; Prol-proliferative; EPDCs-epicardium-derived cells; WBCs-white blood cells; RBCs-red blood cells; Plt-platelets.



Appendix Figure 6.4 No increase in CC3 in E13.5 *Wt1^{CreERT2}; Srsf3$^{fl/fl}$* mutants

Immunostaining for cleaved-caspase 3 (CC3) and tdTomato shows no increase in the number of CC3+ cells in mutants. N=2. Scale bar: 100 μm. epi-epicardium.



Appendix Figure 6.5 Comparison of tdTomato labelling at E17.5 after E9.5 and E9.5/E11.5 tamoxifen administration.

The percentage of tdTomato cells in E17.5 whole hearts is not significantly different after E9.5 and E9.5/E11.5 tamoxifen delivery in controls and Wt1^{CreERT2}; Srsf3$^{fl/fl}$ hearts. n=8 over 3 experiments, E9.5 tamoxifen control, n=4 over one experiment E9.4 mutant, n=6 over 3 experiments E9.5/E11.5 control and n=6 over 2 experiments E9.5/E11.5 mutant.

References

1. Hashimoto, H., Olson, E. N. & Bassel-Duby, R. Therapeutic approaches for cardiac regeneration and repair. *Nat. Rev. Cardiol.* **15**, 585–600 (2018).

2. Cahill, T. J., Choudhury, R. P. & Riley, P. R. Heart regeneration and repair after myocardial infarction: translational opportunities for novel therapeutics. *Nat. Rev. Drug Discov.* **16**, 699–717 (2017).

3. Cao, J. & Poss, K. D. The epicardium as a hub for heart regeneration. *Nat. Rev. Cardiol.* **15**, 631–647 (2018).

4. Kikuchi, K. *et al.* tcf21+ epicardial cells adopt non-myocardial fates during zebrafish heart development and regeneration. *Development* **138**, 2895–2902 (2011).

5. Wang, J., Karra, R., Dickson, A. L. & Poss, K. D. Fibronectin is deposited by injury-activated epicardial cells and is necessary for zebrafish heart regeneration. *Dev. Biol.* **382**, 427–435 (2013).

6. Uygur, A. & Lee, R. T. Mechanisms of Cardiac Regeneration. *Dev. Cell* **36**, 362–374 (2016).

7. Cao, Y. & Cao, J. Covering and Re-Covering the Heart: Development and Regeneration of the Epicardium. *J. Cardiovasc. Dev. Dis.* **6**, 3 (2018).

8. Cao, J. *et al.* Single epicardial cell transcriptome sequencing identifies Caveolin 1 as an essential factor in zebrafish heart regeneration. *Development* **143**, 232–243 (2016).

9. Lepilina, A. *et al.* A Dynamic Epicardial Injury Response Supports Progenitor Cell Activity during Zebrafish Heart Regeneration. *Cell* **127**, 607–619 (2006).

10. Smart, N. & Riley, P. R. The epicardium as a candidate for heart regeneration. *Future Cardiol.* **8**, 53–69 (2012).

11. Smart, N. Prospects for improving neovascularization of the ischemic heart: Lessons from development. *Microcirculation* **24**, 1–15 (2017).

12. Smart, N. *et al.* Thymosin β4 induces adult epicardial progenitor mobilization and neovascularization. *Nature* **445**, 177–182 (2006).

13. Wang, J., Cao, J., Dickson, A. L. & Poss, K. D. Epicardial regeneration is guided by cardiac outflow tract and Hedgehog signalling. *Nature* **522**, 226–230 (2015).

14. Lozano, R. *et al.* Global and regional mortality from 235 causes of death for 20 age groups in 1990 and 2010: a systematic analysis for the Global Burden of Disease Study 2010. *Lancet* **380**, 2095–2128 (2012).

15. Olson, E. N. Gene Regulatory Networks in the Evolution and Development of the Heart. *Science* **313**, 1922–1927 (2006).

16. Alsan, B. H. & Schultheiss, T. M. Regulation of avian cardiogenesis by Fgf8 signaling. *Development* **129**, 1935–1943 (2002).

17. Schwartz, R. J. & Olson, E. N. Building the heart piece by piece: modularity of cis-elements regulating Nkx2-5 transcription. *Development* **126**, 4187–4192 (1999).

18. Harvey, R. P. Patterning the vertebrate heart. *Nat. Rev. Genet.* **3**, 544–556 (2002).

19. Marvin, M. J., Di Rocco, G., Gardiner, A., Bush, S. M. & Lassar, A. B. Inhibition of Wnt activity induces heart formation from posterior mesoderm. *Genes Dev.* **15**, 316–327 (2001).

20. Schultheiss, T. M., Burch, J. B. & Lassar, A. B. A role for bone morphogenetic proteins in the induction of cardiac myogenesis. *Genes Dev.* **11**, 451–462 (1997).

21. Cyganek, L., Chen, S., Borchert, T. & Guan, K. Cardiac Progenitor Cells and their Therapeutic Application for Cardiac Repair. *J Clin Exp Cardiol.* **S11**, 008 (2013).

22. Abu-Issa, R., Waldo, K. & Kirby, M. L. Heart fields: one, two or more? *Dev. Biol.* **272**, 281–285 (2004).

23. Ivanovitch, K., Temiño, S. & Torres, M. Live imaging of heart tube development in mouse reveals alternating phases of cardiac differentiation and morphogenesis. *Elife* **6**, e30668 (2017).

24. Hosseini, H. S., Garcia, K. E. & Taber, L. A. A new hypothesis for foregut and heart tube formation based on differential growth and actomyosin contraction. *Development* **144**, 2381 LP – 2391 (2017).

25. Li, S., Zhou, D., Lu, M. M. & Morrisey, E. E. Advanced Cardiac Morphogenesis Does Not Require Heart Tube Fusion. *Science* **305**, 1619–1622 (2004).

26. Linask, K. K., Knudsen, K. A. & Gui, Y.-H. N-Cadherin–Catenin Interaction: Necessary Component of Cardiac Cell Compartmentalization during Early Vertebrate Heart Development. *Dev. Biol.* **185**, 148–164 (1997).

27. Nakagawa, S. & Takeichi, M. N-cadherin is crucial for heart formation in the chick embryo. *Dev. Growth Differ.* **39**, 451–455 (1997).

28. Sugi, Y. & Markwald, R. R. Endodermal growth factors promote endocardial precursor cell formation from precardiac mesoderm. *Dev. Biol.* **263**, 35–49 (2003).

29. Linask, K. K. N-cadherin localization in early heart development and polar expression of Na+, K+-ATPase, and integrin during pericardial coelom formation and epithelialization of the differentiating myocardium. *Dev. Biol.* **151**, 213–224 (1992).

30. Männer, J. & Yelbuz, T. M. Functional Morphology of the Cardiac Jelly in the Tubular Heart of Vertebrate Embryos. *J. Cardiovasc. Dev. Dis.* **6**, 12 (2019).

31. Gibb, N. *et al.* Hey2 regulates the size of the cardiac progenitor pool during vertebrate heart development. *Development* **145**, dev167510 (2018).

32. Mjaatvedt, C. H. *et al.* The Outflow Tract of the Heart Is Recruited from a Novel Heart-Forming Field. *Dev. Biol.* **238**, 97–109 (2001).

33. Waldo, K. L. *et al.* Conotruncal myocardium arises from a secondary heart field. *Development* **128**, 3179–3188 (2001).

34. Kelly, R. G., Brown, N. A. & Buckingham, M. E. The Arterial Pole of the Mouse Heart Forms from Fgf10-Expressing Cells in Pharyngeal Mesoderm. *Dev. Cell* **1**, 435–440 (2001).

35. Cai, C.-L. *et al.* Isl1 Identifies a Cardiac Progenitor Population that Proliferates Prior to

Differentiation and Contributes a Majority of Cells to the Heart. *Dev. Cell* **5**, 877–889 (2003).

36. Hochgreb, T. *et al.* A caudorostral wave of RALDH2 conveys anteroposterior information to the cardiac field. *Development* **130**, 5363–5374 (2003).

37. Laugwitz, K.-L., Moretti, A., Caron, L., Nakano, A. & Chien, K. R. Islet1 cardiovascular progenitors: a single source for heart lineages? *Development* **135**, 193–205 (2008).

38. Moorman, A., Webb, S., Brown, N. A., Lamers, W. & Anderson, R. H. Development of the heart: (1) formation of the cardiac chambers and arterial trunks. *Heart* **89**, 806–814 (2003).

39. Desgrange, A., Le Garrec, J.-F. & Meilhac, S. M. Left-right asymmetry in heart development and disease: forming the right loop. *Development* **145**, dev162776 (2018).

40. Riley, P., Anaon-Cartwight, L. & Cross, J. C. The Hand1 bHLH transcription factor is essential for placentation and cardiac morphogenesis. *Nat. Genet.* **18**, 271–275 (1998).

41. Christoffels, V. M. *et al.* Chamber Formation and Morphogenesis in the Developing Mammalian Heart. *Dev. Biol.* **223**, 266–278 (2000).

42. Plageman Jr, T. F. & Yutzey, K. E. T-box genes and heart development: Putting the “T” in heart. *Dev. Dyn.* **232**, 11–20 (2005).

43. Lin, C.-J., Lin, C.-Y., Chen, C.-H., Zhou, B. & Chang, C.-P. Partitioning the heart: mechanisms of cardiac septation and valve development. *Development* **139**, 3277–3299 (2012).

44. Wessels, A. *et al.* Epicardially derived fibroblasts preferentially contribute to the parietal leaflets of the atrioventricular valves in the murine heart. *Dev. Biol.* **366**, 111–124 (2012).

45. Chakraborty, S. *et al.* Twist1 promotes heart valve cell proliferation and extracellular matrix gene expression during development in vivo and is expressed in human diseased aortic valves. *Dev. Biol.* **347**, 167–179 (2010).

46. Ma, L., Lu, M.-F., Schwartz, R. J. & Martin, J. F. Bmp2 is essential for cardiac cushion epithelial-mesenchymal transition and myocardial patterning. *Development* **132**, 5601–5611 (2005).

47. Sridurongrit, S., Larsson, J., Schwartz, R., Ruiz-Lozano, P. & Kaartinen, V. Signaling via the Tgf-beta type I receptor Alk5 in heart development. *Dev. Biol.* **322**, 208–218 (2008).

48. Plein, A. *et al.* Neural crest-derived SEMA3C activates endothelial NRP1 for cardiac outflow tract septation. *J. Clin. Invest.* **125**, 2661–2676 (2015).

49. Wu, M. Mechanisms of Trabecular Formation and Specification During Cardiogenesis. *Pediatr. Cardiol.* **39**, 1082–1089 (2018).

50. Samsa, L. A. *et al.* Cardiac contraction activates endocardial Notch signaling to modulate chamber maturation in zebrafish. *Development* **142**, 4080–4091 (2015).

51. Lee, K.-F. *et al.* Requirement for neuregulin receptor erbB2 in neural and cardiac development. *Nature* **378**, 394–398 (1995).

52. Liu, J. *et al.* A dual role for ErbB2 signaling in cardiac trabeculation. *Development* **137**, 3867–3875 (2010).

53. Grego-Bessa, J. *et al.* Notch Signaling Is Essential for Ventricular Chamber Development. *Dev. Cell* **12**, 415–429 (2007).

54. Li, J. *et al.* Single-Cell Lineage Tracing Reveals that Oriented Cell Division Contributes to Trabecular Morphogenesis and Regional Specification. *Cell Rep.* **15**, 158–170 (2016).

55. Passer, D., van de Vrugt, A., Atmanli, A. & Domian, I. J. Atypical Protein Kinase C-Dependent Polarized Cell Division Is Required for Myocardial Trabeculation. *Cell Rep.* **14**, 1662–1672 (2016).

56. Li, G. *et al.* Single cell expression analysis reveals anatomical and cell cycle-dependent transcriptional shifts during heart development. *Development* **146**, dev173476 (2019).

57. D'Amato, G., Luxán, G. & de la Pompa, J. L. Notch signalling in ventricular chamber development and cardiomyopathy. *FEBS J.* **283**, 4223–4237 (2016).

58. Tian, X. *et al.* Vessel formation. De novo formation of a distinct coronary vascular population in neonatal heart. *Science* **345**, 90–94 (2014).

59. Hutchins, G. M., Kessler-Hanna, A. & Moore, G. W. Development of the coronary arteries in the embryonic human heart. *Circulation* **77**, 1250–1257 (1988).

60. Bogers, A. J. J. C., Gittenberger-De Groot, A. C., Poelmann, R. E., Peault, B. M. & Huysmans, H. A. Development of the origin of the coronary arteries, a matter of ingrowth or outgrowth? *Anat. Embryol. (Berl).* **180**, 437–441 (1989).

61. Mikawa, T. & Fischman, D. A. Retroviral analysis of cardiac morphogenesis: discontinuous formation of coronary vessels. *Proc. Natl. Acad. Sci. U. S. A.* **89**, 9504–9508 (1992).

62. Mikawa, T. & Gourdie, R. G. Pericardial Mesoderm Generates a Population of Coronary Smooth Muscle Cells Migrating into the Heart along with Ingrowth of the Epicardial Organ. *Dev. Biol.* **174**, 221–232 (1996).

63. Männer, J. Does the subepicardial mesenchyme contribute myocardioblasts to the myocardium of the chick embryo heart? A quail-chick chimera study tracing the fate of the epicardial primordium. *Anat. Rec.* **255**, 212–226 (1999).

64. Groot, A. C. G., Peeters, M.-P. F. M. V., Mentink, M. M. T., Gourdie, R. G. & Poelmann, R. E. Epicardium-Derived Cells Contribute a Novel Population to the Myocardial Wall and the Atrioventricular Cushions. *Circ. Res.* **82**, 1043–1052 (1998).

65. Zhou, B. & Pu, W. T. Genetic Cre-loxP assessment of epicardial cell fate using Wt1-Driven cre alleles. *Circ. Res.* **111**, 276–280 (2012).

66. Acharya, A., Baek, S. T., Banfi, S., Eskiocak, B. & Tallquist, M. D. Efficient inducible Cre-mediated recombination in Tcf21 cell lineages in the heart and kidney. *Genesis* **49**, 870–877 (2011).

67. Cai, C.-L. *et al.* A myocardial lineage derives from Tbx18 epicardial cells. *Nature* **454**, 104–108 (2008).

68. Katz, T. C. *et al.* Distinct Compartments of the Proepicardial Organ Give Rise to Coronary Vascular Endothelial Cells. *Dev. Cell* **22**, 639–650 (2012).

69. Cano, E. *et al.* Extracardiac septum transversum/proepicardial endothelial cells pattern

embryonic coronary arterio–venous connections. *Proc. Natl. Acad. Sci.* **113**, 656–661 (2016).

70. Metzger, D., Clifford, J., Chiba, H. & Chambon, P. Conditional site-specific recombination in mammalian cells using a ligand-dependent chimeric Cre recombinase. *Proc. Natl. Acad. Sci. U. S. A.* **92**, 6991–6995 (1995).

71. Ambu, R. *et al.* WT1 expression in the human fetus during development. *Eur. J. Histochem.* **59**, 156–163 (2015).

72. Christoffels, V. M. *et al.* Tbx18 and the fate of epicardial progenitors. *Nature* **458**, E8–E9 (2009).

73. Bagchi, R. A. *et al.* The transcription factor scleraxis is a critical regulator of cardiac fibroblast phenotype. *BMC Biol.* **14**, 21 (2016).

74. Aghajanian, H. *et al.* Coronary vasculature patterning requires a novel endothelial ErbB2 holoreceptor. *Nat. Commun.* **7**, 1–9 (2016).

75. Reinert, R. B. *et al.* Tamoxifen-induced cre-loxp recombination is prolonged in pancreatic islets of adult mice. *PLoS One* **7**, e33529 (2012).

76. Pu, W. *et al.* Genetic targeting of organ-specifc blood vessels. *Circ. Res.* **123**, 86–99 (2018).

77. Chen, H. I. *et al.* The sinus venosus contributes to coronary vasculature through VEGFC-stimulated angiogenesis. *Development* **141**, 4500–4512 (2014).

78. Red-Horse, K., Ueno, H., Weissman, I. L. & Krasnow, M. A. Coronary arteries form by developmental reprogramming of venous cells. *Nature* **464**, 549–553 (2010).

79. Kamimura, T., Yamagishi, T. & Nakajima, Y. Avian coronary endothelium is a mosaic of sinus venosus- and ventricle-derived endothelial cells in a region-specific manner. *Dev. Growth Differ.* **60**, 97–111 (2018).

80. Hui, Z. *et al.* Endocardium Minimally Contributes to Coronary Endothelium in the Embryonic Ventricular Free Walls. *Circ. Res.* **118**, 1880–1893 (2016).

81. Acharya, A. *et al.* The bHLH transcription factor Tcf21 is required for lineage-specific EMT of cardiac fibroblast progenitors. *Development* **139**, 2139–2149 (2012).

82. Merki, E. *et al.* Epicardial retinoid X receptor is required for myocardial growth and coronary artery formation. *Proc. Natl. Acad. Sci.* **102**, 18455–18460 (2005).

83. Tomanek, R. J. *et al.* Multiple growth factors regulate coronary embryonic vasculogenesis. *Dev. Dyn.* **221**, 265–273 (2001).

84. Kattan, J., Dettman, R. W. & Bristow, J. Formation and remodeling of the coronary vascular bed in the embryonic avian heart. *Dev. Dyn.* **230**, 34–43 (2004).

85. Olivey, H. E. & Svensson, E. C. Epicardial-myocardial signaling directing coronary vasculogenesis. *Circ. Res.* **106**, 818–832 (2010).

86. Sharma, B. *et al.* Alternative Progenitor Cells Compensate to Rebuild the Coronary Vasculature in Elabela- and Apj-Deficient Hearts. *Dev. Cell* **42**, 655-666.e3 (2017).

87. Chen, H. I. *et al.* VEGF-C and aortic cardiomyocytes guide coronary artery stem development. *J. Clin. Invest.* **124**, 1–10 (2014).

88. Ivins, S. *et al.* The CXCL12/CXCR4 Axis Plays a Critical Role in Coronary Artery Development. *Dev. Cell* **33**, 455–468 (2015).

89. Su, T. *et al.* Single-cell analysis of early progenitor cells that build coronary arteries. *Nature* **559**, 356–362 (2018).

90. Chang, A. H. *et al.* DACH1 stimulates shear stress-guided endothelial cell migration and coronary artery growth through the CXCL12-CXCR4 signaling axis. *Genes Dev.* **31**, 1308–1324 (2017).

91. Wei, K. *et al.* Developmental origin of age-related coronary artery disease. *Cardiovasc. Res.* **107**, 287–294 (2015).

92. Liu, Q. *et al.* Smooth muscle origin of postnatal 2nd CVP is pre-determined in early embryo. *Biochem. Biophys. Res. Commun.* **471**, 430–436 (2016).

93. Arima, Y. *et al.* Preotic neural crest cells contribute to coronary artery smooth muscle involving endothelin signalling. *Nat. Commun.* **3**, 1267 (2012).

94. Chen, Q. *et al.* Endothelial cells are progenitors of cardiac pericytes and vascular smooth muscle cells. *Nat. Commun.* **7**, 12422 (2016).

95. Tian, X. *et al.* Subepicardial endothelial cells invade the embryonic ventricle wall to form coronary arteries. *Cell Res.* **23**, 1075–1090 (2013).

96. Mellgren, A. M. *et al.* Platelet-derived growth factor receptor β signaling is required for efficient epicardial cell migration and development of two distinct coronary vascular smooth muscle cell populations. *Circ. Res.* **103**, 1393–1401 (2008).

97. Sinha, S., Iyer, D. & Granata, A. Embryonic origins of human vascular smooth muscle cells: implications for in vitro modeling and clinical application. *Cell. Mol. Life Sci.* **71**, 2271–2288 (2014).

98. Christoffels, V. M. *et al.* Formation of the venous pole of the heart from an Nkx2-5-negative precursor population requires Tbx18. *Circ. Res.* **98**, 1555–1563 (2006).

99. Kruithof, B. P. T. T. *et al.* BMP and FGF regulate the differentiation of multipotential pericardial mesoderm into the myocardial or epicardial lineage. *Dev. Biol.* **295**, 507–522 (2006).

100. Ma, Q., Zhou, B. & Pu, W. T. Reassessment of Isl1 and Nkx2-5 cardiac fate maps using a Gata4-based reporter of Cre activity. *Dev. Biol.* **323**, 98–104 (2008).

101. van Wijk, B. *et al.* Epicardium and myocardium separate from a common precursor pool by crosstalk between bone morphogenetic protein- and fibroblast growth factor-signaling pathways. *Circ. Res.* **105**, 431–441 (2009).

102. Mommersteeg, M. T. M. *et al.* The sinus venosus progenitors separate and diversify from the first and second heart fields early in development. *Cardiovasc. Res.* **87**, 92–101 (2010).

103. Ishii, Y., Langberg, J. D., Hurtado, R., Lee, S. & Mikawa, T. Induction of proepicardial marker gene expression by the liver bud. *Development* **134**, 3627–3637 (2007).

104. Andrés-Delgado, L. *et al.* Actin dynamics and the Bmp pathway drive apical extrusion of proepicardial cells. *Development* **146**, dev174961 (2019).

105. Hirose, T. PAR3 is essential for cyst-mediated epicardial development by establishing apical cortical domains. *Development* **133**, 1389–1398 (2006).

106. Ishii, Y., Garriock, R. J., Navetta, A. M., Coughlin, L. E. & Mikawa, T. BMP signals promote proepicardial protrusion necessary for recruitment of coronary vessel and epicardial progenitors to the heart. *Dev. Cell* **19**, 307–316 (2010).

107. Lan, Y. *et al.* TETs Regulate Proepicardial Cell Migration through Extracellular Matrix Organization during Zebrafish Cardiogenesis. *Cell Rep.* **26**, 720-732.e4 (2019).

108. Nahirney, P. C., Mikawa, T. & Fischman, D. A. Evidence for an extracellular matrix bridge guiding proepicardial cell migration to the myocardium of chick embryos. *Dev. Dyn.* **227**, 511–523 (2003).

109. Plavicki, J. S. *et al.* Multiple modes of proepicardial cell migration require heartbeat. *BMC Dev. Biol.* **14**, 18 (2014).

110. Dokic, D. & Dettman, R. W. VCAM-1 inhibits TGFβ stimulated epithelial–mesenchymal transformation by modulating Rho activity and stabilizing intercellular adhesion in epicardial mesothelial cells. *Dev. Biol.* **299**, 489–504 (2006).

111. Sengbusch, J. K., He, W., Pinco, K. A. & Yang, J. T. Dual functions of [alpha]4[beta]1 integrin in epicardial development: initial migration and long-term attachment. *J. Cell Biol.* **157**, 873–882 (2002).

112. Tandon, P., Wilczewski, C. M., Williams, C. E. & Conlon, F. L. The Lhx9-integrin pathway is essential for positioning of the proepicardial organ. *Development* **143**, 831–840 (2016).

113. Nieto, M. A., Huang, R. Y.-J., Jackson, R. A. & Thiery, J. P. EMT: 2016. *Cell* **166**, 21–45 (2016).

114. Wu, M. *et al.* Epicardial spindle orientation controls cell entry into the myocardium. *Dev. Cell* **19**, 114–125 (2010).

115. Nakajima, Y. Mitotic spindle orientation in epithelial homeostasis and plasticity. *J. Biochem.* **164**, 277–284 (2018).

116. von Gise, A. *et al.* WT1 regulates epicardial epithelial to mesenchymal transition through β-catenin and retinoic acid signaling pathways. *Dev. Biol.* **356**, 421–431 (2011).

117. Guadix, J. A. *et al.* Wt1 controls retinoic acid signalling in embryonic epicardium through transcriptional activation of Raldh2. *Development* **138**, 1093–1097 (2011).

118. Wang, S. *et al.* Retinoic acid signaling promotes the cytoskeletal rearrangement of embryonic epicardial cells. *FASEB J.* **32**, 3765–3781 (2018).

119. Wang, S. *et al.* Alterations in retinoic acid signaling affect the development of the mouse coronary vasculature. *Dev. Dyn.* **247**, 976–991 (2018).

120. Braitsch, C. M., Combs, M. D., Quaggin, S. E. & Yutzey, K. E. Pod1/Tcf21 is regulated by retinoic acid signaling and inhibits differentiation of epicardium-derived cells into smooth muscle in the developing heart. *Dev. Biol.* **368**, 345–357 (2012).

121. Greulich, F., Farin, H. F., Schuster-Gossler, K. & Kispert, A. Tbx18 function in epicardial development. *Cardiovasc. Res.* **96**, 476–483 (2012).

122. Meng, Z., Moroishi, T. & Guan, K.-L. Mechanisms of Hippo pathway regulation. *Genes Dev.* **30**, 1–17 (2016).

123. Singh, A. *et al.* Hippo Signaling Mediators Yap and Taz Are Required in the Epicardium for Coronary Vasculature Development. *Cell Rep.* **15**, 1384–1393 (2016).

124. Xiao, Y. *et al.* Hippo Signaling Plays an Essential Role in Cell State Transitions during Cardiac Fibroblast Development. *Dev. Cell* **45**, 153-169.e6 (2018).

125. Vieira, J. M. *et al.* BRG1-SWI/SNF-dependent regulation of the Wt1 transcriptional landscape mediates epicardial activity during heart development and disease. *Nat. Commun.* **8**, 16034 (2017).

126. Zhou, B. *et al.* Epicardial progenitors contribute to the cardiomyocyte lineage in the developing heart. *Nature* **454**, 109 (2008).

127. Smith, C. L. *et al.* Epicardial-Derived Cell Epithelial-to-Mesenchymal Transition and Fate Specification Require PDGF Receptor Signaling. *Circ. Res.* **108**, e15–e26 (2011).

128. Duim, S. N., Kurakula, K., Goumans, M.-J. J. & Kruithof, B. P. T. Cardiac endothelial cells express Wilms' tumor-1: Wt1 expression in the developing, adult and infarcted heart. *J. Mol. Cell. Cardiol.* **81**, 127–135 (2015).

129. Parenti, R. *et al.* Immunohistochemical expression of Wilms' tumor protein (WT1) in developing human epithelial and mesenchymal tissues. *Acta Histochem.* **115**, 70–75 (2013).

130. Volz, K. S. *et al.* Pericytes are progenitors for coronary artery smooth muscle. *Elife* **4**, e10036 (2015).

131. Kang, J. *et al.* PDGF-A as an epicardial mitogen during heart development. *Dev. Dyn.* **237**, 692–701 (2008).

132. Li, P. *et al.* IGF signaling directs ventricular cardiomyocyte proliferation during embryonic heart development. *Development* **138**, 1795–1805 (2011).

133. Shen, H. *et al.* Extracardiac control of embryonic cardiomyocyte proliferation and ventricular wall expansion. *Cardiovasc. Res.* **105**, 271–278 (2015).

134. Lavine, K. J. *et al.* Endocardial and Epicardial Derived FGF Signals Regulate Myocardial Proliferation and Differentiation In Vivo. *Dev. Cell* **8**, 85–95 (2005).

135. Pennisi, D. J., Ballard, V. L. T. & Mikawa, T. Epicardium is required for the full rate of myocyte proliferation and levels of expression of myocyte mitogenic factors FGF2 and its receptor, FGFR-1, but not for transmural myocardial patterning in the embryonic chick heart. *Dev. Dyn.* **228**, 161–172 (2003).

136. Lavine, K. J., Long, F., Choi, K., Smith, C. & Ornitz, D. M. Hedgehog signaling to distinct cell types differentially regulates coronary artery and vein development. *Development* **135**, 3161–3171 (2008).

137. Lavine, K. J. *et al.* Fibroblast growth factor signals regulate a wave of Hedgehog activation that is essential for coronary vascular development. *Genes Dev.* **20**, 1651–1666 (2006).

138. Arita, Y. *et al.* Myocardium-derived angiopoietin-1 is essential for coronary vein formation in the developing heart. *Nat. Commun.* **5**, 1–14 (2014).

139. Rhee, S. *et al.* Endothelial deletion of Ino80 disrupts coronary angiogenesis and causes congenital heart disease. *Nat. Commun.* **9**, 368 (2018).

140. Ieda, M. *et al.* Cardiac Fibroblasts Regulate Myocardial Proliferation through b1 integrin Signaling. *Dev. Cell* **16**, 233–244 (2009).

141. Shepard, P. J. & Hertel, K. J. The SR protein family. *Genome Biol.* **10**, 242 (2009).

142. Zahler, A. M., Lane, W. S., Stolk, J. A. & Roth, M. B. SR proteins: a conserved family of pre-mRNA splicing factors. *Genes Dev.* **6**, 837–847 (1992).

143. Shen, H., Kan, J. L. C. & Green, M. R. Arginine-Serine-Rich Domains Bound at Splicing Enhancers Contact the Branchpoint to Promote Prespliceosome Assembly. *Mol. Cell* **13**, 367–376 (2004).

144. Änkö, M.-L. *et al.* The RNA-binding landscapes of two SR proteins reveal unique functions and binding to diverse RNA classes. *Genome Biol.* **13**, R17 (2012).

145. Zhong, X.-Y., Wang, P., Han, J., Rosenfeld, M. G. & Fu, X.-D. SR Proteins in Vertical Integration of Gene Expression from Transcription to RNA Processing to Translation. *Mol. Cell* **35**, 1–10 (2009).

146. Hertel, K. J. Combinatorial Control of Exon Recognition. *J. Biol. Chem.* **283**, 1211–1215 (2008).

147. Jiménez, M. *et al.* Splicing events in the control of genome integrity: role of SLU7 and truncated SRSF3 proteins. *Nucleic Acids Res.* **47**, 3450–3466 (2019).

148. Jumaa, H. & Nielsen, P. J. The splicing factor SRp20 modifies splicing of its own mRNA and ASF/SF2 antagonizes this regulation. *EMBO J.* **16**, 5077–5085 (1997).

149. Müller-McNicoll, M. *et al.* SR proteins are NXF1 adaptors that link alternative RNA processing to mRNA export. *Genes Dev.* **30**, 553–566 (2016).

150. Ratnadiwakara, M. *et al.* SRSF3 promotes pluripotency through Nanog mRNA export and coordination of the pluripotency gene expression program. *Elife* **7**, e37419 (2018).

151. Mure, F. *et al.* The splicing factor SRSF3 is functionally connected to the nuclear RNA exosome for intronless mRNA decay. *Sci. Rep.* **8**, 12901 (2018).

152. Ortiz-Sánchez, P. *et al.* Loss of SRSF3 in cardiomyocytes leads to decapping of contraction-related mRNAs and severe systolic dysfunction. *Circ. Res.* **125**, 170–183 (2019).

153. Park, S. K. & Jeong, S. SRSF3 represses the expression of PDCD4 protein by coordinated regulation of alternative splicing, export and translation. *Biochem. Biophys. Res. Commun.* **470**, 431–438 (2016).

154. Ajiro, M., Jia, R., Yang, Y., Zhu, J. & Zheng, Z. M. A genome landscape of SRSF3-regulated splicing events and gene expression in human osteosarcoma U2OS cells. *Nucleic Acids Res.* **44**, 1854–1870 (2015).

155. Kurokawa, K. *et al.* Downregulation of serine/arginine-rich splicing factor 3 induces G1 cell

cycle arrest and apoptosis in colon cancer cells. *Oncogene* **33**, 1407–1417 (2014).

156. Ke, H. *et al.* Loss of TDP43 inhibits progression of triple-negative breast cancer in coordination with SRSF3. *Proc. Natl. Acad. Sci.* **115**, E3426 LP-E3435 (2018).

157. Peiqi, L. *et al.* Expression of SRSF3 is correlated with carcinogenesis and progression of oral squamous cell carcinoma. *Int. J. Med. Sci.* **13**, 533–539 (2016).

158. Kano, S. *et al.* Truncated serine/arginine-rich splicing factor 3 accelerates cell growth through up-regulating c-Jun expression. *J. Med. Investig.* **60**, 228–235 (2013).

159. Song, X. *et al.* SRSF3-Regulated RNA Alternative Splicing Promotes Glioblastoma Tumorigenicity by Affecting Multiple Cellular Processes. *Cancer Res.* e1504 (2019). doi:10.1158/0008-5472.CAN-19-1504

160. Lin, J.-C. *et al.* RBM4-SRSF3-MAP4K4 splicing cascade modulates the metastatic signature of colorectal cancer cell. *Biochim. Biophys. Acta - Mol. Cell Res.* **1865**, 259–272 (2018).

161. He, X. *et al.* Knockdown of splicing factor SRp20 causes apoptosis in ovarian cancer cells and its expression is associated with malignancy of epithelial ovarian cancer. *Oncogene* **30**, 356–365 (2010).

162. Jia, R., Li, C., McCoy, J. P., Deng, C.-X. & Zheng, Z.-M. SRp20 is a proto-oncogene critical for cell proliferation and tumor induction and maintenance. *Int. J. Biol. Sci.* **6**, 806–826 (2010).

163. Gautrey, H. *et al.* SRSF3 and hnRNP H1 regulate a splicing hotspot of HER2 in breast cancer cells. *RNA Biol.* **12**, 1139–1151 (2015).

164. Kuranaga, Y. *et al.* SRSF3, a Splicer of the PKM Gene, Regulates Cell Growth and Maintenance of Cancer-Specific Energy Metabolism in Colon Cancer Cells. *Int. J. Mol. Sci.* **19**, 3012 (2018).

165. Do, D. V. *et al.* SRSF3 maintains transcriptome integrity in oocytes by regulation of alternative splicing and transposable elements. *Cell Discov.* **4**, 33 (2018).

166. Jumaa, H., Wei, G. & Nielsen, P. J. Blastocyst formation is blocked in mouse embryos lacking the splicing factor SRp20. *Curr. Biol.* **9**, 899–902 (1999).

167. Änkö, M. L., Morales, L., Henry, I., Beyer, A. & Neugebauer, K. M. Global analysis reveals SRp20-and SRp75-specific mRNPs in cycling and neural cells. *Nat. Struct. Mol. Biol.* **17**, 962–970 (2010).

168. Sen, S., Jumaa, H. & Webster, N. J. G. G. Splicing factor SRSF3 is crucial for hepatocyte differentiation and metabolic function. *Nat. Commun.* **4**, 1312–1336 (2013).

169. Xu, X. *et al.* ASF/SF2-Regulated CaMKIIdelta Alternative Splicing Temporally Reprograms Excitation-Contraction Coupling in Cardiac Muscle. *Cell* **120**, 59–72 (2005).

170. Ding, J.-H. H. *et al.* Dilated cardiomyopathy caused by tissue-specific ablation of SC35 in the heart. *EMBO J.* **23**, 885–896 (2004).

171. Feng, Y. *et al.* SRp38 Regulates Alternative Splicing and Is Required for Ca2+ Handling in the Embryonic Heart. *Dev. Cell* **16**, 528–538 (2009).

172. Dubé, K. N. *et al.* Recapitulation of developmental mechanisms to revascularize the ischemic heart. *JCI Insight* **2**, 96800 (2017).

173. Smart, N. *et al.* De novo cardiomyocytes from within the activated adult heart after injury. *Nature* **474**, 640–644 (2011).

174. Bock-Marquette, I., Saxena, A., White, M. D., Michael DiMaio, J. & Srivastava, D. Thymosin β4 activates integrin-linked kinase and promotes cardiac cell migration, survival and cardiac repair. *Nature* **432**, 466–472 (2004).

175. Bock-Marquette, I. *et al.* Thymosin β4 mediated PKC activation is essential to initiate the embryonic coronary developmental program and epicardial progenitor cell activation in adult mice in vivo. *J. Mol. Cell. Cardiol.* **46**, 728–738 (2009).

176. Goldstein, A. L., Hannappel, E. & Kleinman, H. K. Thymosin β4: Actin-sequestering protein moonlights to repair injured tissues. *Trends Mol. Med.* **11**, 421–429 (2005).

177. Smart, N. *et al.* Thymosin β-4 is essential for coronary vessel development and promotes neovascularization via adult epicardium. *Ann. N. Y. Acad. Sci.* **1112**, 171–188 (2007).

178. Austin, A. F., Compton, L. A., Love, J. D., Brown, C. B. & Barnett, J. V. Primary and immortalized mouse epicardial cells undergo differentiation in response to TGFβ. *Dev. Dyn.* **237**, 366–376 (2008).

179. Madisen, L. *et al.* A robust and high-throughput Cre reporting and characterization system for the whole mouse brain. *Nat. Neurosci.* **13**, 133–140 (2010).

180. Abe, T. *et al.* Visualization of cell cycle in mouse embryos with Fucci2 reporter directed by Rosa26 promoter. *Development* **140**, 237–246 (2013).

181. Rossdeutsch, A., Smart, N., Dubé, K. N., Turner, M. & Riley, P. R. Essential Role for thymosin β4 in regulating vascular smooth muscle cell development and vessel wall stability. *Circ. Res.* **111**, 89–102 (2012).

182. Livak, K. J. & Schmittgen, T. D. Analysis of Relative Gene Expression Data Using Real-Time Quantitative PCR and the 2−ΔΔCT Method. *Methods* **25**, 402–408 (2001).

183. Dong, J. *et al.* Single-cell RNA-seq analysis unveils a prevalent epithelial/mesenchymal hybrid state during mouse organogenesis. *Genome Biol.* **19**, 31 (2018).

184. Butler, A., Hoffman, P., Smibert, P., Papalexi, E. & Satija, R. Integrating single-cell transcriptomic data across different conditions, technologies, and species. *Nat. Biotechnol.* **36**, 411 (2018).

185. Stuart, T. *et al.* Comprehensive Integration of Single-Cell Data. *Cell* **177**, 1888-1902.e21 (2019).

186. Maaten, L. van der & Hinton, G. Visualizing data using t-SNE. *J. Mach. Learn. Res.* **9**, 2579–2605 (2008).

187. Picelli, S. *et al.* Full-length RNA-seq from single cells using Smart-seq2. *Nat. Protoc.* **9**, 171–181 (2014).

188. Hafemeister, C. & Satija, R. Normalization and variance stabilization of single-cell RNA-seq data using regularized negative binomial regression. *bioRxiv* 576827 (2019).

doi:10.1101/576827

189. Kowalczyk, M. S. *et al.* Single-cell RNA-seq reveals changes in cell cycle and differentiation programs upon aging of hematopoietic stem cells. *Genome Res.* **25**, 1860–1872 (2015).

190. Qiu, X. *et al.* Reversed graph embedding resolves complex single-cell trajectories. *Nat. Methods* **14**, 979–982 (2017).

191. Becht, E. *et al.* Evaluation of UMAP as an alternative to t-SNE for single-cell data. *bioRxiv* 298430 (2018). doi:10.1101/298430

192. Schulte, I., Schlueter, J., Abu-Issa, R., Brand, T. & Männer, J. Morphological and molecular left–right asymmetries in the development of the proepicardium: A comparative analysis on mouse and chick embryos. *Dev. Dyn.* **236**, 684–695 (2007).

193. Rodgers, L. S., Lalani, S., Runyan, R. B. & Camenisch, T. D. Differential growth and multicellular villi direct proepicardial translocation to the developing mouse heart. *Dev. Dyn.* **237**, 145–152 (2008).

194. Li, J. *et al.* CDC42 is required for epicardial and pro-epicardial development by mediating FGF receptor trafficking to the plasma membrane. *Development* **144**, 1653–1647 (2017).

195. Jenkins, S. J., Hutson, D. R. & Kubalak, S. W. Analysis of the proepicardium–epicardium transition during the malformation of the RXRα−/− epicardium. *Dev. Dyn.* **233**, 1091–1101 (2005).

196. Moore, A. W., McInnes, L., Kreidberg, J., Hastie, N. D. & Schedl, A. YAC complementation shows a requirement for Wt1 in the development of epicardium, adrenal gland and throughout nephrogenesis. *Development* **126**, 1845–1857 (1999).

197. Sham, T. *et al.* Collective cell migration without proliferation: density determines cell velocity and wave velocity. *R. Soc. Open Sci.* **5**, 172421 (2019).

198. Firmino, J., Rocancourt, D., Saadaoui, M., Moreau, C. & Gros, J. Cell Division Drives Epithelial Cell Rearrangements during Gastrulation in Chick. *Dev. Cell* **36**, 249–261 (2016).

199. Tang, Y. *et al.* Downregulation of splicing factor SRSF3 induces p53β, an alternatively spliced isoform of p53 that promotes cellular senescence. *Oncogene* **32**, 2792–2798 (2012).

200. Corbo, C., Orrù, S. & Salvatore, F. SRp20: An overview of its role in human diseases. *Biochem. Biophys. Res. Commun.* **436**, 1–5 (2013).

201. Kim, H. R. *et al.* SRSF3-regulated miR-132/212 controls cell migration and invasion by targeting YAP1. *Exp. Cell Res.* **358**, 161–170 (2017).

202. Markus, M. A. *et al.* WT1 interacts with the splicing protein RBM4 and regulates its ability to modulate alternative splicing in vivo. *Exp. Cell Res.* **312**, 3379–3388 (2006).

203. Gu, H., Zou, Y.-R. & Rajewsky, K. Independent control of immunoglobulin switch recombination at individual switch regions evidenced through Cre-loxP-mediated gene targeting. *Cell* **73**, 1155–1164 (1993).

204. Vooijs, M., Jonkers, J. & Berns, A. A highly efficient ligand-regulated Cre recombinase mouse line shows that LoxP recombination is position dependent. *EMBO Rep.* **2**, 292–297 (2001).

205. Zheng, B., Sage, M., Sheppeard, E. A., Jurecic, V. & Bradley, A. Engineering mouse chromosomes with Cre-loxP: range, efficiency, and somatic applications. *Mol. Cell. Biol.* **20**, 648–655 (2000).

206. Coppoolse, E. R., de Vroomen, M. J., van Gennip, F., Hersmus, B. J. M. & van Haaren, M. J. J. Size Does Matter: Cre-mediated Somatic Deletion Efficiency Depends on the Distance Between the Target lox-Sites. *Plant Mol. Biol.* **58**, 687–698 (2005).

207. Wang, S.-Z., Liu, B.-H., Tao, H. W., Xia, K. & Zhang, L. I. A genetic strategy for stochastic gene activation with regulated sparseness (STARS). *PLoS One* **4**, e4200 (2009).

208. Kim, J. *et al.* Splicing factor SRSF3 represses the translation of programmed cell death 4 mRNA by associating with the 5'-UTR region. *Cell Death Differ* **21**, 481–490 (2014).

209. Böhm, M. *et al.* The transformation suppressor protein Pdcd4 shuttles between nucleus and cytoplasm and binds RNA. *Oncogene* **22**, 4905–4910 (2003).

210. Chen, M. *et al.* Wt1 Is Involved in Leydig Cell Steroid Hormone Biosynthesis by Regulating Paracrine Factor Expression in Mice1. *Biol. Reprod.* **90**, 71 (2014).

211. Jat, P. S. *et al.* Direct derivation of conditionally immortal cell lines from an H-2Kb-tsA58 transgenic mouse. *Proc. Natl. Acad. Sci.* **88**, 5096–5100 (1991).

212. Delaughter, D. M. *et al.* Transcriptional profiling of cultured, embryonic epicardial cells identifies novel genes and signaling pathways regulated by TGFβR3 in vitro. *PLoS One* **11**, 1–21 (2016).

213. Tao, J., Barnett, J. V, Watanabe, M. & Ramírez-Bergeron, D. Hypoxia Supports Epicardial Cell Differentiation in Vascular Smooth Muscle Cells through the Activation of the TGFβ Pathway. *J. Cardiovasc. Dev. Dis.* **5**, 19 (2018).

214. Hubbard, K. & Ozer, H. L. Mechanism of immortalization. *Age (Omaha).* **22**, 65–69 (1999).

215. Brookes, S. *et al.* Evidence for a CDK4-dependent checkpoint in a conditional model of cellular senescence. *Cell Cycle* **14**, 1164–1173 (2015).

216. Obinata, M. Conditionally immortalized cell lines with differentiated functions established from temperature-sensitive T-antigen transgenic mice. *Genes to Cells* **2**, 235–244 (1997).

217. Cantalupo, P. G. *et al.* Cell-type specific regulation of gene expression by simian virus 40 T antigens. *Virology* **386**, 183–191 (2009).

218. Furcht, L. T., Mosher, D. F. & Wendelschafter-Crabb, G. Effects of cell density and transformation on the formation of a fibronectin extracellular filamentous matrix on human fibroblasts. *Cancer Res.* **38**, 4618–4623 (1978).

219. Torlopp, A., Schlueter, J. & Brand, T. Role of fibroblast growth factor signaling during proepicardium formation in the chick embryo. *Dev. Dyn.* **239**, 2393–2403 (2010).

220. Saito, Y., Kojima, T. & Takahashi, N. Mab21l2 Is Essential for Embryonic Heart and Liver Development. *PLoS One* **7**, e32991 (2012).

221. Zhu, J. Y., Abate, M., Rice, P. W. & Cole, C. N. The ability of simian virus 40 large T antigen to immortalize primary mouse embryo fibroblasts cosegregates with its ability to bind to p53. *J. Virol.* **65**, 6872–6880 (1991).

222. Yang, K., Hitomi, M. & Stacey, D. W. Variations in cyclin D1 levels through the cell cycle determine the proliferative fate of a cell. *Cell Div.* **1**, 32 (2006).

223. Dettman, R. W., Denetclaw, W., Ordahl, C. P. & Bristow, J. Common Epicardial Origin of Coronary Vascular Smooth Muscle, Perivascular Fibroblasts, and Intermyocardial Fibroblasts in the Avian Heart. *Dev. Biol.* **193**, 169–181 (1998).

224. Compton, L. A., Potash, D. A., Mundell, N. A. & Barnett, J. V. Transforming growth factor-β induces loss of epithelial character and smooth muscle cell differentiation in epicardial cells. *Dev. Dyn.* **235**, 82–93 (2006).

225. Vega-Hernández, M., Kovacs, A., De Langhe, S. & Ornitz, D. M. FGF10/FGFR2b signaling is essential for cardiac fibroblast development and growth of the myocardium. *Development* **138**, 3331–3340 (2011).

226. Baek, S. T. & Tallquist, M. D. Nf1 limits epicardial derivative expansion by regulating epithelial to mesenchymal transition and proliferation. *Development* **139**, 2040–2049 (2012).

227. Bao, X. *et al.* Human pluripotent stem cell-derived epicardial progenitors can differentiate to endocardial-like endothelial cells. *Bioeng. Transl. Med.* **2**, 191–201 (2017).

228. Wu, B. *et al.* Endocardial cells form the coronary arteries by angiogenesis through myocardial-endocardial VEGF signaling. *Cell* **151**, 1083–1096 (2012).

229. Zamora, M., Manner, J. & Ruiz-Lozano, P. Epicardium-derived progenitor cells require -catenin for coronary artery formation. *Proc. Natl. Acad. Sci.* **104**, 18109–18114 (2007).

230. Soriano, P. Generalized lacZ expression with the ROSA26 Cre reporter strain . *Nat. Genet.* **21**, 70–71 (1999).

231. Park, E. J. *et al.* System for tamoxifen-inducible expression of cre-recombinase from the Foxa2 locus in mice. *Dev. Dyn.* **237**, 447–453 (2008).

232. Danielian, P. S., Muccino, D., Rowitch, D. H., Michael, S. K. & McMahon, A. P. Modification of gene activity in mouse embryos in utero by a tamoxifen-inducible form of Cre recombinase. *Curr. Biol.* **8**, 1323–1326 (1998).

233. Hayashi, S. & McMahon, A. P. Efficient Recombination in Diverse Tissues by a Tamoxifen-Inducible Form of Cre: A Tool for Temporally Regulated Gene Activation/Inactivation in the Mouse. *Dev. Biol.* **244**, 305–318 (2002).

234. Cavallero, S. *et al.* CXCL12 Signaling Is Essential for Maturation of the Ventricular Coronary Endothelial Plexus and Establishment of Functional Coronary Circulation. *Dev. Cell* **33**, 469–477 (2015).

235. M., P. H. *et al.* Non–Cell-Autonomous Roles for the Planar Cell Polarity Gene Vangl2 in Development of the Coronary Circulation. *Circ. Res.* **102**, 615–623 (2008).

236. Ge, J. *et al.* RhoA, Rac1, and Cdc42 differentially regulate αSMA and collagen I expression in mesenchymal stem cells. *J. Biol. Chem.* **293**, 9358–9369 (2018).

237. Martínez-Estrada, O. M. *et al.* Wt1 is required for cardiovascular progenitor cell formation through transcriptional control of Snail and E-cadherin. *Nat. Genet.* **42**, 89–93 (2010).

238. Elbashir, S. M. *et al.* Duplexes of 21-nucleotide RNAs mediate RNA interference in cultured

mammalian cells. *Nature* **411**, 494–498 (2001).

239. Winder, S. J. & Walsh, M. P. Calponin: Thin filament-linked regulation of smooth muscle contraction. *Cell. Signal.* **5**, 677–686 (1993).

240. Wessels, A. & Pérez-Pomares, J. M. The epicardium and epicardially derived cells (EPDCs) as cardiac stem cells. *Anat. Rec. Part A Discov. Mol. Cell. Evol. Biol.* **276A**, 43–57 (2004).

241. Iyer, D. *et al.* Robust derivation of epicardium and its differentiated smooth muscle cell progeny from human pluripotent stem cells. *Development* **143**, 904–904 (2016).

242. Tevosian, S. G. *et al.* FOG-2, a Cofactor for GATA Transcription Factors, Is Essential for Heart Morphogenesis and Development of Coronary Vessels from Epicardium. *Cell* **101**, 729–739 (2000).

243. Krainock, M. *et al.* Epicardial Epithelial-to-Mesenchymal Transition in Heart Development and Disease. *J. Clin. Med.* **5**, E27 (2016).

244. Molin, D. G. M. *et al.* Expression patterns of Tgfβ1–3 associate with myocardialisation of the outflow tract and the development of the epicardium and the fibrous heart skeleton. *Dev. Dyn.* **227**, 431–444 (2003).

245. Pauklin, S. & Vallier, L. The cell-cycle state of stem cells determines cell fate propensity. *Cell* **155**, 135–147 (2013).

246. Du, Y., Taylor, C. G., Aukema, H. M. & Zahradka, P. Importance of extracellular matrix and growth state for the EA.hy926 endothelial cell response to polyunsaturated fatty acids. *PLoS One* **13**, e0197613 (2018).

247. Ruijtenberg, S. & van den Heuvel, S. Coordinating cell proliferation and differentiation: Antagonism between cell cycle regulators and cell type-specific gene expression. *Cell Cycle* **15**, 196–212 (2016).

248. Boilly, B., Vercoutter-Edouart, A. S., Hondermarck, H., Nurcombe, V. & Le Bourhis, X. FGF signals for cell proliferation and migration through different pathways. *Cytokine Growth Factor Rev.* **11**, 295–302 (2000).

249. Bala, K., Ambwani, K. & Gohil, N. K. Effect of different mitogens and serum concentration on HUVEC morphology and characteristics: Implication on use of higher passage cells. *Tissue Cell* **43**, 216–222 (2011).

250. Olsson, A.-K., Dimberg, A., Kreuger, J. & Claesson-Welsh, L. VEGF receptor signalling ? in control of vascular function. *Nat. Rev. Mol. Cell Biol.* **7**, 359–371 (2006).

251. Azhar, M. *et al.* Transforming growth factor beta in cardiovascular development and function. *Cytokine Growth Factor Rev.* **14**, 391–407 (2003).

252. Lie-Venema, H. *et al.* Origin, fate, and function of epicardium-derived cells (EPCDs) in normal and abnormal cardiac development. *ScientificWorldJournal.* **7**, 1777–1798 (2007).

253. Jan, S. & Thomas, B. Subpopulation of Proepicardial Cells Is Derived From the Somatic Mesoderm in the Chick Embryo. *Circ. Res.* **113**, 1128–1137 (2013).

254. Tandon, P., Miteva, Y. V, Kuchenbrod, L. M., Cristea, I. M. & Conlon, F. L. Tcf21 regulates the specification and maturation of proepicardial cells. *Development* **140**, 2409–2421

(2013).

255. Wu, S.-P., Dong, X.-R., Regan, J. N., Su, C. & Majesky, M. W. Tbx18 regulates development of the epicardium and coronary vessels. *Dev. Biol.* **383**, 307–320 (2013).

256. Carmona, R. *et al.* Conditional deletion of WT1 in the septum transversum mesenchyme causes congenital diaphragmatic hernia in mice. *Elife* **5**, e16009 (2016).

257. Maya-Ramos, L., Cleland, J., Bressan, M. & Mikawa, T. Induction of the Proepicardium. *J. Dev. Biol.* **1**, 82–91 (2013).

258. Schlueter, J. & Brand, T. Origin and fates of the proepicardium. *Aswan Hear. Cent. Sci. Pract. Ser.* **2011**, 11 (2011).

259. Levay, A. K. *et al.* Scleraxis is required for cell lineage differentiation and extracellular matrix remodeling during murine heart valve formation in vivo. *Circ. Res.* **103**, 948–956 (2008).

260. Lai, C., Stepniak, D., Sias, L. & Funatake, C. A sensitive flow cytometric method for multi-parametric analysis of microRNA, messenger RNA and protein in single cells. *Methods* **134**–**135**, 136–148 (2018).

261. Nestorowa, S. *et al.* A single cell resolution map of mouse haematopoietic stem and progenitor cell differentiation. *Blood* **128**, e20-31 (2016).

262. Kanamori-Katayama, M. *et al.* LRRN4 and UPK3B are markers of primary mesothelial cells. *PLoS One* **6**, e25391 (2011).

263. Ozerdem, U., Grako, K. A., Dahlin-Huppe, K., Monosov, E. & Stallcup, W. B. NG2 proteoglycan is expressed exclusively by mural cells during vascular morphogenesis. *Dev. Dyn.* **222**, 218–227 (2001).

264. He, L. *et al.* Analysis of the brain mural cell transcriptome. *Sci. Rep.* **6**, 35108 (2016).

265. Liu, X. *et al.* Dermatopontin promotes adhesion, spreading and migration of cardiac fibroblasts in vitro. *Matrix Biol.* **32**, 23–31 (2013).

266. Greulich, F. & Kispert, A. Epicardial Lineages. *J. Dev. Biol.* **1**, 32–46 (2013).

267. Ruiz-Villalba, A., Ziogas, A., Ehrbar, M. & Pérez-Pomares, J. M. Characterization of Epicardial-Derived Cardiac Interstitial Cells: Differentiation and Mobilization of Heart Fibroblast Progenitors. *PLoS One* **8**, 17–19 (2013).

268. Zheng, G. X. Y. *et al.* Massively parallel digital transcriptional profiling of single cells. *Nat. Commun.* **8**, 14049 (2017).

269. Potter, C. M. F. *et al.* Shape and compliance of endothelial cells after shear stress in vitro or from different aortic regions: scanning ion conductance microscopy study. *PLoS One* **7**, e31228 (2012).

270. Miano, J. M., Cserjesi, P., Ligon, K. L., Periasamy, M. & Olson, E. N. Smooth muscle myosin heavy chain exclusively marks the smooth muscle lineage during mouse embryogenesis. *Circ. Res.* **75**, 803–812 (1994).

271. Doppler, S. A. *et al.* Cardiac fibroblasts: more than mechanical support. *J. Thorac. Dis.* **9**, S36–S51 (2017).

272. R., A. S. *et al.* Developmental Heterogeneity of Cardiac Fibroblasts Does Not Predict Pathological Proliferation and Activation. *Circ. Res.* **115**, 625–635 (2014).

273. Bonet, F. *et al.* CCBE1 is required for coronary vessel development and proper coronary artery stem formation in the mouse heart. *Dev. Dyn.* **247**, 1135–1145 (2018).

274. Yoshida, T. *et al.* Smooth and Cardiac Muscle-selective Knock-out of Krüppel-like Factor 4 Causes Postnatal Death and Growth Retardation. *J. Biol. Chem.* **285**, 21175–21184 (2010).

275. Babu, G. J., Bhupathy, P., Carnes, C. A., Billman, G. E. & Periasamy, M. Differential expression of sarcolipin protein during muscle development and cardiac pathophysiology. *J. Mol. Cell. Cardiol.* **43**, 215–222 (2007).

276. Steimle, J. D. & Moskowitz, I. P. TBX5: A Key Regulator of Heart Development. *Curr. Top. Dev. Biol.* **122**, 195–221 (2017).

277. Gaborit, N. *et al.* Cooperative and antagonistic roles for Irx3 and Irx5 in cardiac morphogenesis and postnatal physiology. *Development* **139**, 4007–4019 (2012).

278. England, J. & Loughna, S. Heavy and light roles: myosin in the morphogenesis of the heart. *Cell. Mol. Life Sci.* **70**, 1221–1239 (2013).

279. Cambier, L., Plate, M., M Sucov, H. & Pashmforoush, M. Nkx2-5 regulates cardiac growth through modulation of Wnt signaling by R-spondin3. *Development* **141**, 2959–2971 (2014).

280. Chiplunkar, A. R. *et al.* Krüppel-like factor 2 is required for normal mouse cardiac development. *PLoS One* **8**, e54891 (2013).

281. Tkatchenko, T. V *et al.* Lack of periostin leads to suppression of Notch1 signaling and calcific aortic valve disease. *Physiol. Genomics* **39**, 160–168 (2009).

282. Garside, V. C. *et al.* SOX9 modulates the expression of key transcription factors required for heart valve development. *Development* **142**, 4340–4350 (2015).

283. Li, Y., Urban, A., Midura, D., Simon, H.-G. & Wang, Q. T. Proteomic characterization of epicardial-myocardial signaling reveals novel regulatory networks including a role for NF-κB in epicardial EMT. *PLoS One* **12**, e0174563 (2017).

284. He, L., Tian, X., Zhang, H., Wythe, J. D. & Zhou, B. Fabp4-CreER lineage tracing reveals two distinctive coronary vascular populations. *J. Cell. Mol. Med.* **18**, 2152–2156 (2014).

285. Zhou, X. *et al.* Syncytium calcium signaling and macrophage function in the heart. *Cell Biosci.* **8**, 24 (2018).

286. Baran-Gale, J., Chandra, T. & Kirschner, K. Experimental design for single-cell RNA sequencing. *Brief. Funct. Genomics* **17**, 233–239 (2017).

287. Dunwoodie, S. L. The Role of Hypoxia in Development of the Mammalian Embryo. *Dev. Cell* **17**, 755–773 (2009).

288. Elmasri, H. *et al.* Fatty acid binding protein 4 is a target of VEGF and a regulator of cell proliferation in endothelial cells. *FASEB J.* **23**, 3865–3873 (2009).

289. Summers, K. M., Raza, S., van Nimwegen, E., Freeman, T. C. & Hume, D. A. Co-expression of FBN1 with mesenchyme-specific genes in mouse cell lines: implications for

phenotypic variability in Marfan syndrome. *Eur. J. Hum. Genet.* **18**, 1209–1215 (2010).

290. Wang, J. *et al.* Pim1 kinase synergizes with c-MYC to induce advanced prostate carcinoma. *Oncogene* **29**, 2477–2487 (2010).

291. Wei, X. *et al.* Biological characteristics of embryonic epicardial cells in vitro correlate with embryonic day. *Acta Biochim. Biophys. Sin. (Shanghai).* **49**, 14–24 (2017).

292. Wigle, J. T. *et al.* An essential role for Prox1 in the induction of the lymphatic endothelial cell phenotype. *EMBO J.* **21**, 1505–1513 (2002).

293. Karnik, S. K. *et al.* A critical role for elastin signaling in vascular morphogenesis and disease. *Development* **130**, 411–423 (2003).

294. Airley, R. *et al.* Glucose Transporter Glut-1 Expression Correlates with Tumor Hypoxia and Predicts Metastasis-free Survival in Advanced Carcinoma of the Cervix. *Clin. Cancer Res.* **7**, 928–934 (2001).

295. Jaya, K. *et al.* Essential Role of Developmentally Activated Hypoxia-Inducible Factor 1α for Cardiac Morphogenesis and Function. *Circ. Res.* **103**, 1139–1146 (2008).

296. Heilig, C. *et al.* Implications of glucose transporter protein type 1 (GLUT1)-haplodeficiency in embryonic stem cells for their survival in response to hypoxic stress. *Am. J. Pathol.* **163**, 1873–1885 (2003).

297. Cousins, F. L., Murray, A. A., Scanlon, J. P. & Saunders, P. T. K. Hypoxyprobe™ reveals dynamic spatial and temporal changes in hypoxia in a mouse model of endometrial breakdown and repair. *BMC Res. Notes* **9**, 30 (2016).

298. Lee, M.-J., Kim, J.-Y., Suk, K. & Park, J.-H. Identification of the Hypoxia-Inducible Factor 1α-Responsive HGTD-P Gene as a Mediator in the Mitochondrial Apoptotic Pathway. *Mol. Cell. Biol.* **24**, 3918–3927 (2004).

299. Guo, K. *et al.* Hypoxia induces the expression of the pro-apoptotic gene BNIP3. *Cell Death Differ.* **8**, 367–376 (2001).

300. Bowler, E. *et al.* Hypoxia leads to significant changes in alternative splicing and elevated expression of CLK splice factor kinases in PC3 prostate cancer cells. *BMC Cancer* **18**, 355 (2018).

301. Jiang, H. *et al.* Trichostatin a Protects Dendritic Cells Against Oxygen-Glucose Deprivation via the SRSF3/PKM2/Glycolytic Pathway. *Front. Pharmacol.* **9**, 612 (2018).

302. Villa del Campo, C. *et al.* Myc overexpression enhances epicardial contribution to the developing heart and promotes extensive expansion of the cardiomyocyte population. *Sci. Rep.* **6**, 35366 (2016).

303. Johnston, L. A. Socializing with MYC: cell competition in development and as a model for premalignant cancer. *Cold Spring Harb. Perspect. Med.* **4**, a014274 (2014).

304. von Gise, A. Endocardial and epicardial epithelial to mesenchymal transitions in heart development and disease. *Circ. Res.* **110**, 1628–1645 (2013).

305. Rudat, C., Norden, J., Taketo, M. M. & Kispert, A. Epicardial function of canonical Wnt-, Hedgehog-, Fgfr1/2-, and Pdgfra-signalling. *Cardiovasc. Res.* **100**, 411–421 (2013).

306. Singh, M. K., Lu, M. M., Massera, D. & Epstein, J. A. MicroRNA-processing enzyme Dicer is required in epicardium for coronary vasculature development. *J. Biol. Chem.* **286**, 41036–41045 (2011).

307. Yang, J. *et al.* Epicardial calcineurin–NFAT signals through Smad2 to direct coronary smooth muscle cell and arterial wall development. *Cardiovasc. Res.* **101**, 120–129 (2013).

308. Arora, H. *et al.* Prokineticin receptor-1 signaling promotes Epicardial to Mesenchymal Transition during heart development. *Sci. Rep.* **6**, 25541 (2016).

309. Gonçalves, V., Matos, P. & Jordan, P. Antagonistic SR proteins regulate alternative splicing of tumor-related Rac1b downstream of the PI3-kinase and Wnt pathways. *Hum. Mol. Genet.* **18**, 3696–3707 (2009).

310. Lowe, V. *et al.* Neuropilin 1 mediates epicardial activation and revascularization in the regenerating zebrafish heart. *Development* **146**, dev174482 (2019).

311. Ozpolat, B. *et al.* Programmed Cell Death-4 Tumor Suppressor Protein Contributes to Retinoic Acid-Induced Terminal Granulocytic Differentiation of Human Myeloid Leukemia Cells. *Mol. Cancer Res.* **5**, 95–108 (2007).

312. Liu, X. *et al.* An essential role of PDCD4 in vascular smooth muscle cell apoptosis and proliferation: implications for vascular disease. *Am. J. Physiol. Physiol.* **298**, C1481 (2010).

313. Scholzen, T. & Gerdes, J. The Ki-67 protein: From the known and the unknown. *J. Cell. Physiol.* **182**, 311–322 (2000).

314. Miller, I. *et al.* Ki67 is a Graded Rather than a Binary Marker of Proliferation versus Quiescence. *Cell Rep.* **24**, 1105-1112.e5 (2018).

315. Cossette, S. & Misra, R. The identification of different endothelial cell populations within the mouse proepicardium. *Dev. Dyn.* **240**, 2344–2353 (2011).

316. Pauklin, S., Madrigal, P., Bertero, A. & Vallier, L. Initiation of stem cell differentiation involves cell cycle-dependent regulation of developmental genes by Cyclin D. *Genes Dev.* **30**, 421–433 (2016).

317. Erben, L., He, M.-X., Laeremans, A., Park, E. & Buonanno, A. A Novel Ultrasensitive In Situ Hybridization Approach to Detect Short Sequences and Splice Variants with Cellular Resolution. *Mol. Neurobiol.* **55**, 6169–6181 (2018).

318. You, J.-J., Yang, C.-M., Chen, M.-S. & Yang, C.-H. Regulation of Cyr61/CCN1 expression by hypoxia through cooperation of c-Jun/AP-1 and HIF-1α in retinal vascular endothelial cells. *Exp. Eye Res.* **91**, 825–836 (2010).

319. Pontes-Quero, S. *et al.* High mitogenic stimulation arrests angiogenesis. *Nat. Commun.* **10**, 2016 (2019).